



Interface behaviour of geosynthetics in landfill cover systems under static and seismic loading conditions

Laura Carbone

► To cite this version:

Laura Carbone. Interface behaviour of geosynthetics in landfill cover systems under static and seismic loading conditions. Tectonics. Université de Grenoble; Università degli studi mediterranea (Reggio de Calabre, Italie), 2014. English. NNT : 2014GRENU006 . tel-01551776

HAL Id: tel-01551776

<https://theses.hal.science/tel-01551776>

Submitted on 30 Jun 2017

HAL is a multi-disciplinary open access archive for the deposit and dissemination of scientific research documents, whether they are published or not. The documents may come from teaching and research institutions in France or abroad, or from public or private research centers.

L'archive ouverte pluridisciplinaire **HAL**, est destinée au dépôt et à la diffusion de documents scientifiques de niveau recherche, publiés ou non, émanant des établissements d'enseignement et de recherche français ou étrangers, des laboratoires publics ou privés.



Università degli Studi
Mediterranea
di Reggio Calabria



Dissertation

in partial fulfillment of the requirements for the degree of

Dottore di Ricerca dell'Università “Mediterranea” di Reggio Calabria

SCUOLA DI DOTTORATO IN INGEGNERIA GEOTECNICA E CHIMICA DEI MATERIALI
XXVI CICLO – S.S.D. ICAR/07

DIPARTIMENTO DI INGEGNERIA CIVILE, DELL'ENERGIA, DELL'AMBIENTE E DEI MATERIALI (DICEAM)
and

Docteur de l'Université de Grenoble

ÉCOLE DOCTORALE TERRE, UNIVERS, ENVIRONNEMENT

SPECIALITE: SCIENCES DE LA TERRE ET DE L'UNIVERS ET DE L'ENVIRONNEMENT

Arrêté ministériel : le 6 janvier 2005 -7 août 2006

LABORATOIRE D'ETUDE DES TRANSFERTS EN HYDROLOGIE ET ENVIRONNEMENT (LTHE)

Interface behaviour of geosynthetics in landfill cover systems under static and seismic loading conditions

Ph.D. Candidate

Laura CARBONE

SUPERVISORS

Prof. Eng. Nicola MORACI

Prof. Eng. Jean – Pierre GOURC

CO-SUPERVISOR

Prof. Eng. Paolo CARRUBBA

Publicly defended on April, 28th 2014

GRADUATION COMMITTEE :

Prof. Philippe DELMAS

President and Reviewer, Full Professor, CNAM, Paris

Prof. Michele MAUGERI

Reviewer, Full Professor, Università di Catania

Prof. Francesco CASTELLI

Member, Assistant Professor, Università Kore di Enna

Prof. Roberto PAOLESSE

Member, Full Professor, Università Tor Vergata, Roma

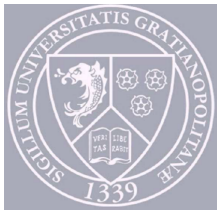
Prof. Jean – Pierre GOURC

Supervisor, Full Professor, Université Joseph Fourier

Prof. Nicola MORACI

Supervisor, Full Professor, Università Mediterranea di Reggio Calabria





UNIVERSITÀ DEGLI STUDI *MEDITERRANEA* DI REGGIO CALABRIA

DOTTORATO DI RICERCA IN
INGEGNERIA GEOTECNICA E CHIMICA DEI MATERIALI
XXVI CICLO – S.S.D. ICAR/07

DIPARTIMENTO DI INGEGNERIA CIVILE, DELL'ENERGIA,
DELL'AMBIENTE E DEI MATERIALI (DICEAM)

UNIVERSITE DE GRENOBLE

ÉCOLE DOCTORALE TERRE, UNIVERS, ENVIRONNEMENT

SPECIALITE: SCIENCES DE LA TERRE ET DE L'UNIVERS ET DE
L'ENVIRONNEMENT

Arrêté ministériel: le 6 janvier 2005 -7 août 2006

LABORATOIRE D'ETUDE DES TRANSFERTS EN
HYDROLOGIE ET ENVIRONNEMENT (LTHE)

**INTERFACE BEHAVIOUR OF GEOSYNTHETICS IN LANDFILL COVER
SYSTEMS UNDER STATIC AND SEISMIC LOADING CONDITIONS**

PH.D. CANDIDATE

Laura Carbone

SUPERVISORS

Prof. Eng. Nicola MORACI

Prof. Eng. Jean – Pierre GOURC

CO – SUPERVISOR

Prof. Eng. Paolo CARRUBBA

HEAD OF THE DOCTORAL SCHOOL

Prof. Eng. Nicola MORACI

REGGIO CALABRIA, JANUARY 2014

Laura Carbone

**INTERFACE BEHAVIOUR OF GEOSYNTHETICS IN
LANDFILL COVER SYSTEMS UNDER STATIC AND
SEISMIC LOADING CONDITIONS**

Scientific Board of the Doctoral School
in Geotechnical Engineering and Materials Chemistry:

Moraci Nicola (Head of the Doctoral School)

Antonucci Pier Luigi

Dente Giovanni

Donato Andrea

Messina Giacomo

Valore Calogero

Conte Enrico

Airò Farulla Camillo

Giovine Pasquale

Musolino Maria Grazia

Santangelo Saveria

Barletta Giuseppina

Calabro' Paolo Salvatore

Candito Pasquale

Cascone Ernesto

Frontera Patrizia

Livrea Roberto

Molica Bisci Giovanni

Mortara Giuseppe

Porcino Daniela Dominica

Ziccarelli Maurizio

*Ce qui s'était abattu sur elle,
ce n'était pas un fardeau,
mais l'insoutenable légèreté de l'être.*

(Milan Kundera, L'insoutenable légèreté de l'être)

Acknowledgements

First, I would like to sincerely thank Prof. Nicola Moraci, his support and his valuable teaching have provided me with new motivation and confidence over the years. Also, I thank him for allowing me to develop this thesis in joint supervision, so having the opportunity to work with three different research teams (in Reggio, Grenoble and Padua), to know a lots of teammates and specialists and to interact with them.

I am deeply grateful to Prof. Jean-Pierre Gourc for his patience, his help, his constant encouragement and his great experience. I always appreciate and keep in my mind his professional and life lessons.

Next, I need to thank Prof. Paolo Carrubba for welcoming to ICEA Department of Padua, for his stimulating conversations and provided suggestions.

I would also like to thank Laurent Briançon for having took time and shared his knowledge about "the world of friction", for his valuable professional and life suggestions.

I am grateful to Ing. Paolo Calabrò for introducing and encouraging me to start this experience.

I also need to thank the Officine Maccaferri S.p.a. for having believed in this project and provided materials.

Also, Henri Mora and Hélène Guyard of Grenoble LTHE Lab, deserve a special thanks because I couldn't have got these results without their patient and tireless help. Thank for having dealt together with a lot of experimental problems, for having always support me and created such a good atmosphere.

I need to further thank Laurent O., Matthieu V. and Loic M. for their help and encouragement, and the administrative LTHE lab staff and TUE Doctoral School for putting patiently up with me and answering all my French bureaucratic questions! I would also to acknowledge LTHE and IsTerre Lab Ph.D. students and colleagues as well as friends: thank you for the good time spent together!

Special thanks to all the DICEAM geotechnical research staff of Reggio Calabria. Especially, I received generous support, valuable suggestions and human warmth from Bruno F., Domenico G., Lidia C., Linda M., Giuseppe C., Paolo S.: with them I have also learned the deepest meaning of working together, that makes work more enjoyable and exciting. I owe my deepest gratitude and appreciation to Stefania for being all the time close to me from the first steps of this experience sharing joy and sorrow: thank you for the stimulating conversations, for the suggestions and overall for the great friendship.

Next, I need to thank the ICEA Department of Padua and all his staff, in particular Eng. Paolo Pavanello for his appreciated suggestions and for the time spent together with the shaking table experimentations, Melissa for her tolerance, Antonio, Mattia, Francesco and Paolo for having brightened the foggy workdays, Maurizio for the support and his good fellowship.

Thanks to all friends of "Casa Prascoli" for having always taken care of me in many circumstances. Thanks to Anita for sharing with me our already ten-year-old path through university and life and thanks to Riccardo for encouraging and motivating me standing.

Finally a big thanks to Grenoble for being my space, time and silence during these years and offering the opportunity to meet wonderful people. A huge "thank you" goes to all of you with whom I have shared this journey, thank you for the refill of love, for the unconditional friendship, for always being there. To Piero "grande fratello", Rachel and Aurore "les plus belles danseuses jamais vues", to Iolanda "cicci", to Emanuele, Fabrizio, Matias, Nando, Helo and Angy "daje", to Juan and Chloé for always having interpreted my invented new languages, to Pierre and Emilia for their constant support and to Lucas for being arrived and for still being there, pushing me always "beyond". Without all of you these years would have never been so incredibly gorgeous.

Thanks to Aurora, Luisa, Patrizia and Raffaella for being my friends, always.

Thank to my family, that cried and enjoyed with silent love, but above all never stopped to believe in me.

Table of contents

INTRODUCTION.....	I
1 GEOSYNTHETIC IN LANDIFILL COVERS	5
1.1 Landfill Generalities	5
1.2 Cover Systems.....	7
1.3 Stability Analysis Of Landfill Covers.....	10
1.3.1 Static stability analysis of cover systems	13
1.3.2 Seismic stability analysis of cover systems.....	26
1.4 Interface Shear Strength Between Geosynthetics	33
1.4.1 Definitions.....	33
1.4.2 Geosynthetic interface shear strength characterization.....	36
2 GEOSYNTHETICS	40
2.1 Generalities	40
2.2 Types, Properties And Main Functions Of Geosynthetics.....	41
2.3 Geosynthetics In Landfill Cover Systems.....	46
2.3.1 Materials tested	47
3 TEST APPARATUS	52
3.1 Inclined Plane Test	52
3.1.1 Introduction	52
3.1.2 Literature review.....	55
3.1.3 Influence of boundary and test conditions	63
3.2 Shaking Table Test.....	66
3.2.1 Introduction	66
3.2.2 Literature review.....	67
3.3 Inclined Plane And Shaking Table Device Adopted In This Study.....	72
4 TEST PROCEDURES AND INTERPRETATION	76
4.1 Interface Shear Strength Evaluation through the Inclined Plane Test (static loading).....	76
4.1.1 Introduction	76

4.1.2	The Standard Procedure (EUROPEAN STANDARD EN ISO 12957-2. 2005)	77
4.1.3	Unified Inclined Plane Procedure (UIPP)	79
4.2	Interface Shear Strength Evaluation using the Shaking Table (dynamic loading).....	84
4.2.1	Introduction.....	84
4.2.2	Theory	85
4.2.3	Shaking table test procedure under harmonic excitations.....	88
4.3	Set Of Available Different Friction Angles	90
5	TEST RESULTS AND DISCUSSION	92
5.1	Inclined Plane Test Results	92
5.1.1	Description and interpretation of a typical test.....	93
5.1.2	Repeatability.....	113
5.1.3	Reproducibility.....	120
5.1.4	Influence of the mean relative velocity.....	123
5.1.5	Influence of the normal stress.....	127
5.1.6	Influence of mechanical damage (wear effect)	133
5.1.7	Influence of temperature	142
5.2	Shaking Table Tests Results	152
5.2.1	Description and interpretation of a typical test.....	154
5.2.2	Influence of frequency	162
5.2.3	Influence of the normal stress.....	165
5.2.4	Influence of the amplitude	168
5.2.5	Influence of the mean relative velocity.....	168
5.2.6	Influence of the mechanical damage (wear effect due to the number of cycles).....	171
5.2.7	Interface response comparison	175
5.2.8	Influence of the nature of the surfaces.....	177
5.2.9	Conclusions.....	182
5.3	Shear Strength Evolution of Geosynthetic Interfaces from Static To Dynamic Loading Conditions.....	183
5.3.1	Introduction.....	183
5.3.2	Influence of the mean relative velocity.....	183
5.3.3	Influence of mechanical damage	190
5.3.4	Influence of normal stress.....	194
6	CONCLUSIONS AND FUTURE PERSPECTIVES	195

6.1	Introduction.....	195
6.2	Inclined Plane And Shaking Table Testing Methods: principal limit and capabilities of test procedures.....	197
6.2.1	Unified Inclined Plane Procedure (UIPP).....	197
6.2.2	Shaking Table Test Procedure	198
6.3	Interface Shear Strength Characterization through the Inclined Plane and the Shaking Table Tests	200
6.4	Inclined Plane And Shaking Table Tests: main conclusions of the first correlation attempt.....	202
6.4.1	Mean relative velocity	202
6.4.2	Mechanical damage.....	204
6.4.3	Normal stress	204
6.4.4	Nature of the surfaces in contact	205
6.5	Recommendations and further Perspectives	206
7	REFERENCES	208

List of figures

Figure 1.1.1. Schematic diagram of a municipal solid waste landfill containment system (modified from Shukla and Yin, 2006)	6
Figure 1.1.2. Components of solid waste containment systems (after Manassero et al., 2000).	7
Figure 1.2.1. Typical landfill cap of municipal waste containment	9
Figure 1.2.2. Landfill covers on slopes.	10
Figure 1.3.1. Landfill failure modes involving sliding along the liner system (after Eid, 2011).	12
Figure 1.3.2. Schematization of the main issues related to the stability of geosynthetic liner systems on landfill slopes (Gourc et al., 2004).	13
Figure 1.3.3. Infinite slope approach (after Koener, 2005).	15
Figure 1.3.4. Finite slope approach according with Giroud-Beech and Koerner-Hwu formulations (after Ling and Leshchinsky, 1997).	16
Figure 1.3.5. Limit equilibrium forces involved in a finite length slope analysis for a uniformly thick cover soil. (after Koener and Soong, 1998).....	18
Figure 1.3.6. Tensile force exceeding the allowable tensile strength of geosynthetic.....	19
Figure 1.3.7. Balance of forces in geosynthetic systems design on slopes.	20
Figure 1.3.8. Schematization of the pull-out strength of the geosynthetic anchorage.....	21
Figure 1.3.9. Anchorage geometries: run-out anchor; ii) “L – shape”; iii) “L – shape” with and additional horizontal bend; iv) “V – shape” or “U – shape” (modified by Briançon et al 2002).....	22
Figure 1.3.10. Schematization of the method proposed by Briançon, (2003).	23
Figure 1.3.11. Comparinon between Koerner (1998) and (Guide technique, 2000) desing methods for “L-shape” anchor.	24
Figure 1.3.12. Force balance considered in the analytical model proposed by Villard et al, 2004.....	25
Figure 1.3.13. In-situ extraction of geotextile layer in a rectangular and “V-shape” trench: i) and iii) before extraction; ii) and iv) at rupture (after Briançon et al. 2006).....	26
Figure 1.3.14. Flowchart for soild waste landfills (adopted by Maugeri and Seco E Pinto, 2005)	27
Figure 1.3.15. Balance of forces considering the infinite slope scheme applying the pseudo-static approach.....	30
Figure 1.3.16. Analytical prediction of rigid block displacements (after Tropeano, 2010).	31

Figure 1.4.1. i) Typical shear strength versus normal load behaviour of geosynthetic interfaces; ii) Typical Shear strength versus displacement behaviour of geosynthetic interfaces (after Blond and Elie, 2006).....	35
Figure 1.4.2. Secant versus tangent friction angle (modified from Blond and Elie, 2006).	36
Figure 2.2.1. Basic mechanisms involved in the separation function: (i) granular fill-soft soil system without the geosynthetic separator; (ii) granular fill-soft soil system with the geosynthetic separator (after Shukla and Yin, 2006).	44
Figure 2.2.2. Basic mechanisms involved in the filtration function (after Shukla and Yin, 2006).....	44
Figure 2.2.3. Basic mechanisms involved in the drainage function (after Shukla and Yin, 2006).....	45
Figure 2.2.4. Basic mechanisms involved in the reinforcement function (after Shukla and Yin, 2006).....	46
Figure 2.3.1. Example of a landfill cover profile.....	46
Figure 2.3.2. Geomembrane used in the experimental programme: i) smooth (GMB _S); ii) textured (GMB _{TMH}); iii) co-extruded - “sandy paper like” (GMB _{RMH}).	48
Figure 2.3.3. Geocomposite drains tested in the experimental programme: i) GCD _N with geonet (GNT) internal core; ii) GCD _W with geomat (GMA) “W” configuration.	49
Figure 2.3.4. Interfaces tested to assess geocomposite drain GCD _N – smooth geomembrane GMB _S interface performance: a) GTX - GMB _S ; b) GNT - GMB _S ; c) GCD _N - GMB _S	50
Figure 3.1.1. Inclined plane device at different configurations of the test: a) geosynthetic – geosynthetic interface; b) soil – geosynthetic interface; c) soil – soil interface (after Pitanga et al., 2009; Reyes Ramirez and Gourc, 2003).....	53
Figure 3.1.2. Inclined Plane test typical diagrams: upper box displacement versus plane inclination angle, β	54
Figure 3.1.3. One of the first inclined plane apparatus: Girard et al. (1990) laboratory tests.	56
Figure 3.1.4. Typical behaviour obtained according to sand density: i) nonwoven geotextile and smooth geomembrane in contact with loose sand; ii) nonwoven geotextile and smooth geomembrane in contact with dense sand (after Lalarakotoson et al., 1999).	57
Figure 3.1.5. Test results of woven geotextile –geospacer interface:i) Shear stress (τ) against displacement (δ) for three different normal stresses (σ_0) through shear box (SB) test; ii) displacement (δ) against slope angle (β) for $\sigma_0 = 5.7$ kPa at the inclined	

plane (IP) test; iii) attempt to compare IP and SB tests on the same diagram (after Reyes Ramirez and Gourc, 2003).	58
Figure 3.1.6. Large inclined plane apparatus (after Briançon et al., 2011).	59
Figure 3.1.7. Box displacement and tensile loads for tests with woven geotextile in contact with fine sand (a) and (b); coarse sand (c) and (d) (after Palmeira et al., 2002) ...	60
Figure 3.1.8. Soil-geosynthetic interface strength characterization on smooth and textured geomembrane interfaces: i) inclined plane and ii) conventional direct shear test; soil - smooth PVC geomembrane after inclined plane tests: (iii) degree of saturation of 5.5% and (iv) degree of saturation of 66%; soil - texturized HDPE geomembrane after inclined plane tests: (iv) degree of saturation of 5.5% and (v) degree of saturation of 66% (modified from Monteiro et al., 2013).	62
Figure 3.1.9. Normal stress distribution along the interface at 15° (i) and 25°(ii) of plane inclinations (after Palmeira et al., 2002).	65
Figure 3.2.1. Schematic diagram of the shaking table setup: (i) geosynthetic-soil interfaces, (ii) geosynthetic-geosynthetic interfaces (Yegian et al., 1995a).	67
Figure 3.2.2. Block and table accelerations versus time performing shaking table tests: i) smooth HDPE geomembrane – nonwoven needle-punched geotextile interface; ii) smooth HDPE geomembrane - soil (Ottawa sand) interface (after Yegian et al., 1995a).	68
Figure 3.2.3. Variation of the peak friction angle with the number of cycles from cyclic direct shear tests: i) a geotextile over a smooth geomembrane; ii) a smooth geomembrane over a geonet; iii) a geotextile over a geonet (after De and Zimmie, 1998).	69
Figure 3.2.4. Block versus table accelerations from shaking table tests: i) a geotextile over a smooth geomembrane; ii) a smooth geomembrane over a geonet (after De and Zimmie, 1998).	70
Figure 3.2.5. Shaking table test performed on a geotextile-geonet interface under a contact force $N=0.338$ kN. Block acceleration and displacement with respect to the at rest position (after Carrubba et al., 2001).	71
Figure 3.3.1. Inclined Plane of LTHE laboratory: a) photo, b) set up schematization	73
Figure 3.3.2. Sensors utilized in the LTHE inclined plane device.	74
Figure 3.3.3. Shaking Table of ICEA laboratory: a) photo, b) arrangement.	75
Figure 4.1.1. Balance of forces in the “Standard Procedure”.	78
Figure 4.1.2. Unified Inclined Plane Procedure (UIPP): Steps of the test.	79
Figure 4.1.3. Different mechanisms of sliding observed in the inclined plane test: i) sudden sliding; ii) jerky sliding and iii) gradual sliding (adopted from Gourc and Reyes Ramirez, 2004).	81

Figure 4.1.4. Kinematic characteristics in gradual and sudden sliding.....	81
Figure 4.1.5. Schematization of the Variant to Step 2.	82
Figure 4.2.1. Freebody diagram of the shaking table test: i) no relative displacement between the box and table; ii) during the relative displacement between the box and table.	86
Figure 4.2.2. Classical Newmark analysis integration scheme (after Matasovic. et al., 1998)	87
Figure 4.2.3. A typical sinusoidal “standard signal” for dynamic loading ($f = 1.5 \text{ Hz}$, $a_{\max} = 0.4g$, $\xi = 0.15 \text{ s}^{-1}$).....	88
Figure 4.2.4. Main phases of the shaking table test procedure under harmonic excitation.	89
Figure 5.1.1. Upper and lower layers of interfaces involving the geotextile (GTX), the geonet (GNT) and the geocomposite drain (GCD_N) in contact with the smooth geomembrane GMB_S : a) GTX - GMB_S ; b) GNT - GMB_S ; c) GCD_N - GMB_S	95
Figure 5.1.2. Typical results of the Inclined Plane tests performed at LTHE laboratory following the Unified Procedure ($\sigma_{v0} = 5 \text{ kPa}$; $T = 20^\circ\text{C}$) displaying upper box displacement versus plane inclination (Step 1 and 2 on the left side) and mobilized tensile force in the cable and friction angle versus plane inclination (Step 3 on the right side): a ₁) and a ₂) GTX – GMB_S interface; b ₁) and b ₂) GNT – GMB_S interface; c ₁) and c ₂) GCD_N – GMB_S interface.	96
Figure 5.1.3. Inclined Plane test at fixed inclinations of the plane (Variant to Step 2 of UIPP). Test results obtained at LTHE laboratory for $\beta = 20^\circ$, at $T = 20^\circ\text{C}$ and under $\sigma_{v0} = 5 \text{ kPa}$: displacement, velocity and acceleration of the upper box versus the time. a) GTX – GMB_S interface; b) GNT – GMB_S interface; GCD – GMB_S interface.	98
Figure 5.1.4. Comparative behaviour (gradual sliding) for different interfaces applying the Unified Procedure ($\sigma_{v0} = 5 \text{ kPa}$) to GTX – GMB_S , GNT – GMB_S and GCD_N – GMB_S interfaces: i) upper box displacement versus plane inclination; ii) mobilized force and friction angle versus plane inclination.	101
Figure 5.1.5. Upper and lower layers of interfaces involving geocomposite drains (GCD_N and GCD_W) in contact with GMB_{TMH} and GMB_{RMH} geomembranes: d) GCD_N - GMB_{TMH} ; e) GCD_W - GMB_{TMH} ; f) GCD_N - GMB_{RMH} ; g) GCD_W - GMB_{RMH} interfaces.	102
Figure 5.1.6. Typical plot of the Inclined Plane test results applying the Unified Procedure ($\sigma_{v0} = 5 \text{ kPa}$; $T = 20^\circ\text{C}$) to GCD_N - GMB_{TMH} and GCD_W - GMB_{TMH} interfaces: d ₁) and e ₁) upper box displacement versus plane inclination; d ₂) and e ₂) enlarged view of	

the uniformly accelerated motion during Step 2; d ₃) and e ₃) mobilized force and friction angle versus plane inclination in Step3.....	103
Figure 5.1.7. Typical plot of the Inclined Plane test results applying the Unified Procedure ($\sigma_{v0} = 5$ kPa; $T = 20^\circ\text{C}$) to GCD _N - GMB _{RMH} ; GCD _W - GMB _{RMH} interfaces: f ₁) and g ₁) upper box displacement versus plane inclination; f ₂) and g ₂) zoomed view of the uniformly accelerated motion during Step 2; f ₃) and g ₃) mobilized force and friction angle versus plane inclination; g ₄) zoomed view of the stabilization of the mobilized friction angle during Step 3 for GCD _W - GMB _{RMH} interface.....	104
Figure 5.1.8. Sketch of interaction mechanisms between nonwoven geotextiles and textured geomembranes at different normal stresses (adapted from Hebel et al. 2005).	106
Figure 5.1.9. Comparative behaviour of the two geocomposite drains (GCD _N and GCD _W) in contact with the different textured geomembranes (structured - GMB _{TMH} and co-extruded - GMB _{RMH}) applying the Unified Procedure ($\sigma_{v0} = 5$ kPa; $T = 20^\circ\text{C}$): i) upper box displacement versus plane inclination; ii) mobilized force and friction angle versus plane inclination.....	108
Figure 5.1.10. Images of geotextile specimens of GCD _N and GCD _W , representing the upper layer, after shearing: d) GCD _N in contact with the GMB _{TMH} ; e) GCD _W in contact with the GMB _{TMH} ; f) GCD _N in contact with the GMB _{RMH} ; g) GCD _W in contact with the GMB _{RMH}	109
Figure 5.1.11. Comparative behaviour of the geocomposite drain (GCD _N) in contact with the smooth (GMB _S), the structured (GMB _{TMH}) and the co-extruded (GMB _{RMH}) geomembranes applying the Unified Procedure ($\sigma_{v0} = 5$ kPa; $T = 20^\circ\text{C}$): i) upper box displacement versus plane inclination; ii) mobilized force and friction angle versus plane inclination.	110
Figure 5.1.12. Loss in shear strength for smooth and textured geomembrane – non-woven geotextile interfaces passing from peak to residual value: i) and ii) peak and residual failure envelope carrying out direct shear tests (after Frost and Lee, 2001); iii) peak and residual failure envelope carrying out torsional ring shear test (after Stark et al. 1996).	111
Figure 5.1.13. Geotextile filaments hooked to the structured geomembrane (GCD _N – GMB _S interface) during the Inclined Plane test (LTHE laboratory).	119
Figure 5.1.14. Detail of the upper layer (GCD _N) in contact with the “sandy paper like” geomembrane (GMB _{RMH}) after shearing (LTHE laboratory).....	119

Figure 5.1.15. Influence of the mean relative velocity, v , on the dynamic interface friction angles obtained for uniform ($v_{\text{box}} = \text{const}$) and uniformly accelerated motions ($a_{\text{box}} = \text{const}$) using ICEA and LTHE inclined plane devices.	125
Figure 5.1.16. Dynamic friction angle versus sliding velocity provided by the ICEA inclined plane ($\sigma_{v0} = 5\text{kPa}$) of GTX - GMB _S interface.	126
Figure 5.1.17. a) Dynamic friction coefficient versus the sliding velocity for the tests showing uniform motion (ICEA laboratory) of GTX - GMB _S interface; b) Zoomed view of the low relative velocity range of values.	128
Figure 5.1.18. Normalized dynamic friction coefficient versus sliding velocity (GTX - GMB _S interface - ICEA laboratory).	129
Figure 5.1.19. Variation of the limit interface coefficient of friction with vertical load (GTX - GMB _S interface - ICEA laboratory).	130
Figure 5.1.20. Effect of normal stress level on the test results: non-woven geotextile – smooth geomembrane (after Wasti and Özdüzgün, 2001).	131
Figure 5.1.21. Comparison between static failure envelopes on GTX-GMB _S interface.	132
Figure 5.1.22. Shear stress vs normal stress non-woven geotextile - geomembrane: i) inclined plane tests (after Wasti and Özdüzgün, 2001); ii) direct shear tests (after Jones and Dixon, 1998).	133
Figure 5.1.23. Schematization of the kinematic processes of the upper and the lower geosynthetics.	135
Figure 5.1.24. Wear effect on GTX – GMB _S , GNT – GMB _S , GCD _N – GMB _S interfaces simulated by retesting materials (multiple sliding of the upper box) at the inclined plane ($T = 20^\circ$, $\sigma_{v0} = 5\text{ kPa}$ – LTHE laboratory): a ₁), b ₁) and c ₁) Step 1 and Step 2 of the UIPP; a ₂), b ₂) and c ₂) Step 3 of the UIPP.	138
Figure 5.1.25. Wear effect simulated by retesting materials (multiple sliding of the upper box) at the inclined plane ($T = 20^\circ$, $\sigma_{v0} = 5\text{ kPa}$ – LTHE laboratory): d) Step 1 and 2 of UIPP of GCD _N – GMB _{TMH} interface; e) Step 1 and 2 of UIPP of GCD _W – GMB _{TMH} interface; f ₁) Step 1 and 2 of UIPP of GCD _N – GMB _{RMH} interface; f ₂) zoomed view of Step1 for GCD _N – GMB _{RMH} interface; g ₁) Step 1 and 2 of UIPP of GCD _W – GMB _{RMH} interface; g ₂) enlargement view of Step1 for GCD _W – GMB _{RMH} interface.	140
Figure 5.1.26. Damage of the surface in contact: GCD _N after testing in contact with GMB _{TMH} . i) before sliding; ii) after the first passage of the upper box; iii) after three sliding of the upper box ($T = 20^\circ$, $\sigma_{v0} = 5\text{ kPa}$ – LTHE laboratory).	141

Figure 5.1.27. Friction angles corresponding to peak and post peak conditions as a function of temperature for GMT-GTX and GMS-GTX interfaces (after Akpinar and Benson, 2005).	144
Figure 5.1.28. Smooth HDPE geomembrane- nonwoven needle-punched geotextile interface: i) shear stress – horizontal displacement; ii) coefficient of friction-temperature (Karademir and Frost, 2013).	145
Figure 5.1.29. Inclined Plane test results applying the UIPP at $\sigma_{v0} = 5\text{kPa}$: (a) GTX-GMB _S interface; (b) GNT-GMB _S interface; (c) GCD _N -GMB _S interface (LTHE laboratory).	149
Figure 5.1.30. Static, limit and dynamic interface strength response in terms of coefficient of friction in function of the laboratory temperature for GTX-GMB _S (a), GNT-GMB _S (b) and GCD _N -GMB _S (c) interfaces at $\sigma_{v0} = 5\text{kPa}$ (Inclined Plane test – LTHE laboratory).....	150
Figure 5.2.1. Evolution of the table and the box accelerations during a shaking table test (“standard” table solicitation, $f = 1.5\text{ Hz}$ and $\sigma_{v0} = 5\text{ kPa}$): a) GTX – GMB _S interface; b) GNT – GMB _S interface; c) GCD _N – GMB _S interface.....	155
Figure 5.2.2. Box peak acceleration versus table peak acceleration (“standard” table solicitation, $f = 1.5, 3\text{ and }6\text{ Hz}$ and $\sigma_{v0} = 5\text{ kPa}$): GTX – GMB _S interface during the entire test a ₁); zoom on Phases 2 and 3 a ₂); GNT – GMB _S interface during the entire test b ₁), zoom on Phases 2 and 3 b ₂); GCD _N – GMB _S interface during the entire test c ₁), zoom on Phases 2 and 3 c ₂).	157
Figure 5.2.3. Box peak acceleration versus table peak acceleration: i) HDPE geomembrane – nonwoven needle-punched geotextile interface (after Yegian et al.1995); ii) geocomposite clay liner – s,pptH HDPE geomembrane (after Park et al., 2004); iii) and iv) HDPE geomembrane – nonwoven needle-punched geotextile interface (after De and Zimmie,1998.....	158
Figure 5.2.4. Typical trend of table and box critical acceleration with the number of cycles of GTX – GMB _S , GNT – GMB _S and GCD _N – GMB _S interfaces during Phases 2 and 3 of shaking table tests (“standard” table solicitation, $f = 1.5, 3\text{ and }6\text{ Hz}$ and $\sigma_{v0} = 5\text{ kPa}$).	159
Figure 5.2.5. Influence of the Transitory phase on the dynamic shear strength of GTX – GMB _S interface (“faster” and “slower” TARs, $f = 1.5\text{ Hz}$ and $\sigma_{v0} = 5\text{ kPa}$).	161
Figure 5.2.6. Influence of frequency and of the number of cycles on the dynamic shear strength of GTX – GMB _S interface (“standard” TAR , $a_{\text{max}}=0.4g$, Phases 2 and 3): a ₁)	

and a ₂) a/g and ϕ_{dyn}^{ST} values at $\sigma_{v0} = 5$ kPa; a ₃) and a ₄) a/g and ϕ_{dyn}^{ST} values at $\sigma_{v0} = 12$ kPa.....	163
Figure 5.2.7. Influence of frequency and of the number of cycles on the dynamic shear strength of GNT – GMB _S interface (“standard” TAR , a _{max} =0.4g, Phases 2 and 3): b ₁) and b ₂) a/g and ϕ_{dyn}^{ST} values at $\sigma_{v0} = 5$ kPa; b ₃) and b ₄) a/g and ϕ_{dyn}^{ST} values at $\sigma_{v0} = 12$ kPa.....	164
Figure 5.2.8. Influence of frequency and of the number of cycles on the dynamic shear strength of GCD _N – GMB _S interface (“standard” TAR , a _{max} =0.4g, Phases 2 and 3): c ₁) and c ₂) a/g and ϕ_{dyn}^{ST} values at $\sigma_{v0} = 5$ kPa; c ₃) and c ₄) a/g and ϕ_{dyn}^{ST} values at $\sigma_{v0} = 12$ kPa.....	165
Figure 5.2.9. Influence of normal stress on dynamic friction angle (“standard” TAR and a _{max} =0.4 g): (a) GTX – GMB _S , (b) GNT – GMB _S , (c) GCD _N – GMB _S interfaces. ...	166
Figure 5.2.10. Effect of normal stress on the dynamic friction angle for geotextile – smooth geomembrane interface (after Park et al. 2004).....	167
Figure 5.2.11. Influence of the maximum table acceleration on dynamic friction coefficient (“standard” TAR, f= 3 Hz and $\sigma_{v0} = 5$ kPa) a) GTX – GMB _S , b) GNT – GMB _S , c) GCD _N – GMB _S interfaces.....	168
Figure 5.2.12. Relative velocity in shaking table tests. Results of GTX – GMB _S interface subjected to “standard signal” solicitation at frequency, f = 1.5 Hz and $\sigma_{v0} = 5$ kPa: i) evolution of the table and the box accelerations; ii) evolution of the relative velocity with the time.	169
Figure 5.2.13. Evolution of the dynamic friction angle with respect to the mean relative velocity during a single test for GTX – GMB _S ; GNT – GMB _S and GCD _N – GMB _S interfaces (“standard signal” solicitation, frequency, f = 1.5 Hz and $\sigma_{v0} = 5$ kPa).170	
Figure 5.2.14. Evolution of the dynamic friction angle with respect to the mean relative velocity during a single test for GTX – GMB _S interface (“standard signal” solicitation, frequency, f = 1.5 Hz and $\sigma_{v0} = 5$ kPa).....	171
Figure 5.2.15. Influence of the number of cycles, N _d , on the dynamic interface friction angle (“standard” TAR, f = 1.5 Hz, a _{max} = 0.4 g and $\sigma_{v0} = 5$ kPa) for GTX – GMB _S (a); GNT – GMB _S (b) and GCD _N – GMB _S interfaces (c).	174
Figure 5.2.16. Variation of the peak friction angle with the number of cycles from cyclic direct shear tests run at a frequency equal to 0.25 Hz for a number of loading cycles equal to 50: i) a geotextile over a smooth geomembrane; ii) a smooth geomembrane over a geonet (after De and Zimmie, 1998).	175

Figure 5.2.17. Comparative behaviour of GTX – GMB _S , GNT – GMB _S and GCD _N – GMB _S interfaces during Phases 2 and 3 of shaking table tests under harmonic excitations (“standard” signal”, $f = 1.5$ Hz (i), 3 Hz (ii) and 6Hz(iii) at $\sigma_{v0} = 5$ kPa).	177
Figure 5.2.18. Dynamic interface response comparison (“standard” TAR, $f = 3$ Hz and $\sigma_{v0} = 5$ kPa): d) table and the box accelerations during Phases 1, 2, and 3 of GCD _N – GMB _{TMH} interface; c) table and the box accelerations during Phases 1, 2, and 3 of GCD _N – GMB _S interface	179
Figure 5.2.19. Comparative behaviour of the dynamic shear strength trend versus the number of cycles (N_d) in the case of “gradual” (GCD _N – GMB _S) and “sudden” sliding behaviour (GCD _N – GMB _{TMH}).	181
Figure 5.3.1. Mobilised interface friction angle with respect to the mean relative velocity determined through the inclined plane and the shaking table test. GTX -GMB _S interface: a ₁) whole set of interface friction angle measured in both tests and a ₂) enlarged view on the range of low-medium velocities; GNT -GMB _S interface: b ₁) whole set of interface friction angle measured in both tests and b ₂) enlarged view on the range of low-medium velocities; GCD _N -GMB _S interface: c ₁) whole set of interface friction angle measured in both tests and c ₂) enlarged view on the range of low-medium velocities.	185
Figure 5.3.2. Comparative analysis between interface friction angles ($v = 0$) obtained through inclined plane (ϕ_0 and ϕ_{lim}) and shaking table $\phi_{dyn}^{ST}(N_d = 1)$ tests.....	187
Figure 5.3.3. Comparison of the mechanical damage effect on ϕ_0 and ϕ_{lim} (incline plane test) and on $\phi_{dyn}^{ST}(N_d = 1)$ (shaking table tests: a ₁) and a ₂) GTX-GMB _S interface; b ₁) and b ₂) GNT-GMB _S interface; c ₁) and c ₂) GCD _N -GMB _S interface.....	191
Figure 5.3.4. Mechanical damage effect on dynamic friction angles simulated by successive monotonic shear experiments (a ₁ , b ₁ and c ₁) and dynamic shearing due to the stress reversal loading (a ₂ , b ₂ and c ₂):a ₁) and a ₂) GTX-GMB _S interface; b ₁) and b ₂) GNT-GMB _S interface; c ₁) and c ₂) GCD _N -GMB _S interface.....	193

List of tables

Table 1.3.1. Generic allowable calculated seismic displacements for MSW landfills (after Kavazanjian, 1999).....	32
Table 1.4.1. Summary of advantages and disadvantages associated with test devices for measuring interface shear strength (modified from Bouazza et al., 2002).....	37
Table 2.2.1. Abbreviations and graphical symbols of geosynthetic products as recommended by the International Geosynthetics Society.....	41
Table 2.2.2. Polymers commonly used for geosynthetics.....	42
Table 2.2.3. Properties and parameters of geosynthetic	43
Table 2.2.4. Types and functions of various geosynthetics. ✓ main function; ★ secondary function (after Bouazza et al., 2002).....	43
Table 2.3.1. Characteristics of tested geosynthetics.	50
Table 2.3.2. Description of geosynthetic interfaces.	51
Table 5.1.1. Schematization of the parameter analysed in the experimental program at the Inclined Plane device (Geosynthetics presented in § 2.3.1).....	93
Table 5.1.2. Interface friction angles of GTX - GMB _S ; GNT - GMB _S and GCD _N - GMB _S interfaces calculated during the different Steps of the UIPP (T = 20°C; σ_{v0} = 5 kPa).	99
Table 5.1.3. Interface friction angles of the geocomposite drains in contact with the textured geomembranes at 20°C under a vertical stress of 5 kPa.	107
Table 5.1.4. Variability in test results. Interface friction angles and coefficient of friction of GTX – GMB _S ; GNT - GMB _S and GCD ^A -GMB _S interfaces at 10°C, 20°C and 32°C under a vertical stress of 5 kPa.	115
Table 5.1.5. Variability in test results. Interface friction angles and coefficient of friction of the geocomposite drains in contact with the textured geomembranes at 20°C under a vertical stress of 5 kPa	116
Table 5.1.6. Characteristics of the Inclined Plane devices available at LTHE and ICEA laboratories.	121
Table 5.1.7. Friction angles of GTX – GMB _S interface obtained at the LTHE and ICEA laboratories applying the UIPP (T = 20°C and σ_{v0} = 5 kPa).	122
Table 5.1.8. Influence of the mean relative velocity, v, on the dynamic interface friction angles.	124

Table 5.1.9. Dynamic interface friction angles of GTX – GMB _S interface obtained applying the variant to Step 2 of the UIPP with plane inclinations $\beta \gg \beta_0$ ($\sigma_{v0} = 5$ kPa; T = 20°C; ICEA laboratory).....	127
Table 5.1.10. Effect of wear on interface friction angles of GTX - GMB _S ; GNT - GMB _S and GCD _N - GMB _S evaluated for virgin and retested specimens (four and six upper box sliding) (T = 20°C; $\sigma_{v0} = 5$ kPa, LTHE laboratory).....	137
Table 5.1.11. Effect of wear on interface friction angles of GCD _N - GMB _{TMH} , GCD _W - GMB _{TMH} , GCD _N - GMB _{RMH} and GCD _W - GMB _{RMH} evaluated for virgin and retested specimens (four and six upper box sliding) (T = 20°C; $\sigma_{v0} = 5$ kPa, LTHE laboratory).	139
Table 5.1.12. Summary of temperature measurements in landfills (adopted from Karademir, 2011).	143
Table 5.1.13. Physical properties of some polymeric materials commonly used in manufacturing geosynthetics (after Moraci, 2011).....	146
Table 5.1.14. Interface friction angles at different temperatures applying the UIPP at the Inclined plane test ($\sigma_{v0} = 5$ kPa).	148
Table 5.2.1. Schematization of the parameter analysed in the experimental program at the Inclined Plane device.	153
Table 5.2.2. Interface friction angles of GTX - GMB _S ; GNT - GMB _S and GCD _N - GMB _S interfaces calculated during the different phases of the shaking table test (f = 1.5, 3 and 6 Hz; T = 20°C; $\sigma_{v0} = 5$ kPa).....	160
Table 5.2.3. Comparison of the dynamic interface friction angles of GTX - GMB _S ; GNT - GMB _S and GCD _N - GMB _S interfaces at $\sigma_{v0} = 5$ and 12 kPa (f = 1.5, 3 and 6 Hz; T = 20°C).	167
Table 5.2.4. Shaking table test results after three successive tests and increasing the number of cycles to 300.	172
Table 5.2.5. Comparison between dynamic interface friction angles of geocomposite drain (GCD _N) in contact with the smooth and the structured geomembrane (GMB _{TMH}).	180
Table 5.3.1. Mobilized interface friction angle at zero relative velocity obtained under static and dynamic loading conditions.	186
Table 5.3.2. Dynamic interface friction angles, obtained in monotonic and dynamic tests, with respect of the mean relative velocity	189
Table 5.3.3. Mechanical damage effect of ϕ_0 and ϕ_{lim} (incline plane test) and of $\phi_{dyn}^{ST}(N_d = 1)$ (shaking table tests).....	190

Table 5.3.4. Mechanical damage effect of the dynamic friction angles $\phi_{\text{dyn}}^{\text{IP}}$ (incline plane test) and of $\phi_{\text{dyn}}^{\text{ST}}$ (shaking table tests).....	192
---	-----

Nomenclature

$a_{\text{box}}(t)$: upper box acceleration at any time t

a_{const} : constant acceleration of the upper box during the slide (Inclined Plane test - Step 2 of UIPP)

a_{crit} : critical acceleration of the box corresponding to the relative sliding between the box and the table (Shaking Table test - Phases 2 and 3)

a_{max} : maximum amplitude of the table acceleration (Shaking Table test - Phase 3)

$a_{\text{table}}(t)$: table acceleration at any time t of the test (Shaking Table test)

f : frequency of the table acceleration (Shaking Table test)

$F(\beta)$: force required to hold back the upper box (Inclined Plane test – Step 3 of UIPP)

N_d : number of cycles of the upper box starting from the beginning of the relative motion between the box and the table (Shaking Table test)

TAR: table acceleration rate (Shaking Table test)

UIPP: Unified Inclined Plane Procedure

u : upper box displacement (Inclined Plane test)

u_{lim} : maximum upper box displacement (Inclined Plane test - Step 3 of UIPP)

v : upper box average velocity

β : plane inclination angle (Inclined Plane test)

β_0 : plane inclination corresponding to beginning of the upper box movement $u = 1 \text{ mm}$ (Inclined Plane test - Step 1 of UIPP)

β_s : plane inclination during the uniformly accelerated motion, $a_{\text{box}} \cong a_{\text{const}}$ (Inclined Plane test - Step 2 of UIPP)

β_{50} : plane inclination angle corresponding to the upper box displacement equal to 50 mm (Inclined Plane test - Step 2 of UIPP)

ϕ : interface friction angle

ϕ_0 : maximum static interface friction angle (Inclined Plane test – Step 1 of UIPP)

ϕ_{dyn}^{IP} : dynamic interface friction angle (Inclined Plane test – Step 2 of UIPP)

ϕ_{lim} : static friction angle after the interface shearing, at large displacements (Inclined Plane test – Step 3 of UIPP)

ϕ_{dyn}^{ST} : dynamic interface friction angle (Shaking Table test)

ϕ_{stand} : standard interface friction angle as defined by EN ISO 12957-2 (2005) (Inclined Plane – Step 2 of UIPP)

$\tan\phi$: coefficient of friction

σ : normal stress

σ_{v0} : vertical stress

ξ : increase factor

INTRODUCTION

Many geotechnical and hydraulic works require the use of several typologies of geosynthetics to handle specific functions such as: reinforcement, filtration, drainage, waterproofing, separation, protection and erosion control.

To accomplish these functions, geosynthetics are often coupled in multi-layer systems and may be placed on slopes. In such cases, the interface shear resistance between different materials may control the stability of the composite system. Therefore, in geotechnical applications such as geosynthetic liner systems on slopes of landfill sites (cap cover or bottom liner) or reservoirs, dams, an in-depth knowledge of the friction behaviour of both soil–geosynthetic and geosynthetic–geosynthetic interfaces is required. In particular, the correct assessment of the interface shear properties between different types of geosynthetics is of paramount importance considering the fact that interfaces with low in-plane shear resistance act as potential failure planes and in opposite case, high shear stresses at the interface can induce high tensile forces in geosynthetic with possible tensile failure. In fact, the functional engineering properties of geosynthetic interfaces should remain within acceptable limits, as it is a critical factor governing the integrity of the structure as well as the stability of these modern liner systems. If the stability of composite systems is not properly addressed, failure can occur. For example, failures of cover soils on geosynthetic layers in slopes of waste disposal areas have been reported in the literature (Blight, 2007; Palmeira, 2009).

Geosynthetic composite installations may be greatly affected by both static and seismic loadings. The behaviour of each interface can be different depending on the interactions of the materials in contact under the different load conditions. Though the knowledge

regarding stability analyses and monitoring the slope movement and also the stabilization techniques improved substantially in recent years, instabilities of geosynthetic composite slopes is still being an important issue in several regions especially during seismic events. Slopes which are quite stable under static conditions may not withstand or be seriously damaged by seismic forces induced during an earthquake.

In compliance with the more recent regulations, the design should take into account the performance of composite systems under both static and seismic conditions. In spite of this, only few studies are available in literature on the assessment of geosynthetic interface response in both conditions.

In light of this, a comprehensive study on the geosynthetic interface shear strength is carried out in this work. The assessment of the interface shear strength is very complex as it mainly depends on the nature of the surfaces in contact but also on the test conditions such as: mode of shear loading, normal stress, temperature and humidity. An alteration of the interface shear strength can also occur due to mechanical damage, time-dependent processes (ageing), stress dependent processes (such as repeated loading), coupled effects of both time and stress-strain dependent processes (creep or relaxation).

An extensive experimental research program was performed to investigate the evolution of the interface shear strength from static (gravity as driving force) to seismic (dynamic excitations) loading conditions in several geosynthetic – geosynthetic interfaces including geocomposite drains in contact with geomembranes (smooth and textured). Taking into account the wide range of geosynthetic structures, only a few interfaces among the more common ones are experimented. However, the original test method proposed, is extendable to new interfaces.

Static conditions were studied through the inclined plane while seismic conditions were simulated by shaking table tests. In fact, the inclined plane (Briançon et al., 2011, 2002; Palmeira, 2009; Reyes Ramirez and Gourc, 2003; Wasti and Özdüzgün, 2001; Wu et al., 2008b) and the shaking table (Carrubba et al. 2001; De and Zimmie, 1998; Yegian and Kadakal, 1998) are the most suitable tests in order to investigate the interface shear behaviour under low vertical stresses typically encountered in many applications such as landfill cap covers.

This study presents the results and the findings of research studies on the influence of interface shear behaviour under different loading conditions with the goal of better understanding the complex interactions and mechanisms occurring at the interface.

In light of this, the first part of the thesis was devoted to the development and validation of methodologies to carry out in the testing program considering also the experimental conditions affecting the different test results of both the inclined plane and the shaking table tests.

In the inclined plane test a new procedure (named “Unified Procedure”) able to characterize the interface shear strength in all the phases of the test and under different kinematic conditions was proposed. Thanks to this new procedure, it is possible to study, during a single test, the interface shear strength angle in static (at both small and large displacements) and dynamic conditions. In the shaking table test, a specific procedure was defined in order to study the dynamic interface shear strength angle in all the phases of the test, conditions not always taken into account in the previous researches.

Subsequently, the attention was focused on the factors affecting the interface shear strength. Firstly, the influence of the kinematic conditions, characterized by the relative velocity at the interface, was assessed in both tests. Several interface friction angle were defined representing different physical conditions. Furthermore, since the focus of this study is on construction and low normal stress interaction mechanisms, the influence of normal stress varying from 0.08 to 12 kPa was studied. Finally, as the many steps in the construction of the cover liners, and the repeated loading induced during an earthquake may cause damage in the liners, also the wear effect of the surfaces was simulated and investigated.

In addition, since landfill cover liners are subjected to harsh environmental conditions, and in particular the properties and behaviour of polymeric geosynthetics are sensitive to temperature changes, a first insight on the influence of temperature in static conditions was also provided.

The scope of the thesis can be divided into six main sections: (Chapter 1) general description of landfill covers and stability problems related to the use of geosynthetics in cap liners; (Chapter 2) geosynthetics main properties and functions; (Chapter 3) review of previous studies and the resultant current state of knowledge concerning interface behaviour of geosynthetic systems using the inclined plane and the shaking table tests; (Chapter 4) description of the new procedure proposed and adopted in this study; (Chapter 5) interface shear strength results obtained through the inclined plane and the shaking table tests with the analysis of the effect of some experimental parameters. Preliminary correlation of the interface shear strength results from static to dynamic conditions. Finally a summary of the main conclusions and advancements made during the current research

study and additionally, recommendations for future work on the topic are provided (Chapter 6).

1 GEOSYNTHETIC IN LANDFILL COVERS

1.1 LANDFILL GENERALITIES

Human activities create several types of waste such as municipal solid waste (MSW), industrial waste, and hazardous waste. The environmental impact of disposing solid waste has been long recognized. Many waste management strategies aimed to reduce production, to recycle and to re-use waste have been introduced in recent years. However, large amounts of waste must still be disposed in the environment; and as far as municipal solid waste (MSW) is concerned, the main alternative for its safe disposition continues to be the sanitary landfill.

A sanitary landfill is usually conceptualized as a biochemical reactor. In this giant reactor, waste and water are the main inputs, while gas and leachate are the major outputs (Manfredi and Christensen, 2009).

A conventional landfill, as typically defined, is a landfill carefully designed and constructed to encapsulate the waste and to prevent the escape of pollutants into the environment.

A correct waste containment philosophy consists of:

- optimisation of the landfill location;
- construction of high performance lining and capping systems;
- optimisation of waste storage;
- short and long term careful monitoring;
- a convenient re-use of the landfill area after closure.

The geotechnical engineer, in particular can effectively deal with the design, construction quality control and monitoring of the lining and cover systems, the waste storage and compaction procedure, and the foundation and improving treatments for constructions above waste deposits (Manassero et al., 2000).

Modern engineered landfills are designed and constructed to minimize or eliminate the release of constituents into the environment. Thus, landfills consist of multi-barrier systems including the bottom and side lining systems and covers (Figure 1.1.1).

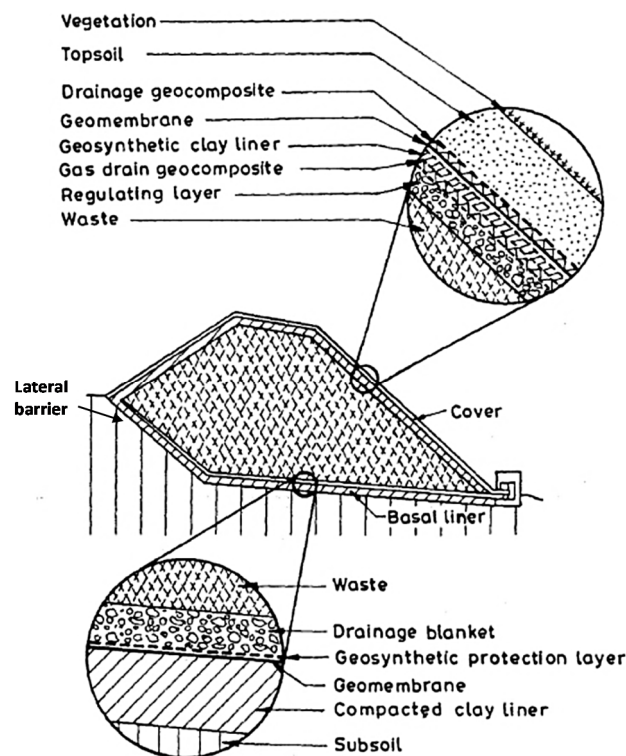


Figure 1.1.1. Schematic diagram of a municipal solid waste landfill containment system (modified from Shukla and Yin, 2006)

Referring to the three liner components (i.e. bottom, side and cover liners) of a containment system as shown in Figure 1.1.1, it is possible to summarize their main functions as schematized in Figure 1.1.2 (see also Manassero et al., 2000).

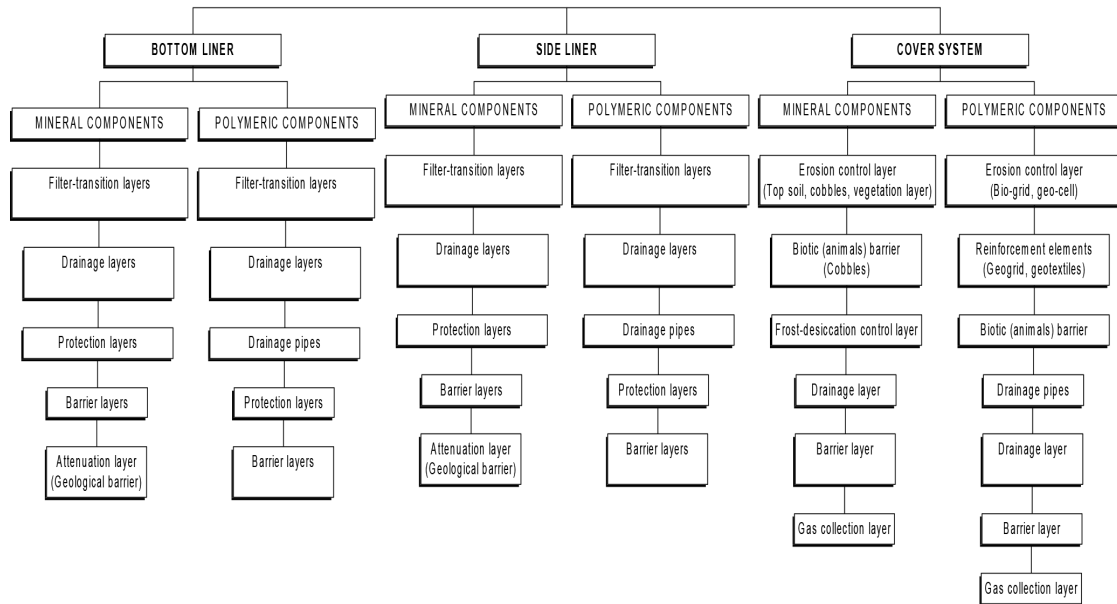


Figure 1.1.2. Components of solid waste containment systems (after Manassero et al., 2000).

Geosynthetics play an important role to minimize contaminant migration into the surrounding environment to levels that will result in negligible impact. Their application has been triggered by the economic and technical advantages that geosynthetics can offer in relation to more traditional materials (Bouazza et al., 2002).

The loading conditions expected will vary throughout the design life of the landfill. For instance, for the slopes of the bottom liner the following main considerations can be done (Jones and Dixon, 1998):

- short-term loading immediately post-construction with the relatively low normal stress due to protection/drainage materials only,
- intermediate loading as waste placement proceeds,
- long-term loading under full height of waste and the expected waste settlements.

1.2 COVER SYSTEMS

Landfill covers are ruled by the European Union Directive 1999/31/EC on waste landfilling. The cover system has to fulfil numerous functions:

- isolate the waste body from the environment, including the insurance of controlled removal of the landfill gas and odours;

- limit the infiltration of rainwater to the waste so to minimize generation of leachate that could possibly escape to ground-water sources;
- reduce the maintenance requirement;
- minimize erosion problems;
- resist to settling and localized subsidence phenomena.

Furthermore, the cover system provides a lot of other tasks; among them it is possible to include: separate waste from animals and insects, favourite the vegetation growth and post-closure developments on the landfill area. Thus, the tasks of a cover system are much more numerous than for a base and side liners considering also that in the long term the water and pollutant balance of almost all the landfills are governed by the capping performance.

In general, the nature of liner design varies, both within and between countries, depending on waste management strategies and practices, public concern and political will. The type of a waste containment facility is dictated by the type of waste to be disposed of.

Waste classification can be broadly grouped into three types:

- inert;
- municipal or domestic and industrial non-hazardous;
- industrial hazardous.

A landfill cap of municipal solid waste containment usually consists of the following layers (from bottom to top):

- ✓ **Base (levelling) layer:** this layer forms a base for the capping construction;
- ✓ **Gas vent layer:** it should be able to control the volume of gas that may be formed during anaerobic decomposition of the waste (biogas);
- ✓ **Bottom low-permeability layer:** this layer has to provide a level of protection against infiltration. It consists of a low permeability soil (i.e., compacted clay) or of material with an equivalent performance;
- ✓ **Drainage layer:** the functions of the drainage layer are: removing the excess of rainwater, minimizing the infiltration through the low permeability layer and enhancing the stability of the cover soil on side slopes;
- ✓ **Protective soil layer:** the purpose of this soil layer is to sustain the vegetative cover and protect the underlying layers from frost damage and excessive loads.

The mineral layers may be replaced by a different material (usually geosynthetics) with equivalent performances as it is schematized in Figure 1.2.1. Thus, since the modern trend is to optimize the capacity of landfill storage, the use of geosynthetic is becoming very widespread in cap covers thanks to their low thickness value, their easier implementation in comparison with conventional solutions and their economic viability.

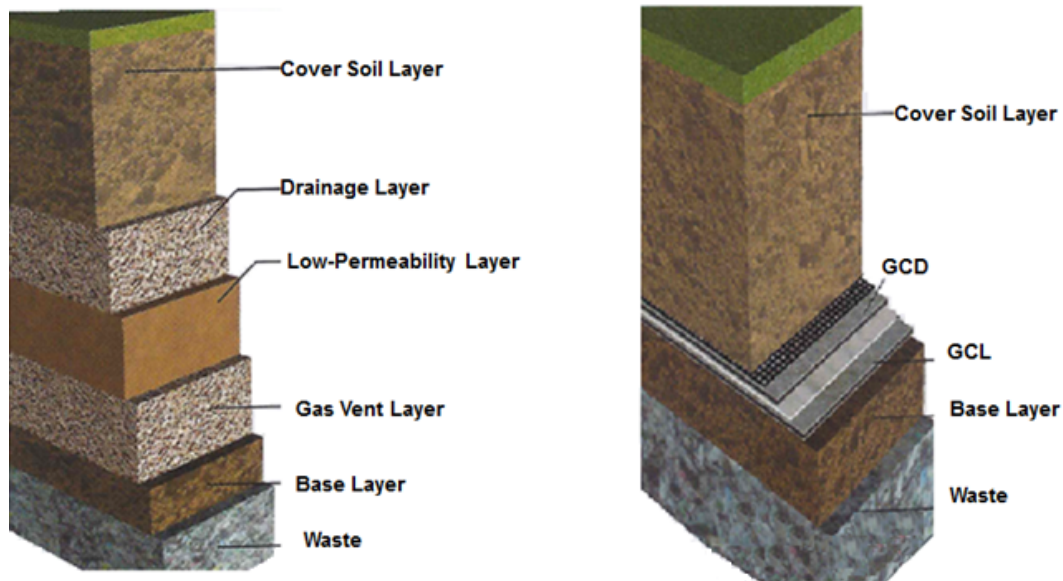


Figure 1.2.1. Typical landfill cap of municipal waste containment (modified by TeMa –Technologies and Materials brochure).

This design is aimed at limiting percolation of water into the underlying waste, allowing minimization of the transport of contaminants from the landfill to the groundwater. However, it's worth noting that limiting wetting of the waste body presents a disadvantage, since decrease of waste moisture could stop the biodegradation. Consequently, in a modern bioreactor landfill, a systems of injection by chambers or wells of water or leachate completes the control of the percolation of rainfall water.

Usually, lateral and cover lining systems are designed to accommodate two factors: land saving (smaller landfill foot print) and increase of landfill capacity. To achieve these goals, the inclination of the slopes (Figure 1.2.2) is generally increased to improve the ratio between the volumetric capacity and the print of the landfill (Bouazza et al., 2002).

In this respect, the main concerns regarding the integrity of the cover systems are landfill settlements and the stability of the liners. In particular, the stability is a key point when the multi-layer system involving soil and geosynthetics is laid on slope.



Figure 1.2.2. Landfill covers on slopes.

1.3 STABILITY ANALYSIS OF LANDFILL COVERS

The overall integrity of a landfill is closely linked to the slope stability of the lateral and cover barriers under static and seismic loading conditions. The interfaces between the different material layers composing a multi-layered liner system often represent potential slip surfaces that need to be considered in slope stability analyses. The failure at the interfaces occurs when the driving forces exceed the shear resistance force mobilized at the interface.

The stability of landfill liner system is influenced by many variables and the most important factors that influence the multiplayer landfill liner system stability are:

- interface shear strength between various geosynthetic materials,
- interface shear strength between geosynthetics and soil materials,
- internal shear strength of geocomposite clay liners,
- internal shear strength of solid waste and
- slope and height of waste fill during each lift,

- length of the slope,
- anchorage of the geosynthetics at the top.

Geocomposite liner of the cover systems, may experience harsh environmental conditions such as extreme high and low temperatures or excessive loading in their life time (Akpınar and Benson, 2005; Rowe, 2005). Geosynthetics placed on slopes of a landfill can experience tension due to various factors (Jones and Dixon, 1998). For example, during construction of the liner systems, wind up-lift on uncovered areas, movement of heavy vehicles and frictional forces from the cover soil. After the closure of a landfill, the down-drag caused by settling waste must be taken into the account.

In the design, the geosynthetics to be used in the project, the associated local soils at their targeted density and moisture content should be tested at appropriate normal stresses, strain rates and temperatures. The measured interface shear strength parameters should be compared to those existing in the literature, and then can be utilized in the evaluation of the potential sliding failure in the landfill liners to assess the stability of the structure.

Several different critical equilibrium situations involving geosynthetics can be considered. In all these cases, the interface properties require an accurate assessment. One can distinguish:

- Sliding along the slope of the bottom liner;
- Sliding along the slope of the cap cover.

The first difference between the two cases is the value of the normal stress on the liner, increasing until high values in the first case, due to the waste progressive storage, and on the other hand, systematically low in the second case, seeing that the normal stress is related to the weight of the veneer.

Among the examples of failures related to sliding along the bottom liner, the most famous is the slope failure of Kettleman Hills, a hazardous waste landfill in southern California, USA (Mitchell et al. 1990, Seed et al. 1990, Byrne et al. 1992). This failure occurred primarily at the interface between the clay and smooth geomembrane of the secondary lining system, with sliding in the upper part of the side slopes occurring along the primary geomembrane/secondary geotextile interface. This failure however was not attributed to seismic loading but to the low shear strength at the interfaces.

If the stability of composite systems is not properly addressed, failure can occur. For example, failures of cover soils on geosynthetic layers in slopes of waste disposal areas,

reservoirs and ponds have been reported in the literature (Blight, 2007; Palmeira, 2009; Wu et al., 2008).

The present research will be dedicated to the stability of landfill covers with an experimental program considering geosynthetic interfaces subjected to low values of normal stresses.

Furthermore, landfill slopes can experience different types of failure modes, some of which involve sliding along the composite liner system (Eid, 2011). Figure 1.3.1 shows two of these modes in which failure surface passes entirely along the liner system [e.g. Kettleman Hills landfill failure (Seed et al., 1990)] or through the waste at a steep inclination and then to the underlying liner system [e.g. Mahoning landfill failure (Stark et al., 1998)].

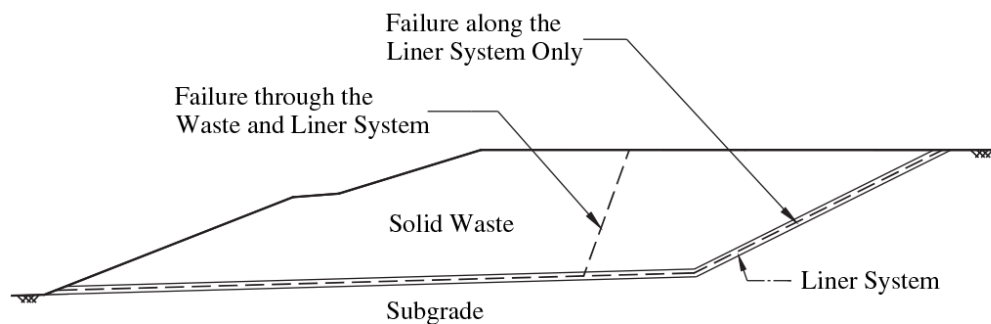


Figure 1.3.1. Landfill failure modes involving sliding along the liner system (after Eid, 2011).

As with any stability study, the selection of the most probable mode of failure and the accurate assessment of the necessary physical and mechanical properties and hydraulic conditions of the waste and the foundation soils are the most critical aspects (Bouazza et al., 2002). Although different definitions for the factor of safety have been reported in literature, stability against direct sliding is satisfied if shear resisting force available at the displaying a lower frictional resistance is greater than or equal to the driving force.

Other important characteristic of the failure mode is the localisation of the critical interface corresponding to the sliding motion. The liner system is a composite with soil and geosynthetic layers and the prediction of the slip surface requires a relevant knowledge of the shear properties of every interface between the different elements of the system and also the shear properties internal to the materials (soils and geosynthetic clay liners).

The stability of the liner system can be regarded as ensuring there is no uncontrolled slippage between the components of the system. Such slippage may produce excessive local stressing on the geosynthetic and lead to tearing, or may induce a global slope failure

(Jones and Dixon, 1998). Current design methods for geosynthetic liner system stability rely for the most part on limit equilibrium methods: the most widely used are the block method (Giroud and Beech 1989; Koerner and Hwu 1991).

1.3.1 Static stability analysis of cover systems

Afterwards, only the case of liner systems corresponding to the cap cover will be considered.

In the simple case of the Figure 1.3.2, the main conditions of stability are presented.

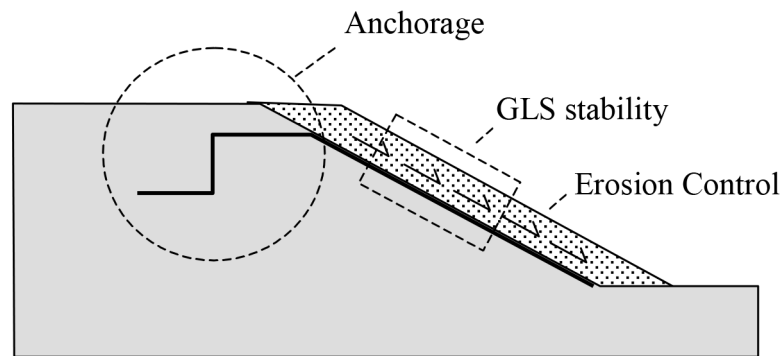


Figure 1.3.2. Schematization of the main issues related to the stability of geosynthetic liner systems on landfill slopes (Gourc et al., 2004).

The limit equilibrium of the liner system is complex. Two different approaches of limit stability should be considered:

- sliding at the interface soil-geosynthetic with a limit equilibrium of the soil veneer above the geosynthetic,
- sliding at the interface between two geosynthetics, considering the global equilibrium of the geosynthetic on slope and its anchorage which supplies a pull-out strength.

In the two cases, tangential stresses are mobilized along the geosynthetic interfaces and consequently, tensile forces are mobilized in the different geosynthetics. There is a possible combination of sliding on an interface soil-geosynthetic or geosynthetic-geosynthetic with a tensile failure at the top edge corresponding either the maximal tensile force of the geosynthetic or the maximal pull-out strength of the anchorage.

The approach of the first sliding mode is identical to the approach of a conventional slope stability problem. The principle is summarized below.

The analysis assumes the cover soil to be a rigid block resting on the geomembrane or other geosynthetic, where the interface between the soil and geosynthetic or between geosynthetics acts as a well-defined failure plane. Stability analysis may be conducted by assuming the cover soil to be infinitely long such that the passive wedge is ignored, or of a finite length. These conditions are called as infinite and finite slopes, respectively.

The main features to differentiate infinite (Figure 1.3.3) and finite equilibrium (Figure 1.3.5) are the conditions at the top and at the bottom of the slope:

- at the bottom, a buttress is considered with a wedge which acts as a passive block to sustain the layer along the slope;
- at the top, generally a tensile crack in the soil veneer is considered, since the low cohesion of soil can be discarded. As far as the geosynthetics are included, if the considered slip line is beneath one or several geosynthetics. Tensile forces, T , in these layers should be included in the equilibrium, since a virtual cutting of these layers by the slip line is taken into account (Figure 1.3.6).

In the second mode of sliding, presented in § 1.3.1.2, the global equilibrium of the geosynthetic on slope and its anchorage which supplies a pull-out strength are considered.

1.3.1.1 Sliding at the interface soil veneer - geosynthetic

1.3.1.1.1 Infinite slope approach

In an infinite slope, stability under static loading can be maintained if the slope angle is less than the angle of friction between the most critical interface, where the adhesion at the interface, seepage and external forces are ignored.

Such analyses neglect the influence of reinforcement forces on the soil stresses along the potential failure surface and may result in factors of safety significantly different than those calculated using more rigorous approaches (Bouazza et al., 2002). Considering the normal and shear forces acting in a control volume (Figure 1.3.3) along the veneer slope (or infinite slope), and assuming a Mohr-Coulomb shear strength envelope, the factor of safety can be expressed as:

$$FS = \frac{N \cdot \tan \delta}{W \cdot \sin \beta} = \frac{N \cdot \cos \beta \tan \delta}{W \cdot \sin \beta} = \frac{\tan \delta}{\tan \beta} \quad 1.3-1$$

where W is the top cover weight; N the normal load; β the slope inclination angle and δ the interface friction angle between the geosynthetic and the cover soil.

Following the scheme (Figure 1.3.3) adopted by Koerner (2005), it is assumed that failure will occur at the cover soil interface.

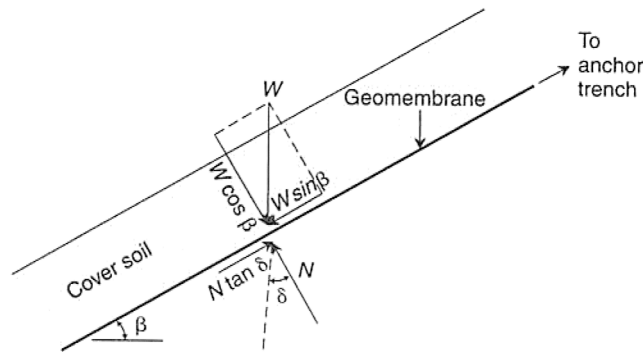


Figure 1.3.3. Infinite slope approach (after Koerner, 2005).

1.3.1.1.2 Finite slope approach

The finite slope methods take into account the toe end effects in design. Giroud and Beech (1989) and Koerner and Hwu (1991) formulated the finite slope problem to determine the factor of safety and the geosynthetic reinforcement force required to restore static stability. These formulations were based on a two-part wedge mechanism in which the inter-wedge force acts parallel to the slope angle. There are, however, several differences between the Koerner-Hwu and Giroud-Beech equations. The top end of the soil cover of the Giroud-Beech and Koerner-Hwu formulations are shown in Figure 1.3.4.

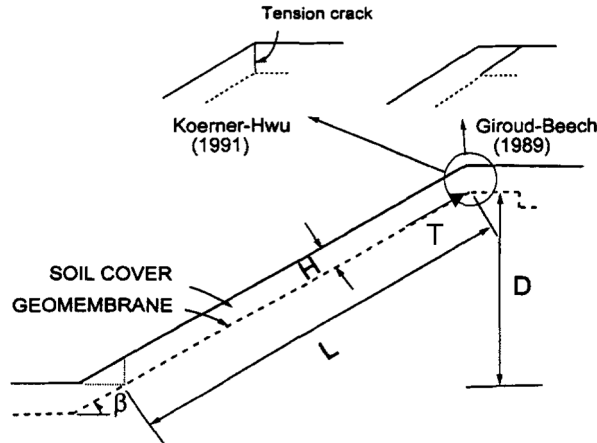


Figure 1.3.4. Finite slope approach according with Giroud-Beech and Koerner-Hwu formulations (after Ling and Leshchinsky, 1997).

The limiting equilibrium method of Giroud and Beech (1989) has been used extensively and this approach divides the system into two wedges and balances forces in the vertical and horizontal directions. The resistance to failure is provided by mobilised soil resistance at the toe, mobilised interface friction along the bottom of the potential sliding surface and a mobilised tensile load in the geosynthetics above the plane of sliding. A major drawback in this method is that the distribution of tensile loads within the geosynthetic layers is not determined.

Subsequently, Giroud et al. 1995a modified the previous method to include also the soil cohesion and the soil-geosynthetic adhesion. In the method proposed, only three elements must be considered in the analysis of the stability:

- the slip surface;
- the soil located above the slip surface;
- geosynthetics if located above the slip surface.

The factor of safety is expressed following Equation 1.3-2:

$$FS = \frac{F_{R, \text{slope}}}{F_{D, \text{slope}}} \quad 1.3-2$$

where $F_{R, \text{slope}}$ is the projection on the slope of the resisting forces and $F_{D, \text{slope}}$ the projection on the slope of the driving forces. The safety factor equation consists of the sum of five terms (Equation 1.3-3): the interface friction angle, interface adhesion along the slip surface, the internal friction angle of the soil component of the layered system located above

the slip surface, the cohesion of soil component of the layered system located above the slip surface and the tensile strength of the geosynthetic located above the slip surface.

The factor of safety according can be express as follows:

$$FS = \frac{\tan \delta}{\tan \beta} + \frac{a}{\gamma \cdot T \sin \beta} + \frac{T}{D} \frac{\tan \phi / (2 \sin \beta \cos^2 \beta)}{1 - \tan \beta \tan \delta} + \frac{c}{\gamma D} \frac{1 / (\sin \beta \cos \beta)}{1 - \tan \beta \tan \delta} + \frac{T_a}{\gamma D T} \quad 1.3-3$$

where γ , c and ϕ are the unit weight, the cohesion and the interface shear strength angle of the soil; a is the interface adhesion along the slip surface; T_a allowable tensile strength of geosynthetic reinforcement; β slope angle and δ the interface friction angle along the slip surface, D the height of the slope. As for a conventional slope stability problem, different slip lines selecting successive interfaces, should be assessed.

Thanks to this definition of the factor of safety, it is easier to identify the contribution of the different terms to the stability of the slope. Further, Giroud et al (1995b) analyse stability analysis considering also seepage forces.

The Koerner-Hwu equation is mainly based on the solution of a quadratic equation from which the factor of safety is determined. Koerner and Soong (1998) improved the previous method including also the effect of construction equipment, seepage forces, seismic forces, and the stabilizing effects of toe berms, tapered slopes and slope reinforcements. In the simplest case illustrated in Figure 1.3.5, they consider a cover soil placed directly on a geosynthetic at a slope angle β , and the effect of two zones (i.e. the active and the passive wedges) is analysed. It is assumed that the cover soil is of uniform thickness and constant unit weight and that the failure will occur along the continuity with the remaining cover soil at the crest. The factor of safety is obtained solving a quadratic equation ($aFS^2 + bFS + c = 0$) as follows:

$$FS = \frac{-b \pm \sqrt{b^2 - 4ac}}{2a} \quad 1.3-4$$

with:

$$a = (W_a - N_a \cos \beta) \cos \beta \quad 1.3-5$$

$$b = -(W_a - N_a \cos \beta) \sin \beta \tan \delta + (N_a \tan \delta + C_a) \sin \beta \cos \beta + \sin \beta (C + W_p + \tan \delta) \quad 1.3-6$$

$$c = (N_a \tan \delta + C_a) \sin 2\beta \tan \delta \quad 1.3-7$$

where W_a and W_p are respectively the active and passive wedge weight; N_a is the normal load of the active wedge; C_a adhesion between soil and geosynthetic; C adhesion force along the passive wedge; β the slope inclination angle and δ the interface friction angle between the geosynthetic and the cover soil.

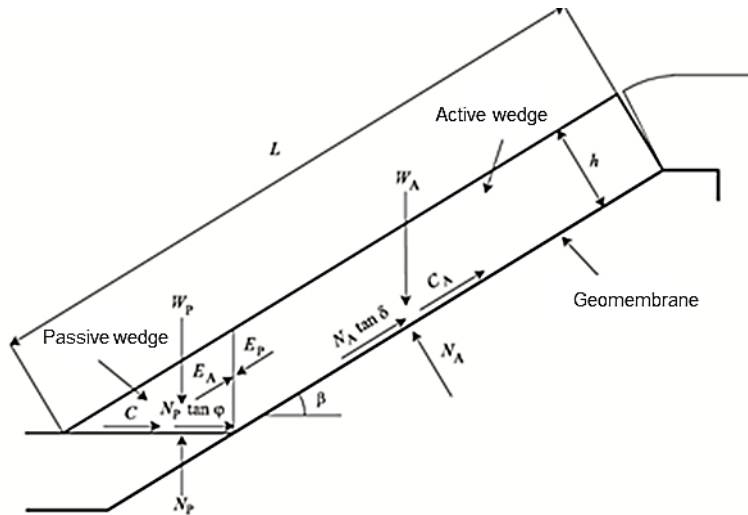


Figure 1.3.5. Limit equilibrium forces involved in a finite length slope analysis for a uniformly thick cover soil. (after Koener and Soong, 1998)

In the limit equilibrium methods, the tensile strength within individual components of a layered system are determined by a force equilibrium procedure. To assure the stability, the shear strength should balance the forces in a direction parallel to the slope.

1.3.1.2 Tensile force transmitted to the geosynthetic

Although these methods, according to which both material and interface behaviour is assumed to be rigid-plastic, generally yield a conservative design, they are not able to explain the complex behaviour observed within the composite system. Computations using the finite element method, in association with more elaborate constitutive laws (Feki 1996), have demonstrated behavioural sensitivity to small modifications in, for example, the friction interface relationship.

The design methods above require an evaluation of the interface friction between soil and geosynthetics corresponding tests were presented by Pitanga et al., (2009). The physical behaviour could be complex, because with some specific geosynthetics with surfaces allowing soil grains penetration, the critical shear interface is difficult to localize accurately.

Even if the stability of the cover is assured, the aforementioned methods do not investigate the tensile strength transmitted to the geosynthetics. This condition is of paramount importance because the forces involved cannot be consistent with the allowable tensile strength of the geosynthetic, T_a . In fact, if T_a is exceeded, a tensile crack in the geosynthetic can occur as represented in Figure 1.3.6.

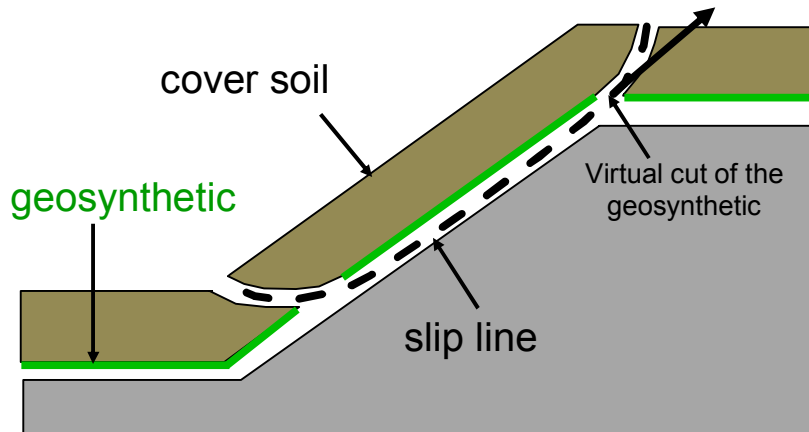


Figure 1.3.6. Tensile force exceeding the allowable tensile strength of geosynthetic.

In the present research, only friction properties for geosynthetic-geosynthetic interfaces are considered so that the sliding at the interface between two geosynthetics, considering the global equilibrium of the geosynthetic on slope and its anchorage which supplies a pull-out strength should be considered.

This case is more complex and less conventional, seeing the equilibrium of every geosynthetic. The different forces to consider are the shear stresses along the slope for both sides of the interface (i.e. T is the tensile strength resulting from the difference between the tensile mobilization of the upper and lower part of the geosynthetic considered) and the anchorage strength (Gourc et al., 2004).

Even if, in this section, only the risk of plane slippage along the geosynthetic system is treated, the stability of the system should also take into account the internal stability of the protective earth cover installed on the slope on either side of the geosynthetic complex, as well as the global stability of the slope.

When geosynthetics are laid on slopes, the weight of the materials above them induces a destabilizing force moving the system downward. For this reason, the behaviour of geosynthetic sheets at the top of the slope is a decisive factor to withstand to the tensile force generated along the slope and the consequent pull out strength.

Following the scheme presented in Figure 1.3.7 the resulting force T that depends on the weight of the cover soil, on the slope inclination and on the interface friction angles on both geosynthetic surfaces, does not exceed the allowable tensile strength of the geosynthetic, T_a .

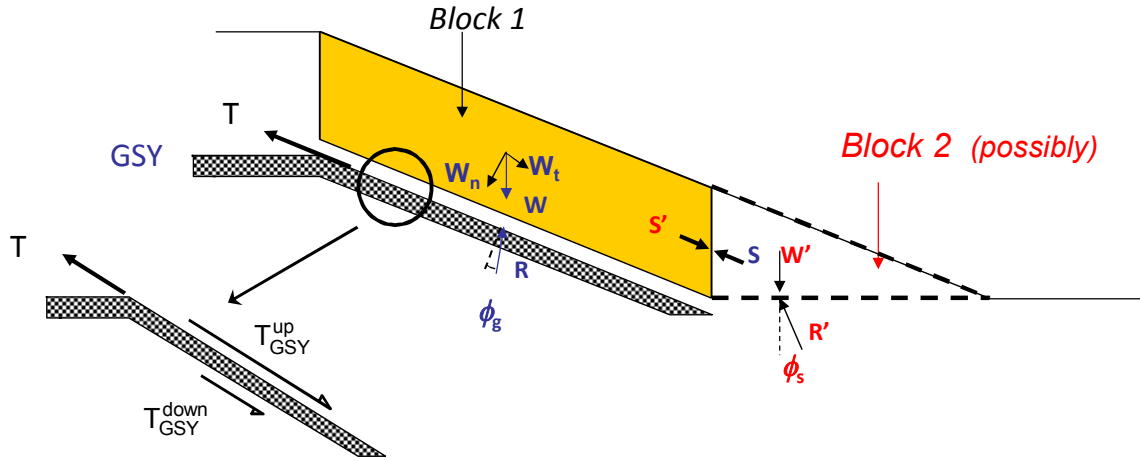


Figure 1.3.7. Balance of forces in geosynthetic systems design on slopes.

Furthermore, the basic conceptual scheme to design anchorage is presented in Figure 1.3.8 in which the simplest case (hydraulic conditions are not taken into account) is presented.

In the case of infinite slope, the analysis of stability corresponds simply to the balance between the driving forces due to the weight W of the protection itself and the stabilising forces constituted by the friction force F that can be mobilised on the interface being studied, to which is then added any anchor force T at the top of the slope (Figure 1.3.8):

$$T + F = W \cdot \sin \beta \quad 1.3-8$$

$$F = W \cdot \cos \beta \cdot \tan \phi_g \quad 1.3-9$$

It is important to note that, for the calculation of the friction that can be mobilised, ones should take into account the uplift force given by the sum of hydraulic pressure, F_w , that can occur at the geosynthetic interface in case of total or partial saturation of the protective layer(s). In this case, F is defined by the relation:

$$F = (W \cdot \cos \beta - F_w) \cdot \tan \phi_g \quad 1.3-10$$

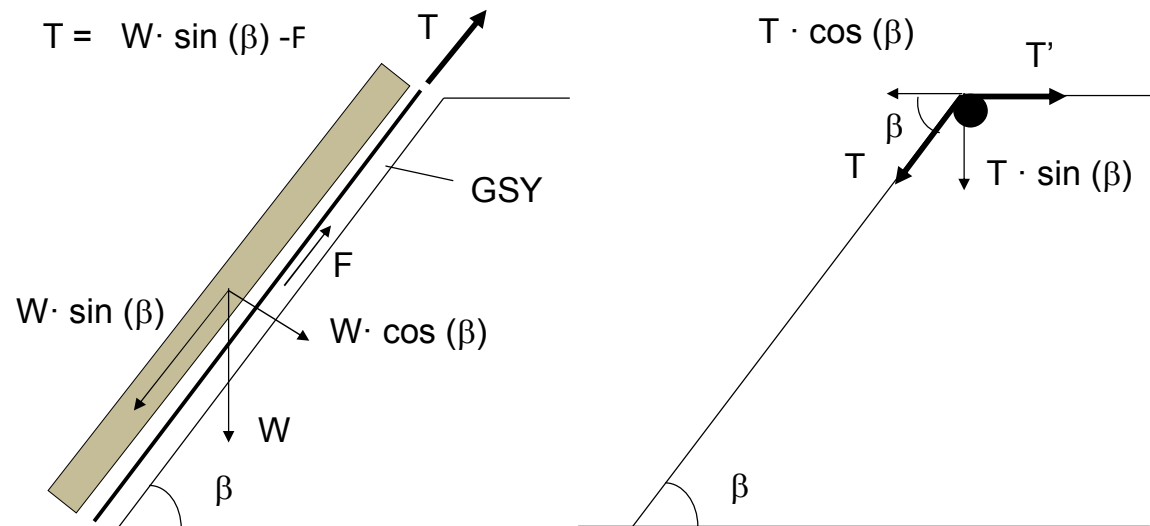


Figure 1.3.8. Schematization of the pull-out strength of the geosynthetic anchorage.

1.3.1.3 Anchorage capacity of geosynthetics in trenches

In the basic calculation of the anchorage capacity (i.e. the force, T , required to pull the sheet out), the geometric characteristics of the anchorage and the friction characteristics of the materials used are required. More complex calculation, take into account the forces and stresses that develop at each curved portion of the anchorage and other mechanisms of the soil cover behaviour.

The anchorage can be of several types depending on the specific characteristics of the site, on the available area and on the applied load (Chareyre et al. 2002). Figure 1.3.9 shows the most typical geometries for the anchorage: the “linear” (simple *run-out*), or as more common, installed in trenches with “L – shape”, “V – shape” or “U – shape”.

The trenches are dug by a trenching machine and then they are backfilled with the same soil that was originally, properly compacted in several layers

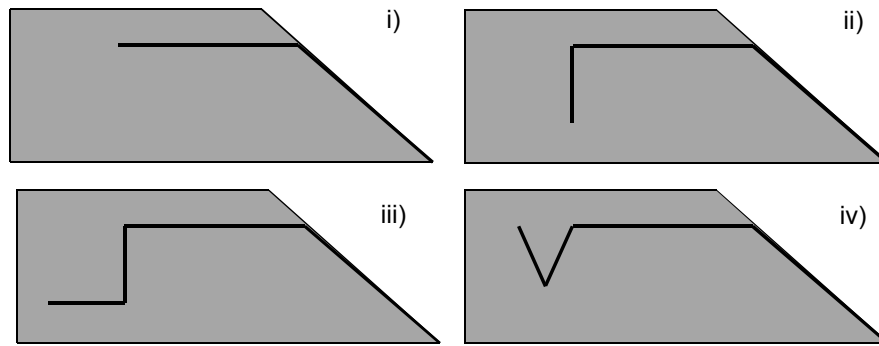


Figure 1.3.9. Anchorage geometries: run-out anchor; ii) “L – shape”; iii) “L – shape” with and additional horizontal bend; iv) “V – shape” or “U – shape” (modified by Briançon et al 2002).

For every kind of anchorage, different design methods were developed in literature (Briançon, 2003; Koerner, 1998 and 2005; Huling et Sansone, 1997; Villard and Chareyre, 2004). The common hypotheses are (Gourc et al., 2004):

- the geometry of the anchor is represented schematically by linear segments (numbered in an increasing order from the outside towards the inside of the soil mass),
- the anchor fails only by relative displacement at the critical interface,
- the shear stresses τ that can be mobilised at the interface are equal to the maximum stresses τ_{\max} corresponding to the slip limit state (on one or both sides of the geosynthetic),
- friction is governed by a Mohr-Coulomb interface law: $\tau_{\max} = \sigma_n \cdot \tan \phi_g$ with ϕ_g and σ_n the friction angle and normal stress acting at the interface before pull-out,
- the contribution of the i^{th} segment to the total anchorage can be assimilated to a force F_i calculated by integrating the shear stress of intensity τ_{\max} on either side of that portion of geosynthetic sheet.

The main differences between the various design methods are in the following assumptions:

- behaviour of the cover soil,
- edge effect on the pull-out strength,
- stress state in the vertical segment.

In the first assumption, if the soil is considered as rigid mass, the geosynthetic moves in relation with the soil that is considered fixed. The maximum forces that can be mobilised correspond to the limit equilibrium state at all points of the soil/geosynthetic interface (i.e.

$\tau_{\max} = \sigma_n \cdot \tan \phi_g$). The value of the anchoring capacity is therefore determined by considering the distribution of the normal stress σ_n on each segment of the interface. Otherwise, if it is considered that during the movement, the soil can deform and cracks and also its behaviour at failure should be taken into account.

The second hypothesis implies that the change in direction at the angle can modify the tension in the sheet ($T \rightarrow T'$ on Figure 1.3.12).

The third hypothesis takes into account a different stress state in the vertical segment to be considered.

The first analytical formulae put forward to calculate the anchorage capacity (Hulling and Sansone 1997) assumed that the loads on the anchorage were taken up only by friction on the linear parts of the geosynthetic without the existence of angle effects. The friction loads were governed by a Coulomb - type law: $\tau_{\max} = \sigma_n \cdot \tan \phi_g$ where σ_n and ϕ_g are the normal stress and the friction angle of the interface in question, respectively. In particular, the parameter σ_n is the normal stress acting on the interface, equal to σ_v (vertical stress) on the horizontal portions of the sheet, and equal to σ_h (horizontal stress) for the vertical portions of the sheet. The parameter σ_h is calculated using the coefficient of earth pressure at rest, K_0 .

With similar hypothesis, Briançon, (2003), defined another method, schematized in (Figure 1.3.10) in which the anchor capacity, T_{\max} , is equal to the sum of the friction forces that can be mobilised on the linear parts of the anchor system ($T_{\max} = T_{A1} + T_{A2} + T_{A3}$). Furthermore, as a result of a series of experimental tests in situ, the effect of any angles which tend to increase the anchorage capacity, is not taken into account because the contribution of these angle effects was found to be generally low. The value of the friction T_{A1} that can be mobilised along the horizontal length L is generally low compared with T_{A2} and T_{A3} .

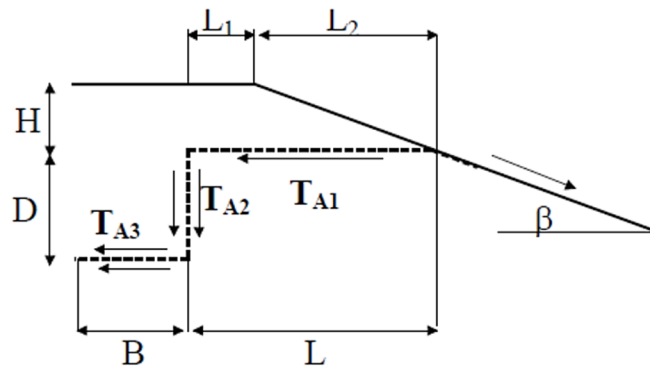


Figure 1.3.10. Schematization of the method proposed by Briançon, (2003).

Considered a simple “L-shape” anchor, Koerner (1998, 2005) assumed that the vertical component of the tensile strength on the geosynthetic along the slope induced, on the horizontal section of the sheet, additional normal stresses at the soil-geosynthetic interface, hence, an increase in the interface friction forces. In this method the cover soil applies normal stress due to its weight but its contribution to the frictional resistance at the interface is considered negligible. The total tensile force required in the anchor takes into account the sum of the different forces acting on both sides (up and down) of the geosynthetic. Furthermore, in the vertical segment, active and passive earth pressures are considered (Figure 1.3.11, method A).

In the Guide technique (2000) different authors introduced, in order to consider the change in direction of each geosynthetic sheet, an amplification coefficient K_1 that depends on the inclination of the bend (Figure 1.3.11, method B) and, in the vertical segment, the K_0 coefficient is considered.

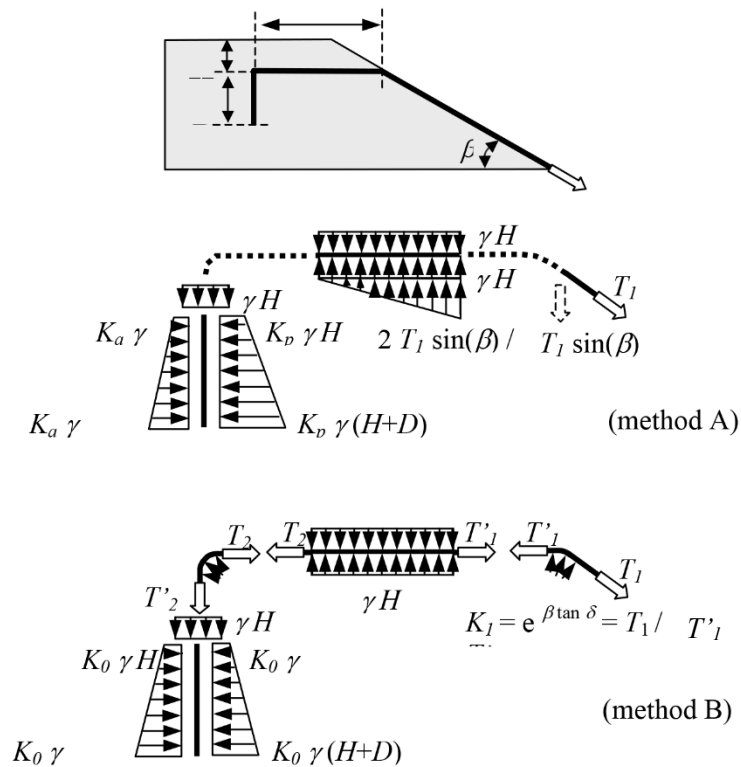


Figure 1.3.11. Comparison between Koerner (1998) and (Guide technique, 2000) design methods for “L-shape” anchor.

Villard and Chareyre, (2004), schematized in Figure 1.3.12, proposed another analytical model where the tension T , applied parallel to the slope, is obtained by considering the

angle effect and behaviour of the cover soil: two failure mechanisms are considered depending on whether the soil failure is taken into account or not.

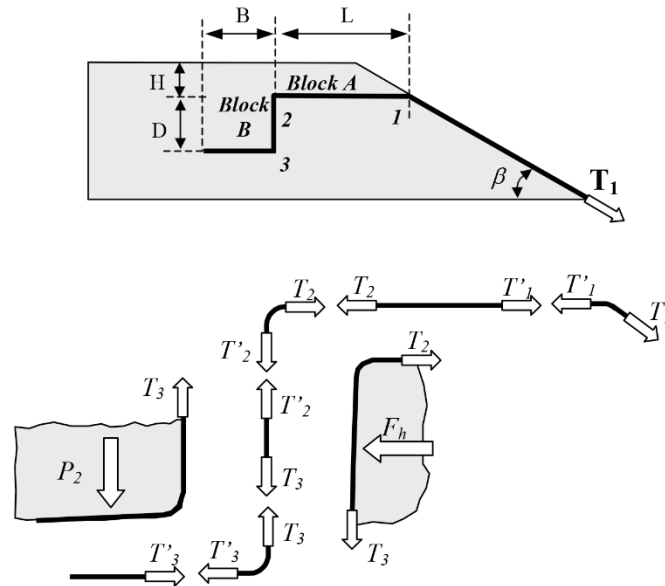


Figure 1.3.12. Force balance considered in the analytical model proposed by Villard et al, 2004.

Briançon et al. (2006) performing experimental tests in-situ highlighted some important mechanisms. They noted that, depending on the geometry of trench considered and on the soil properties, the failure mechanisms of the soil can occur and can be different depending on the trench geometry and soil properties as reported in Figure 1.3.13. It is also underlined that the normal stress applied to the different interfaces at failure can be different from the initial stress state and the soil-geosynthetic interface friction can be not fully mobilized if failure occurs in the soil. Therefore, assessing the law governing the interface tensile force, T , with respect to the displacement, u , is of paramount importance. In this context, the inclined plane test permits assessing the evolution of the tensile strength from very small to large displacement.

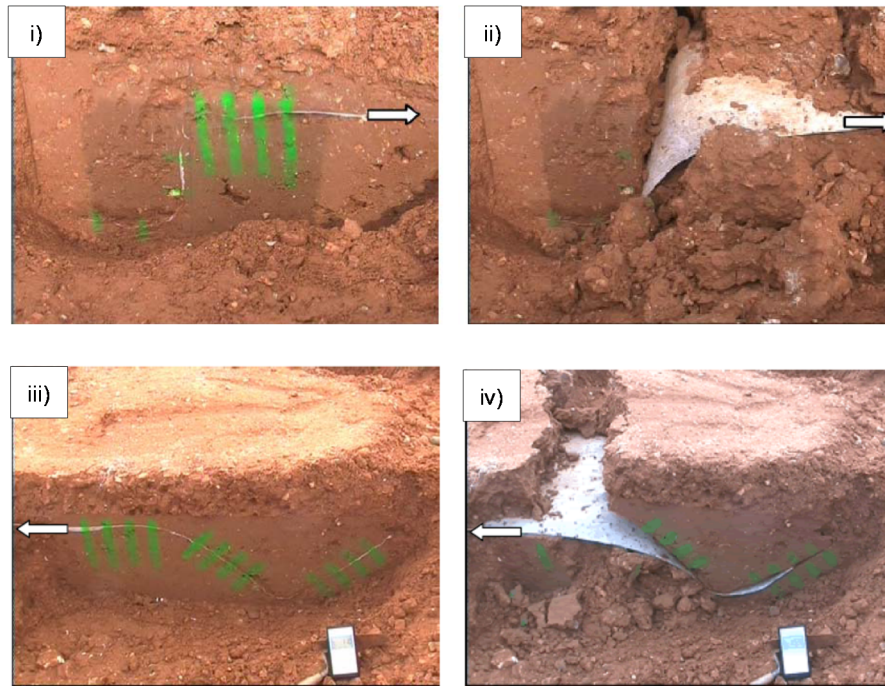


Figure 1.3.13. In-situ extraction of geotextile layer in a rectangular and “V-shape” trench: i) and iii) before extraction; ii) and iv) at rupture (after Briançon et al. 2006).

1.3.2 Seismic stability analysis of cover systems

The performance of solid waste containment facilities subjected to seismic loading, demonstrated that modern solid waste landfills have generally shown a good ability to withstand strong earthquakes without damages to human health and the environment (Kavazanjian, 1999; Matasovic. et al., 1998; Maugeri and Seco E Pinto, 2005). Twenty-two landfills were influenced by the Northridge earthquake (U.S.A.) (Augello et al., 1995), and a few solid waste landfills located in the Kobe/Osaka area of Japan were reported to be damaged by the severe earthquake (Park et al., 2004).

For landfills located in seismic regions, the most critical loading to the liner system and the geomembrane may be expected during an earthquake.

Maugeri and Seco E Pinto, (2005) summarized the major failure mechanisms for landfills under earthquake loadings as follows:

- Sliding or shear distortion of landfill or foundation or both;
- Landfill settlement;
- Transverse and longitudinal cracks of cover soils;
- Cracking of the landfill slopes;
- Damage to the gas system pipes;

- Tears in the geomembrane liners;
- Disruption of the landfill by major fault movement in foundation;
- Differential tectonic ground movements;
- Cracks through the contact between refuse landfill and canyon; and
- Liquefaction of landfill or foundation.

In particular, performance of the cover and lateral slopes under seismic conditions is an important aspect to consider in the design. The slopes which are quite stable under static conditions can simply collapse during earthquakes due to several reasons, including ground shaking leading to excessive vibrations and deformations, loss of bearing strength of the foundation soil due to liquefaction and reduction in the safety factor of the slope due to transient shooting up of the pore water pressures. Any of these events can impair the functionality of the liner and cause leakage of leachate leading to ground water pollution or a failure of landfill.

The stability analysis of solid waste landfills can be established by following the procedures outlined in the flow chart presented in Figure 1.3.14. In general, the behaviour of solid waste landfills during the occurrence of earthquakes can be analysed by experimental methods or mathematical methods.

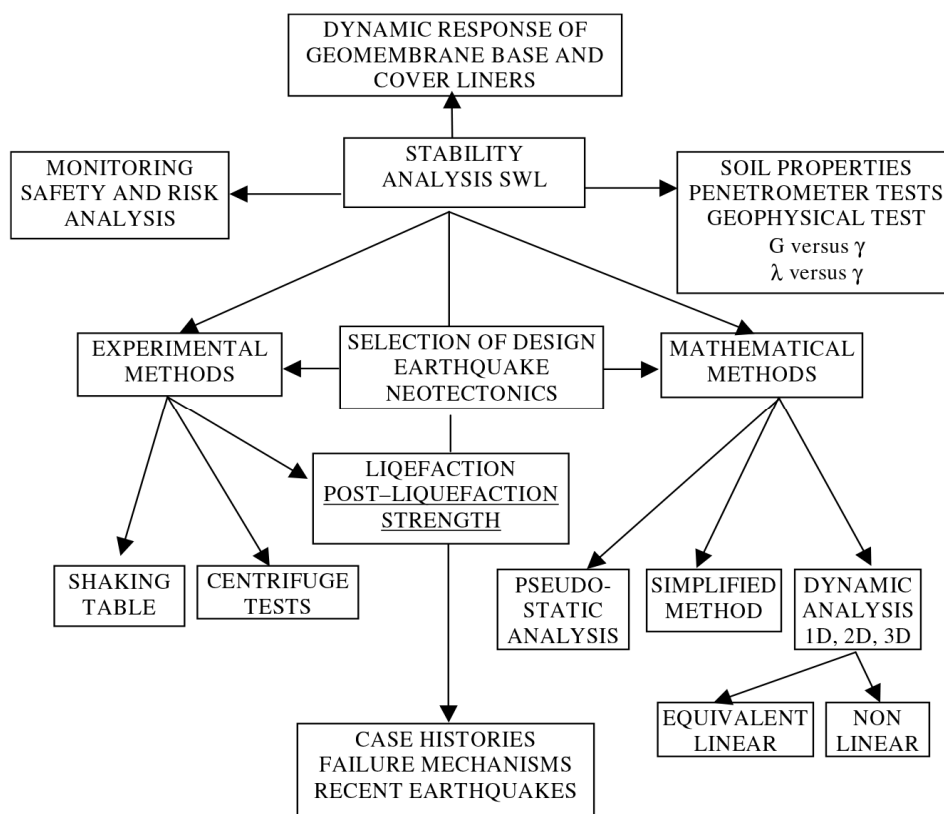


Figure 1.3.14. Flowchart for solid waste landfills (adopted by Maugeri and Seco E Pinto, 2005)

Seismic evaluations of slope stability range from using relatively simple pseudo-static procedures to advanced nonlinear finite element analyses.

1.3.2.1 Pseudo-static analysis

Seismic stability analysis of cover systems may be conducted using a pseudo-static approach. In this method, based on limit equilibrium analysis, the following hypothesis are made:

- ✓ the behaviour of the soil is rigid-plastic;
- ✓ failure is reached simultaneously from all the point of the failure surface;
- ✓ the shear strength versus normal load relation can be defined by a mohr-coulomb envelope;
- ✓ seismic inertia force is considered through an equivalent static force; the vertical and the horizontal component of the dynamic force can be expressed:

$$F_h = k_h \cdot W \quad 1.3-11$$

$$F_v = k_v \cdot W \quad 1.3-12$$

where k_h and k_v are the horizontal and the vertical seismic coefficient.

1.3.2.2 Seismic coefficient

The slope stability of waste landfills is generally evaluated by limit equilibrium slope method. In the analysis conducted applying the pseudo-static approach, the distribution of the acceleration is assumed uniform along the entire slope and the horizontal and the vertical components of the seismic inertia forces are applied at the centroid of the cover cross section. In order to take into account the possible amplification effects, the peak ground acceleration a_g (acceleration expected on the bedrock), is usually multiplied by some amplification coefficients which take into account the subsoil and the local site effects. However, in this case, the maximum acceleration used in the design, a_{max} , can overestimate the effect of the earthquake (Tropeano, 2010).

To simplify, the horizontal seismic coefficient, k_h , is often expressed as a part of the peak ground acceleration, a_g , and the vertical seismic coefficient, k_v , is generally evaluated as a part of k_h . In literature, there are not many examples to calculate the seismic coefficient.

The Eurocode 8 (prEN 1998-5 – 2003), indicates k_h as follows:

$$k_h = 0.5 \cdot \gamma_I \cdot S \cdot a_g / g \quad 1.3-13$$

where γ_I is a coefficient depending on the importance of the structure considered; S is a coefficient taking into account the subsoil (S_S) and the topographic (S_T) effects. The vertical seismic coefficient can be equal to:

$$k_v = \pm 0.5 \cdot k_h \quad 1.3-14$$

$$k_v = \pm 0.33 \cdot k_h \quad 1.3-15$$

Equations 1.3-14 or 1.3-15 are used if the ratio between the vertical and the horizontal acceleration of the earthquake is higher or smaller than 0.6 respectively.

Similarly, in Italy, the current legislation, “Norme Tecniche per le Costruzioni” (NTC, 2008), indicates, at the limit state, the horizontal and vertical seismic coefficients as follows:

$$k_h = \beta_m \cdot \frac{a_{\max}}{g} = \beta_m \cdot S_T \cdot S_S \cdot a_g \quad 1.3-16$$

$$k_v = 0,5 \cdot k_h \quad 1.3-17$$

with k_h and k_v horizontal and vertical seismic coefficients respectively, a_{\max} is the maximum acceleration, a_g is peak ground acceleration, β_m is a reduction coefficient that takes into account the ductility; S_T and S_S amplification coefficients depending on the subsoil and the site effects.

1.3.2.3 Factor of safety – limit equilibrium slope method

Limit equilibrium methods considering the infinite slope, are often applied in the current practice

The factor of safety, considering the translational equilibrium across and along the slope as schematized in Figure 1.3.15, in absence of seepage, can be expressed as:

$$W \cdot \cos \beta - k_h \cdot W \cdot \sin \beta = N \quad 1.3-18$$

$$k_h \cdot W \cdot \cos \beta + W \cdot \sin \beta = T \quad 1.3-19$$

$$FS = \frac{\tan \phi \cdot (1 - k_h \tan \beta) + c/\gamma \cdot h \cos^2 \beta}{k_h + \tan \beta} \quad 1.3-20$$

where k_h is the horizontal seismic coefficient; γ , c and ϕ are the unit weight, the cohesion, and the interface shear strength angle of the soil respectively; β and h the inclination angle and the height of the cover soil.

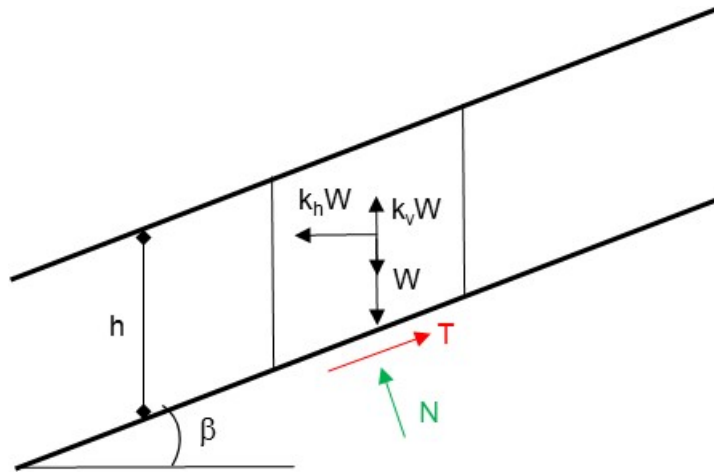


Figure 1.3.15. Balance of forces considering the infinite slope scheme applying the pseudo-static approach.

The principal limitation of this approach is that the equivalent pseudo-static force takes into account only the effect of the acceleration, a_{max} , while the seismic response is also linked to the frequency and the duration of the seismic event.

1.3.2.4 Dynamic simplified analysis

The dynamic simplified methods are mainly based on the sliding block theory (Newmark, 1965). These methods permit to overcome the limitations of the pseudo-static approach considering the evaluation of the acceleration time history. The seismic force is typically defined by an accelerogram, while the slope response is evaluated in terms of permanent displacements by integrating the function of the relative motion between the rigid mass and

the surface in the time. Slope stability is evaluated comparing the calculated permanent seismic displacement with the allowable displacement of the structure. The method consists of the following steps: (1) the identification of the failure surface corresponding to $FS = 1$ using the pseudo – static analysis; (2) determination of the seismic coefficient $k_y = a_y/g$ (corresponding to $FS = 1$); (3) selection of the proper accelerogram; (4) comparison between the calculated permanent displacement with respect to the allowable displacements of the structure.

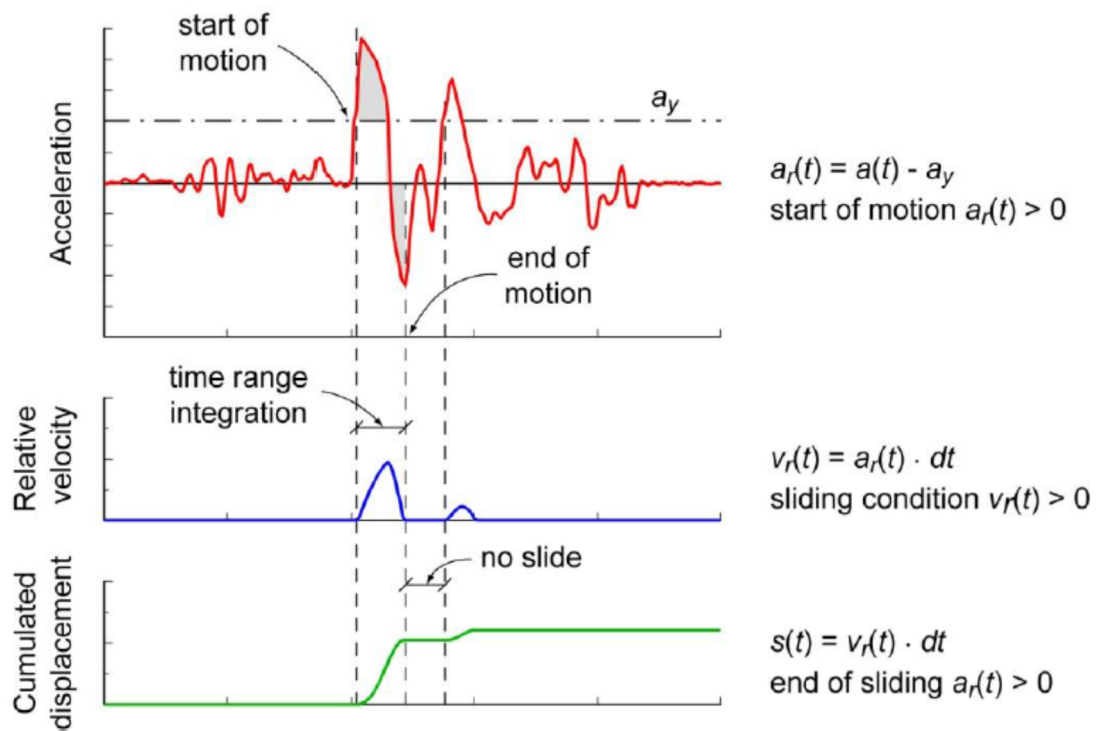


Figure 1.3.16. Analytical prediction of rigid block displacements (after Tropeano, 2010).

In practice, the calculated permanent seismic displacement is the most commonly used index of seismic performance of landfills (Kavazanjian, 1999; Ling and Leshchincky, 1997; Matasovic. et al., 1998; Maugeri and Seco E Pinto, 2005). In design the maximum allowable values of calculated permanent seismic displacement is considered. Allowable displacement depends on the ability to predict seismic deformation, the ability to sustain deformation without loss of function, the impact of a release due to loss of function, the ability to detect loss of function, and the feasibility (and associated cost) of repair (or replacement) (Kavazanjian, 1999).

Kavazanjian, (1999) provided a list of containment system components with typical values for the allowable calculated seismic displacement schematized in Table 1.3.1. These values are based upon the assumption that seismic displacements are calculated in the

typical fashion used in conventional practice: using one-dimensional equivalent linear response analyses, yield accelerations calculated with residual shear strengths, and Newmark-type seismic displacement analyses.

Table 1.3.1. Generic allowable calculated seismic displacements for MSW landfills (after Kavazanjian, 1999).

Component	Allowable Calculated Displacement	Comment
Liner System	150 to 300 mm	Actual expected deformation is very small.
Cover System	300 mm to 1 m	Damage is repairable.
Waste Mass	1 m	For displacement not impacting cover or liner.
Roadways, Embankments	1 m	Conventional geotechnical criteria.
Surface Water Controls	1 m	Conventional geotechnical criteria.
Gas Collection System	No Limit	Breakage common under normal operating conditions.

The final cumulated displacement depends on:

- amplitude, duration and number of cycles of the accelerogram $a(t)$;
- block-plane sliding resistance (a_{crit}).

The permanent displacement evaluated by the sliding block theory (Newmark, 1965) is assumed to accumulate whenever the yield acceleration is exceeded during the duration of excitation. In this case, it determines the acceleration value corresponding to the collapse of the structure assuming the behaviour of the soil as rigid-plastic. Acceleration in the reverse direction is usually not considered. The yield acceleration is usually obtained through the pseudo-static approach when the factor of safety is equal to one. According to Equation 1.3-20, in the case of infinite slope as reported in Figure 1.3.15, the yield seismic coefficient is obtained as:

$$k_y = k_h = \tan \phi + \frac{c}{\gamma \cdot h \cdot \cos^2 \beta \cdot (1 + \tan \beta \tan \phi)} \quad 1.3-21$$

The yield coefficient (k_y) represents the critical seismic coefficient of the structure, which depends primarily on the dynamic shear strength of the material along the critical sliding surface and the structure's geometry and weight.

1.4 INTERFACE SHEAR STRENGTH BETWEEN GEOSYNTHETICS

1.4.1 Definitions

When a body moves or tends to move over another body, a force opposing the motion, develops at the contact surfaces (Bowden and Tabor, 1954). This force which opposes the movement or the tendency of movement is called frictional force or simply friction. Friction is due to the resistance offered to the motion by minutely projecting particles at the contact surfaces. This maximum value of frictional force is known as limiting friction. It may be noted that when the applied force is less than the limiting friction, the body remains at rest and such frictional force is called static friction, which may have any value between zero and the limit friction. If the value of the applied force exceeds the limiting friction, the body starts moving over the other body and the frictional resistance experienced by the body while moving is known as dynamic friction. Dynamic friction may be grouped into the following two:

- Sliding friction: it is the friction experienced by a body when it slides over the other body;
- Rolling friction: it is the friction experienced by a body when it rolls over a surface.

Friction theory was first revealed by Leonardo da Vinci in the 15th century as a relationship governing the resistance between bodies in intimate contact. Amontons (1699) presented the nature of friction in terms of surface irregularities and the force required to raise the weight pressing the surfaces together and published the basic theory of friction as: i) Friction force is proportional to normal load; ii) Friction force is independent of contact area (Bowden and Tabor, 1954).

Finally, Coulomb (1785) investigated the influence of four main factors on friction: the nature of the materials in contact and their surface coatings; the extent of the surface area; the normal pressure (or load); and the length of time that the surfaces remained in contact (time of repose). Coulomb further considered the influence of sliding velocity, temperature

and humidity, in order to decide between the different explanations on the nature of friction that had been proposed.

The coefficient of friction (shear resistance normalized by normal force) is constant based on the fundamental rules of basic theory of friction. Most materials obey Amonton's Law. However, the interfaces comprised of polymeric materials do not obey these fundamental rules of friction. The friction force, (F) is governed by fundamental shear strength mechanisms as well as is being composed of one or more components as follows. For most continuous materials forming multi-asperity contacts, two components have been identified as: i) adhesion component; ii) "plowing" or plastic deformation component (Bowden and Tabor, 1954). For interfaces comprised of polymers, as the normal load increases, the coefficient of friction (normalized friction: proportion of shear force to normal load) decreases.

In fact, for average ranges of normal loads, the shear strength properties of geomembrane/soils or geomembrane/geosynthetics systems are characterized as follows (Blond and Elie, 2006):

- The shear strength versus normal load relation can be defined by a Mohr-Coulomb envelope, or a friction angle and an adhesion. However, the relation is not linear over a very large range of normal loads Figure 1.4.1(i).
- For most interfaces involving geosynthetics, a peak as well as a residual shear strength can be defined in a shear test with a constant displacement rate. This means that the shear strength mobilized after some displacement of one surface versus the other will typically be lower than the maximum shear strength, as shown on Figure 1.4.1(ii). For this reason, a rigorous assessment of the stability of a landfill liner with geosynthetics requires the knowledge of the full shear stress-displacement curve for the level of anticipated normal stress (Jones and Dixon, 1998).

In particular, the importance of strain softening interfaces, i.e. the decrease in interface shear strength with increasing displacement was outlined also by Byrne (1994). He concluded that if the degradation of the interface shear strength from the peak to the residual value is not considered, a non-conservative assessment of stability can be provided. Depending on the geometry and the distribution of strains within the lining system, progressive failure may occur (Jones and Dixon, 1998). In such circumstances, the use of the peak shear strength to calculate the factor of safety would not give a conservative assessment of stability. The work of Byrne (1994) and Long et al. (1994) has led to the need

to characterise the full stress/strain behaviour of interfaces in laboratory tests, in order to obtain the relevant parameters for use in these more rigorous analysis techniques.

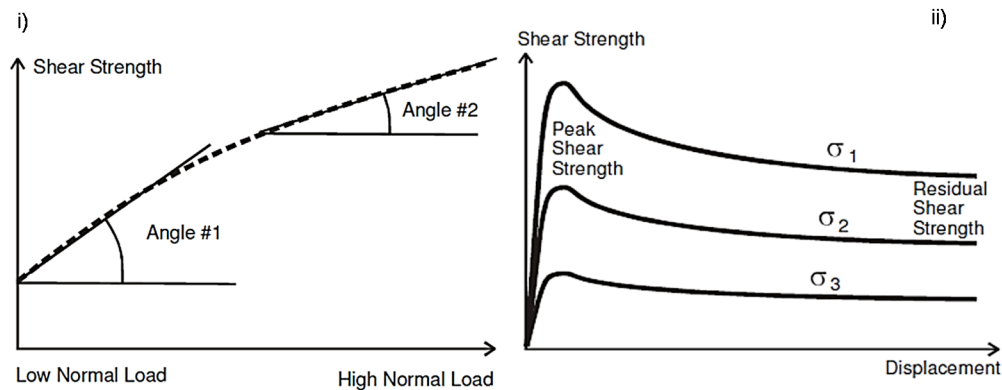


Figure 1.4.1. i) Typical shear strength versus normal load behaviour of geosynthetic interfaces; ii) Typical Shear strength versus displacement behaviour of geosynthetic interfaces (after Blond and Elie, 2006).

It shall be mentioned that EN ISO 10318 (Geosynthetics - Terms and Definitions) as well as EN ISO 12957 (Geosynthetics – Determination of friction characteristics) define the friction angle of a geosynthetic interface as the angle which tangent is defined by “the ratio of the friction force per unit area to the normal stress between two materials”.

If a design method involving the ‘secant’ angle (Figure 1.4.2) is chosen, this angle shall be determined using test results conducted under the exact design normal load.

If a ‘tangent’ angle (Figure 1.4.2) is used for design, the relevance of incorporating the adhesion in the design shall be evaluated. A common approach is to neglect this adhesion and to consider it as an additional safety.

Generally speaking, the main target of a typical interface friction test is to assess a limit value of the shear stress τ at the interface under a normal effective stress σ' . The characteristic parameter deduced from this kind of test is $\tan \phi = \tau / \sigma'$ where $\sigma' = \sigma$, if the tests are performed in dry conditions (as in the case of this study). The shear stress does not vary quite linearly with the normal stress. For this reason, it is worth noting that ϕ is the secant friction angle corresponding to the normal stress σ and, in the following, it is called “friction angle”. Similarly, $\tan \phi$ is called “coefficient of friction” as usually in the literature.

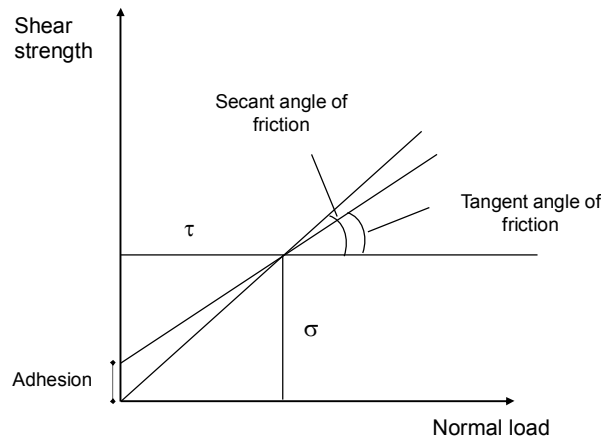


Figure 1.4.2. Secant versus tangent friction angle (modified from Blond and Elie, 2006).

1.4.2 Geosynthetic interface shear strength characterization

When the barrier is installed in the inclined surface for side and cover barriers, due to self-weight of the soil for protection layer and possibly, in case of bottom liner the solid waste disposed into the landfill, the sliding force will arise along the barrier system that results in shearing force applying the barrier (Kotake et al., 2011).

The comprised liner and cover systems must withstand the possibly applied stresses without being affected in its function during, after construction and in the post closure phase. A careful estimation of these stresses as well as shear strength of liner and cover systems serves as a basis for safe landfill construction, operation, and post-closure. Shear stresses that develop during the installation of the geosynthetic composite systems on landfill sloped base and surfaces are of a major concern.

There are several devices currently in use to test the shear strength of the different interfaces present in liner systems under static loading conditions including: the large scale direct shear box, the conventional direct shear box, the torsional or ring shear device, the inclined plane and the cylindrical shear device. Bouazza et al., (2002) summarize the principal advantages and disadvantages of these tests reported in Table 1.4.1.

The seismic response of geosynthetic – geosynthetic interfaces is commonly investigated by cyclic direct shear tests, shaking table tests and shaking table on geotechnical centrifuge.

Table 1.4.1. Summary of advantages and disadvantages associated with test devices for measuring interface shear strength (modified from Bouazza et al., 2002).

TEST DEVICE	ADVANTAGES	DISVANTAGES
Large scale direct shear box	Industry standard Large scale Minimal boundary effects Expedient specimen preparation	Machine friction Load eccentric Limited continuous displacement Expensive
Large displacement shear box	Large area of interface Capable of detecting and effects Determination of residual strength with a linear displacement device	Influence of end effects Availability
Conventional direct shear box	Experience with soil Inexpensive Large normal stress Expedient specimens preparation	Small geosynthetic experience base Machine friction Load eccentricity Small scale Limited displacement Boundary effects
Ring shear device	Unlimited continuous displacement	Machine friction Mechanism of friction not comparable to that exhibited in the field Small scale Expensive No lateral restrain for migration of plastic soil
Inclined Plane	Minimal machine effects Minimal boundary effects Large displacement Ability to monitor tensile forces Low normal stresses Inexpensive <i>and easy to perform</i>	Limited normal stresses
Cylindrical shear	Unlimited continuous displacement Better controlling confined during shearing Large sample size with less ledge effects Area of shear plane remains constant Constant direction of shear displacement	Availability Experience with dry materials only No restrain for migration of plastic soils

As several studies demonstrated, both the inclined plane (Briançon et al., 2011, 2002; Palmeira, 2009; Reyes Ramirez and Gourc, 2003; Wasti and Özdüzgün, 2001; Wu et al., 2008b) and the shaking table (Carrubba et al. 2001; De and Zimmie, 1998; Yegian and Kadakal, 1998) are the most suitable tests in order to investigate low normal stresses.

In particular, the inclined plane is a very suitable tool to simulate the interface response because, it is possible to reproduce field conditions:

1. gravity is the driving force;
2. large specimens can be tested;
3. the materials are subjected to different relative displacements, from low up to very large; in addition and this kind of device is versatile, comparing with the shear box, in order to simulate different kinematic conditions as unrolling of geosynthetics, implementation of the soil cover, assessment of dynamic conditions, etc.
4. the behaviour at very low normal stress can be assessed.

In particular, the third and the fourth points represent relevant advantages. As geosynthetic interfaces generally exhibit strain softening behaviour (Figure 1.4.1, *ii*), after shearing the peak shear strength is mobilized within a small amount of displacement and then the shear strength decreases to a residual strength at significantly larger displacement. As fully described in §4.1.3, through the inclined plane test, the behaviour of the interface can be evaluated for displacements ranging from few millimetres until greater values of the order of one meter.

Furthermore, in the field, the liners of cover systems are usually subjected to low normal stresses. In fact, the density of soil cover, which is generally not properly compacted, could be evaluated to 1.7 t/m^3 . The corresponding thickness of soil veneer is ranging between 0.30m and 1.0m which corresponds to normal stress varying between 5 and 17 kPa respectively.

The shaking table test allows investigating the dynamic interface shear strength subjecting materials to sinusoidal inputs (characterization test) or the seismic interface response sending earthquake-type excitations (performance test). Through this test it is possible to determinate the maximum shear stress transmitted at the interface and the permanent displacement at low normal stress.

Consequently, the assessment of the geosynthetic interface shear strength is very complex as it depends mainly on the mechanical surface properties such as surface roughness but also on the test conditions such as: applied shear loading (De and Zimmie, 1998; Kotake et al., 2011), normal stress (Bergado et al., 2006; Jones and Dixon, 1998; Lalarakotoson et al., 1999), temperature (Akpınar and Benson, 2005; Karademir and Frost, 2013) and moisture content (Maugeri and Seco E Pinto, 2005). An alteration of the interface strength can also occur due to mechanical damage (Pitanga et al., 2011; Reyes Ramirez and Gourc, 2003), time-dependent processes (ageing), stress dependent processes (such as repeated loading, Moraci and Cardile, 2009), coupled effects of both time and stress-strain dependent processes (creep or relaxation).

To summarize, the parameter influencing the interface shear strength are:

- Physical and chemical properties of the surfaces in contact;
- Geometry and manufacturing of the surfaces;
- Temperature and humidity of the environment;
- Interface contact stress;
- Velocity of loading (static or dynamic);

- Loading conditions (monotonic, cyclic or dynamic);
- Mechanical damage of the surfaces;
- Long-term variation of interface shear strength.

2 GEOSYNTHETICS

2.1 GENERALITIES

Geosynthetic is “A generic term describing a product, at least one of whose components is made from a synthetic or natural polymer, in the form of a sheet, a strip or a three dimensional structure, used in contact with soil and/or other materials in geotechnical and civil engineering applications” (EN ISO 10318, 2005). They are plastic, organic or textile materials, commercialized in rolls that could be classified in different categories.

Geosynthetics have been used in civil engineering construction since the late 1970s, and their use is currently growing rapidly. Nowadays they are employed in a range of applications in many areas of civil engineering, especially geotechnical, transportation, water resources, environmental (geoenvironmental), coastal, and sediment and erosion control engineering for achieving technical benefits and/or economic benefits. The wide use of geosynthetic is mainly due to their lower cost, their simpler installation and their ability to partially or completely replace natural resources such as gravel, sand, bentonite clay, etc. Other favourable basic characteristics are (Shukla and Yin, 2006):

- non-corrosiveness
- highly resistant to biological and chemical degradation
- high flexibility
- minimum volume
- lightness
- ease of storing and transportation
- speeding the construction process
- making economical and environment-friendly solution

- providing good aesthetic look to structures.

This chapter provides a general description of geosynthetics including their basic characteristics, manufacturing processes and their main functions.






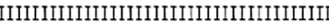

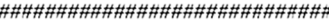
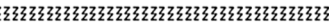






2.2 TYPES, PROPERTIES AND MAIN FUNCTIONS OF GEOSYNTHETICS

Geosynthetics include a variety of synthetic polymer materials that can be broadly classified into different categories according with the method of manufacture, physical properties and specific function.

Various types of geosynthetics can be recognized: geotextiles, geogrids, geonets, geomembranes and geocomposite (including bentonitic geocomposites and drainage geocomposites), geocells, geocontainers, geofoam etc. which are used in contact with soil, rock and/or any other civil engineering-related material as an integral part of a man-made project, structure - or system.

For convenience geosynthetic products can be represented by abbreviations and/or graphical symbols as recommended by the International Geosynthetics Society (Table 2.2.1).

Table 2.2.1. Abbreviations and graphical symbols of geosynthetic products as recommended by the International Geosynthetics Society

Notation	Graphical Symbols	Geosynthetic products
GTX		Geotextile (generic)
GMB		Geomembrane (generic)
GBA		Geobar (generic)
GBL		Geobanket (generic)
GCD		Geocomposite drain (generic) – with geotextile on both sides
GCE		Geocell (generic)
GCL		Geocomposite clay liner (generic)
GEC		Surficial geosynthetic erosion control (generic)
GEK		Electrokinetic geosynthetic (generic)
GGR		Geogrid (generic)
GMA		Geomat (generic)
GMT		Geomattress (generic)
GNT		Geonet (generic)
GSP		Geospacer (generic)
GST		Geostrip (generic)

Geosynthetics are polymer-based products that influence their global performance. Furthermore other several factors such as the ambient temperature, the level of stress, the duration of the applied stress and the rate at which the stress is applied (Shukla and Yin, 2006) can affect their behaviour. The main polymers used to manufacture geosynthetic are specified in Table 2.2.2.

Table 2.2.2. Polymers commonly used for geosynthetics

Geosynthetic materials	Polymer materials
GEOMEMBRANES	Polyethylene (HDPE and LLDPE) Plasticized PVC Polypropylene
GEONETS	HDPE
GEOGRIDS	HDPE Polyesters Polypropylene
GEOPIPES	HDPE PVC
GEOTEXTILES	Polypropylene Polyester

The number of monomers in a polymer chain determines the length of the polymeric chain and the resulting molecular weight. Molecular weight can affect physical and mechanical properties, heat resistance and durability (resistance to chemical and biological attack) properties of geosynthetics. The physical and mechanical properties of the polymers are also influenced by the bonds within and between chains, the chain branching and the degree of crystallinity. An increase in the degree of crystallinity leads directly to an increase in rigidity, tensile strength, hardness, and softening point and to a decrease in chemical permeability (Shukla and Yin, 2006).

The material influences the geosynthetic mechanical behaviour, the shear resistance, the hydraulic behaviour, the UV, chemical and biological resistance.

To summarize, the various types of geosynthetics have a variety of properties. A comprehensive set of tests has been developed to evaluate the properties of geosynthetics. These tests include physical tests, hydraulic tests, mechanical tests, and tests to evaluate durability (Giroud, 2012).

For geosynthetic, the material properties can be mainly grouped under six types as listed in Table 2.2.3 in which there are also summarizes the parameters evaluated for each group.

Table 2.2.3. Properties and parameters of geosynthetic (after Vashi et al. 2010).

Type of property	Parameters
Physical	Thickness, specific gravity, mass per unit area, porosity, apparent opening size.
Chemical	Polymer type, filler material, carbon black percentage, plasticizer and additive details, manufacturing process for fiber and geosynthetics.
Mechanical	Tensile strength, compressibility, elongation, tear/impact/puncture resistance, burst strength, seam strength, fatigue resistance, interface friction with soil, anchorage in soil
Hydraulic	Permittivity (cross-plane permeability), transmissivity (in-plane permeability), clogging potential.
Endurance	Installation damage potential – tear/impact/puncture resistance, abrasion resistance, creep.
Degradation	Resistance to ultra-violet radiation, temperature, oxidation, etc.

In particular, mechanical properties are important in those applications where a geosynthetic is required to perform a structural role under applied loads or where it is required to survive installation damage and localized stresses. Among the different mechanical parameters, the tensile strength that is the maximum resistance to deformation developed for a geosynthetic when it is subjected to tension by an external force, is the significant one.

Due to the variety of properties, geosynthetics can perform a several of functions such as: reinforcement, separation, filtration, drainage, fluid barrier, protection and erosion control (Moraci, 2011). Even if the basic principal is “one geosynthetic, one function”, the advanced technologies allow one or more functions to be handled from the same product. In general, the use of geosynthetic in a specific application needs classification of tis functions as primary or secondary listed in Table 2.2.4.

Table 2.2.4. Types and functions of various geosynthetics. ✓ main function; ★ secondary function (after Bouazza et al., 2002)

Geosynthetic types	Function					
	Separation	Drainage	Filtration	Reinforcement	Hydraulique/ gas barrier	Protection
Non woven geotextile	✓	★	✓		✓ ¹	✓
Woven geotextile	✓		★	✓		
Geogrids				✓		
Geomembranes					✓	
Geocells	✓			✓		
Geosynthetic clay liners					✓	★
Geocomposites	★	✓	★	★	✓	✓
Geonet		✓				
Geopipe		✓				

Separation: In this kind of application, the geosynthetic has to avoid the co-penetration and mixing of different soil layer. Figure 2.2.1 shows a geosynthetic layer preventing the intermixing of soft soil and granular fill, thereby keeping the structural integrity and functioning of both materials intact.

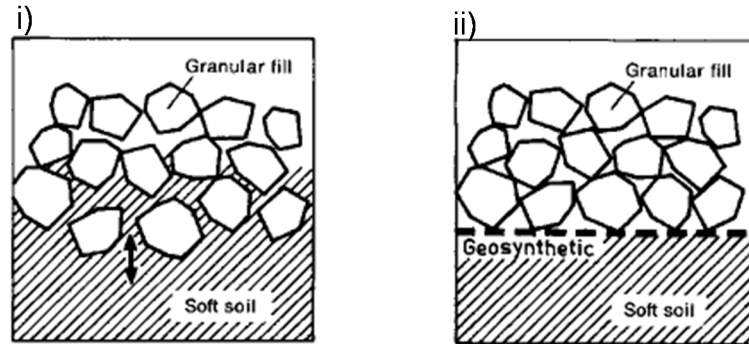


Figure 2.2.1. Basic mechanisms involved in the separation function: (i) granular fill-soft soil system without the geosynthetic separator; (ii) granular fill-soft soil system with the geosynthetic separator (after Shukla and Yin, 2006).

Filtration: A geosynthetic may function as filter, between two materials with different particle size distribution, allowing for adequate fluid flow with limited migration of soil particles across its plane over a projected service lifetime of the application under consideration. Figure 2.2.2 shows that a geosynthetic allows passage of water from a soil mass while preventing the uncontrolled migration of soil particles.

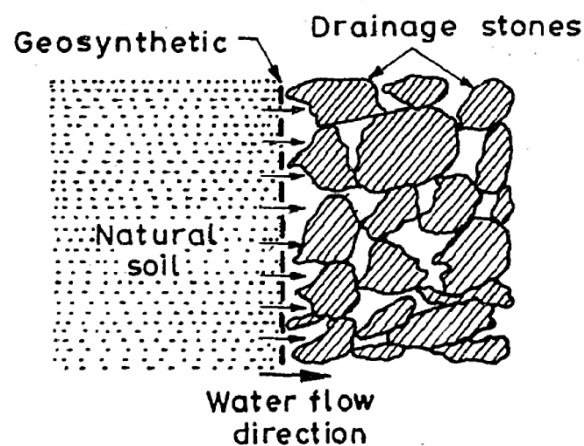


Figure 2.2.2. Basic mechanisms involved in the filtration function (after Shukla and Yin, 2006).

It is important to understand that the filtration function also provides separation benefits. However, a distinction may be drawn between filtration function and separation function

with respect to the quantity of fluid involved and to the degree to which it influences the geosynthetic selection (Shukla and Yin, 2006).

Drainage: in this function a high permeable geosynthetic, collects and conveys fluids and gases to flow through the plane of the material. It facilitates also the surface water runoff (Figure 2.2.3).

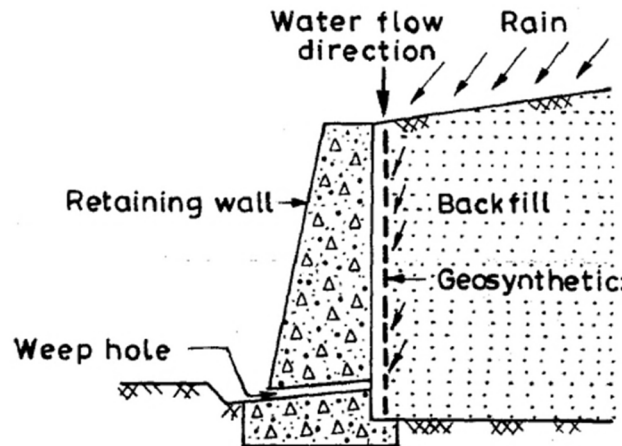


Figure 2.2.3. Basic mechanisms involved in the drainage function (after Shukla and Yin, 2006).

Geosynthetic acts to reduce *soil erosion* caused by rainfall impact and surface water runoff on slopes preventing dispersion of surface soil particles subjected to erosion actions, often allowing or promoting growth of vegetation.

Protection: a geosynthetic, placed between two materials, performs the protection function when it prevents acute damage caused by adjacent materials or distributes stresses and strains transmitted to the material to be protected against any damage (Shukla and Yin, 2006). In some applications, a geosynthetic layer is needed as a localized stress reduction layer to prevent or reduce local damage to a geotechnical system.

Reinforcement: the geosynthetic improves the mechanical properties of a soil mass providing additional strength to soils as a result of its inclusion. When soil and geosynthetic reinforcement are combined, a composite material, “reinforced soil”, possessing high compressive and tensile strength is produced. In fact, any geosynthetic applied as reinforcement has the main task of resisting applied stresses or preventing inadmissible deformations in geotechnical structures. In this process, the geosynthetic acts as a tensioned member coupled to the soil/fill material by friction, adhesion, interlocking or confinement and thus maintains the stability of the soil mass (Figure 2.2.4).

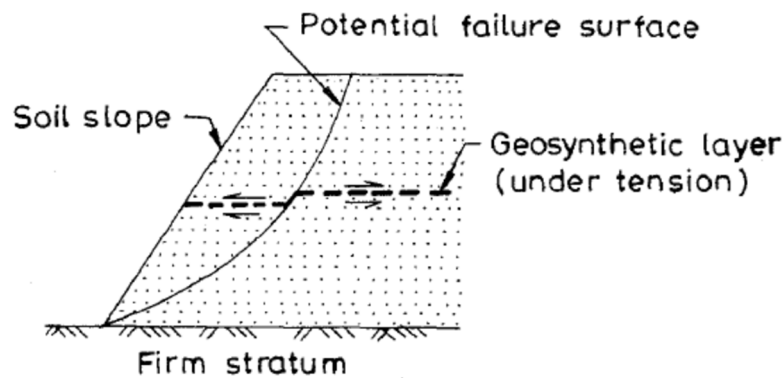


Figure 2.2.4. Basic mechanisms involved in the reinforcement function (after Shukla and Yin, 2006).

Fluid/Gas barrier: Total separation of the volume considered, realization of an impermeable barrier to fluids or gases.

2.3 GEOSYNTHETICS IN LANDFILL COVER SYSTEMS

Landfills employ geosynthetics to varying degrees depending on the designer and the applicable regulatory requirements. The liner system is designed taking into account the different functions and the efficiency of materials used. In cover liner systems, for example, these components are used (see Figure 2.3.1) to serve one or several purposes, such as watertightness (geomembrane and compacted clay liner), drainage and filtration (geotextile, geonet or geocomposite drain) and protection (cover soil).

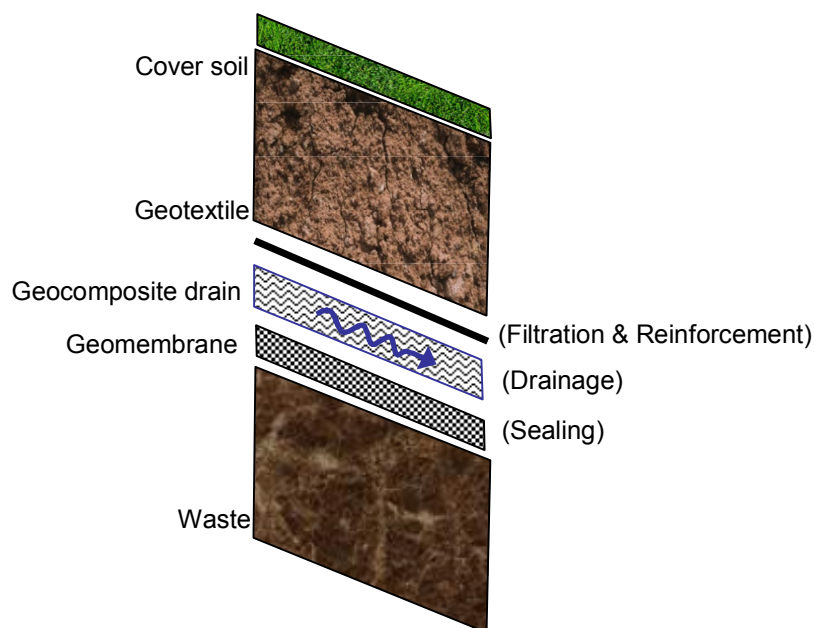


Figure 2.3.1. Example of a landfill cover profile.

In this respect geogrids can be used to reinforce slopes beneath the waste as well as for veneer reinforcement of the cover soils above geomembranes (Bouazza et al., 2002). The geogrids or high strength geotextiles (woven, knitted geosynthetics or composites) are used as support systems for geomembranes placed above them in resisting differential settlement of the underlying waste. Geotextiles are commonly used for filtration purpose or as cushion to protect the geomembrane from puncture. Geonets are unitized sets of parallel ribs positioned in layers such that liquid can be transmitted within their open spaces. Their primary function is in-plane drainage. Geomembranes are impermeable sheets of polymeric formulations used as a barrier to liquids and/or vapors. Geocomposites represent a subset of geosynthetics whereby two or more individual materials are utilized together. The type of geocomposite most commonly used in landfills is a geotextile/geonet composite. The geotextile serves as both a separator and a filter, and the geonet or built-up core serves as a drain. Geosynthetic clay liners represent a composite material consisting of bentonite and geosynthetics where the geosynthetics are either geotextiles or geomembranes.

2.3.1 Materials tested

The stability of modern lining systems is often controlled by interface strengths between geosynthetic components. In particular, the present study focuses on the interface between geocomposite drain in contact with geomembrane because the range of use this interface is very widespread in geotechnical and environmental engineering and more specifically in landfill barriers on slopes.

Geomembranes are polymeric continuum sheet materials manufactured uniformly from a variety of polymer resins, to possess homogeneity in terms of physical and mechanical properties as well as a uniform distribution of material characteristics throughout a large lining sheet. The most common types of polymer resins are polyvinyl chloride (PVC), chlorosulfonated polyethylene (CSPE), and polyethylene (PE).

PE membranes are manufactured as either smooth or textured sheets using a screw extrusion process and classified by resin density as high density polyethylene (HDPE), linear low density polyethylene (LLDPE), or very low density polyethylene (VLDPE) (Koerner, 1998). The most common polymer used in geosynthetic landfill cover systems is currently HDPE, and is the focus of the current experimental program. The manufacturing process consists of solid resin pellets, and other additives such as antioxidants and process stabilizers being blended in a hopper attached to a barrel system.

Smooth geomembranes has been used for decades over a wide range of applications; textured geomembranes are often chosen to allow for better compliance and interaction between the synthetic materials or geosynthetic and soil.

In particular, the texturing techniques, processes, and finished textures can vary widely. Manufacturing methods used to texture geomembranes include: co-extrusion, impingement, lamination, and structuring. In this study two different kinds of textured geomembranes are tested: a structured, GMB_{TMH} (with spikes) and a coextruded “sandy paper like” (GMB_{RMH}) membranes.

The structuring process forces a hot flat die extruded geomembrane through two counter-rotating rollers with patterned surfaces. The texture of the embossing rollers is sometimes a box and point pattern, but can be of almost any geometry. An advantage of structuring is the ability to create vastly different textures on the upper and lower geomembrane surfaces. Improper cooling can result in residual stresses under the macrotextural features making the membrane more susceptible to stress cracking in the presence of active surface agents.

The co-extrusion method uses one or two secondary extruders on the preferred or both sides of a main extruder to deliver a molten resin with an added blowing agent, typically nitrogen. Properly executed, co-extrusion texturing produces high bond strengths between the geomembrane core and the textured surfaces consisting of variably sized macrotexture with significant microtexturing due to the rapid expansion of the blowing agent (Hebeler et al. 2005).

For the present research, three different kinds of geomembrane, representing in all the tests the lower layer, are used (Figure 2.3.2): smooth (GMB_S), structured (GMB_{TMH}) and co-extruded - “sandy paper like” (GMB_{RMH}).

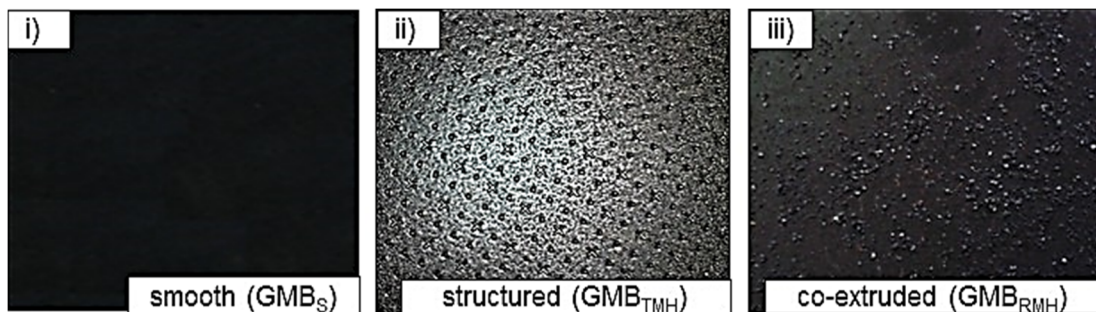


Figure 2.3.2. Geomembrane used in the experimental programme: i) smooth (GMB_S); ii) textured (GMB_{TMH}); iii) co-extruded - “sandy paper like” (GMB_{RMH}).

In particular, GMB_S is a smooth geomembrane on both sides; GMB_{TMH} and GMB_{RMH} have only one face (the surface tested) textured.

Geocomposite drains (GCD) consist in two or more geosynthetics solving different functions such as separation, filtration and drainage. In a GCD two principal parts can be distinguished:

- Internal drainage component;
- External separation-filtration part.

In this investigation, two types of geocomposite drains, usually glued to the upper box, are tested (Figure 2.3.3): GCD_N and GCD_W . The first one (GCD_N) consists of a thermobonding draining core - HDPE geonet (GNT) done by two sets of parallel overlaid ribs integrally connected to have a rhomboidal shape enclosed by two nonwoven geotextiles (GTX) on both sides, working as separation, filtration and protection layers.

In the GCD_W the internal core is composed by a geomat (GMA) realized by thermobonded extruded monofilaments with two filtering nonwoven geotextiles that may also be working as separation or protecting layers. The draining three dimensional core will have a “W” configuration as longitudinal parallel channels.

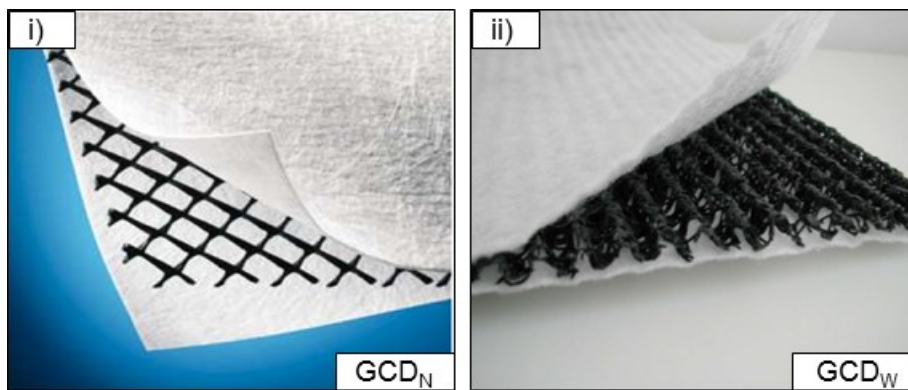


Figure 2.3.3. Geocomposite drains tested in the experimental programme: i) GCD_N with geonet (GNT) internal core; ii) GCD_W with geomat (GMA) “W” configuration.

Furthermore, just for the specific interface between the GCD_N and the smooth geomembrane (GMB_S), the influence of the different materials which constitute the geocomposite layer (geonet and geotextile) is assessed by testing them separately in direct contact with the geomembrane. Thereby, in the experimental program three different interfaces are tested (Figure 2.3.4):

- geotextile (GTX) – geomembrane (GMB_S);

- geonet (GNT) – geomembrane (GMB_S);
- geocomposite drain (GCD_N) – geomembrane (GMB_S).

In this last case the direct contact is between the geotextile and the geomembrane as in the first one. However, the geonet support could influence the surface of the geotextile glued to the geonet

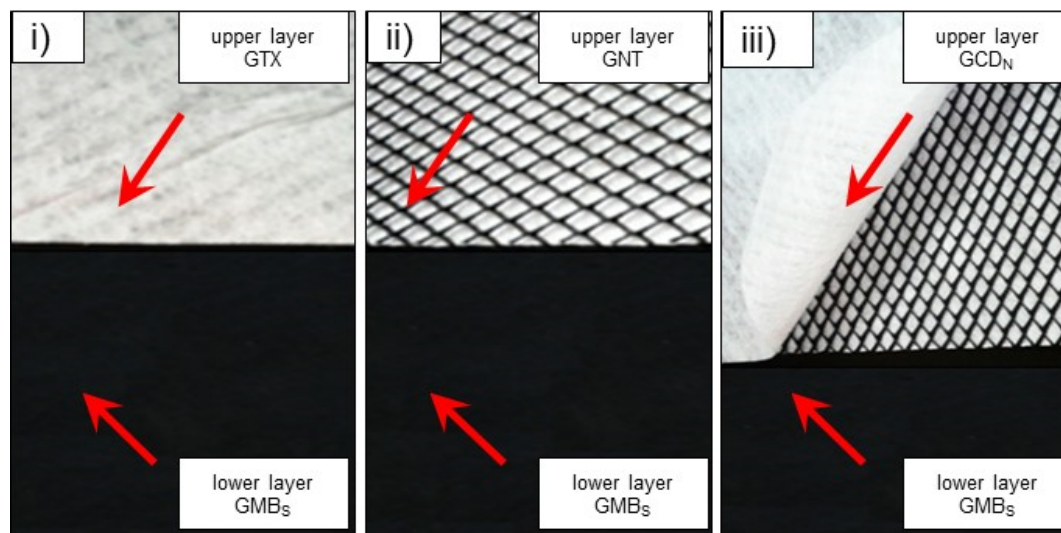


Figure 2.3.4. Interfaces tested to assess geocomposite drain GCDN – smooth geomembrane GMB_S interface performance: a) GTX - GMB_S; b) GNT - GMB_S; c) GCDN - GMB_S.

The physical properties of the materials are given in Table 2.3.1.

Table 2.3.1. Characteristics of tested geosynthetics.

Type of geosynthetic	Material	Thickness at 2 kPa (mm)	Mass per Unit Area (g/m ²)
Geotextile (GTX)	Needlepunched and/or thermobonded nonwoven	1	130
Geonet (GNT)	Thermobonded rhomboidal shape (HDPE)	3.5	520
Geocomposite drain (GCD_N)	GTX (external filter) + GNT (drainage core)	5.5	780
Geocomposite drain (GCD_w)	GTX (external filter) + GMA (drainage core)	6.2	600
Geomembrane (GMB_S)	Smooth (HDPE)	2	2000
Geomembrane (GMB_{TMH})	Structured (HDPE)	2	/
Geomembrane (GMB_{RMH})	Co-extruded “sandy paper like” (HDPE)	2	/

The experiments described in the current study were conducted on seven different interfaces as indicated in Table 2.3.2, formed through various combinations of the geosynthetics listed in Table 2.3.1.

All the geosynthetics material were provided by Officine Maccaferri S.p.a.

Table 2.3.2. Description of geosynthetic interfaces.

Interface identification	Upper geosynthetic	Lower geosynthetic	Notation
<i>a</i>	Geotextile (GTX)	Geomembrane (GMB _S)	GTX - GMB _S
<i>b</i>	Geonet (GNT)	Geomembrane (GMB _S)	GNT - GMB _S
<i>c</i>	Geocomposite drain (GCD _N)	Geomembrane (GMB _S)	GCD _N - GMB _S
<i>d</i>	Geocomposite drain (GCD _N)	Geomembrane (GMB _{TMH})	GCD _N - GMB _{TMH}
<i>e</i>	Geocomposite drain (GCD _W)	Geomembrane (GMB _{TMH})	GCD _W - GMB _{TMH}
<i>f</i>	Geocomposite drain (GCD _N)	Geomembrane (GMB _{RMH})	GCD _N - GMB _{RMH}
<i>g</i>	Geocomposite drain (GCD _W)	Geomembrane (GMB _{RMH})	GCD _W - GMB _{RMH}

3 TEST APPARATUS

3.1 INCLINED PLANE TEST

3.1.1 Introduction

In geotechnical applications such as geosynthetic liner systems on slopes of landfill sites either at the cap cover, and on dams and riverbanks, an in-depth knowledge of the shear strength behaviour of both soil–geosynthetic and geosynthetic–geosynthetic interfaces is required. The correct assessment of the interface shear properties between the geosynthetics and soils or between different types of geosynthetics becomes an important issue considering the fact that interfaces with low in-plane shear resistance act as potential failure planes.

As noticed in the previous chapter, the Inclined Plane test is the most appropriate tool (Lalarakotoson et al., 1999; Izgin and Wasti, 1998; Wasti and Özdüzgün, 2001; Palmeira et al., 2002; Reyes Ramirez and Gourc, 2003; Pitanga et al., 2009) for the characterization of the interaction between soil - geosynthetic and geosynthetic - geosynthetic interfaces at low normal stress typically found in such applications.

A typical device, schematized in Figure 3.1.1, is composed of an upper box sliding along an inclined support (a lower box or a plane). The test consists in studying the sliding behaviour of the upper box while the inclination of the plane continuously increases. The typical diagram reports the upper box displacement versus the plane inclination angle, β as in Figure 3.1.2.

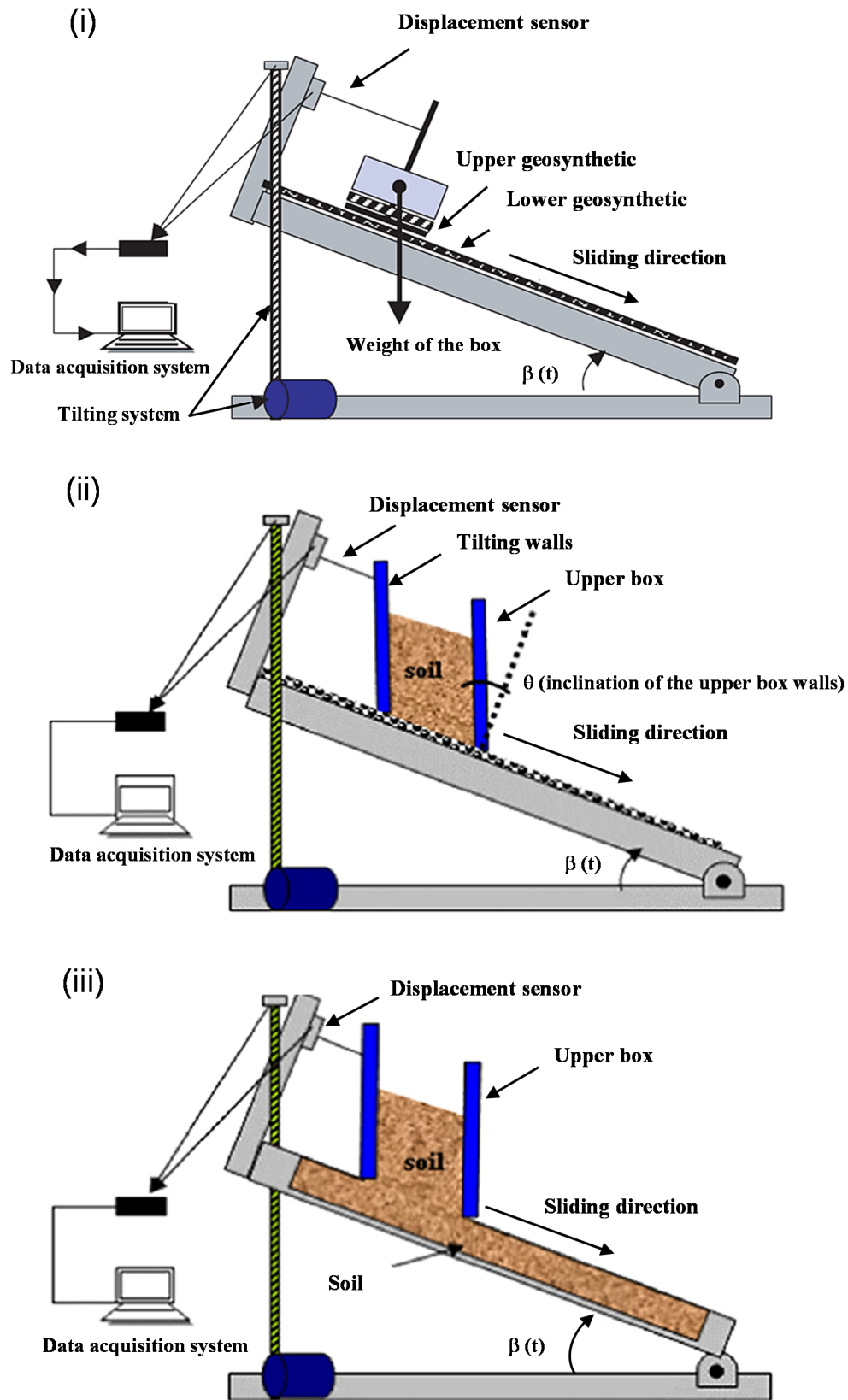


Figure 3.1.1. Inclined plane device at different configurations of the test: a) geosynthetic – geosynthetic interface; b) soil – geosynthetic interface; c) soil – soil interface (after Pitanga et al., 2009; Reyes Ramirez and Gourc, 2003)

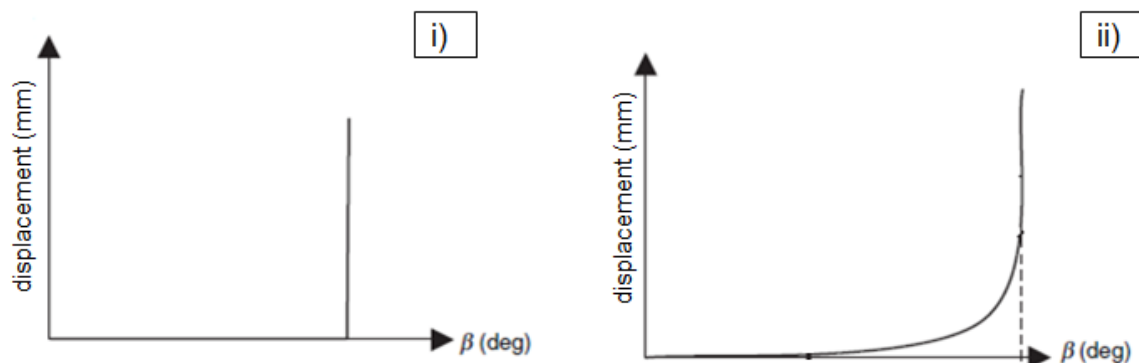


Figure 3.1.2. Inclined Plane test typical diagrams: upper box displacement versus plane inclination angle, β .

Several works on inclined plane test (tilting table or ramp test) can be found in literature (Briançon et al., 2002, 2011; Girard et al., 1990; Gourc et al., 1996; Izgin and Wasti, 1998; Lalarakotoson et al., 1999; Ling et al., 2002; Lopes et al., 2001; Monteiro et al., 2013, Palmeira, 2009; Palmeira et al., 2002; Pitanga et al., 2009, 2011; Reyes Ramirez and Gourc, 2003). In these works, despite the test is based on simple geometrical and mechanical concepts, variations between testing equipment can be found regarding apparatus arrangement, testing methodology, results interpretation and experimental conditions.

The first studies (Girard et al., 1990; Gourc et al., 1996; Izgin and Wasti, 1998; Lalarakotoson et al., 1999; Reyes Ramirez and Gourc, 2003; Wasti and Özdüzgün, 2001) on the inclined plane, mainly investigated the experimental condition of the test, the possibility of testing for every type of interfaces, the selection of the direct shear or tilting test in function of the application, the classification of these tests as index or performance tests.

Subsequently, the attention of researchers was focused on the in-depth investigation of the test by redefining:

- ✓ the procedure (taking into account the influence of some parameters);
- ✓ the interpretation of the results (considering the current kinematic conditions during the entire test);
- ✓ alternative approaches of testing in order to simulate additional conditions (i.e. testing multiple layers during a single experiment, abrasion tests, creep tests) existing in the field.

3.1.2 Literature review

The use of the inclined plane test for the characterization of the interface interaction between soil – geosynthetic and geosynthetic – geosynthetic interaction has been fully demonstrated.

In literature, especially before the European standardization (EN ISO 12957-2, 2005), the incline plane test was conducted with various testing methods and result interpretations. An in-depth bibliographical analysis was carried out on the existing experimental procedures and on the main findings about the interface shear strength assessment by means of the incline plane apparatus.

Firstly, in order to validate the test, several investigations drew a parallel study between the inclined plane and the shear box test results (Girard et al., 1990; Gourc et al., 1996; Izgin and Wasti, 1998; Lalarakotoson et al., 1999; Reyes Ramirez and Gourc, 2003; Wasti and Özdüzgün, 2001) conducted both on soil – geosynthetic and geosynthetic – geosynthetic interfaces.

Girard et al. (1990) studied a failure occurred between lining system at Aubrac Dam (France) along a PVC-needle-punched geotextile interface through the inclined plane (Figure 3.1.3) and the direct shear tests. The authors reported an overestimation of the direct shear test results compared with those obtained through the inclined plane and with those determined by the back – analysis of the failure. Similar conclusions were drawn by Giroud et al. (1990) using an inclined plane as well as direct shear tests on the rough geomembrane - hard geonet and rough geomembrane - nonwoven geotextile interfaces. The normal stresses applied in both devices are between 25 and 160 kPa in the direct shear test and of 0.7 kPa in inclined plane tests. Test results were consistent for the hard geonet - rough geomembrane interface while, for the rough geomembrane – nonwoven needle - punched geotextile interface the results of these two methods of testing yielded quite dissimilar results.

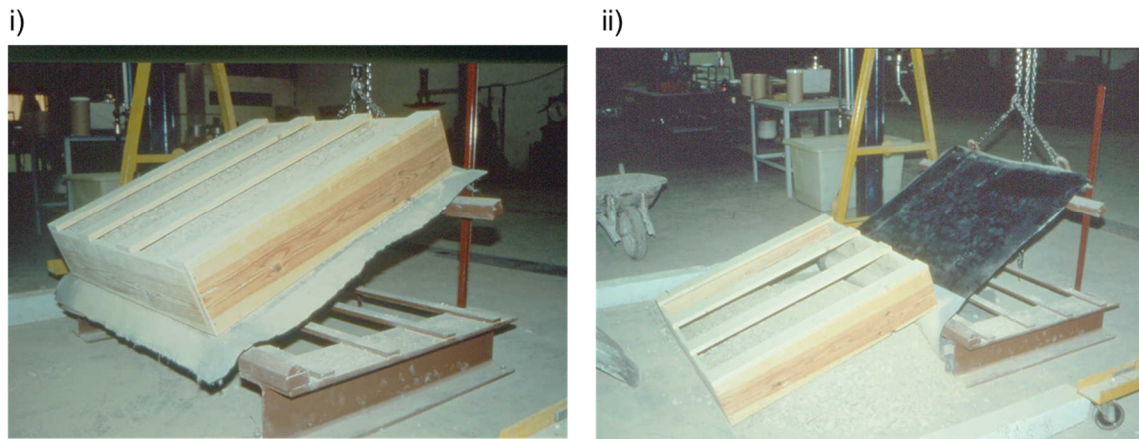


Figure 3.1.3. One of the first inclined plane apparatus: Girard et al. (1990) laboratory tests.

Izgin and Wasti, (1998) compared inclined plane tests with direct shear tests equipped with boxes of different dimensions (from 0.12 m² to 0.6 m²) under a normal stress level ranging from 5 – to 50 kPa, with $\sigma' = 14 - 200\text{kPa}$. The tests were carried out on soil (Ottawa sand) – HDPE smooth and rough geomembrane interfaces considering the sliding angle (i.e. the slope of the inclined board at which the box slides) as the main parameter of the test. They concluded that the direct shear test overestimate the interface shear strength angle, furthermore they noted higher discrepancy if the small size box dimensions are considered. Wasti and Özdüzgün (2001) extended the work of Izgin and Wasti, (1998) assessing the shear strength properties of geotextile-geomembrane interfaces at both devices. They observed that the interface shear behaviour and the agreement between the results of direct shear box and inclined plane tests depend on the type of interface. For smooth geomembrane - geotextile interfaces a good agreement of test results was found. Conversely, for rough geomembrane - geotextile interfaces, direct shear tests predicted significantly higher interface shear strengths than those of inclined board tests as a result of large adhesion intercept values in direct shear envelopes.

Gourc et al., (1996) performed a series of inclined plane and direct shear tests on several types of geomaterials (soils and geosynthetics) under the European project for standardization (CEN – Interlab). In their study, they evaluated the influence of some experimental parameters (i.e. box dimensions, tilting walls, fixation of specimens, placing and compaction of soil) and then they compared the results obtained testing: the standard sand (EN206/196) – (HDPE and PVC) geomembranes, the sand (EN206/196) - non-woven needle punched polyester and woven geotextiles and sand (EN206/196) –geogrids (with thick and with flat ribs) interfaces at both devices. Interpreting the inclined plane test through two kinds of interface shear strength angles (i.e. ϕ_0 defined by the following conditions: the

differential ratio $du/d\beta$ greater than two for more than three datasets with u upper box displacement and β inclination of the plane and ϕ_r corresponding to the angle of the slippage without interruption up to the end of allowed displacement) and comparing them with direct shear test results, it is concluded that both tests give consistent results (difference lower than 10%) if the variation of normal stress level is taken into the account.

Similar conclusions were found by Lalarakotoson et al., (1999) investigating the shear strength at the interface between dense ($Dr = 0.85$) and loose ($Dr = 0.2$) sand (EN206/196) in contact with different geosynthetics (i.e. HDPE smooth and textured geomembranes, with woven and non-woven geotextiles, and with geogrids). The shear strength is considered as purely frictional with no cohesive component and the interpretation of test results is conducted taking into account two main angles: ϕ_{gp} maximum shear strength angle representing the maximum friction resistance obtained for a given σ value (calculated during slip applying static equilibrium); ϕ_{gr} residual shear strength angle after slip for the same σ value. A completely different sliding behaviour is observed testing interfaces involving loose and dense sand (Figure 3.1.4). Independently of the geosynthetic tested, the interfaces involving the loose sand showed a stick-slip behaviour (Figure 3.1.4ii) while, a continuous slip was observed when dense sand was tested (Figure 3.1.4i). These interface behaviours (in particular the stick-slip) can be observed easier in the inclined plane than in the direct shear box test because the different test kinematics.

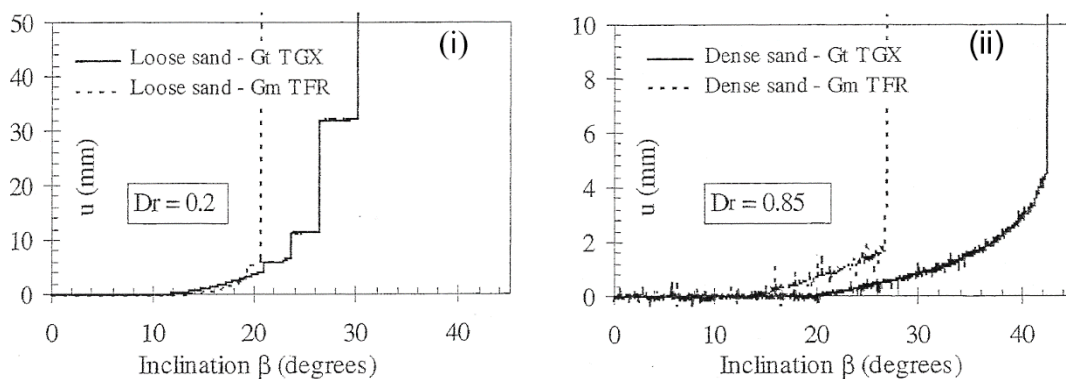


Figure 3.1.4. Typical behaviour obtained according to sand density: i) nonwoven geotextile and smooth geomembrane in contact with loose sand; ii) nonwoven geotextile and smooth geomembrane in contact with dense sand (after Lalarakotoson et al., 1999).

Reyes Ramirez and Gourc, (2003) performed some inclined plane and direct shear tests on geosynthetic – geosynthetic interfaces (see Figure 3.1.5). The materials tested involved a HDPE grid – type geospacer in contact with a non-woven geotextile and a PP and HDPE smooth geomembranes respectively. Assuming the threshold angle ϕ_{gg} (with ϕ value

corresponding to $\tau_{lim}/\sigma' = \tan \phi$ for an upper box displacement equal to 10mm, 50mm and 100mm), as the critical angle determined with the inclined plane test, they found a drop in the shear strength angle passing from the inclined plane to the direct shear test results. They attributed the difference in test results to due to the increase in normal stress acting on the interface; considering this difference, comparable results are obtained.

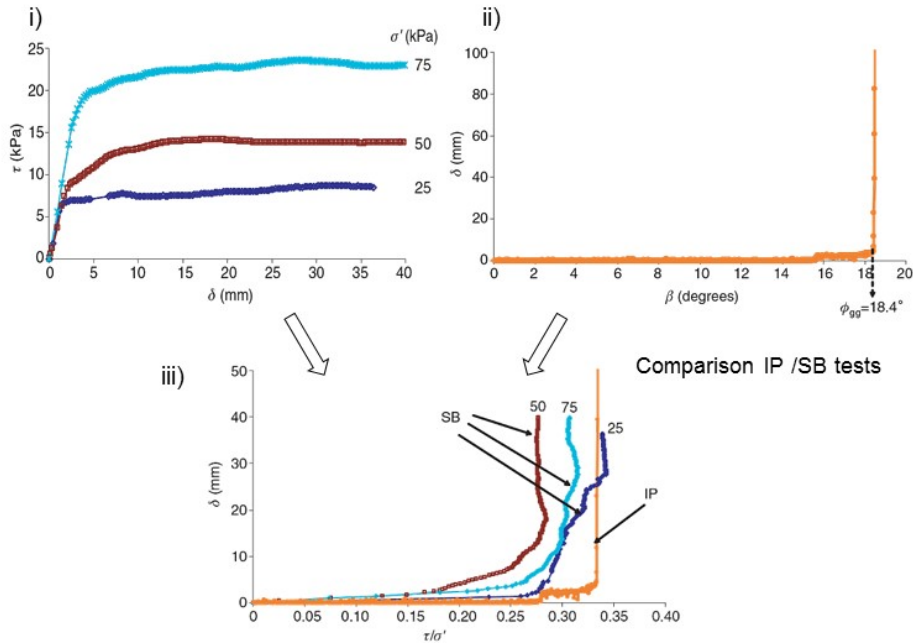


Figure 3.1.5. Test results of woven geotextile –geospacer interface:*i) Shear stress (τ) against displacement (δ) for three different normal stresses (σ_0) through shear box (SB) test; ii) displacement (δ) against slope angle (β) for $\sigma_0 = 5.7$ kPa at the inclined plane (IP) test; iii) attempt to compare IP and SB tests on the same diagram (after Reyes Ramirez and Gourc, 2003).*

After the validation of the inclined plane test, researchers focused the attention on improving test method (Briançon et al., 2011, 2002; Gourc and Reyes Ramirez, 2004; Pitanga et al., 2009), the assessment of test results (Briançon et al., 2002; Palmeira et al., 2002) and the analysis of the influence of other factors (i.e. presence of reinforcement, dry and wet conditions, creep, abrasion, temperature) in shear strength evaluation (Briançon et al., 2002; Monteiro et al., 2013; Palmeira and Viana, 2003; Pitanga et al., 2011; Reyes Ramirez and Gourc, 2003).

Briançon et al., (2002) used a large inclined plane apparatus (Figure 3.1.6) capable to perform tests under dry and wet conditions to develop and apply three different testing methods able to calculate the interface shear strength by (i) measuring the displacement of the upper box as the plane is inclined (test described in the standards); (ii) monitoring the displacement of the upper box and of the tensions in the geosynthetics (fixed to the lower box) in relation to the slope of the plane; (iii) the force required to hold back the upper box

as the plane is inclined. The interfaces tested included soil – geotextiles (different types), geotextile – geomembrane (HDPE smooth and rough) and soil – geomembrane. The results obtained with such apparatus were validated by the authors in comparisons with results from large field experiments. Furthermore, the great influence of seepage of the upper soil on test results was highlighted.

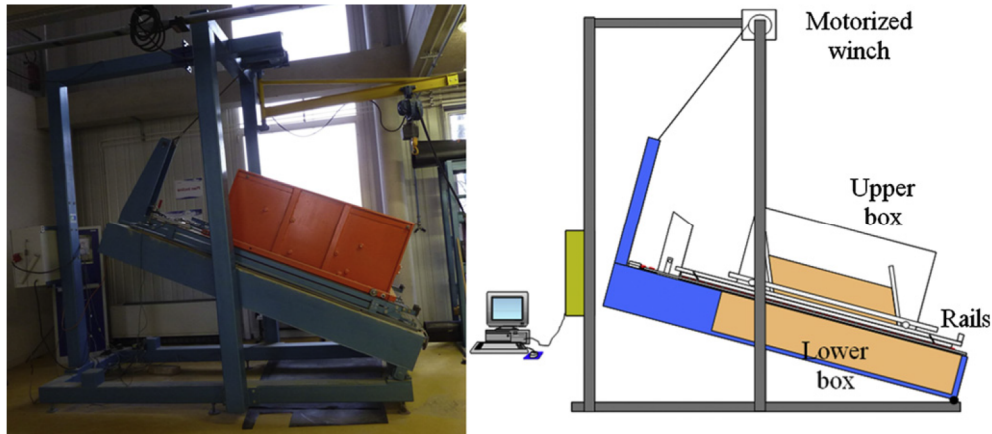


Figure 3.1.6. Large inclined plane apparatus (after Briançon et al., 2011).

Palmeira et al., (2002) presented theoretical and experimental investigations on the use of a large ramp test apparatus to study the interaction between soil and geosynthetics and between different layers of geosynthetics. In this study, the soils tested were a fine and a coarse sand and clayey soil while, several types of geosynthetics were used involving non-woven and woven geotextiles, geogrids, geonets, and PVC and HDPE smooth and rough geomembranes. The tests were carried out in a diverse manner with respect to those presented in literature. In fact, the lower specimen, usually fastened to the plane, was just laid on the ramp (preliminary tests to investigate the friction between the lower specimen and the ramp were conducted) and connected to a load cells through the clamps. In order to investigate the effect of multiple geosynthetic layers in contact with soil, different geosynthetics were put on the lower specimen and through load cells, the tensile load mobilized at each geosynthetics was measured. The upper box was in general filled with soil, just in one configuration a geosynthetic was fastened under the box. The displacement transducer monitored the upper box displacement and the test finished when the complete slide of the box along the ramp is accomplished. Hence, the interface properties are expressed in terms of tensile load of the geosynthetic and considering the upper box displacement versus the plane inclination. The principal findings of this study are: (1) the shear strength angles between geosynthetics occurred first along the weakest interface usually represented by geosynthetic – geosynthetic contact; (2) in terms of displacement,

tests with the fine sand yielded greater box displacements and geosynthetic forces at failure (Figure 3.1.7 i and ii) than those observed in tests with the coarse sand (Figure 3.1.7 iii and iv); (3) the presence of a geotextile layer between a geogrid and a geomembrane increased the box displacements, but caused a reduction of the geomembrane tensile force of 30% in comparison to the situation without the geotextile; (4) the sequence of slippage along interfaces in tests with multiple geosynthetic layers influenced the magnitude and the variation of tensile forces in the underlying geomembrane layer.

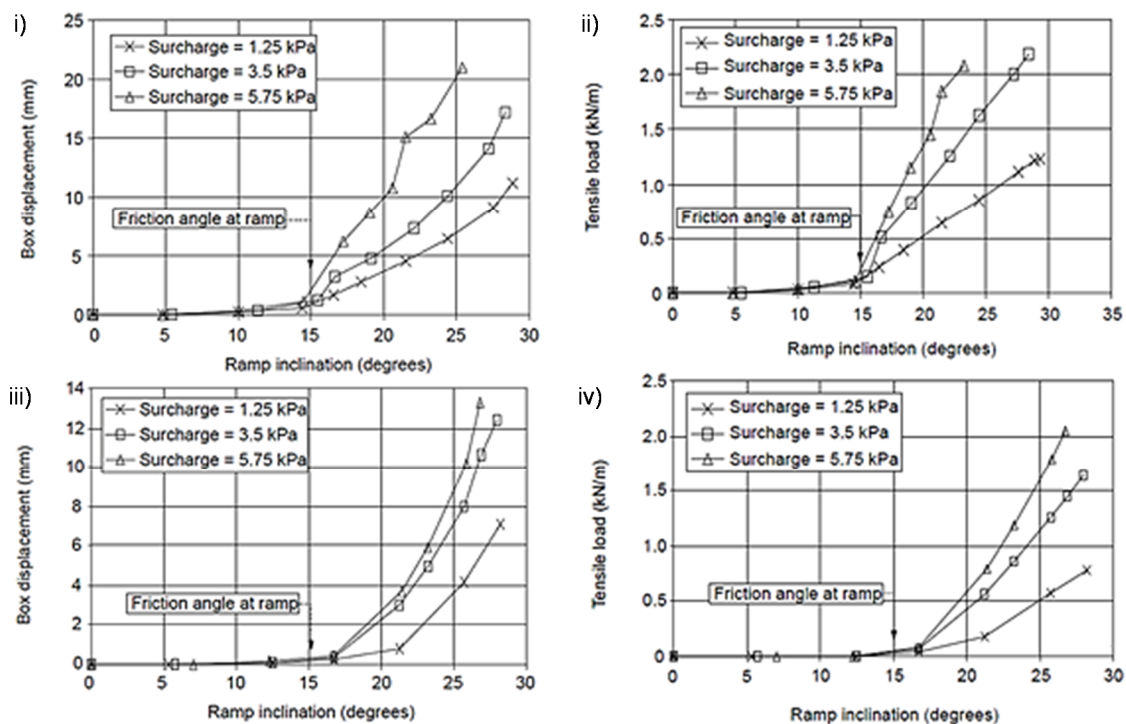


Figure 3.1.7. Box displacement and tensile loads for tests with woven geotextile in contact with fine sand (a) and (b); coarse sand (c) and (d) (after Palmeira et al., 2002)

Using the same large-scale inclined plane device, Palmeira and Viana, (2003) presented an experimental investigation on the use of geogrids buried in cover soils of slopes. The tests involved the use of geogrids with varying values of tensile stiffness and bearing capacity (number of bearing members) installed at different elevations above the geomembrane representing always the lower layer. The influence of the use of a geotextile layer on the geomembrane on the behaviour of the system was also assessed. The results show that the presence of a geogrid in the cover soil, and particularly of a geogrid with a geotextile on the geomembrane, can significantly reduce the deformability of the cover soil and the tensile forces mobilised in the geomembrane, as well as increase the inclination of

the slope at failure. Furthermore, they found that the optimum elevation of the geogrid layer above the geomembrane is of the order of one-third of the cover soil thickness.

Thanks to a reduction of the upper box dimensions with respect to those described by the European Standard (EN ISO 12957-2, 2005), Gourc and Reyes Ramirez (2004) detailed the upper box sliding behaviour and proposed a new interpretation of test results taking into account the dynamic conditions during the upper box slide (as described in §4.1.3). They defined two different friction angles: ϕ_0 and ϕ_{dyn} corresponding to the initialization of the sliding and to the sliding state respectively. Therefore, the static and the dynamic shear strength angles were determined for interfaces involving dense and loose sand (Leucate) in contact with smooth HDPE geomembrane, and HDPE geospacer in contact with smooth HDPE geomembrane and with a non – woven geotextile respectively. For sand-geomembrane results, they found (i) a decrease of ϕ_0 decreasing sand density and (ii) a dynamic friction angle, ϕ_{dyn} , lower than the static one. Furthermore, calculating the dynamic friction angle ϕ_{dyn} , with two different approaches (β continuously increased and fixed at a constant inclination) they found a stabilization of this value which remains almost constant. This fact, demonstrated the “intrinsic” character of the dynamic friction angle for all the interfaces considered. Pitanga et al., (2009) extended the study of Gourc and Reyes Ramirez (2004) considering the interface behaviour between different geosynthetic materials (comprising geotextile, reinforced geomat (geotextile + geomat), geomembrane) and compacted soil (silty sand). The main findings of this study are: (i) the shear strength angles tend to decrease significantly with normal stress ranging between 5.9 kPa and 10.4 kPa; (ii) the gradual and the sudden sliding can be compared, as a first approximation, with the strain hardening and strain softening behaviour observed in direct shear tests; (iii) the interfaces presenting gradual sliding exhibits $\phi_0 < \phi_{dyn}$, while the sudden sliding corresponds to $\phi_0 > \phi_{dyn}$. Furthermore, the behaviour of compacted soil with geosynthetics, led to the observation of failures throughout the cover soil instead of between interfaces. For the first time, some tests were performed to characterize, the soil – soil interface (Figure 3.1.1) showing that the shear zone enters in the layer of the soil support (upper box) and it is not limited to the interface.

Recently, Monteiro et al., (2013), present the results of inclined plane and direct shear tests conducted on different geomembrane products (PVC and smooth and textured HDPE) in contact with a sandy soil prepared at various degrees of saturation. The results presented show that the interface shear strength angle between soil and geomembranes was insensitive to the variation of the soil degree of saturation. A progressive interface failure mechanism was observed in the tests with PVC geomembrane due to the more extensible

nature of this type of geomembrane. The largest values of interface shear strength angles were obtained as expected with the textured HDPE geomembrane, whereas similar lower values were obtained with the smooth PVC and HDPE geomembranes.



Figure 3.1.8. Soil-geosynthetic interface strength characterization on smooth and textured geomembrane interfaces: i) inclined plane and ii) conventional direct shear test; soil - smooth PVC geomembrane after inclined plane tests: (iii) degree of saturation of 5.5% and (iv) degree of saturation of 66%; soil - textured HDPE geomembrane after inclined plane tests: (v) degree of saturation of 5.5% and (vi) degree of saturation of 66% (modified from Monteiro et al., 2013).

Finally, the inclined plane test enables the acquisition of much more complete information than the merely threshold shear strength angle. In light of this, the effect of creep (Reyes Ramirez and Gourc, 2003), of the surfaces abrasion (Carbone et al., 2013; Pitanga et al., 2011; Reyes Ramirez et al., 2002) and of temperature (discussed in § 5.1.7) on the determination of shear strength angles can be assessed.

3.1.3 Influence of boundary and test conditions

A review of the studies reported in literature highlighted the influence of some experimental parameters in the determination of the interface shear strength such as:

- upper and lower box dimensions,
- spacing between upper box and lower specimen,
- non-uniformity of normal stress distribution,
- plane inclination rate.

The influence of each parameter is fully treated below.

3.1.3.1 Box dimensions

The interfaces tested at the inclined plane involve contacts between soil - geosynthetic, geosynthetic - geosynthetic and soil – soil. Therefore, the dimensions of the boxes, especially when testing interfaces involving the soil, should take into the account the need for a contact surface ensuring a representative tested interface, the need to minimize edge effects and the difficulties of placing a large volume of soil.

In literature, the interface area tested varies from 0.005 m² (Ling et al., 2002) to 2.304 m² (Palmeira et al., 2002), depending on the work considered.

Izgin and Wasti, (1998) comparing interface shear strength values of smooth and rough geomembranes in contact with soil obtained, testing specimens of different dimensions (0.12 m², 0.4 mm² and 0.6 mm²), that a minimum area of 0.4 mm² is required to have representative specimens for similar materials.

According to the EN ISO 12957-2 (2005), for the upper box, the minimum dimensions are $L_U = 0.30$ m (length along the displacement direction) and $B_U = 0.30$ m (width) while, for the lower support they are $L_L = 0.40$ m and $B_L = 0.325$ m.

It is worth noting that, the upper box dimensions are coincident with those encountered in large-scale direct shear devices and smaller dimensions of the upper box when testing geosynthetic interfaces can be still representative (taking into the account the size of the mesh for certain type of product as geogrids).

3.1.3.1.1 Spacing between upper box and lower sample

To avoid friction between upper box (filled with soil) and the lower surface (geosynthetic or compacted soil), a spacing (s) between the upper box and lower layer is necessary. The European Standard (EN ISO 12957-2 (2005) suggests $s = 5$ mm, but some tests carried out firstly by Gourc et al., (1996) and subsequently by Pitanga et al., (2009) varying the spacing from 1 mm to 10 mm, showed that the ideal spacing was equal to 6.5 mm.

It should be pointed out that this parameter is not taken into account when testing geosynthetic – geosynthetic interfaces. In fact, in particular it is linked to the size of the grains in order to avoid the leakage of the soil at the interface.

3.1.3.2 Normal stress distribution

In literature, inclined plane tests were performed at different normal stress levels ranging between 1.1kPa (Girard et al., 1990) to 50kPa (Izgin and Wasti, 1998) even if it is typically carried out at 5kPa.

As in other types of tests, the dimensions of the box used to confine the soil in inclined plane tests influences the normal stress distribution on the interface being tested. In particular, the effective normal stress acting on the interface, decreases ($\sigma' = \sigma'_0 \cdot \cos \beta$) as the inclination β increases (Girard et al., 1990; Gourc et al., 1996; Palmeira et al., 2002). Thus, the level of non-uniformity of the normal stress distribution along the interface is directly proportional to the tilting angle and the height of the box centre-mass, and inversely proportional to the box length. Its influence on test results was found to be relevant if progressive failure takes place as typical when testing dense soils on extensible geosynthetic layers (Palmeira et al., 2002).

Therefore, in order to limit the uneven shear stress along the interface tested, Palmeira et al., (2002) suggested large box dimensions while Gourc et al. (1996) adopted the use of inclined walls of the upper box especially when testing soil-geosynthetic interfaces. Thus, the front and rear sides of the upper box are kept parallel and their inclination is fixed in order to be close to the vertical during the sliding phase. To determine the walls inclination, preliminary tests are required. In particular, they indicate that, for the tests with resulting angles between 20° and 35°, the walls should be fixed to 27° while, for angles higher than 35°, the walls can be put to 40°.

Palmeira et al., (2002) performing numerical analyses of inclined plane tests using the computer code PLAXIS and considering different lengths (0.5, 2, and 10 m) of a soil box

with varying thickness and different plane inclinations validated both solutions. In fact, the results obtained by the numerical analyses (Figure 3.1.9) showed that, assuming a trapezoidal normal stress distribution, the difference between maximum and minimum normal stress values increases considerably as the length of the upper box is reduced, while, adopting inclined walls as suggested by Gourc et al. (1996), a very uniform stress distribution is obtained.

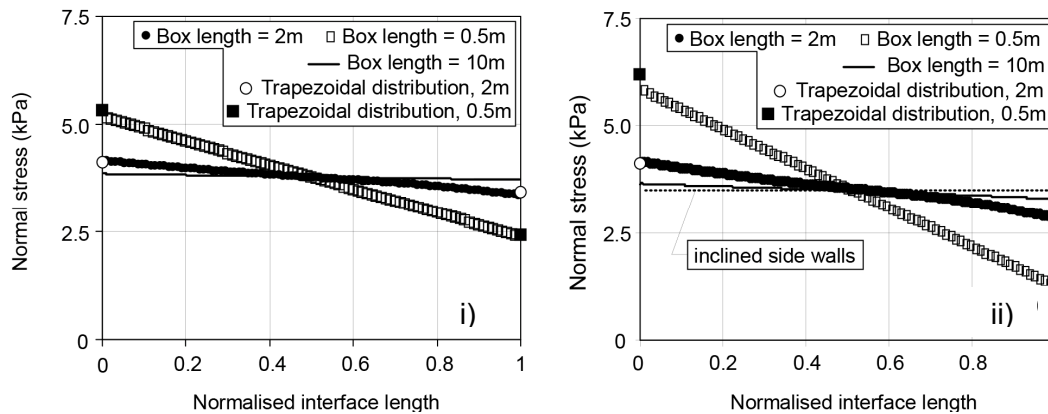


Figure 3.1.9. Normal stress distribution along the interface at 15° (i) and 25° (ii) of plane inclinations (after Palmeira et al., 2002).

3.1.3.3 Plane inclination rate

In general, during the test, the plane inclination is increased at a constant rate ranging, depending on the work considered, from 0.2°/min to 390°/min. The influence of the plane inclination rate, $d\beta/dt$, was investigated in literature by Izgin and Wasti, (1998) performing tests at rising speeds of 1, 1.65 and 6.5°/sec and found no significant effect of speed on test results. Further researches conducted by Reyes-Ramirez et al., (2002) for a range of rates between 0.58°/min to 3.08°/min demonstrated that the plane inclination speed has no significant effect on test results.

The European Standard EN ISO 12957-2 (2005) establishes that, during the test, the plane inclination, β , must be increased at a constant low rate $d\beta/dt = 3.0 \pm 0.5^\circ/\text{min}$.

3.2 SHAKING TABLE TEST

3.2.1 Introduction

The response of a landfill to seismic forces is closely linked to both the slope stability and the interface shear strength between the liner and the soil. The interface shear strength between geosynthetics under dynamic loads has been the subject of recent concern due to the increased emphasis on the design of landfills against possible seismic disturbance.

The conventional Newmark seismic deformation analyses have been used extensively for seismic design of geosynthetic liners and covers for landfills and other waste containment systems (Matasovic. et al., 1998). Such analysis, fully described in § 4.2.2, is based on the study of a rigid block sliding on a plane; when the table is excited by a horizontal motion, inertia forces are transferred to the upper box by means of the mobilized shear strength at the interface. Experimental evidence on the accuracy of conventional Newmark analyses applied to geosynthetic interfaces is noted in literature performing both geotechnical centrifuge testing (Hushmand and Martin 1990) and shaking table tests (Kavazanjian et al. 1991; Yegian and Lahlaf 1992; Yegian and Harb, 1995; Yegian et al., 1995a, 1995b) under a variety of experimental conditions.

The use of geosynthetics in landfill, built in seismic regions, should be considered from two points of view: the base isolation action performed by these discontinuities (Yegian et al., 1995a) and the occurrence of non-predicted slip movements in localised areas of the landfill (Carrubba et al., 2001). These two implications are due to the limited acceleration that these discontinuities can transmit to the overhanging materials. Once this limited acceleration is achieved, relative displacements will occur.

The cyclic tests are performed with direct or torsional cyclic shear devices, while the dynamic tests are usually carried out by large or small scale shaking table apparatus.

In particular, shaking table test permits to study the behaviour of the interfaces under dynamic/seismic loadings conditions. It is possible to have two typical configurations of the apparatus allowing the analysis of geosynthetic-soil (Figure 3.2.1 *i*) or geosynthetic-geosynthetic (Figure 3.2.1 *ii*) interfaces. In the case of soil-geosynthetic interface, the geosynthetic is fixed to the surface and the soil is placed inside the box; in geosynthetic-geosynthetic configuration, one geosynthetic is attached to the table surface and the other is fastened to a solid block placed on top of the table.

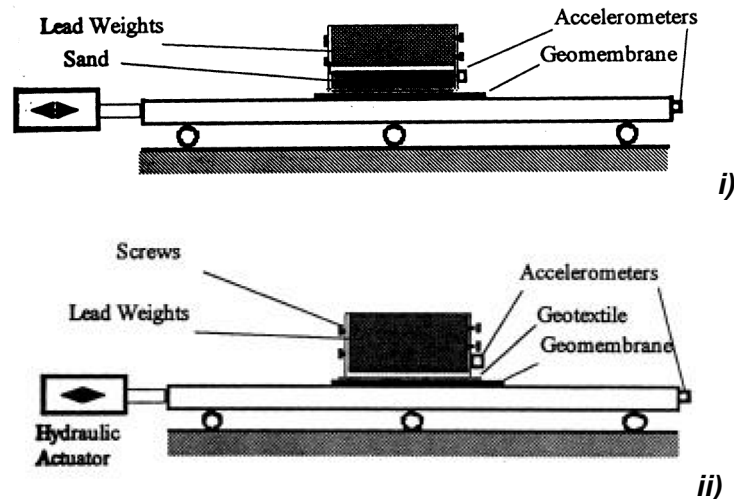


Figure 3.2.1. Schematic diagram of the shaking table setup: (i) geosynthetic-soil interfaces, (ii) geosynthetic-geosynthetic interfaces (Yegian et al., 1995a)

3.2.2 Literature review

A review of previous studies on shaking table tests performed on geosynthetic – geosynthetic or geosynthetic – soil interfaces is presented herein.

The first studies conducted by Kavazanjian et al. (1991) report a slight decrease in interface shear strength with increasing frequency for sinusoidal loading between 1 and 5 Hz for several geosynthetic/geosynthetic interfaces. Conversely, Yegian and Lahlaf (1992) evaluating the dynamic response of geosynthetic interfaces under harmonic excitations, found an increase of these value with respect to the static ones. The main finding of this study is that a limiting shear force, hence acceleration, can be transmitted at the interface (i.e. from a geomembrane to a geotextile in this case). Beyond this limit, relative displacements will occur along the geosynthetic interface. Therefore, in both investigations, response analyses indicate that relative displacement at an interface during an earthquake can have a “base isolation” effect. The use of geosynthetics as base isolators, leads to a reduction of the peak intensity of motions above the interface and shifts the predominant period of the response of the overlying mass.

Yegian et al., (1995a) presented shaking table test results to evaluate the dynamic response of smooth HDPE geomembrane – nonwoven needle-punched geotextile and smooth HDPE geomembrane - soil (Ottawa sand) interfaces excited by harmonic and earthquake excitations. For both interfaces, the materials were placed on a shaking table and the accelerations and displacements (slip) of the lead block weights (12.4 kPa) and of the table were recorded. From the steady state harmonic excitations they found that the

sand - geomembrane interface is able to transmit more shear stress between the two components than the geotextile - geomembrane interface, where smaller slip is observed (Figure 3.2.2).

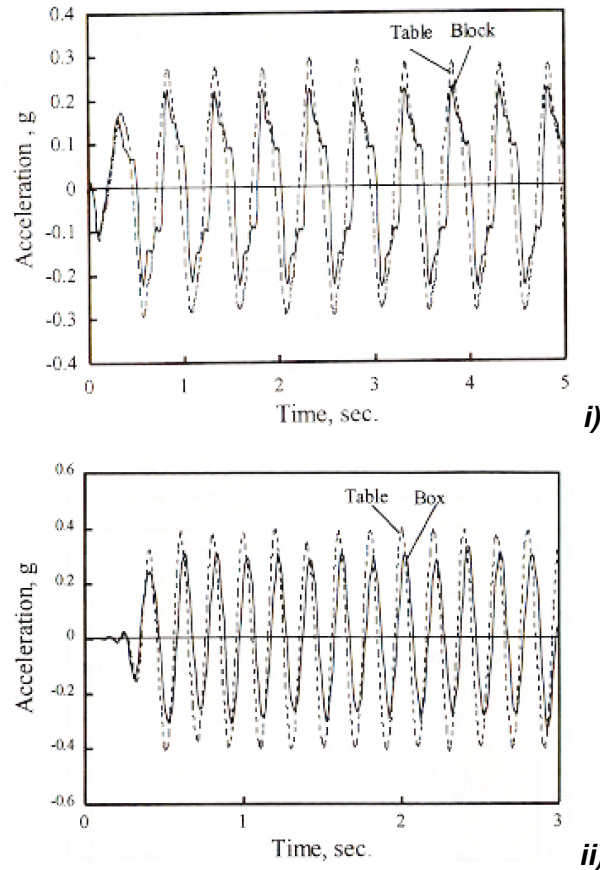


Figure 3.2.2. Block and table accelerations versus time performing shaking table tests: i) smooth HDPE geomembrane – nonwoven needle-punched geotextile interface; ii) smooth HDPE geomembrane - soil (Ottawa sand) interface (after Yegian et al., 1995a).

Subsequently, the dynamic response of the sand - geomembrane interface submitted to earthquake - type excitations was carried out. In the case of earthquake excitations, the response is more complex than for steady state harmonic excitations and it was observed that the yield acceleration was not constant and was difficult to define. This observation is important to bear in mind when deformation analyses for a landfill is performed using methodologies that typically consider a constant yield acceleration associated with a slip surface. Finally, Yegian et al., (1995b) studied the smooth HDPE geomembrane – nonwoven needle punched geotextile also under earthquake excitation and found that the presence of a geosynthetic interface, which has a weaker shear strength properties than that of the surrounding soil or landfill materials, causes absorption of energy through slip acting as base isolator as described by Kavazanjian et al. (1991) and Yegian and Lahlaf

(1992). They also observed that the maximum slip deformation (i.e. the transitory deformation during the relative movement) can be important as the permanent slip if the integrity of a geosynthetic is concerned.

Yegian and Harb, (1995) investigated the dynamic response of geosynthetic interfaces commonly used in municipal solid waste landfill using a shaking table facility, where geosynthetic interfaces placed horizontally and on inclined surface were tested to simulate bottom and cover barriers. Studying the behaviour of the inclined interfaces is more complex than a horizontal one. The main concern was in defining a single parameter of the yield acceleration and relating this value with that measured in a horizontal interface.

De and Zimmie, (1998) estimated the dynamic frictional properties using cyclic direct shear tests, shaking table tests conducted at a normal g-level of 1g as well as at high levels, and on a 100g-ton geotechnical centrifuge. The tests involved eight different interface formed through various combinations of three geosynthetics: geotextile, smooth geomembrane and geonet. First, the different interfaces were tested by monotonic and cyclic (frequency of 0.25 Hz) direct shear tests. Under monotonic loading, shear stress versus displacement curves was almost linear, up to a maximum point (peak). Past this point, the curves dropped, even though some showed a residual stress larger than the peak value. Under cyclic loading, the final shear stresses can be either larger or smaller than the initial value depending on the nature of the interface; moreover, the difference between initial and terminal values is a function of the normal stress applied (Figure 3.2.3).

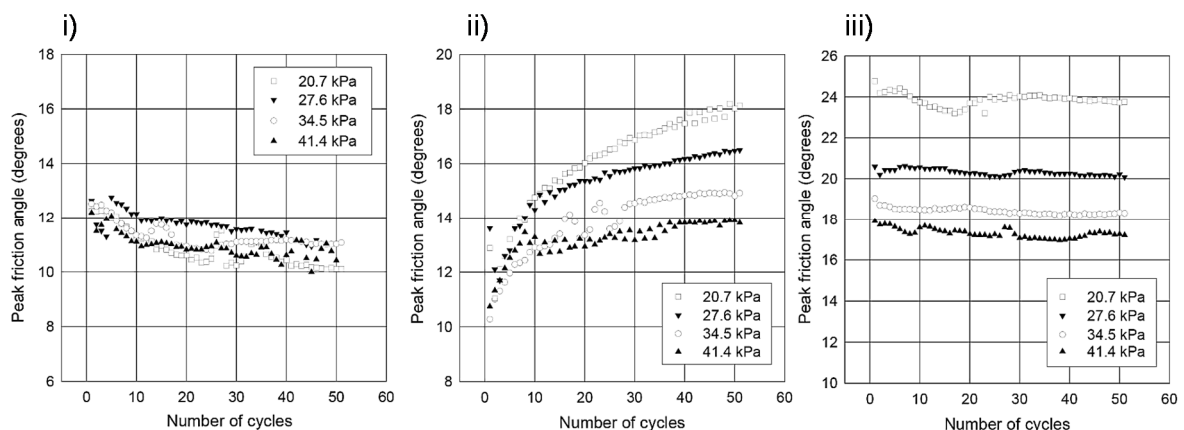


Figure 3.2.3. Variation of the peak friction angle with the number of cycles from cyclic direct shear tests: i) a geotextile over a smooth geomembrane; ii) a smooth geomembrane over a geonet; iii) a geotextile over a geonet (after De and Zimmie, 1998).

The second part of this study addressed shaking table tests, which allow the determination of the dynamic friction angle and therefore, the shear force. Small as well as

large values of acceleration were used for the table excitation. Test results demonstrated that the dynamic behaviour of most interfaces could be complicated by the dependence on the normal stress and on the frequency of excitation. It could decrease or increase depending on the interfaces tested (Figure 3.2.4).

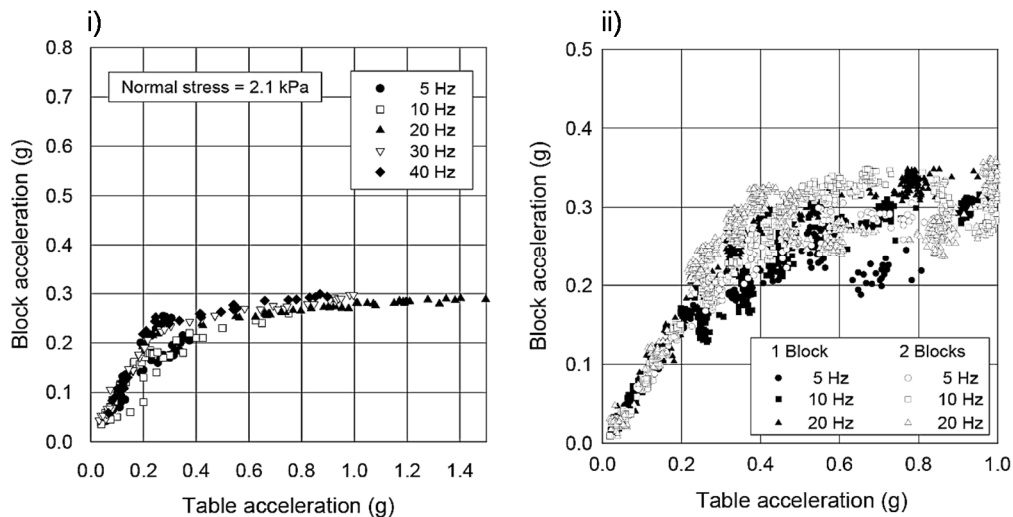


Figure 3.2.4. Block versus table accelerations from shaking table tests: i) a geotextile over a smooth geomembrane; ii) a smooth geomembrane over a geonet (after De and Zimmie, 1998).

Finally, an interesting finding was that the geonet transverse and longitudinal interfaces exhibit the same behaviour indicating that orientation is not a factor in the shear strength at interface.

Yegian and Kadakal, (1998) utilized a shaking table to investigate the frictional interface properties of a smooth HDPE geomembrane and nonwoven geotextile interface. Two test configurations were used, one for cyclic load tests, and the other for shaking table tests. Cyclic load tests were performed to investigate the effect of displacement rates. The difference between friction coefficients at displacement rates of 13 and 64 mm/s indicated that the friction coefficient increases with the sliding velocity. Shaking table tests were used to simulate the dynamic loads induced in the smooth HDPE geomembrane-nonwoven geotextile interface during earthquakes. Tests were run with harmonic base excitations as well as using earthquake-type base excitation resulting in comparable friction coefficients.

Carrubba et al., (2001) proposed a numerical model for predicting the dynamic frictional properties of non-woven geotextile – geonet interface. The model was validated by shaking table test results. Experimental results, plotted in Figure 3.2.5, have confirmed that for a non-woven geotextile-geonet interface dynamic friction is independent from vertical contact

stress; therefore, the Coulomb friction criterion may be adopted also in numerical simulations. However, they concluded that more improvements were necessary in the numerical interface model to describe the little growth of friction during slippage. The authors attributed this latter effect, noticed in the experimental data, to visco-plastic properties of the contact.

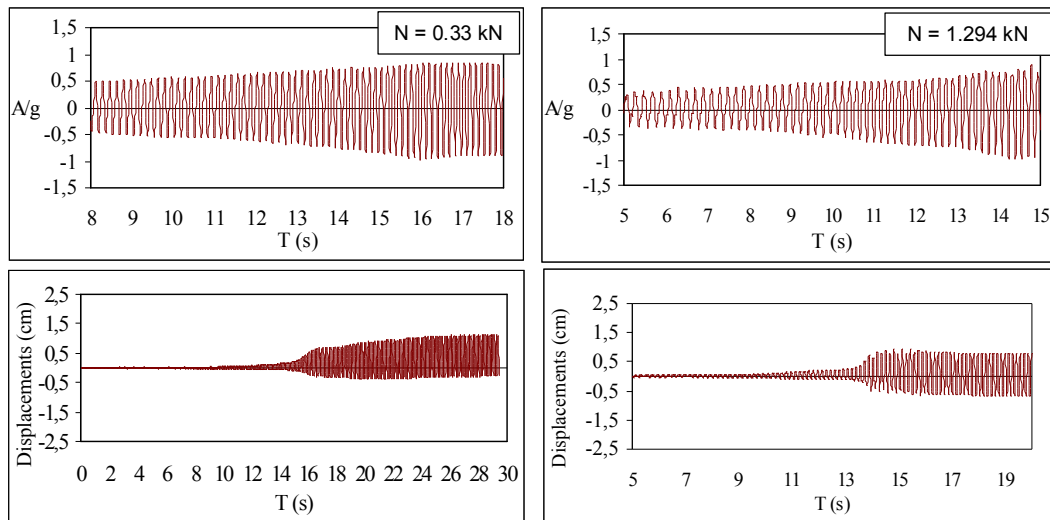


Figure 3.2.5. Shaking table test performed on a geotextile-geonet interface under a contact force $N=0.338$ kN. Block acceleration and displacement with respect to the at rest position (after Carrubba et al., 2001).

Kim (2003) carried out an experimental study of geosynthetic interfaces on a shaking table (fixed block setup) to investigate the relationship between dynamic friction resistance and shear displacement rate of geosynthetic interfaces. The subsequent multiple rate tests showed that geotextile-involved interfaces continue to degrade as displacement increase until they reach an apparent steady-state (or residual strength). Under dry condition, the shear strengths of geotextile-involved interface were observed to increase almost linearly as the displacement rate increases in logarithm scale. However, once submerged with water, the shear strength appeared to be no longer dependent on the displacement rate. This phenomenon appeared to relate to lubrication effect of water trapped inside the interface. Finally, Kim (2003) reported that shear strength parameters are generally not sensitive to the magnitude of normal stress within the range of normal stresses tested (from 7.0 kPa to 63.3 kPa).

Park et al., (2004) tested smooth geomembrane, non-woven geotextile, and two kinds of geocomposite clay liner at the shaking table under dry and wet conditions. During the experimental program, also the influence of normal stress and the frequency of excitation were investigated. While the normal stress and the frequency appeared to have no

significant effect on the dynamic interface friction angle, the dynamic interface friction angle, in wet condition, was $1^\circ - 2^\circ$ lower than that in the dry condition except that for geosynthetic clay liner (GCL) in contact with the smooth geomembrane interface. The authors attributed these variations to the water existing in the interface or to the intruded bentonite from GCL into the interface.

Kotake et al., (2011) performed shaking table tests in order to assess the dynamic behaviour of smooth HDPE geomembrane in contact with non-woven geotextile and gravel – non-woven geotextile interfaces. The table was excited by a sinusoidal excitation varying the frequency and the acceleration. The dynamic friction coefficient of geosynthetic interfaces was given from the critical acceleration corresponding to the beginning of the block motion. The comparison between the dynamic and the static friction coefficients, obtained in the latter case performing inclined plane tests, provides a satisfactory agreement between the results. Furthermore, the authors noticed that, in the case of gravel – geotextile interface, the first slide occurred at the peak friction and the residual one was mobilized afterward.

3.3 INCLINED PLANE AND SHAKING TABLE DEVICE ADOPTED IN THIS STUDY

A typical inclined plane device is composed of an upper box sliding along an inclined support (a lower box or a plane). During the test, the upper box displacement is monitored and the plane inclination, β , is increased at a constant low rate $d\beta/dt = 3.0 \pm 0.5^\circ/\text{min}$ (EN ISO 12957-2, 2005). The vertical stress σ_{v0} , typically lower than 10 kPa, is applied to the upper box and it is maintained constant during the test; consequently, normal stress ($\sigma_{v0} \cos \beta$) decreases as the inclination β increases. When testing a geosynthetic-geosynthetic interface the upper and the lower specimens are fastened to the respective supports. According to the EN ISO 12957-2 (2005), for the upper box the minimum dimensions are $L_U = 0.30$ m (length along the displacement direction) and $B_U = 0.30$ m (width) while, for the lower support, they are $L_L = 0.40$ m and $B_L = 0.325$ m.

The devices used in this research, at LTHE (University of Grenoble) and ICEA Department (University of Padova) laboratories, maintain some common characteristics of the standard experimental conditions (EN ISO 12957-2), such as a sliding upper box, a

plane with inclination increasing at constant rate and vertical stress maintained constant during the test.

The inclined plane available at the LTHE laboratory (Figure 3.3.1) has the following dimensions: $L_U = 0.18$ m and $B_U = 0.70$ m, for the upper box, and $L_L = 1.30$ m, $B_L = 0.80$ m for the lower support (Gourc and Reyes Ramirez, 2004). In the current configuration of this apparatus, the system is fitted according to the recent advances of the research (Carbone et al., 2012). The device is equipped with a displacement sensor that allows measurement of the box displacement, u , while the plane continuously tilts. Furthermore, a force sensor fixed to the plane framework and linked to the upper box by means of a cable, allows monitoring the tensile force, F , after the full box sliding (cable completely stretched).

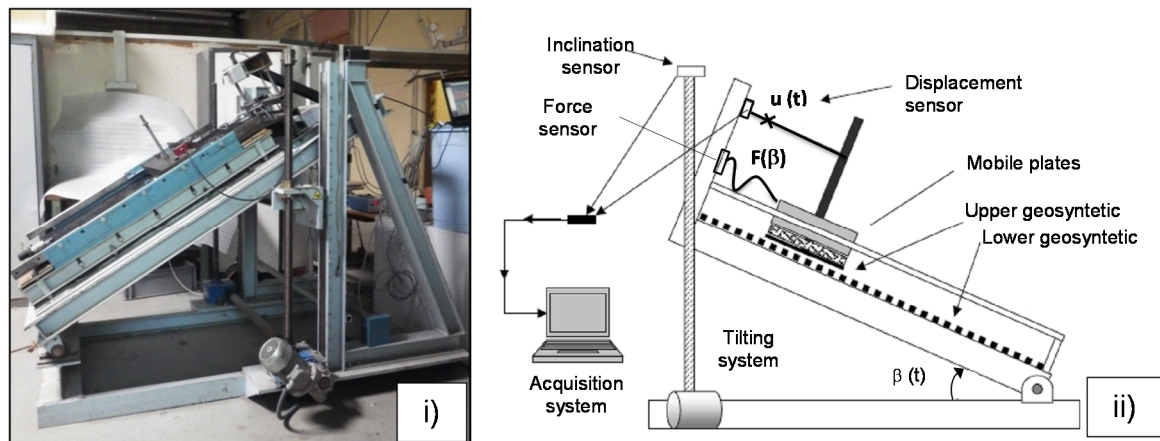


Figure 3.3.1. Inclined Plane of LTHE laboratory: a) photo, b) set up schematization

During the experiment, the parameters recorded by the different sensor displayed in Figure 3.3.2 are:

- Time (milliseconds);
- Plane angle inclination ($^{\circ}$);
- Upper box acceleration (g);
- Upper box displacement (mm);
- Force required to restrain the upper box (N).

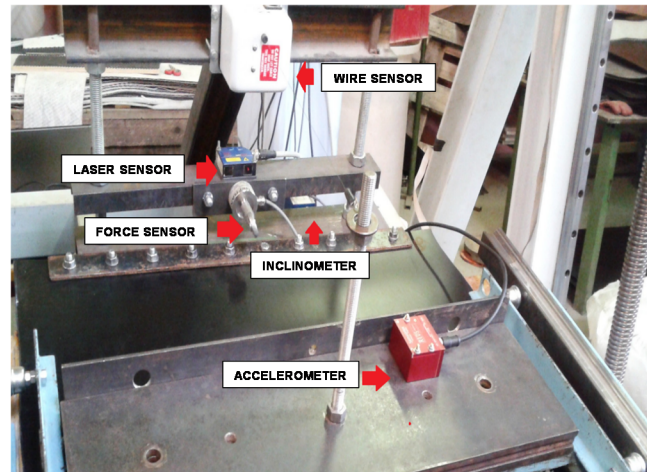


Figure 3.3.2. Sensors utilized in the LTHE inclined plane device.

The shaking table is a device permitting a dynamic approach for the interface shear strength characterization (Figure 3.3.3). The table oscillates back and forth along the horizontal direction; moreover the facility available at the geotechnical laboratory of the ICEA Department (Pavanello and Carrubba, 2012) was designed to simulate static and seismic loading conditions also on slope. For this purpose, an additional reclining support was developed and applied to the horizontal table with the aim of carrying out sliding tests on the inclined support under static and dynamic loading conditions. In order to study geosynthetic - geosynthetic interfaces, one specimen is anchored to the upper box and the other one is fixed to the table. The dimensions of the upper box are $L_U = 0.35$ m, along the displacement direction, and $B_U = 0.20$ m in width. The inclined plane, fixed to the shaking table, has length $L_L = 1.10$ m and width $B_L = 0.24$ m and carries two lateral rails to ensure one-dimensional displacement of the box without introducing additional friction forces. By staking steel plates inside the box, it is possible to apply a vertical stress up to a maximum value of $\sigma_{v0} = 12$ kPa.

The table motion is provided by an oleo-dynamic actuator with a maximum stroke of 0.25 m (peak to peak). The table motion is controlled by a servo-valve with time stepping 10^{-3} s and it is monitored by a high precision dynamic displacement transducer. The box movement is monitored by an accelerometer and by a displacement transducer.

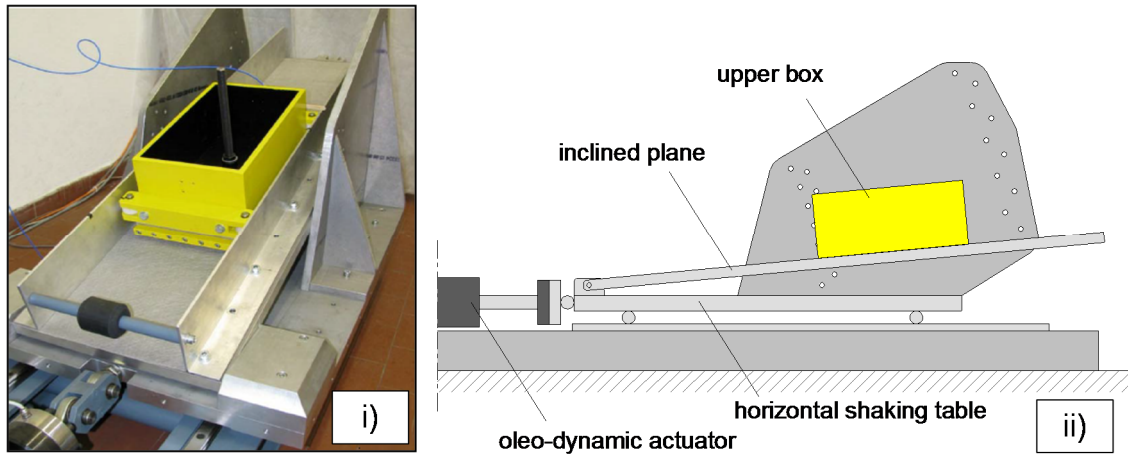


Figure 3.3.3. Shaking Table of ICEA laboratory: a) photo, b) arrangement.

4 TEST PROCEDURES AND INTERPRETATION

4.1 INTERFACE SHEAR STRENGTH EVALUATION THROUGH THE INCLINED PLANE TEST (STATIC LOADING)

4.1.1 Introduction

Due to the various characteristics of inclined plane equipment available in literature, differences in performing the test and interpreting the results were observed.

Some studies considered the interface shear strength angle as the angle corresponding to the inclination of the plane at which the box slides (Girard et al., 1990; Izgin and Wasti, 1998; Wasti and Özdüzgün, 2001). Gourc et al., (1996) and Lalarakotoson et al., (1999), differentiated the interface shear strength angle corresponding to the beginning of the slide with respect to that at failure (i.e. when the upper box arrives at the end of the plane). Finally, in some researches (Briançon et al., 2002; Palmeira and Viana, 2003; Palmeira et al., 2002) the interface shear strength properties, were assessed in terms of tensile load exerted on the geosynthetics and of the upper box displacement versus the plane inclination.

In this context, the European Standard (EN ISO 12957-2, 2005) tried to homogenise the procedure and the result interpretation describing the method and the shear strength angle determination. Advances in the interpretation of test results, highlight that the evaluation of the interface friction according to EN ISO 12957-2, here defined as “Standard Procedure”, can lead to a misleading value because this method does not consider the actual kinematic conditions existing during the test. Furthermore, as noted by Carbone et al., 2013a, 2013b, the Standard Procedure, restrict the interface behaviour to a merely threshold value.

Two other procedures were suggested by Gourc and Reyes Ramirez (2004) and Briançon et al. (2011), here called “Displacement Procedure” and “Force Procedure” respectively. The “Displacement Procedure” focuses the attention on the analysis of the box motion during the sliding. According to this method, two interface friction angles are determined: the first corresponding to the beginning of the slide and the second during the sliding approximating the motion as uniformly accelerated. The main limit of this method is to assess the upper box acceleration, especially when is very low to be calculated.

The “Force Procedure”, tried to overcome experimental problems encountered in the Displacement Procedure only considering the upper box static conditions instead of the dynamic one. In this case the characteristic friction angle is calculated measuring the force required to restrain the upper box maintained stationary along the plane, while it continuously tilts.

Both procedures were proposed as an alternative to the Standard Procedure. Consequently, different studies (Briançon et al., 2011; Gourc and Reyes Ramirez, 2004; Pitanga et al., 2011, 2009) comparing the friction angles determined according to the different procedures, are available in literature. As outlined by Carbone et al., (2013a, 2013b) and fully demonstrated in the present research work, these angles cannot be compared as they belong to different kinematic conditions. In fact, these values are complementary and provide information about the interface behaviour under static, pseudo-static and dynamic conditions.

In this research, after a presentation of the European Standard procedure, a comprehensive methodology feasible, easy to perform and able to fully characterize the evolution of the friction angle during the entire duration of the test, is proposed and discussed. Hence, the so called “Unified Inclined Plane Procedure (UIPP)” is validated and applied to different geosynthetic interfaces.

4.1.2 The Standard Procedure (EUROPEAN STANDARD EN ISO 12957-2. 2005)

The European Standard is nowadays the unique standard that rules the inclined plane test. The EN ISO 12957-2 proposes an interpretation of the test here called “Standard Procedure”. According to this standard, the interface friction angle is evaluated at the plane inclination, β_{50} , corresponding to a conventional displacement of 50 mm of the upper box. The conventional upper box displacement, $u = 50$ mm, was chosen because, test results

obtained testing the same interfaces at different European laboratories (experimental program: CEN-Interlab), showed that the determination of $\beta_{50} = \phi_{\text{stan}}$ from the displacement – inclination curve gave satisfying results in terms of repeatability (Gourc et al., 1996).

The relative friction angle, ϕ_{stan} , is calculated considering a static equilibrium along the plane direction:

$$W \cdot \sin \beta_{50} - N \cdot \tan \phi_{\text{stan}} = 0 \quad 4.1-1$$

$$W \cdot \cos \beta_{50} = N \quad 4.1-2$$

where N is the reactive force balancing the normal component of the weight, W , of the upper box.

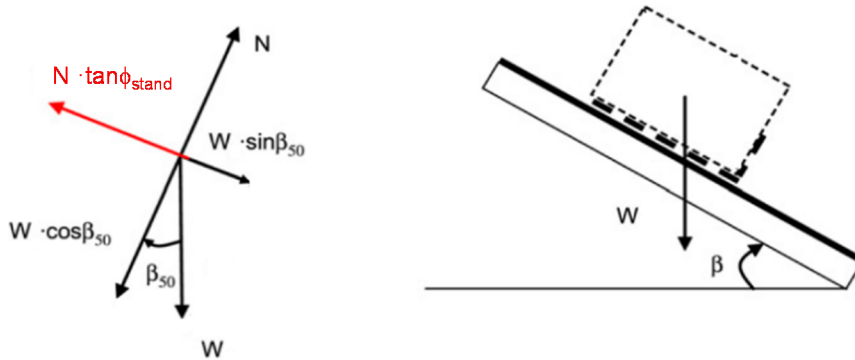


Figure 4.1.1. Balance of forces in the “Standard Procedure”.

The value of ϕ_{stan} , is obtained combining Equations 4.1-1 and 4.1-2 to yield the following:

$$\tan \phi_{\text{stan}} = \tan \beta_{50} \quad 4.1-3$$

Since the standard interface friction angle, ϕ_{stan} , is evaluated during the upper box sliding, the static interpretation is not fully correct and the friction angle could be overestimated in many cases (Briançon et al., 2011; Carbone et al., 2012; Gourc and Reyes Ramirez, 2004; Pitanga et al., 2009).

4.1.3 Unified Inclined Plane Procedure (UIPP)

The Unified Procedure, here presented, allows assessing the frictional properties of different interfaces at various kinematic conditions. Comparing with the standard box, a cable with a tensile force sensor fixed to the frame is added. In this way, the force required to stabilize the upper box can be assessed. The new test consists of three following steps (Figure 4.1.2):

- **Step 1.** The plane starts to tilt and the box keeps still, the cable of the force sensor is loose and the interface shear strength is not completely mobilized until the box starts to slide. At the beginning of the motion, the static interface friction angle ϕ_0 , corresponding to the beginning of the motion can be determined at the end of this step.
- **Step 2.** The upper box slides along the plane. During the sliding the cable is still loose ($u < u_{lim}$) and the dynamic shear strength angle, ϕ_{dyn}^{IP} , can be evaluated according to the type of motion. For comparison, the standard friction angle, ϕ_{stand} , can be also determined when the box reaches the displacement of 50 mm.
- **Step 3.** The upper box moves until the cable is completely stretched (for $u = u_{lim}$). In this step the retaining force $F(\beta)$, necessary to hold back the box, is continuously measured meanwhile the plane increases the tilting angle β . At this stage the friction angle ϕ_{lim} is evaluated.

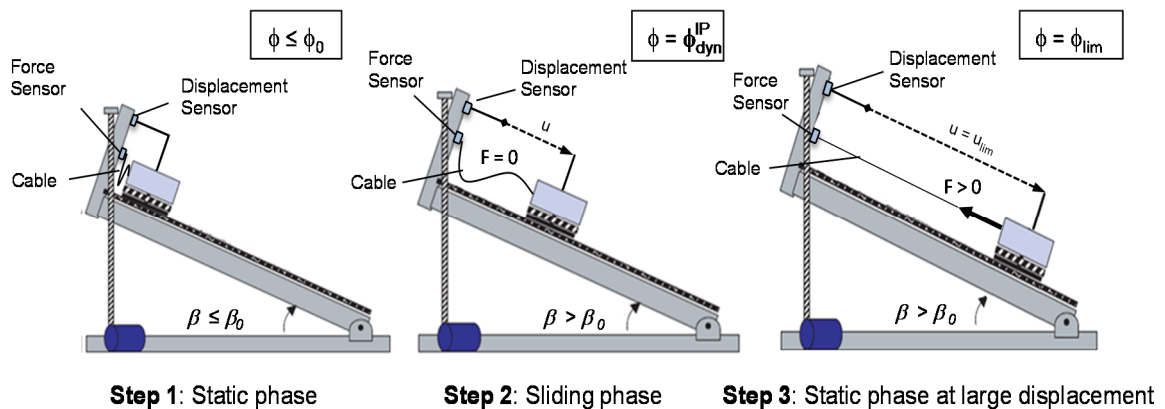


Figure 4.1.2. Unified Inclined Plane Procedure (UIPP): Steps of the test.

4.1.3.1 Interface shear strength parameters assessed at every step of the Unified Inclined Plane Procedure (UIPP)

As soon as the box begins to move (end of Step 1), the static friction angle, ϕ_0 , is evaluated by the equilibrium equation:

$$\tan \phi_0 = \tan \beta_0 \quad 4.1-4$$

being β_0 the plane inclination at which the sliding starts.

During Step 2, the sliding motion of the upper box can be described by the following dynamic equilibrium:

$$mg \cdot \sin \beta(t) - mg \cdot \cos \beta(t) \cdot \tan \phi_{dyn}^{IP}(t) = m \cdot a_{box}(t) \quad 4.1-5$$

where m is the mass of the upper box, β is the plane inclination angle, a_{box} is the box acceleration and g the gravity acceleration. Starting from Equation 4.1-5, the dynamic friction angle can be calculated:

$$\tan \phi_{dyn}^{IP}(t) = \tan \beta(t) - \frac{1}{\cos \beta(t)} \cdot \frac{a_{box}(t)}{g} \quad 4.1-6$$

The general relationship of Equation 4.1-6 takes different forms depending on the type of box motion. As found by Gourc and Reyes Ramírez, (2004), the interface shear strength mobilization during the slide can occur according to three main mechanisms: sudden sliding, jerky and gradual sliding (Figure 4.1.3).

Furthermore, this research work introduced the box acceleration, a_{box} , as the principal feature to characterize them. Depending on the acceleration of the box, two end-members can be considered:

- *Sudden sliding*: the upper box slides abruptly with an approximately constant acceleration ($a_{box} \cong a_{const} > 0$);
- *Gradual sliding*: the upper box slides with an approximately zero acceleration ($a_{box} \cong 0$) and, consequently, the velocity is almost constant.

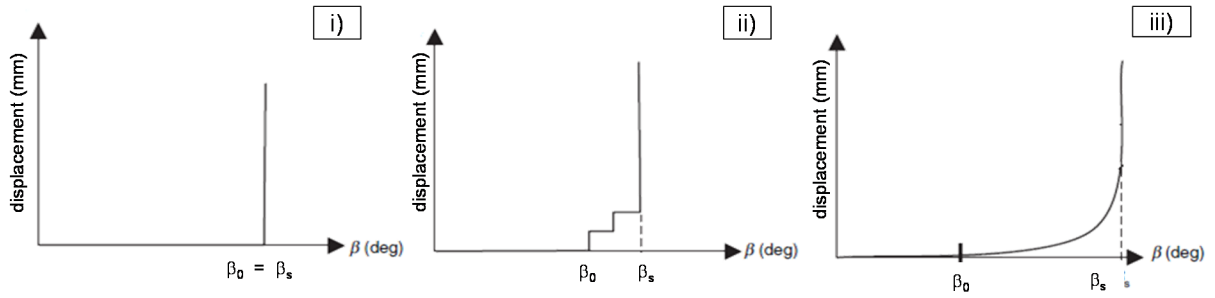


Figure 4.1.3. Different mechanisms of sliding observed in the inclined plane test: i) sudden sliding; ii) jerky sliding and iii) gradual sliding (adopted from Gourc and Reyes Ramirez, 2004).

Figure 4.1.4 summarizes the principal features of both sliding. Note that, as the plane inclination increases linearly with the time ($\beta = at + b$), the x axis of Figure 4.1.4 can be plotted versus the time as well as in the plane inclination β .

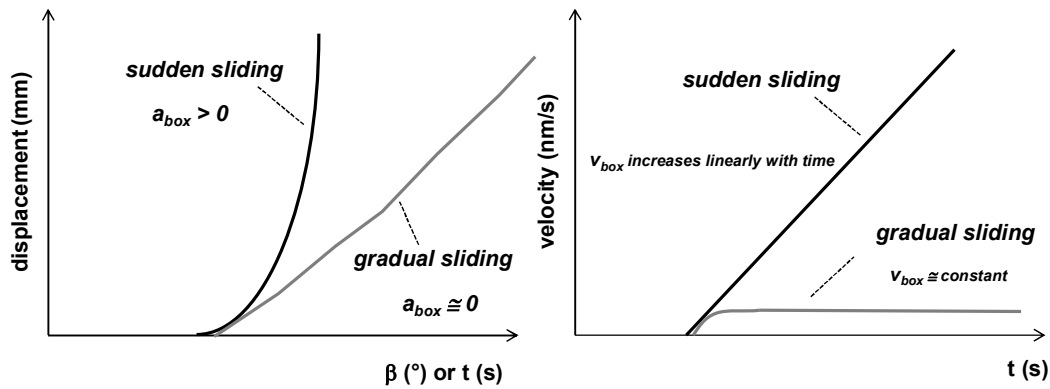


Figure 4.1.4. Kinematic characteristics in gradual and sudden sliding.

In the sudden sliding, the ϕ_{dyn}^{IP} can be obtained approximating the motion as uniformly accelerated. The upper box acceleration can be directly measured by an accelerometer or deduced from the progressive displacements monitored in the time. In this case, when the motion becomes uniformly accelerated, the displacement history versus time can be fitted by a parabola and the constant acceleration a_{const} is obtained through a double derivation. If the motion is fast enough, the variation of the inclination β during the dynamic phase can be considered negligible, so that β may be assumed as constant ($\beta = \beta_s$) during the motion. In this case, the Equation 4.1-6 can be rewritten as proposed by Gourc and Reyes Ramirez, (2004) in the “Displacement Procedure”:

$$\tan \phi_{dyn}^{IP} = \tan \beta_s - \frac{1}{\cos \beta_s} \cdot \frac{a_{const}}{g} \quad 4.1-7$$

where β_s is the current inclination of the plane. Since in this case the motion is fast enough, β_s value is generally equal to β_0 , and the dynamic friction angle ϕ_{dyn}^{IP} is lower than the static one (Equation 4.1-4), being $\tan \beta_s \equiv \tan \phi_0$

On the other hand, some interfaces display a motion with very slow velocity so that β cannot be considered constant and the acceleration cannot be appreciated. This limitation is encountered in those interfaces showing a gradual type of sliding (Briançon et al., 2011). Thus, as in this case the acceleration is close to zero, Equation 4.1-6 can be written as:

$$\tan \phi_{dyn}^{IP}(t) = \tan \beta(t) \quad 4.1-8$$

where ϕ_{dyn}^{IP} is not a unique value because β is changing continuously. It is worth noting that, being the upper box acceleration equal to zero, this angle would properly be defined as kinetic friction angle.

For this reason, since the interpretation may be sometimes difficult, an alteration of Step 2 is suggested. In this supplementary experimental approach, the plane is fixed at different inclinations, greater than β_0 and the box is released to move along the plane (Figure 4.1.5). This allows the analysis of the box motion under the hypothesis of β constant, irrespective of the time. In this case, the dynamic friction angle can be calculated according to Equation 4.1-7 if the uniformly accelerated movement is established (i.e. usually when $\beta \gg \beta_0$) or according to Equation 4.1-8 with $\beta(t) = \beta_{fixed}$ if the uniform motion is evaluated (i.e. typically when β is only slightly higher than β_0).

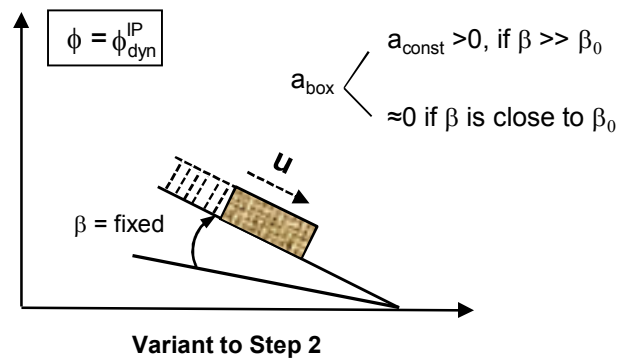


Figure 4.1.5. Schematization of the Variant to Step 2.

After the complete sliding of the upper box along the plane, until $u = u_{lim}$, when the box is stationary, Step 3 starts. At this stage, following the “Force Procedure” (Briançon et al., 2011), the force required to restrain the upper box is measured by means of the sensor

linked to the cable, meanwhile the plane continues to tilt. In this phase, being the rotation of the plane very slow ($d\beta/dt \cong 3.0^\circ/\text{min}$), inertial forces are negligible and the mobilized friction angle ϕ can be obtained from the equilibrium equation:

$$\tan \phi(t) = \tan \beta(t) - \frac{F(\beta(t))}{W \cdot \cos \beta(t)} \quad \mathbf{4.1-9}$$

where W is the weight of the upper box and F is the tensile load of the cable. Despite the increase of the tilting angle β , a stabilization of the friction angle is observed (Briançon et al., 2011): the force $F(t)$ increases with $\beta(t)$ in such a way that $\tan \phi$ does not vary further. After stabilization the constant value of the friction angle is indicated as ϕ_{lim} .

It is worth noting that preliminary tests were carried out in order to assess the effect of the limit displacement value, u_{lim} , on the friction angle. In the study reported by Carbone et al., (2012) that extends the previous work of Briançon et al., (2011), it could be noticed that, even varying the limit displacement u_{lim} between 30 cm and 90 cm, the limit friction angle ϕ_{lim} results do not change.

Furthermore, it should emphasize that the main advantages of applying the UIPP are:

- ✓ the possibility to investigate, during a single test, the transition of the interface shear strength from static - dynamic – pseudo-static conditions
- ✓ the assessment of the static friction mobilized at little deformations, ϕ_0 , or at very large displacement, ϕ_{lim} , that is particularly relevant since geosynthetic interfaces generally show strain softening behaviour (as reported in §1.4.1),
- ✓ the study of the own mode of failure of the interface (i.e. the test is not displacements controlled).
- ✓ This latter point is important as the proper characterization of the sliding behaviour not only permits the determination of the dynamic friction angle but also allows identifying the failure mode and consequently the mechanical characterization of the interface (i.e. if the interface displays a strain-softening rather than a hardening behaviour).

4.2 INTERFACE SHEAR STRENGTH EVALUATION USING THE SHAKING TABLE (DYNAMIC LOADING)

4.2.1 Introduction

The dynamic shear strength is investigated by the shaking table device of the ICEA laboratory in the vibrating configuration at zero inclination β of the table.

The test permits to investigate the interface response to harmonic and earthquake-type excitations.

The most common approach to interpret the test is the conventional Newmark seismic deformation analysis. The formal conventional Newmark seismic deformation analysis described below (§ 4.2.2), involves the following five simplifying assumptions:

1. the potential failure mass is rigid (noncompliant);
2. the dynamic response of the failure mass is not influenced by (coupled with) the permanent displacement (slip) that occurs along the failure surface;
3. permanent displacement accumulates in only one direction (the downslope direction);
4. the vertical component of the ground motion does not influence the calculated permanent displacement;
5. the yield acceleration of the potential failure mass is constant.

A study conducted by Matasovic. et al., (1998), indicates that the assumptions of decoupled seismic response and displacement and of a noncompliant failure mass are of relatively minor significance for assessing the deformation potential of geosynthetic covers for solid waste landfills and other facilities, resulting in overprediction of the permanent displacement by at most a factor of 2. Furthermore, the effects of two-way sliding and of the vertical component of the earthquake ground motions are, for most practical purposes, negligible for geosynthetic cover systems. On the other hand, the effect of degradation of the yield acceleration from an initial peak value to an ultimate residual value may be an important factor impacting the accuracy of conventional Newmark analyses which use a constant yield acceleration.

In this context, a test procedure able to fully characterize the dynamic friction angle and its degradation during the entire test is presented and discussed. In the study, harmonic excitations are applied to the table and the effect of the dynamic parameters on the interface shear strength, such as: acceleration, frequency and duration of loading are evaluated.

4.2.2 Theory

The most common approach to seismic deformation analysis is the rigid block sliding on a plane approach described by Newmark (1965). In such an analysis, schematically illustrated in Figure 4.2.1 it is assumed that a rigid box of weight $W = mg$, where m is the mass of the block and g is the acceleration due to gravity, is resting on a horizontal plane. When the table is excited by a horizontal acceleration, a seismic inertia force, T_{in} , is induced in the box. At any time t , the forces at the box-table interface are:

$$W + N = 0 \quad 4.2-1$$

$$T_{in}(t) = m \cdot a_{box}(t) \quad 4.2-2$$

$$T_{friction}(t) = N \cdot \mu(t) = mg \cdot \mu(t) \quad 4.2-3$$

where N is the interface normal force, T_{in} is the box inertia force and $T_{friction}$ is the shear strength of the interface expressed using the Mohr-Coulomb failure criterion with $\mu(t)$ representing the friction angle coefficient of the box-table interface.

By force equilibrium, the interface shear force is equal to the box inertia force and the interface normal force is equal to the weight of the box. The magnitude of T_{in} is limited by the shear strength of the interface, $T_{friction}$.

If the table acceleration, $a_{table}(t)$, does not exceed the critical acceleration of the box (a_{crit}), the box oscillates in synchronism with the table [$a_{box}(t) = a_{table}(t)$]:

$$T_{in}(t) = m \cdot a_{box}(t) \quad 4.2-4$$

$$T_{friction}(t) = mg \cdot \mu(t) = mg \cdot \tan \delta(t) \quad 4.2-5$$

with δ interface friction not completely mobilized.

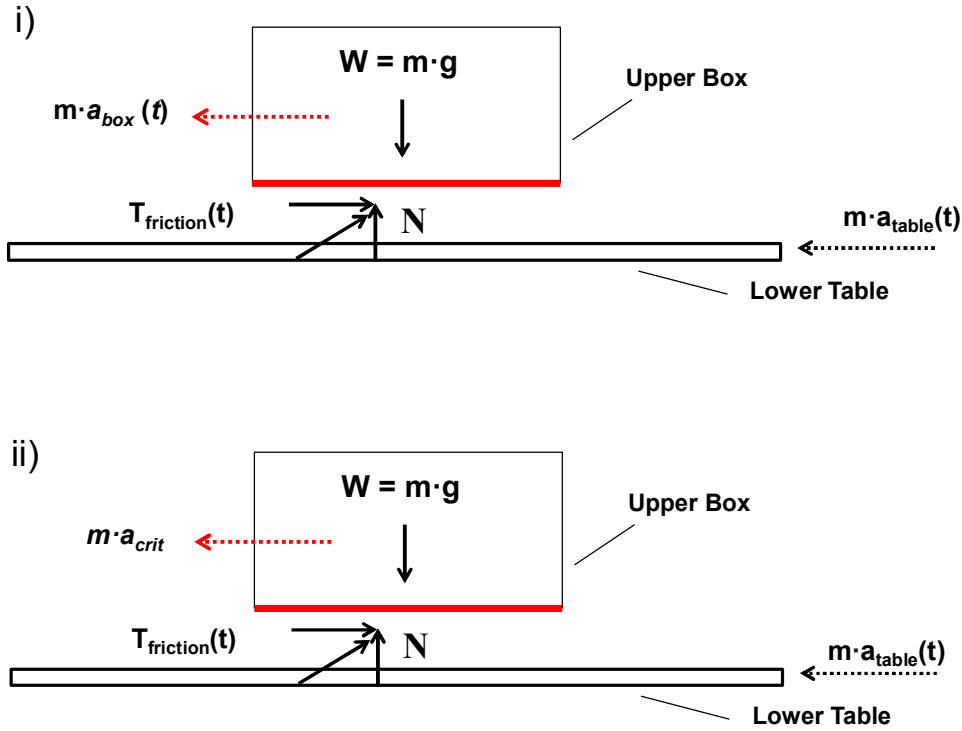


Figure 4.2.1. Freebody diagram of the shaking table test: i) no relative displacement between the box and table; ii) during the relative displacement between the box and table.

When the box acceleration $a_{box}(t)$ reaches a_{crit} , the shearing resistance of the interface is fully mobilized and the box begins to slide with respect to the table. In the case of horizontal plane, the dynamic equilibrium allows to evaluate the dynamic friction coefficient according to the following expression:

$$T_{in}^* = m \cdot a_{crit} \quad 4.2-6$$

$$T_{friction}^* = mg \cdot \tan \phi_{dyn}^{ST} \quad 4.2-7$$

$$\tan \phi_{dyn}^{ST} = \frac{a_{crit}}{g} \quad 4.2-8$$

where a_{crit} is the maximum acceleration sustainable by the box before the relative sliding displacement; exceeding this value no more acceleration can be transferred to the box. T_{in}^* and $T_{friction}^*$ are the box inertia force and the shear strength of the interface when the relative movement starts.

Because it represents the threshold above which relative movement (yielding) between the block and plane occurs, a_{crit} is usually called in literature as “yield acceleration” and the ratio a_{crit}/g is usually known as seismic coefficient k_h as reported in §1.3.2.

As illustrated in Figure 4.2.2, the classical Newmark procedure may be implemented by numerical integration of the acceleration and velocity time histories of the block. First, the velocity time history of the relative movement between the box and the table is calculated by integration of the acceleration time history of the table modified by the yield acceleration of the block, with relative block movement (sliding) beginning each time the yield acceleration is exceeded in the out-of-slope direction and continuing until zero velocity is calculated for the sliding block. The cumulative relative displacement of the sliding block is then calculated by integrating the relative velocity time history, as shown in Figure 4.2.2. Since relative displacement of the block only occurs between the time the earthquake acceleration exceeds the yield acceleration in the out-of-slope direction and the time when the relative velocity drops to zero, quiet intervals exist during which there are no increments in the relative block displacement. The value of relative displacement at the end of the base plane excitation is commonly called the (calculated) permanent seismic displacement or (calculated) seismic deformation.

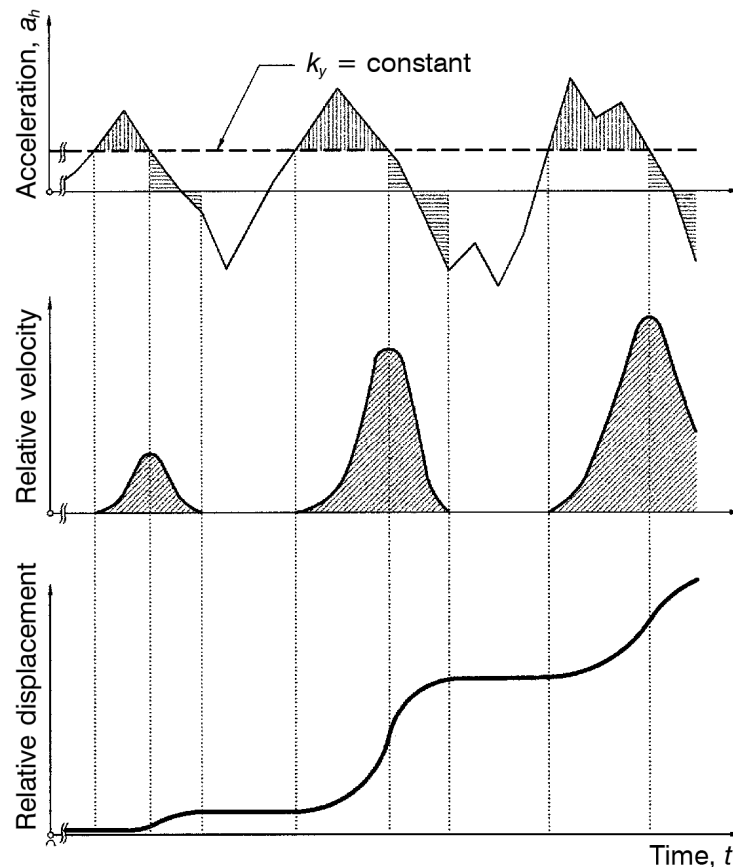


Figure 4.2.2. Classical Newmark analysis integration scheme (after Matasovic. et al., 1998)

4.2.3 Shaking table test procedure under harmonic excitations

In the experimental program the table is forced by a sinusoidal signal. In order to avoid an abrupt start of the table motion, the acceleration of the table at any time t , $a_{\text{table}}(t)$, was increased gradually up until the maximum acceleration amplitude called a_{max} was reached.

The sinusoidal signal can be expressed as follows:

$$a_{\text{table}}(t) = a_{\text{max}} \cdot \sin(2\pi ft) \cdot \left(1 - e^{-\xi \frac{f}{f_0} t}\right) \quad 4.2-9$$

where a_{max} represents the maximum amplitude of the table acceleration, t the time in seconds, f is the frequency (Hz) and the term $\left(1 - e^{-\xi \frac{f}{f_0} t}\right)$ determines the Table Acceleration Rate (TAR) as shown in Figure 4.2.3.

In particular, regarding the TAR, ξ is the increase factor, f_0 is the reference frequency (1 Hz) and the term (f/f_0) allows reaching the maximum acceleration a_{max} for the same number of cycles also by modifying the frequency. This means that, even changing the frequency of vibration, the interface is subjected to a given value of the table acceleration, for the same number of cycle of the table.

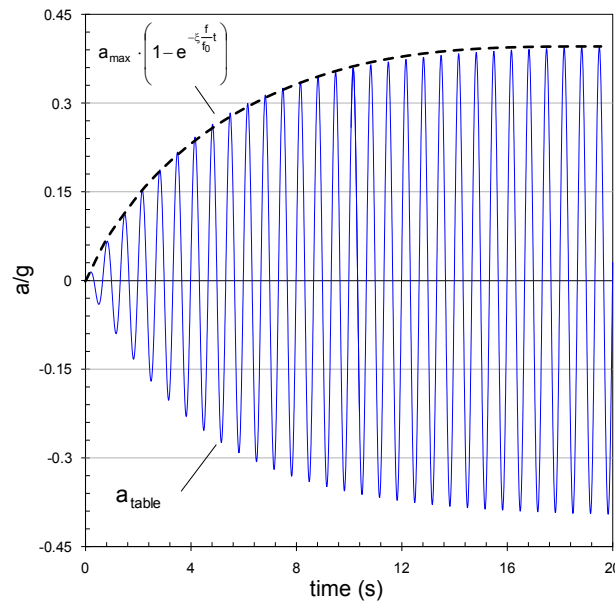


Figure 4.2.3. A typical sinusoidal “standard signal” for dynamic loading ($f = 1.5$ Hz, $a_{\text{max}} = 0.4g$, $\xi = 0.15 \text{ s}^{-1}$).

Following this approach, the test can be divided into three main phases (Figure 4.2.4):

- **Phase 1** (Initial phase): the table acceleration increases and the upper box and the table move in synchronization, $a_{\text{box}}(t) = a_{\text{table}}(t)$;
- **Phase 2** (Transitory phase): $a_{\text{table}}(t)$ continues to increase following the selected TAR but at a given time, it exceeds the shearing resistance of the interface [$a_{\text{table}}(t) > a_{\text{box}}(t) = a_{\text{crit}}(t)$] determining the start of the relative movement between the box and the table;
- **Phase 3** (Steady-state phase): the table acceleration reaches the steady state value (a_{max}) while the box continues to slide along the table.

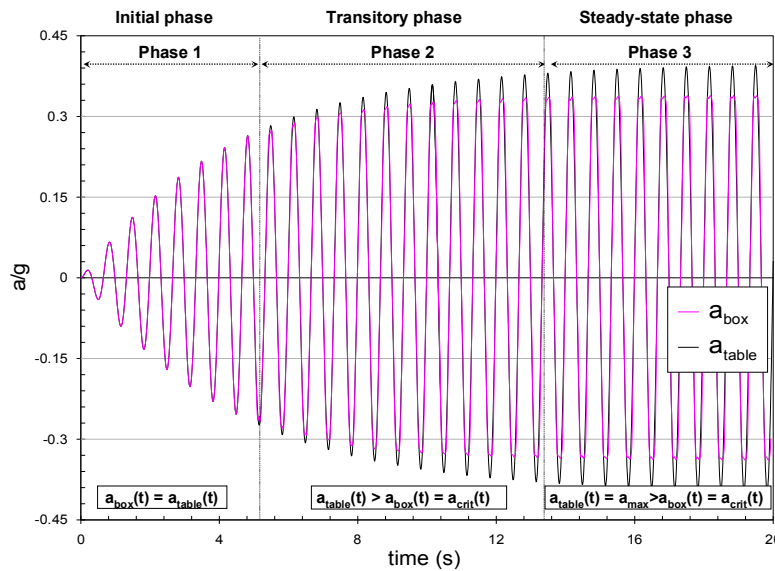


Figure 4.2.4. Main phases of the shaking table test procedure under harmonic excitation.

It must be pointed out that if the table acceleration a_{table} attains a_{crit} during the steady-state phase (Phase 3), Phase 2 does not occur.

The characteristic parameter during the transitory phase (Phase 2) is the TAR while Phase 3 is characterized by the amplitude of the table acceleration, a_{max} generally determined through preliminary tests.

Furthermore, the parameter N_d , referring to the number of cycles accomplished by the box during the sliding, was introduced in order to study the evolution of the dynamic friction coefficient, $\tan \phi_{\text{dyn}}^{\text{ST}}$, during Phases 2 and 3. Taking into account that the first cycle ($N_d = 1$) corresponds to the first relative movement of the box with respect to the table ($a_{\text{box}}(t) = a_{\text{crit}}$)

the dynamic friction coefficient $\tan\phi_{\text{dyn}}^{\text{ST}}$ is evaluated during the entire test by considering $N_d = 10, 25, 50$ and 100 cycles.

In this investigation, except for some specific sets of tests, the interfaces were subjected to a sinusoidal signal, here called “standard signal”. The standard signal is characterized by:

- TAR with an increase factor ξ , equal to 0.15 s^{-1} ,
- maximum acceleration a_{max} fixed at $0.4g$ (preliminary test to determine a_{max} are required),
- frequency ranging between $1.5 \text{ Hz} \leq f \leq 6 \text{ Hz}$.

For each frequency, the applied vertical stress, σ_{v0} , varies in the range between 5 kPa and 12 kPa .

Other complementary tests were carried out in order to verify the possible influence of the TAR (Phase 1 and 2). For this reason, a series of tests where the table was forced by sinusoidal signals characterized by different TARs (here called “faster” where $\xi = 0.3 \text{ s}^{-1}$ and “slower” with $\xi = 0.05 \text{ s}^{-1}$, with respect to the “standard” one) was performed.

The effect of the amplitude of the table acceleration, a_{max} , (Phase 3) on the interface response was also studied by performing tests at a fixed frequency (3Hz), maintaining the same TAR, and varying a_{max} in the range between $0.34g$ up to $0.60g$.

4.3 SET OF AVAILABLE DIFFERENT FRICTION ANGLES

Summarizing, the following symbolism are selected to indicate the friction angles obtained through the inclined plane and the shaking table tests:

- ✓ ϕ_0 : maximum mobilized static interface friction angle (Inclined Plane - Step1 – Equation 4.1-4);
- ✓ $\phi_{s \tan d}$: interface friction angle as defined by EN ISO 12957-2 (2005) (Inclined Plane - Step2 – Equation 4.1-3);
- ✓ $\phi_{\text{dyn}}^{\text{IP}}$: dynamic interface friction angle (Inclined Plane - Step2 - Equations 4.1-7 and 4.1-8);
- ✓ ϕ_{lim} : static friction angle after the interface shearing (Inclined Plane - Step3 – Equation 4.1-9).

- ✓ $\phi_{\text{dyn}}^{\text{ST}}$: dynamic friction angle evaluated with the shaking table test (Equation 4.2-8).

5 TEST RESULTS AND DISCUSSION

5.1 INCLINED PLANE TEST RESULTS

A wide experimental program was conducted at the Inclined Plane, in particular focusing the attention on the interface shear strength characterization of geocomposite drains layer overlying geomembranes.

The experimental program was carried out with the following aims:

- Development and validation of the Unified Incline Plane Procedure (UIPP);
- Interpretation of the interface shear strength with the current kinematic conditions;
- Analysis of the parameters influencing the interface shear strength (as described § 1.4.2).

Table 5.1.1 summarizes the parameters analysed in every test series specifying for each case the experimental conditions.

Table 5.1.1. Schematization of the parameter analysed in the experimental program at the Inclined Plane device (Geosynthetics presented in § 2.3.1).

Parameter analysed	Inclined Plane device	Interface tested GSY _{UP} /GSY _{DOWN}	Vertical stress σ_{v0} (kPa)	Temperature (°C)
Repeatability	LTHE	a. GTX - GMB _S	5	10,20 and 30
		b. GNT - GMB _S	5	10,20 and 30
		c. GCD _N - GMB _S	5	10,20 and 30
		d. GCD _N - GMB _{TMH}	5	20
		e. GCD _W - GMB _{TMH}	5	20
		f. GCD _N - GMB _{RMH}	5	20
		g. GCD _W - GMB _{RMH}	5	20
Reproducibility and size effect	LTHE and ICEA	a. GTX - GMB _S	5	20
Upper box velocity	ICEA	a. GTX - GMB _S	0.08	20
			0.8	20
			5	20
			12	20
		GNT - GMB _S	5	20
		GCD _N - GMB _S	5	20
Normal stress	ICEA	a. GTX - GMB _S	0.08	20
			0.8	20
			5	20
			12	20
Mechanical damage (wear test)	LTHE and ICEA	a. GTX - GMB _S	5	20
	LTHE	b. GNT - GMB _S	5	20
	LTHE	c. GCD _N - GMB _S	5	20
	LTHE	d. GCD _N - GMB _{TMH}	5	20
	LTHE	e. GCD _W - GMB _{TMH}	5	20
	LTHE	f. GCD _N - GMB _{RMH}	5	20
	LTHE	g. GCD _W - GMB _{RMH}	5	20
Temperature	LTHE	a. GTX - GMB _S	5	10,20 and 30
		b. GNT - GMB _S	5	10,20 and 30
		c. GCD _N - GMB _S	5	10,20 and 30

5.1.1 Description and interpretation of a typical test

A total of more than 100 inclined plane tests involving geocomposite drains in contact with smooth and textured geomembranes were carried out. Each pair of geosynthetics is designated by a letter (see Table 5.1.1).

As discussed in §4.1.3.1, the failure mechanism can be mainly classified following to two basic behaviours: *sudden sliding* and *gradual sliding* (Figure 4.1.3 and Figure 4.1.4).

Therefore, the mechanical characterization of the interface properties is different depending on the mode of sliding (see § 4.1.3.1).

For this reason the analysis of inclined plane test results will be divided, in the following section, into two main categories:

- Interfaces displaying *gradual sliding* behaviour;
- Interfaces displaying *sudden sliding* behaviour.

In the first case, the interfaces involved are *a*, *b* and *c* while, in the second case, the behaviours of interfaces *d*, *e*, *f* and *g* are presented (Table 2.3.2).

It should be pointed out that all the tests presented in this section, except for §5.1.6 were the mechanical damage on wear specimens is treated, are performed on virgin specimens, along the machine direction under a vertical stress σ_{v0} equal to 5 kPa.

5.1.1.1 Analysis in the case of gradual sliding

5.1.1.1.1 Typical diagrams

Unified Inclined Plane Procedure

The Unified Inclined Plane Procedure (UIPP) was applied to the GTX – GMB_s, GNT – GMB_s and GCD_N – GMB_s interfaces (Figure 5.1.1). The typical diagrams of inclined plane test results are shown in Figure 5.1.2 in terms of the upper displacement (*u*) versus plane inclination angle (β) on the left side for Steps 1 and 2 and in terms of force versus the plane inclination angle (β) on the right side for the Step 3 (as described § 4.1.3.1). The corresponding evolution of the mobilized friction angle ϕ was also inserted on the diagrams during Step3.

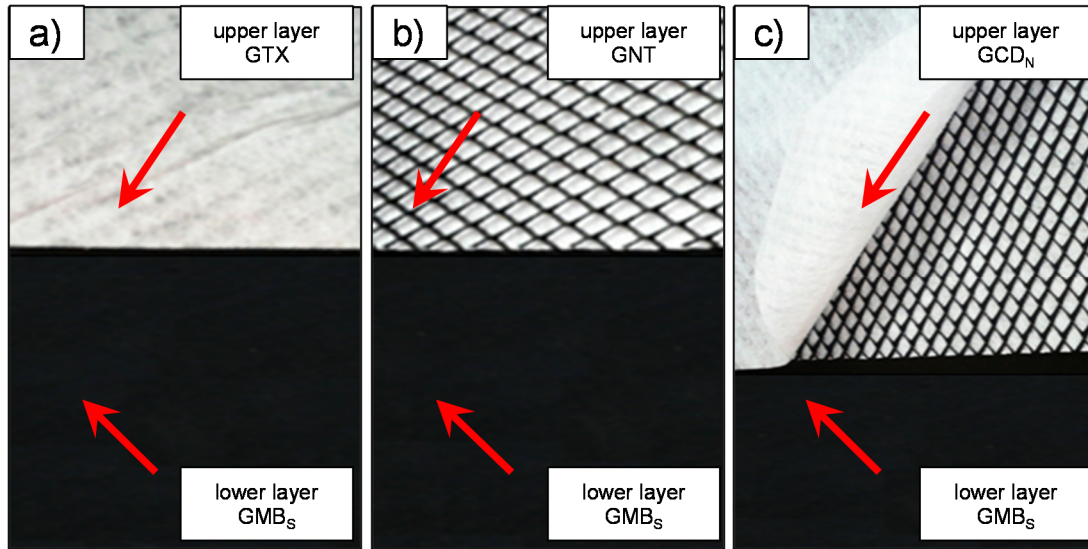


Figure 5.1.1. Upper and lower layers of interfaces involving the geotextile (GTX), the geonet (GNT) and the geocomposite drain (GCD_N) in contact with the smooth geomembrane GMB_S: a) GTX - GMB_S; b) GNT - GMB_S; c) GCD_N - GMB_S.

Whatever the different shape of the curves, for the three interfaces tested, the box motion can be mainly classified as a gradual sliding type (Step 2). The motion is characterized by a very low and almost constant velocity (Figure 5.1.2 a₁, b₁ and c₁), while the plane is continuously tilting.

During the test, the interface friction angles can be determined as follows. At the beginning of the motion, for an initial upper box displacement of 1mm the static interface friction ϕ_0 (Step 1) is conventionally determined. Afterwards the gradual sliding takes place (Step 2) resulting in a very low upper box velocity ($a_{\text{box}} \cong 0$). The dynamic (or kinematic) friction angle $\phi_{\text{dyn}}^{\text{IP}}$ is given by Equation (4.1-8) and is continuously increasing since it varies with the inclination of the plane. In these tests, uniformly accelerated motion is not occurring until $u = u_{\text{lim}}$ (600 mm). Only a lower bound for $\phi_{\text{dyn}}^{\text{IP}}$ is get from these tests reported in Table 5.1.2. Furthermore, during Step 2, in order to compare test results, also the “Standard Procedure” is carried out and, for an upper box displacement of 50 mm, the standard interface friction angle (ϕ_{stand}) is determined according to Equation 4.1-3. At the end of the sliding (Step 3) the cable is totally stretched ($u = u_{\text{lim}}$), here for a displacement u_{lim} equal to 600 mm. The tensile force in the cable equilibrates the box and, as previously discussed (§ 4.1.3.1), the mobilized shear strength (Equation 4.1-9) attains a constant value corresponding to the limit interface friction angle ϕ_{lim} (Figure 5.1.2 a₂, b₂ and c₂).

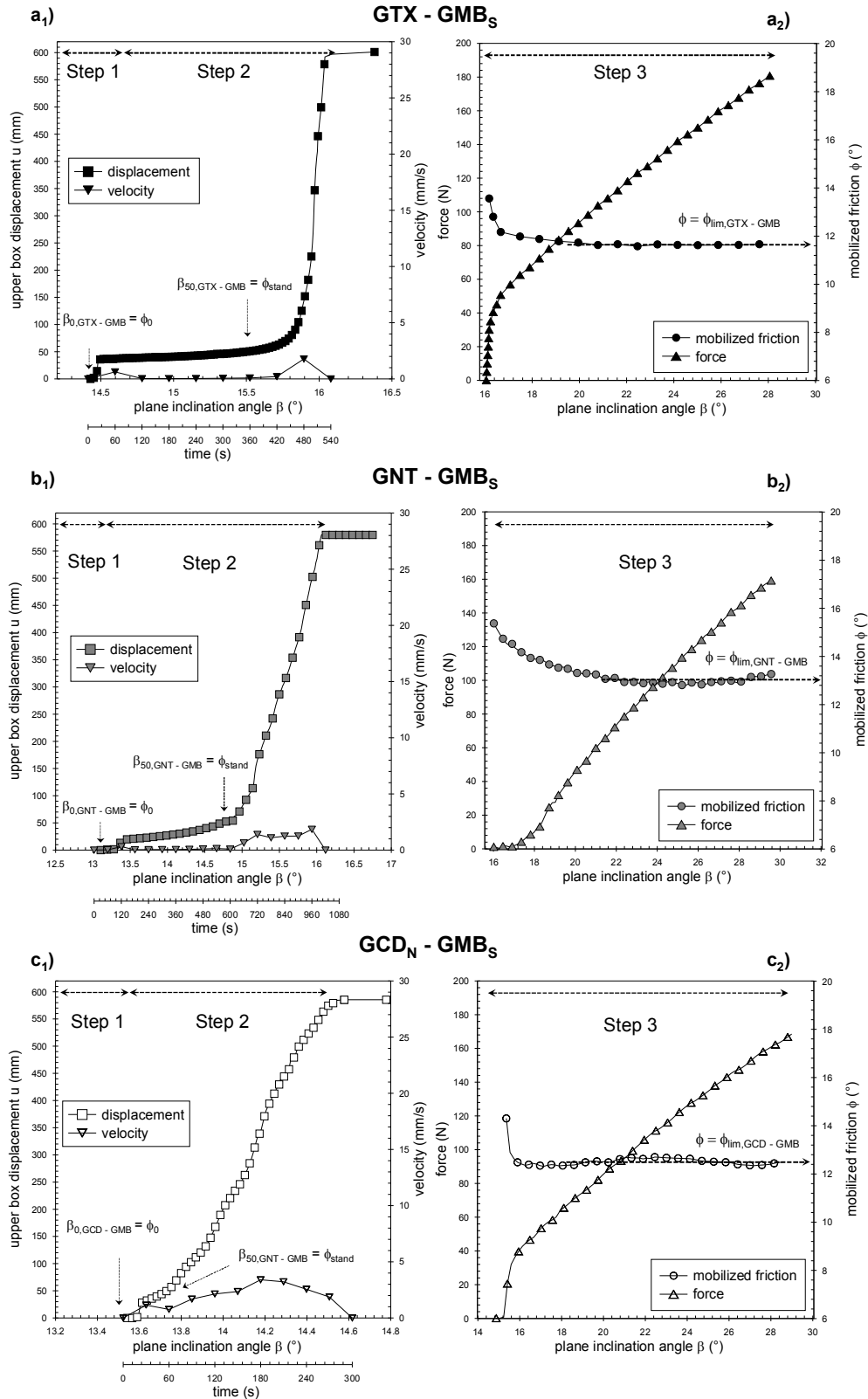


Figure 5.1.2. Typical results of the Inclined Plane tests performed at LTHE laboratory following the Unified Procedure ($\sigma_{v0} = 5 \text{ kPa}$; $T = 20^\circ\text{C}$) displaying upper box displacement versus plane inclination (Step 1 and 2 on the left side) and mobilized tensile force in the cable and friction angle versus plane inclination (Step 3 on the right side): a₁) and a₂) GTX – GMB_s interface; b₁) and b₂) GNT – GMB_s interface; c₁) and c₂) GCD_N – GMB_s interface.

Variant to Step 2

As noticed in Figure 5.1.2, the movement of the upper box is very slow and the box acceleration is difficult to assess during the sliding (Step 2). The Variant to Step 2 is applied in order to estimate the dynamic friction angle. Following this approach, the plane is fixed at a certain inclination ($\beta \gg \beta_0$) and the upper box is kept stationary at the beginning of the plane. Then, the upper box is left free to slide: since the plane inclination is significantly higher than β_0 , a uniformly accelerated motion (the velocity increases linearly in the time and the acceleration reaches a constant value) of the upper box during the sliding is obtained. Thus, in these conditions, the upper box acceleration can be directly measured by the accelerometer and/or calculated by double derivation of the box displacement (see § 4.1.3.1) and the dynamic interface friction angle, ϕ_{dy}^P , is computed following Equation (4.1-7).

It is worth noting that, in the test series where the Variant to Step 2 was applied, different inclinations of the plane were used with β varying between 18° and 25° . A higher value of $u_{lim} = 800$ mm is obtained, thanks to the cable which is missing in this configuration.

Figure 5.1.3 shows, for the three interfaces investigated, the displacement, the velocity and the acceleration of the upper box during an Inclined Plane test applying the Variant to Step 2 of the UIPP with $\beta = 20^\circ$ which is higher than β_0 for every interface.

The results of the tests plotted in Figure 5.1.2 (described in § 5.1.1.1.1) and Figure 5.1.3, are summarized in Table 5.1.2. It can be checked that an approximately constant acceleration of the upper box is observed in every case *a*, *b*, and *c*.

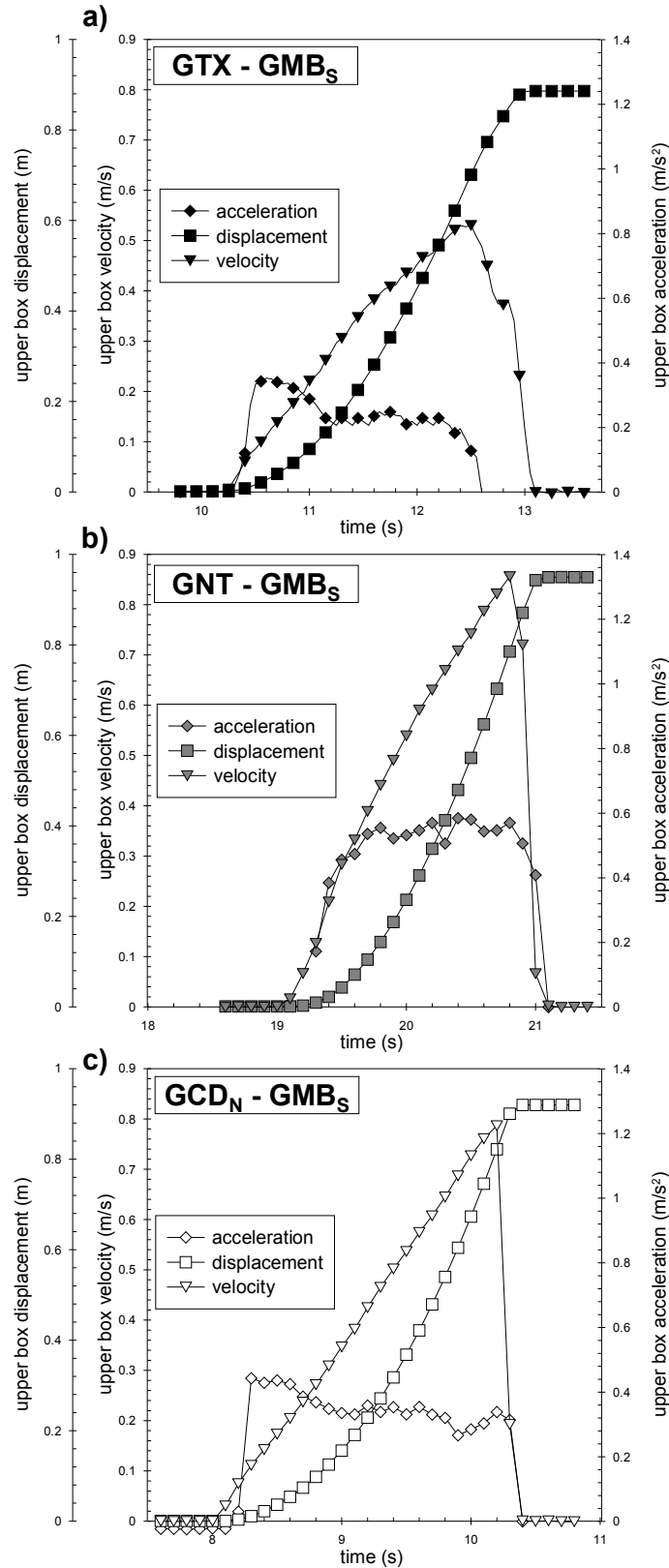


Figure 5.1.3. Inclined Plane test at fixed inclinations of the plane (Variant to Step 2 of UIPP). Test results obtained at LTHE laboratory for $\beta = 20^\circ$, at $T = 20^\circ\text{C}$ and under $\sigma_{v0} = 5 \text{ kPa}$: displacement, velocity and acceleration of the upper box versus the time. a) GTX – GMB_s interface; b) GNT – GMB_s interface; c) GCD – GMB_s interface.

Table 5.1.2. Interface friction angles of GTX - GMB_s; GNT - GMB_s and GCD_N - GMB_s interfaces calculated during the different Steps of the UIPP ($T = 20^\circ\text{C}$; $\sigma_{v0} = 5 \text{ kPa}$).

Interface tested		Step 1	Step 2		Variant to Step 2		Step 3
		ϕ_0	ϕ_{stand}	ϕ_{dyn}^{IP}	ϕ_{dyn}^{IP}	a_{box}	ϕ_{lim}
		(°)	(°)	lower bound (°)	($a_{box}=\text{const}$) (°)	(m/s ²)	(°)
a	GTX - GMB_s	14.4	15.5	15.7-15.9	17.6	0.24	11.6
b	GNT - GMB_s	13.3	14.8	15.8-15.9	16.0	0.53	13.1
c	GCD_N - GMB_s	13.6	13.7	14.1-14.2	16.3	0.36	12.6

* $\phi_{dyn}^{IP}(a_{box} = \text{const})$ values are determined applying the variant to Step 2 of the UIPP for a plane inclination $\beta = 20^\circ$ and the lower bound are provided during Step 2 $\phi_{dyn}^{IP}(v_{box} = \text{const})$.

5.1.1.1.2 Basic interpretation

Test results indicate that the interface shear strength strictly depends on the current kinematic conditions, a static equilibrium is considered in the evaluation of ϕ_0 , ϕ_{stand} and ϕ_{lim} while a dynamic equilibrium is taken into account when assessing ϕ_{dyn}^{IP} .

Starting the discussion from the static condition, shear strength may be identified as ϕ_0 or ϕ_{lim} , for the cases in which displacement has previously occurred or not. In particular, the limit interface friction angle ϕ_{lim} , represents the mobilized shear strength after sliding.

Test results (Table 5.1.2) show a loss in shear strength passing from ϕ_0 and ϕ_{lim} values that can be mainly attributed to the additional shear displacement at which the materials were previously subjected.

The dynamic friction angles, ϕ_{dyn}^{IP} , depend on the type of motion. In the three cases, during the Step 2, the box slides at low velocity (Figure 5.1.2): the maximum average velocity was determined for GCD_N – GMB_s interface and equal to 3.4 mm/s. Since it can also be considered as constant, the box acceleration is very low (the maximum box acceleration computed, $a_{box,GCDN - GMBs} = 0.0064 \text{ mm/s}^2$) and negligible. In this case, only a

lower bound of for the dynamic interface friction angle can be defined. The ϕ_{dyn}^{IP} values obtained with the Variant to Step 2, resulted higher than the static ones confirming what already found by Gourc and Reyes Ramirez (2004) in the interfaces showing a gradual sliding motion. It's worth noting that the value of ϕ_{dyn}^{IP} is also compatible with the value of the lower bound.

5.1.1.1.3 Influence of the kind of interface

This specific test series was also dedicated to study the influence of the geosynthetics which form the geocomposite drain in its interface performance. For this purpose the geotextile (GTX), the geonet (GNT) and the geocomposite drain (GCD_N) were separately tested in direct contact with the smooth geomembrane (GMB_S). Firstly, it could be noticed that, despite the great difference in the upper layer surface structural pattern (i.e. the geotextile is porous and fibrous material consisting of irregularly oriented long filaments varying in terms of spatial distribution, curvature, orientation, size, and mass density while the geonet is composed of sets of parallel ribs overlaid and integrally connected having a rhomboidal shape), for all the tested interfaces a common failure mechanism (gradual sliding) is observed. This suggests that, the shear resistance response developed at the interface can be mainly attributed to geomembrane surface properties (for the smoothness in the present case).

Figure 5.1.4 displays the comparative behaviour of the three interfaces during the inclined plane tests. This figure is illustrative of the significant differences of behaviour between interfaces and justifies the use of several parameters of friction to attempt to distinguish the interfaces. The comparison between the different test results indicates that:

- the interface friction angles ϕ_0 , ϕ_{lim} and ϕ_{dyn}^{IP} of the GTX – GMB_S interface with respect to those of the geotextile with its support geonet (GCD_N - GMB_S interface) are influenced by the geonet which decreases drastically ϕ_0 and ϕ_{dyn}^{IP} and increases the ϕ_{lim} .
- the contact between GNT – GMB_S is in general quite different than GTX – GMB_S interface with a variation that depends on the nature of the surfaces and on the resulting possible damage effect at large displacements. In fact, GNT – GMB_S seems to be less resistant in terms of initial sliding with $\phi_{0,GNT-GMB_S} < \phi_{0,GTX-GMB_S}$. Increasing the displacement, the GNT – GMB_S interface shows a shear strength

increase resulting in a limit interface friction angle higher than that found for GTX – GMB_S interface ($\phi_{lim,GNT-GMBs} < \phi_{lim,GTX-GMBs}$).

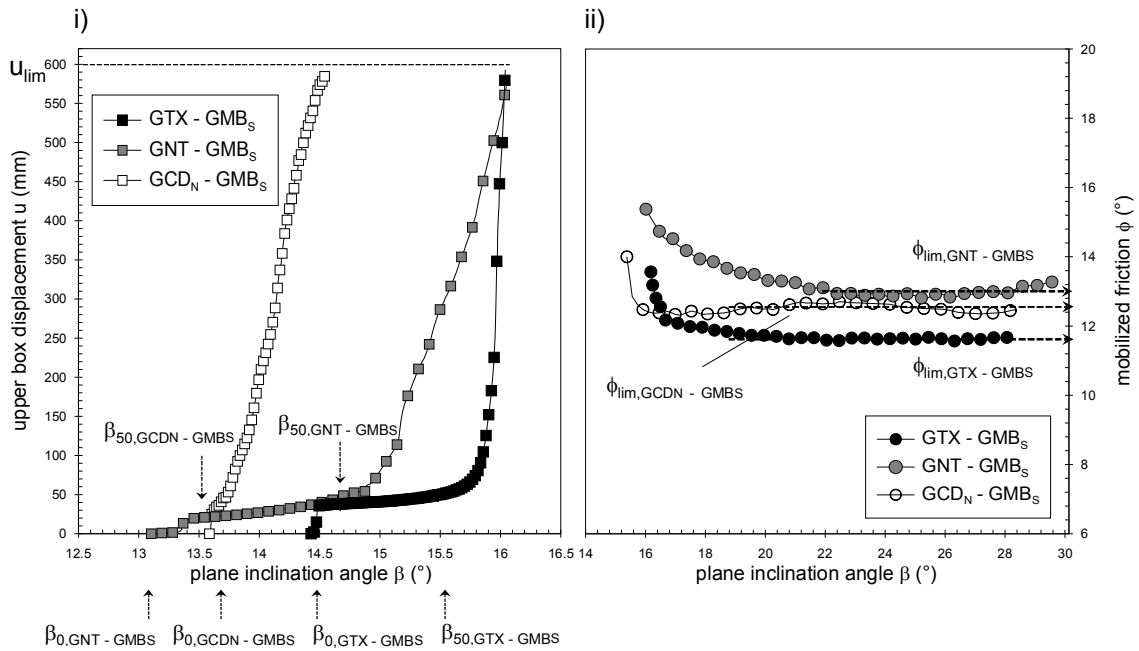


Figure 5.1.4. Comparative behaviour (gradual sliding) for different interfaces applying the Unified Procedure ($\sigma_{v0} = 5$ kPa) to GTX – GMB_S, GNT – GMB_S and GCD_N – GMB_S interfaces: i) upper box displacement versus plane inclination; ii) mobilized force and friction angle versus plane inclination.

5.1.1.2 Analysis in the case of sudden sliding

5.1.1.2.1 Typical diagrams

A total of four interfaces (*d*, *e*, *f* and *g* listed in Table 2.3.2), involving geocomposite drains (GCD_N and GCD_W) in contact with GMB_{TMH} and GMB_{RMH} geomembranes are tested with the Inclined Plane available at LTHE laboratory applying the UIPP even if, it is worth noting that the direct contact is between the nonwoven geotextile forming the geocomposite drains and the geomembrane (Figure 5.1.5).

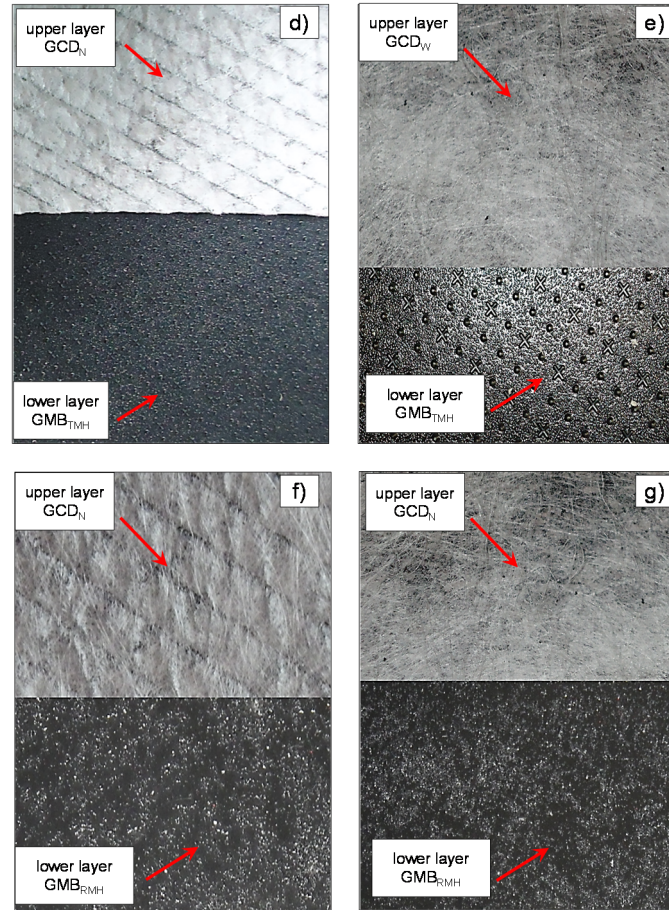


Figure 5.1.5. Upper and lower layers of interfaces involving geocomposite drains (GCD_N and GCD_W) in contact with GMB_{TMh} and GMB_{RMh} geomembranes: d) GCD_N - GMB_{TMh} ; e) GCD_W - GMB_{TMh} ; f) GCD_N - GMB_{RMh} ; g) GCD_W - GMB_{RMh} interfaces.

Figure 5.1.6 and Figure 5.1.7 display the typical plot of inclined plane test results during the different steps. Note that, in this test series, u_{lim} is equal to 900 mm. In order to compare test results during the sliding (Step 2), also the “Standard Procedure” is carried out and, for an upper box displacement of 50 mm, the standard interface friction angle (ϕ_{stand}) is determined according to Equation 4.1-3.

For the four interfaces tested, the box motion can be mainly classified as sudden sliding: the upper box slides with very high velocity along the plane and the motion can be approximated as uniformly accelerated (Figure 5.1.6 d_2 , e_2 and Figure 5.1.7 f_2 , g_2). It's easy to understand that this condition is more hazardous in field conditions because once the driving forces exceed the friction-resistant forces a brutal failure occurs at the interface.

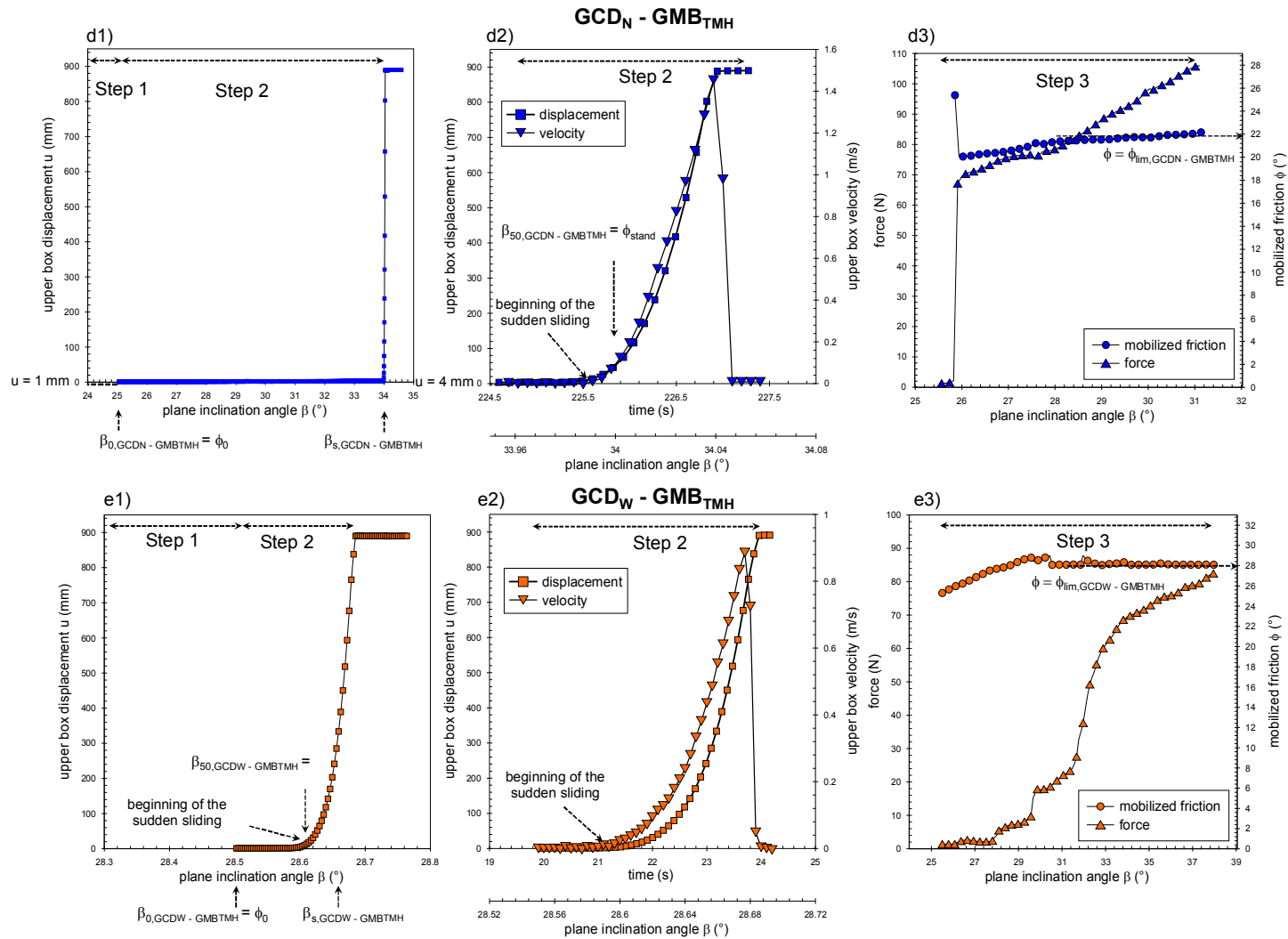


Figure 5.1.6. Typical plot of the Inclined Plane test results applying the Unified Procedure ($\sigma_v = 5 \text{ kPa}$; $T = 20^\circ\text{C}$) to $\text{GCD}_N - \text{GMB}_{TMH}$ and $\text{GCD}_W - \text{GMB}_{TMH}$ interfaces: d₁) and e₁) upper box displacement versus plane inclination; d₂) and e₂) enlarged view of the uniformly accelerated motion during Step 2; d₃) and e₃) mobilized force and friction angle versus plane inclination in Step 3.

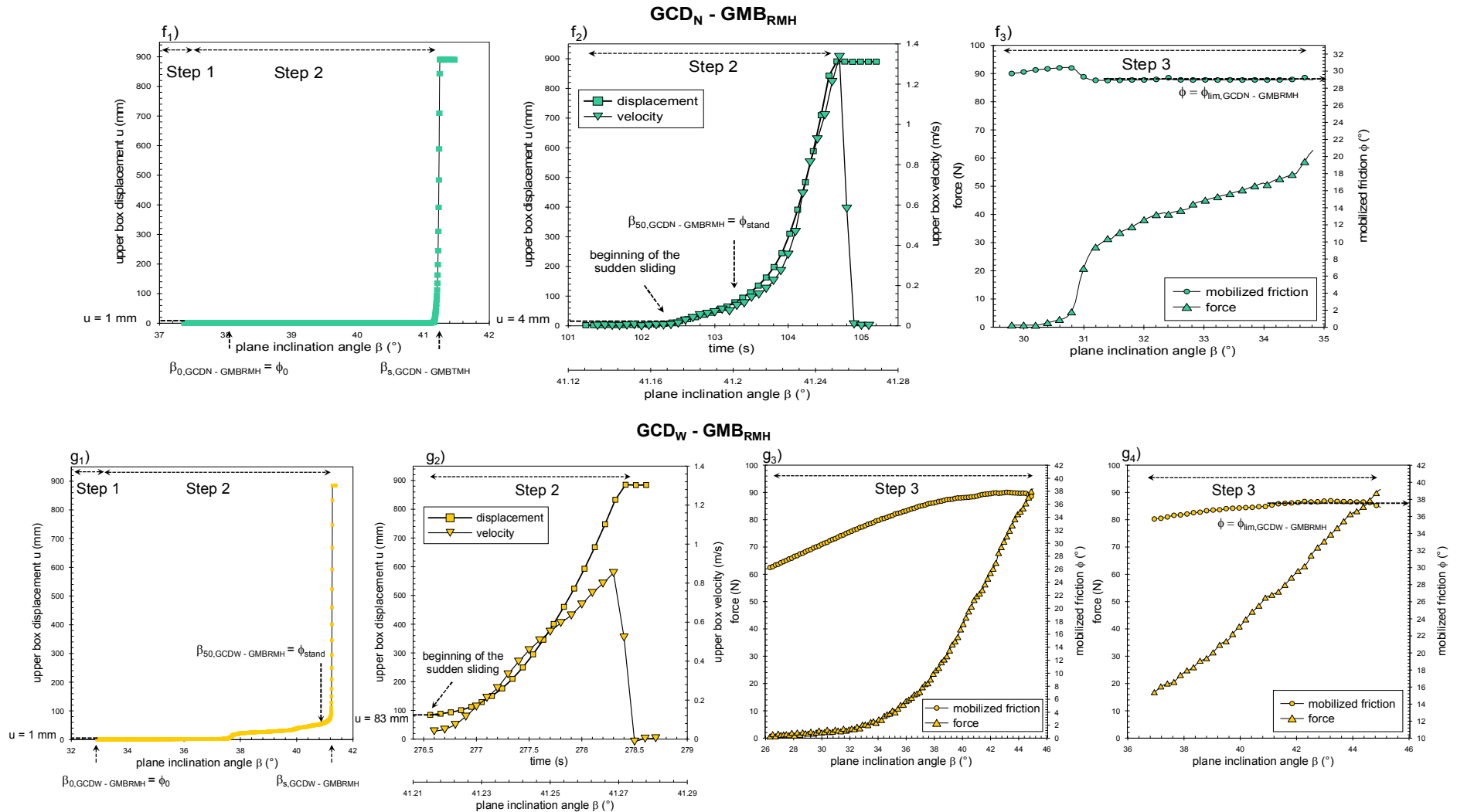


Figure 5.1.7. Typical plot of the Inclined Plane test results applying the Unified Procedure ($\sigma_{v0} = 5$ kPa; $T = 20^\circ\text{C}$) to GCD_N - GMB_{RMH}; GCD_W - GMB_{RMH} interfaces: f₁) and g₁) upper box displacement versus plane inclination; f₂) and g₂) zoomed view of the uniformly accelerated motion during Step 2; f₃) and g₃) mobilized force and friction angle versus plane inclination; g₄) zoomed view of the stabilization of the mobilized friction angle during Step 3 for GCD_W - GMB_{RMH} interface.

5.1.1.2.2 Basic interpretation

Applying the UIPP, the interface friction angles are determined as follows. During Step 1 for an upper box displacement equal to 1mm, ϕ_0 is determined according to Equation (4.1-4). During Step 2 the upper box slides along the plane. At the beginning of the uniformly accelerated motion, the slide is fast enough so that the variation of the inclination β during the dynamic phase can be considered negligible. This implies that β may be assumed as constant ($\beta = \beta_s$) and the dynamic friction angle ϕ_{dy}^P can be computed applying Equation (4.1-7) for $a_{box} = a_{const}$ (linear variation of velocity, Figure 5.1.6 and Figure 5.1.7). The limit interface friction angle ϕ_{lim} is evaluated during Step 3 of the UIPP. At this regard, an important aspect highlighted during the test procedure, is that the evaluation of the limit interface friction angle ϕ_{lim} at Step 3 of the UIPP may be complicated for interfaces involving textured and roughened geomembranes. In fact, since the motion can start at very high inclinations, it is difficult to reach the stabilization of the mobilized friction during Step 3 as described by the UIPP. This limit is mainly attributed to the capability of the device that can reach 47° , as maximum plane inclination. Therefore, in order to overcome this restriction and to estimate the limit interface friction angle, a specific approach was used: at the end of the slide, when the cable is still loose, the plane inclination is decreased enough, in such a way that the test can subsequently restart as usual.

Even if the interface response can be mainly classified as “sudden sliding” some results differ from what previously observed in the literature for the interfaces showing the same behaviour. The main findings presented in literature in the case of sudden sliding interfaces are:

- $\phi_0 > \phi_{lim}$ (Briançon et al. 2011);
- $\phi_0 > \phi_{dyn}^{IP}$ (Gourc and Reyes Ramirez, 2004).

As it could be noticed from test results summarized in Table 5.1.3, the general trend follows what previously reported in literature. However, in the case of $GCD_W - GMB_{RMH}$ interface, the limit interface friction angle is higher than the static one ($\phi_0 < \phi_{lim}$), while, for $GCD_N - GMB_{TMH}$, $GCD_W - GMB_{RM}$ the static friction angle is smaller than the dynamic one ($\phi_0 < \phi_{dyn}^{IP}$). The divergences obtained in the results mainly depend on the use of the textured geomembranes causing an alteration of the surface of the non-woven geotextile. Considering that no punching effect by the geomembrane spikes was observed since tests are performed at low normal stress, as found by Hebeler et al. (2005) in these cases, the

interaction between the geotextile filaments and the geomembrane surfaces consists mostly of individual filaments being engaged by the geomembrane texture (Figure 5.1.8).

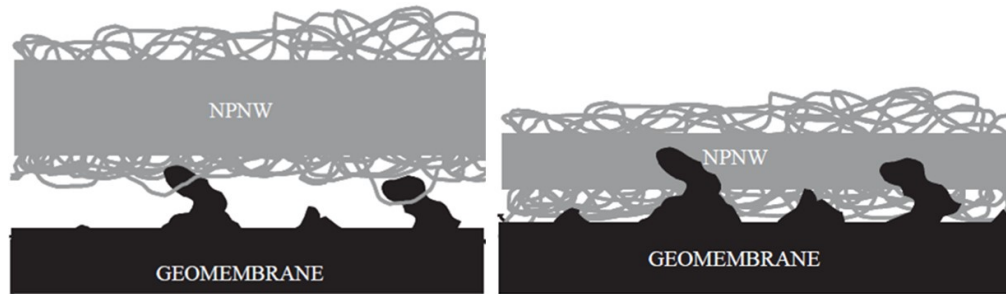


Figure 5.1.8. Sketch of interaction mechanisms between nonwoven geotextiles and textured geomembranes at different normal stresses (adapted from Hebelier et al. 2005).

As a consequence of the “hoop and lock” contribution, the upper box cannot slide continuously along the plane (Figure 5.1.6 d_1 , d_2 and e_1 , e_2 ; Figure 5.1.7 f_1 , f_2 and g_1 , g_2). Therefore, the behaviour can be divided in two main phases. In the first phase, for a displacement $u = 1$ mm, ϕ_0 corresponds to the mobilization of non-woven fibers. After tensile failure of the geotextile filaments, a second motion starts ($\beta = \beta_s$) where the sudden sliding takes place.

Furthermore, the standard interface friction angle ϕ_{stand} (Table 5.1.3) systematically overestimates the interface friction angle with respect to both ϕ_0 and ϕ_{lim} .

With the foregoing bases:

- ϕ_0 could be not relevant following the conventional test interpretation;
- since $\beta_s > \beta_0$ (in the interfaces d , f and g) consequently also $\phi_{\text{dyn}}^{\text{IP}} > \phi_0$;
- ϕ_{stand} , systematically overestimates the interface friction angle with respect to the static ones.

To summarize the behaviour of interfaces with textured geomembranes can be equivalent to a stick-slip behaviour with the failure of the fibers or of the bonds between fibers. Stick – slip subcategory (Figure 4.1.3 ii) induces a new value of the plane inclination, corresponding to the beginning of the sudden sliding, to be considered as outlined in Figure 5.1.6 and Figure 5.1.7.

Table 5.1.3. Interface friction angles of the geocomposite drains in contact with the textured geomembranes at 20°C under a vertical stress of 5 kPa.

Interface tested		Step 1	Step 2				Step 3
		ϕ_0 (°)	ϕ_{stand} (°)	ϕ_{dyn}^{IP} (°)	β_s (°)	a_{box} (m/s ²)	ϕ_{lim} (°)
d	GCD_N - GMB_{TMH}	25.9	34.0	27.9	34.0	1.19	21.3
e	GCD_W - GMB_{TMH}	28.5	28.6	25.8	28.5	0.53	28.3
f	GCD_N - GMB_{RMH}	38.2	41.2	35.9	41.2	1.11	28.9
g	GCD_W - GMB_{RMH}	33.4	40.6	39.0	41.2	0.49	37.7

The analysis of test results schematized in Table 5.1.3, leads to the following considerations.

Starting the discussion from the static and the limit interface friction angles, a reduction in shear strength passing from ϕ_0 to ϕ_{lim} can be noted. The loss in shear strength may be attributed to the pulling out, the reorientation and the breakage of the geotextile filaments from the matrix causing continuous changes in the contact area.

The dynamic friction angles were calculated during Step 2 of the UIPP and resulted in two cases higher than ϕ_0 . Until now, in the interfaces studied in literature (Briançon et al., 2011; Gourc and Reyes Ramirez, 2004; Pitanga et al., 2009) the upper box slides continuously until the end of the plane so that, considering $\beta_s \cong \beta_0$, the dynamic friction angle ϕ_{dyn}^{IP} resulted lower than the static one (Equation 4.1-4). Conversely, in the interfaces *d*, *f* and *g*, due to the “seating response” of the interface, the start of the upper box motion does not always correspond to the beginning of the uniformly accelerated movement: β_s is higher than β_0 and, consequently, also the dynamic friction angle ϕ_{dyn}^{IP} can result higher than the static angle ϕ_0 . It is worth noting that this result is not related to the type of motion (sudden or gradual) but to the nature of the geomembrane surfaces.

5.1.1.2.3 Influence of the kind of interface

In this section, being the interfaces *d*, *e*, *f* and *g* a combination of two kinds of geocomposite drain with two different types of textured geomembranes, a first insight into the behavioural differences resulting on the use of these products is provided.

Figure 5.1.9 reports Inclined Plane test results involving the two geocomposite drains (GCD_N and GCD_W) in contact with the different textured geomembranes (structured - GMB_{TMH} and co-extruded - GMB_{RMH})

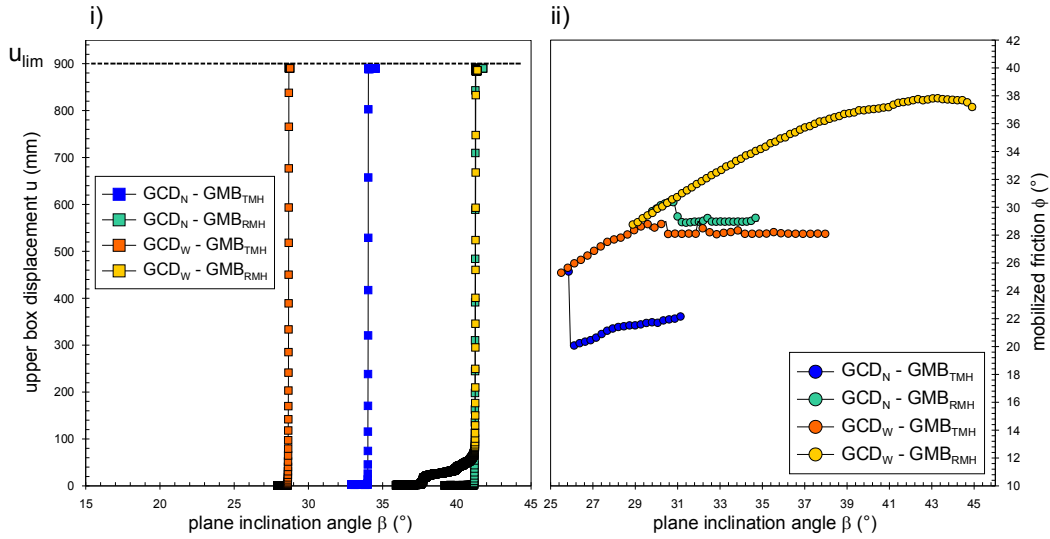


Figure 5.1.9. Comparative behaviour of the two geocomposite drains (GCD_N and GCD_W) in contact with the different textured geomembranes (structured - GMB_{TMH} and co-extruded - GMB_{RMH}) applying the Unified Procedure ($\sigma_{v0} = 5 \text{ kPa}$; $T = 20^\circ\text{C}$): i) upper box displacement versus plane inclination; ii) mobilized force and friction angle versus plane inclination.

Comparing the test results it can be pointed out that:

- ϕ_0 values obtained when the “sandy paper like” (co-extruded) geomembrane GMB_{RMH} is used, are higher than those determined in interfaces involving the structured geomembrane GMB_{TMH} ($\phi_{0,GMB_{RMH}} > \phi_{0,GMB_{TMH}}$). This can be mainly related to the fact that at low normal stresses, the “hook and loop” contribution (see Figure 5.1.6 and Figure 5.1.7) is more marked in the co-extruded geomembrane interfaces than in the structured ones. Moreover, the damage of the upper layers in terms of loose geotextile filaments, is higher for GCD_N than GCD_W . In fact, the contact points between the geonet and the geotextile in GCD_N are lower and more fragile with respect to those obtained between the geomat and the geotextile in GCD_W as it could be noticed after visual inspection of the tested specimens (Figure 5.1.10);
- in co-extruded geomembrane interfaces (f and g) the limit friction angles, ϕ_{lim} , are higher than in the interfaces involving structured geomembranes (d and e) ($\phi_{lim,GMB_{RMH}} > \phi_{lim,GMB_{TMH}}$); the values obtained utilizing the GCD_N are, generally lower than ϕ_0 while if GCD_W is used, ϕ_{lim} and ϕ_0 values are very close;

- the same considerations can be drawn for ϕ_{dyn}^{IP} values for the interfaces analysed.

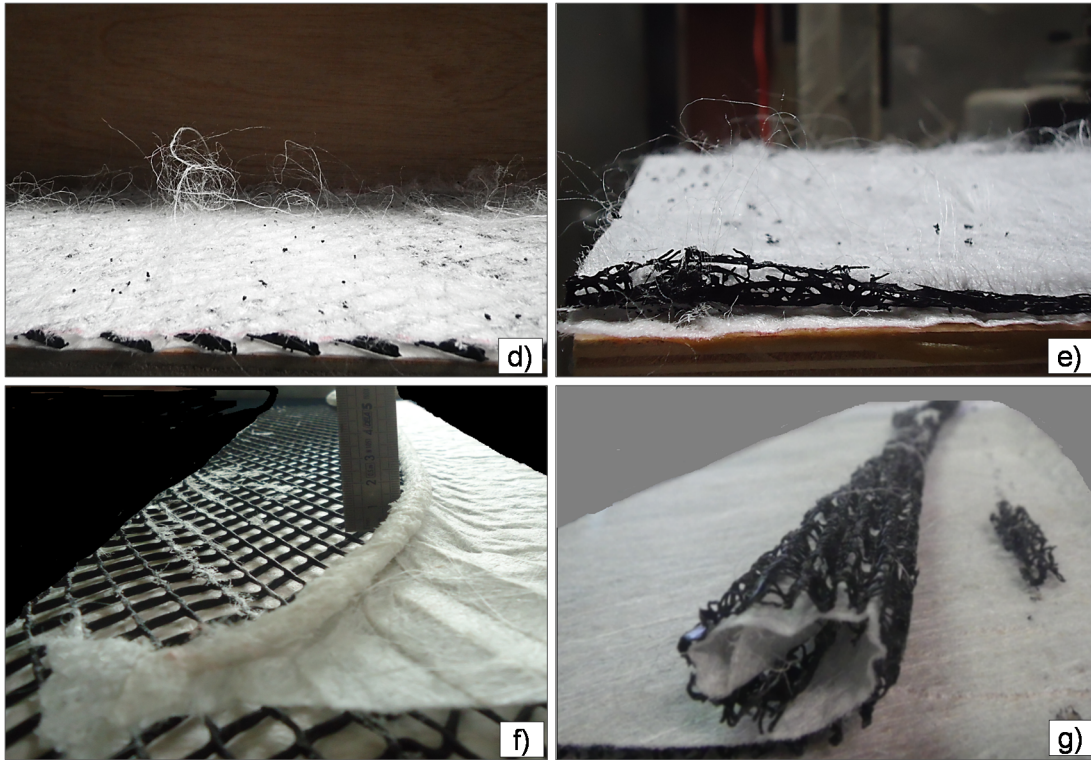


Figure 5.1.10. Images of geotextile specimens of GCD_N and GCD_W , representing the upper layer, after shearing: d) GCD_N in contact with the GMB_{TMh} ; e) GCD_W in contact with the GMB_{TMh} ; f) GCD_N in contact with the GMB_{RMh} ; g) GCD_W in contact with the GMB_{RMh} .

5.1.1.3 Influence of the nature of the surfaces

Research studies (Dove, 1996, Lee, 1998) into the behaviour of interfaces have shown that the roughness of the geomembrane is one of the main factors in the development of interface strength.

In order to deepen this aspect, the behaviour of the geocomposite drain (GCD_N) in contact with the smooth (GMB_S), the structured (GMB_{TMh}) and the co-extruded (GMB_{RMh}) geomembranes are analysed in this section (interfaces *c*, *d* and *f* listed in Table 2.3.2).

Figure 5.1.11 shows the behaviour of GCD_N when tested with the different geomembranes.

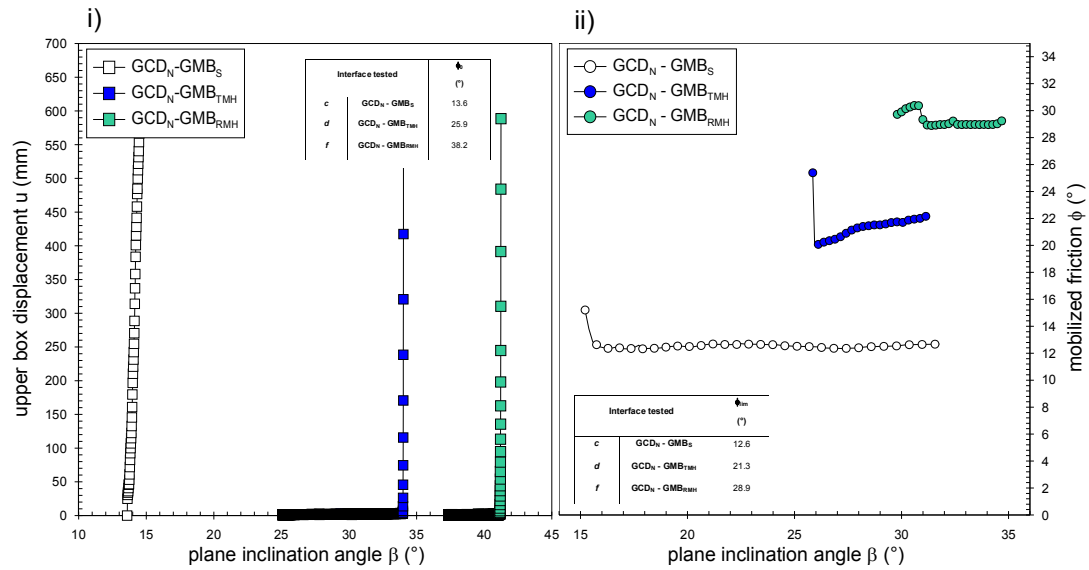


Figure 5.1.11. Comparative behaviour of the geocomposite drain (GCD_N) in contact with the smooth (GMB_S), the structured (GMB_{TMH}) and the co-extruded (GMB_{RMH}) geomembranes applying the Unified Procedure ($\sigma_{v0} = 5 \text{ kPa}$; $T = 20^\circ\text{C}$): i) upper box displacement versus plane inclination; ii) mobilized force and friction angle versus plane inclination.

From test results represented in Figure 5.1.11, it could be noticed that the interfaces *d* and *f* (interfaces involving textured geomembranes) are characterized by friction angles significantly higher than those obtained in the interface involving the smooth geomembrane. This is in agreement with other studies on geomembrane-geotextile interface (Frost and Lee, 2001) and on a geomembrane-soil interface as well (Dove et al., 1997). In particular, they reported that the peak and residual interface strengths increased approximately 300% and 200%, respectively by the use of textured geomembranes instead of smooth geomembranes.

Similar results are obtained with the Inclined Plane for the static and the limit interface friction angles that increase approximately 180% and 130% respectively passing from the smooth to the co-extruded geomembrane. Among the different parameters usually influencing test results, the increase in interface shear strength, may be also attributed to the engagement of the “loop” structure by the “hook” material occurring in systems where textured geomembranes are in contact with the geotextiles.

Regarding the static friction angles ϕ_0 and ϕ_{lim} , a similar trend consisting in a decrease of interface shear strength passing from the static to the limit interface friction can be observed. However, the limit shear strength loss is substantially greater with a textured geomembrane.

In the case of $GCD_N - GMB_S$ interface, visual inspection of the specimens after testing seems to indicate that the shear strength loss may be primarily due to polishing of the interface as also found by Akpınar (1997).

Therefore, when the contact is between the geocomposite drain and the textured geomembranes, the reductions in interface shear strength passing from ϕ_0 to ϕ_{lim} may be attributed to the pulling out, the breakage and the reorientation of the geotextile filaments from the matrix causing continuous changes in the contact area. Consequently, in these cases the interface shear strength is a function of the tensile and pull-out strength of the geotextile filaments. A similar result in terms of peak and residual interface strength (Figure 5.1.12), testing textured HDPE geomembranes in contact with nonwoven geotextiles, was found by Frost and Lee, (2001) using large direct shear box and by Stark et al. (1996) performing torsional ring shear tests.

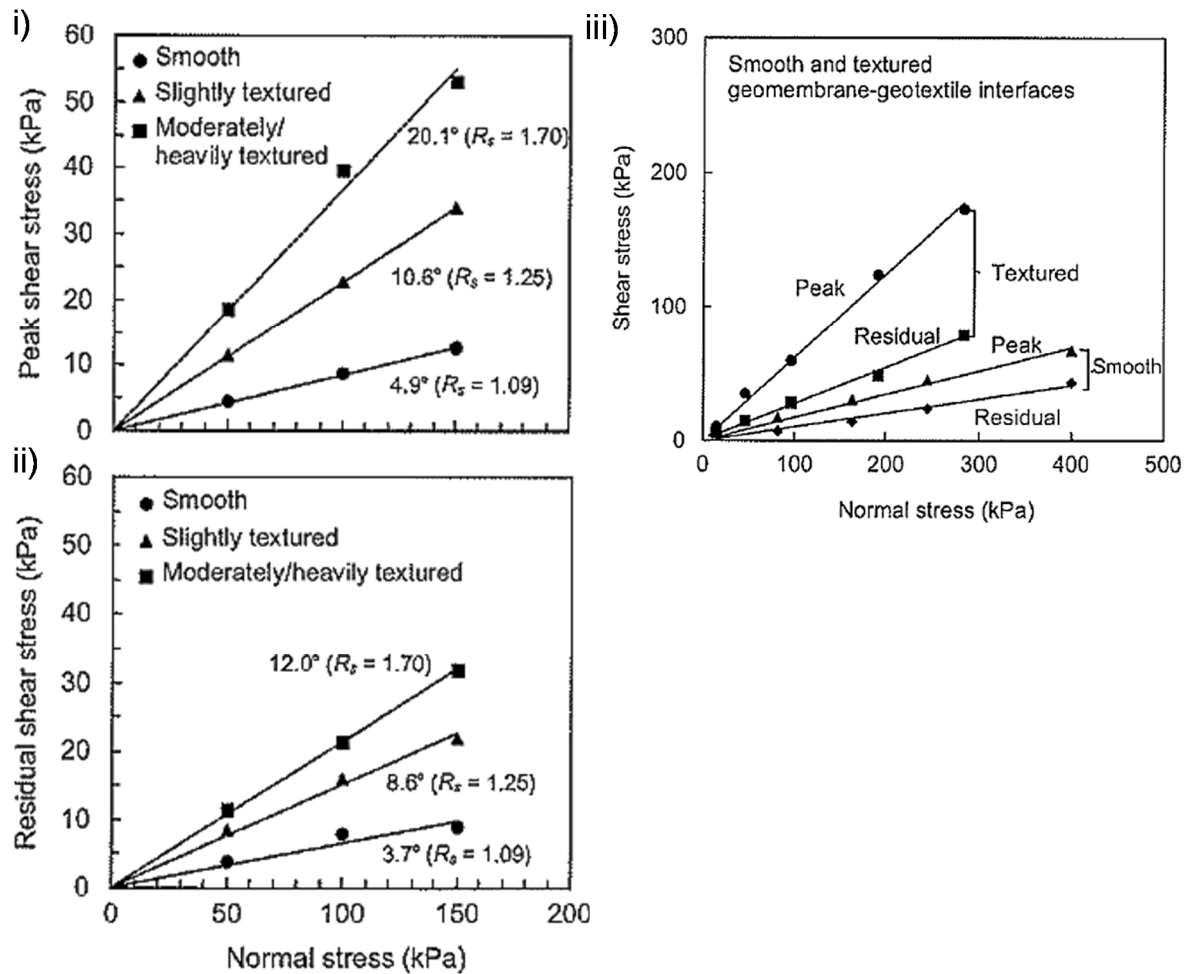


Figure 5.1.12. Loss in shear strength for smooth and textured geomembrane – non-woven geotextile interfaces passing from peak to residual value: i) and ii) peak and residual failure envelope carrying out direct shear tests (after Frost and Lee, 2001); iii) peak and residual failure envelope carrying out torsional ring shear test (after Stark et al. 1996).

The nature of the surfaces in contact also affected the mechanism of sliding (gradual or sudden) and, consequently, the dynamic friction angle.

Concluding, the selection of textured geomembrane results in an increase of the interface friction angles. This leads to an increase of shearing stresses in geomembrane and, since the sudden sliding is observed, once the failure limit is reached, a brutal rupture takes place.

5.1.1.4 Inclined Plane test general conclusions

The Inclined Plane test is suitable for the assessment of friction in case of low normal stresses as it is the case of landfill cap covers. However, in spite the handiness in performing the test, its interpretation can be rather difficult.

The Inclined Plane results lead to the principal general conclusions.

- The interface shear strength is very sensitive to the existing kinematic conditions.
- The interface shear strength cannot be characterised by a single parameter, as proposed by the European Standard EN ISO 12957-2 (2005) depending on the existing kinematic conditions of the interface during the test. Furthermore, since the standard friction angle refers to a conventional displacement of 50 mm, it may correspond to various kinematic conditions, depending on the behaviour of the tested interface, not known a priori. In particular, in the case of sudden sliding, this approach in general overestimates the interface friction angle because a static approach is applied in dynamic conditions.
- The approach proposed and applied in this study tries to overcome the limitations of the “Standard Procedure”. In fact, thanks to the Unified Inclined Plane Procedure (UIPP) it is possible to evaluate, during a single test, different friction angles varying according to the current kinematic conditions (ϕ_0 , ϕ_{dyn}^{IP} and ϕ_{lim}). In particular, the evolution of the interface shear strength in static - dynamic – pseudo-static at large deformations conditions can be investigated during the same test.
- The UIPP seems to be a suitable method even if, in some cases, its application can be difficult and some modifications must be performed. For the interfaces *a*, *b* and *c* (involving smooth geomembrane) the dynamic friction angle is difficult to determine during Step 2 (i.e. the upper box acceleration is very low) while, in the case of interfaces *d*, *e*, *f* and *g* (involving textured geomembranes) some difficulties were encountered in carrying out Step 3. However, in this latter case, the difficulties are related to the capabilities of the device. In fact, as the interfaces are

characterized by very high values, the stabilization of ϕ , during Step 3, is not easy to reach following the method described in the UIPP.

- The sliding mode is the first parameter that must be taken into account in the analysis of the interface response: following the mode of failure the considerations about interface friction angles behaviour can be different.
- The Inclined Plane test allows determining the behaviour of the interface in various conditions. The resulting properties obtained, have direct implications on the design of structure involving composite systems; thus, the very useful information about the evolution of the interface shear strength under different conditions, can help designers in the stability analysis of cover liners on slopes.

5.1.2 Repeatability

The interface shear strength can exhibit significant variability in test results overall at low effective normal stresses (Dellinger et al. 2013). Knowledge of variability is fundamental for evaluation of characteristic values for use in design as well as inputs for reliability analyses (Sia and Dixon, 2007). The variability of test results may be attributed to the testing method (i.e. the procedure used, measurement and procedural errors, statistical error and model uncertainty) as well as to the material properties (i.e. physical properties, local variations within the sheets and between rolls).

5.1.2.1 Methodology and materials

A repeatability testing program is conducted to investigate the variability that can be expected by using single operator, equipment, procedure, and materials from single source. The repeatability testing programme consisted of inclined plane tests carried out along the machine direction of the products, at an initial vertical stress $\sigma_{v0} = 5$ kPa and in dry conditions. The results presented refer to virgin specimens, corresponding to specimens which have experienced no previous displacement, for ϕ_0 evaluation, or only corresponding to u_{lim} , for ϕ_{lim} determination.

The experimental program was conducted on the seven interfaces listed in Table 2.3.2. The investigation of results variability is a key issue, in particular for interfaces involving textured geomembranes (*d*, *e*, *f* and *g*) as underlined by different studies (Dove and Frost 1996, Stark et al. 1996 and Frost and Lee 2001), seeing that the variability of the interface

could be higher than for smooth geomembranes, specifically for the co-extruded “sandy paper like” geomembrane in contact with non-woven thermo-bounded geotextile.

Two main factors should be taken into account when studying the variability of the different interfaces:

- homogeneity of the surface and,
- contact between two geosynthetics.

For the interfaces *a*, *b* and *c*, the repeatability was also studied at different temperature conditions ($T = 10^{\circ}\text{C}$, 20°C and 30°C).

In agreement with the EN ISO 12957-2, at least three different specimens for each interface are tested. Therefore, test results are summarized in Table 5.1.4 and Table 5.1.5 in terms of the average value instead of individual values or the minimum value. Furthermore, also the scatter (coefficient of variation) indicating the dispersion of the results with respect to the mean value, is reported.

5.1.2.2 Results and discussion

Table 5.1.4 and Table 5.1.5 summarize test results of the experimental program carried out on the seven interfaces. In particular, in Table 5.1.4 are schematized test results involving interfaces with the smooth geomembrane while Table 5.1.5 deals with interfaces involving textured geomembranes. As highlighted by the results, this is a crucial aspect towards the repeatability. In fact, it could be noticed that the use of smooth geomembrane as lower layer (Table 5.1.4) provides a maximum scatter of 1.7° , which is smaller than that found when textured geomembranes are used (Table 5.1.5). In the latter case, the scatter can reach even 4° . In fact, as the roughness of textured geomembranes is a three-dimensional object, the variability in the interface shear strength is related not only to the height of the asperities but also to their distribution along the surface (Dellinger et al., 2013) that can vary in the specimens used in the different tests even belonging to the same roll.

Therefore, the analysis of repeatability will be divided into two sections in order to take into account the surface properties of the geomembranes used.

Table 5.1.4. Variability in test results. Interface friction angles and coefficient of friction of GTX – GMB_s; GNT - GMB_s and GCD^A-GMB_s interfaces at 10°C, 20°C and 32°C under a vertical stress of 5 kPa.

T	GTX - GMB _s			GNT - GMB _s			GCD - GMB _s		
	ϕ_0	ϕ_{lim}	ϕ_{dyn}^{IP}	ϕ_0	ϕ_{lim}	ϕ_{dyn}^{IP}	ϕ_0	ϕ_{lim}	ϕ_{dyn}^{IP}
	(°)	(°)	(°)	(°)	(°)	(°)	(°)	(°)	(°)
(°C)	$\tan\phi_0$	$\tan\phi_{lim}$	$\tan\phi_{dyn}^{IP}$	$\tan\phi_0$	$\tan\phi_{lim}$	$\tan\phi_{dyn}^{IP}$	$\tan\phi_0$	$\tan\phi_{lim}$	$\tan\phi_{dyn}^{IP}$
10	16.7±0.6	17.1±0.1	17.5±0.1	15.0±1.4	16.5±0.6	17.3±0.4	16.3±0.1	13.6±0.5	15.0±0.5
	0.300±0.01	0.308±0.001	0.315±0.001	0.268±0.02	0.296±0.01	0.311±0.007	0.292±0.001	0.242±0.009	0.268±0.009
20	14.0±1.0	11.7±0.2	17.3±0.8	13.5±1.0	13.1±0.4	16.9±0.4	14.0±1.1	12.6±0.5	16.5±0.6
	0.249±0.02	0.207±0.003	0.311±0.01	0.240±0.02	0.233±0.007	0.304±0.007	0.249±0.019	0.223±0.009	0.296±0.010
30	15.5±1.5	13.7±0.1	18.0±0.6	15.5±1.0	16.2±0.6	17.7±0.6	15.7±1.7	14.7±0.6	17.7±0.5
	0.277±0.03	0.243±0.001	0.324±0.01	0.277±0.02	0.290±0.01	0.319±0.01	0.281±0.03	0.273±0.01	0.319±0.009

* ϕ_{dyn}^{IP} values are determined applying the variant to Step 2 of the UIPP

Table 5.1.5. Variability in test results. Interface friction angles and coefficient of friction of the geocomposite drains in contact with the textured geomembranes at 20°C under a vertical stress of 5 kPa

GCD _N - GMB _{RMH}			GCD _W - GMB _{RMH}			GCD _N - GMB _{TMH}			GCD _W - GMB _{TMH}		
ϕ_0	ϕ_{lim}	ϕ_{dyn}^{IP}	ϕ_0	ϕ_{lim}	ϕ_{dyn}^{IP}	ϕ_0	ϕ_{lim}	ϕ_{dyn}^{IP}	ϕ_0	ϕ_{lim}	ϕ_{dyn}^{IP}
(°)	(°)	(°)	(°)	(°)	(°)	(°)	(°)	(°)	(°)	(°)	(°)
$\tan\phi_0$	$\tan\phi_{lim}$	$\tan \phi_{dyn}^{IP}$	$\tan\phi_0$	$\tan\phi_{lim}$	$\tan \phi_{dyn}^{IP}$	$\tan\phi_0$	$\tan\phi_{lim}$	$\tan \phi_{dyn}^{IP}$	$\tan\phi_0$	$\tan\phi_{lim}$	$\tan \phi_{dyn}^{IP}$
34.7±3.5	30.7±1.8	34.6±4	34.1±2.1	36.3±1.3	39.9±3.1	28.7±2.9	21.3±1.5	27.1±1.9	26.4±2.0	27.4±1.4	25.2±0.6
0.692±0.06	0.593±0.03	0.690±0.07	0.677±0.04	0.734±0.02	0.836±0.05	0.547±0.05	0.390±0.03	0.512±0.03	0.496±0.03	0.496±0.02	0.470±0.01

* ϕ_{dyn}^{IP} values are determined during Step 2 of the UIPP

5.1.2.2.1 Repeatability of geosynthetic interface friction angles involving smooth geomembrane

In the following section a detailed discussion about test results involving smooth geomembrane as lower layer (Table 5.1.4) is presented.

The variability analysis of test results should take into account a variability due to the material properties and also the typical variability of the different interface friction angles determined (static, limit and dynamic).

Considering the interface friction angles, test results (Table 5.1.4) show that the value of the friction angle ϕ_0 , in general, displays a greater dispersion (higher coefficient of variability) than those found for the limit (ϕ_{lim}) and the dynamic (ϕ_{dyn}^{IP}) ones. It is believed that many random factors such as initial adhesion, temperature, contact stress and elapsed time before sliding can affect the static friction increasing the dispersion of its values.

The maximum scatter found in GTX – GMB_S interface regarding ϕ_0 is $\pm 1.5^\circ$ (± 0.03 in terms of friction coefficient). For GNT – GMB_S and GCD_N – GMB_S interfaces the maximum coefficient of variability is $\pm 1.4^\circ$ (± 0.02 in terms of friction coefficient) and $\pm 1.7^\circ$ (± 0.03 in terms of friction coefficient) respectively.

The limit interface friction ϕ_{lim} , represents the friction after shearing. For the virgin interfaces (reminding that in this case, the upper layer is already subjected to a displacement during the sliding), the scatter related to ϕ_{lim} is no more than $\pm 0.6^\circ$ (± 0.01 in terms of friction coefficient) for the three interfaces investigated. It could be noticed that, for interfaces involving smooth geomembranes, the scatter associated to ϕ_{lim} is in general smaller than the scatter related to ϕ_0 .

Regarding the dynamic friction angle (ϕ_{dyn}^{IP}) it should be borne in mind that as the interfaces showed a gradual sliding motion, the dynamic friction angles are obtained at fixed inclinations of the plane with $\beta \gg \beta_0$ (Variant to Step 2) as suggested in the case of gradual sliding behaviour (see § 4.1.3). The mean value of ϕ_{dyn}^{IP} is higher than ϕ_0 according to the failure behaviour of the gradual sliding type. Looking at the repeatability, it could be noticed that the dynamic interface friction angles does not vary significantly for the virgin specimen (i.e. values obtained for specimen tested for the first time), being its variation no more than $\pm 0.8^\circ$ corresponding to a variation of about or ± 0.01 in terms of friction coefficient.

For comparison, Gilbert et al. (1995) and Allen and Gilbert (2002) carrying out direct shear tests, found a coefficient of variations in the friction coefficient for interfaces between a nonwoven geotextile and a smooth geomembrane typically less than 0.05. Sia and Dixon, (2007) conducted a variability study of the peak and large displacement interface shear strength evaluated with the direct shear test of three different interfaces: non-woven needle-punched geotextile against coarse grained soil (NWGT-coarse), textured high polyethylene geomembrane against non-woven needlepunched geotextile (TGM-NWGT) and textured high polyethylene geomembrane against fine grained soil (TGM-fines). They observed that interface shear strengths between two geosynthetics display less variability compared to interfaces involving soils. For the NWGT-coarse interface, the variability computed for peak and large displacement interface shear strengths is in the range of 4–7%. For the TGM-NWGT interface, variability for peak interface shear strength is about 5% and about 4–8% for large displacement interface shear strengths. For the TGM-fines interface, peak interface shear strengths demonstrate as maximum a variability of about 13% (for a normal stress less than 10 kPa). Concluding, in the perspective of the engineering allowance, the results may be considered repeatable, for all the GTX – GMB_s, GNT – GMB_s and GCD_N – GMB_s interfaces.

5.1.2.2.2 Repeatability testing programme of interfaces involving textured geomembranes

The texturing process of geomembrane surfaces can be locally erratic within a sheet as well as between rolls (i.e. for spikes the problem is linked to the size of the specimen compared to the distance between spikes). With the foregoing bases, the height and density of asperities, as well as their shapes, can vary. Thus, repeatability analysis of the interfaces involving textured geomembranes is more complex. Furthermore, another important aspect that must be taken into account in the interpretation of test results is that textured geomembranes are in direct contact with geotextiles forming the geocomposite drain so that the “hook and loop effect” (Figure 5.1.13) leads to an increase of the variability of test results.

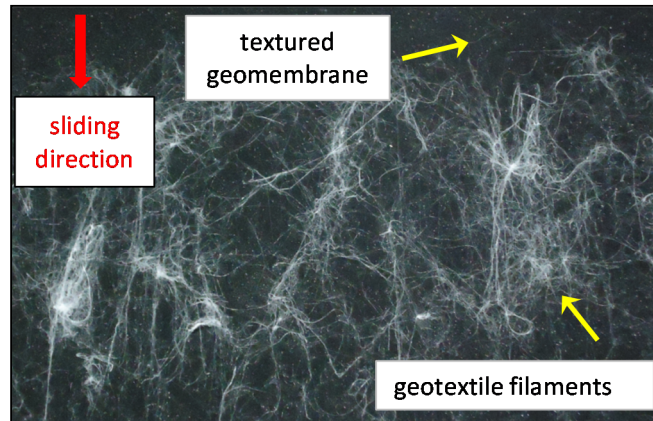


Figure 5.1.13. Geotextile filaments hooked to the structured geomembrane (GCD_N – GMB_S interface) during the Inclined Plane test (LTHE laboratory).

In fact, the typical coefficients of variability found for these interfaces are significantly higher (until 4° or 0.07 in terms of friction coefficient) with respect to the previous ones.

Contrary to what previously stated about repeatability of test results involving smooth geomembrane interfaces, it is more difficult to draw a typical trend of the results according to the different friction angles (ϕ_0 ; ϕ_{lim} and ϕ_{dyn}^{IP}). This may be attributed to the fact that during the same test, along the entire specimen, as geotextile fibers are caught on geomembrane asperities, the direct contact can be not only between the geotextile and the geomembrane but also between the geonet and the geomembrane (Figure 5.1.14).

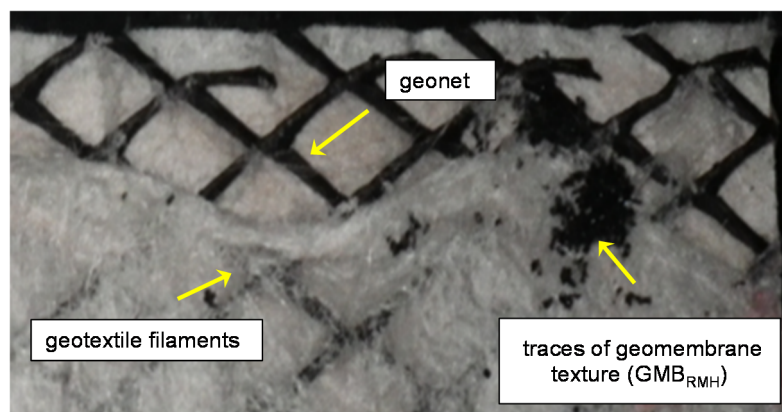


Figure 5.1.14. Detail of the upper layer (GCD_N) in contact with the “sandy paper like” geomembrane (GMB_{RMH}) after shearing (LTHE laboratory).

Studying these local variations in test results is very important to establish the proper number of tests required to characterize the interface shear strength. In this regard,

Dellinger et al., (2013) recommended a minimum of five to ten tests to assess the average interface shear strength for these interfaces.

5.1.2.3 Conclusions

Repeatability for laboratory test results are presented and analysed. The variability of results in geosynthetic interfaces can vary depending on the surface properties of the materials in contact. For this reason, a separate analysis of test results was conducted distinguishing the interfaces involving the smooth geomembrane and the interface involving textured geomembranes.

In the former category, the variability computed for the three interfaces (GTX - GMB_S, GNT - GMB_S and GCD_N - GMB_S) regarding the three interface friction angles (ϕ_0 , ϕ_{lim} and ϕ_{dyn}^{IP}) is in the range of 0.7 - 9% for normal stresses equal to 5kPa.

Much more complex is repeatability analysis of interfaces involving textured geomembranes. In this case, the coefficients of variability are in the range of approximately 3 - 11% for the same level of normal stress.

5.1.3 Reproducibility

A special testing program was conducted in order to investigate the reproducibility of test results. Reproducibility here refers to the possibility to obtain comparable friction values by working with different devices under the same laboratory conditions. For this purpose, the Inclined Plane devices available at LTHE and ICEA laboratories were used even if the two device present different characteristics (Table 5.1.6). Furthermore, thanks to the different specimen dimensions used in both devices (the LTHE device requires specimens of area about 1.5 times greater than the ICEA one) also the influence of the size effects was investigated.

Table 5.1.6. Characteristics of the Inclined Plane devices available at LTHE and ICEA laboratories.

Inclined Plane device	Dimensions	Fixation upper support	Limit upper box displacement (u_{lim})	Vertical stress application
LTHE	LOWER LAYER: $L_L = 1.3\text{m}$; $B_L = 0.8\text{m}$ UPPER LAYER: $L_U = 0.18\text{m}$; $B_U = 0.7\text{m}$	Upper layer glued to wood support	0.9m	Metal plates
ICEA	LOWER LAYER: $L_L = 1.1\text{m}$; $B_L = 0.24\text{m}$ UPPER LAYER: $L_U = 0.35\text{m}$; $B_U = 0.2\text{m}$	Upper layer anchored to steel support	0.6m	Metal plates

5.1.3.1 Methodology and materials

To assess the reproducibility and the size effects different inclined plane tests were carried out at LTHE and ICEA laboratories on GTX-GMB_s interface which gives the best repeatability, along the machine direction of the products, at a vertical stress $\sigma_{v0} = 5 \text{ kPa}$ and at a temperature $T = 20^\circ\text{C}$.

The friction angles were evaluated with the two devices and results were compared. Both virgin and wear specimens were used; the latter category refers to specimens subjected to multiple sliding (at least three) of the upper box along the plane.

Test results regarding virgin specimens are reported in terms of the mean value (calculated as the average of all the values obtained) while, a range of values is reported for the wear specimens because the results depend on the level of damage.

5.1.3.2 Results, discussion and conclusions

Table 5.1.7 displays friction angles of GTX – GMB_s interface obtained at LTHE and ICEA laboratories. It should be pointed out that some slight differences in the test results may arise from the operative conditions of the different devices: for example the techniques for fixing the interface layers (continuous gluing or discontinuous anchoring) or the stiffness and planarity of the support even made of different materials (wood, steel).

Referring to the reproducibility, the results of the tests carried out on virgin specimens with both different devices, show for ϕ_0 a maximum scatter of about $\pm 0.8^\circ$ ($\pm 5.7\%$ respect to the mean value or ± 0.001 in terms of friction coefficient). For ϕ_{lim} the analogous scatter is of about $\pm 0.5^\circ$ ($\pm 4.3\%$ respect to the mean value or ± 0.009 in terms of friction coefficient). A greater difference of about $\pm 1.1^\circ$ ($\pm 4.3\%$ respect to the mean value or ± 0.01 in terms of friction coefficient) was found for the dynamic friction angles. As ϕ_{dyn}^{IP} values are calculated during the sliding phase, one of the possible causes of the difference may be attributed to the different length of the plane.

A more delicate issue is matching test results of wear specimens being them dependent on the damaging induced by the multiple sliding. In spite of the different level of damaging (the maximum available displacement, u_{max} , is 0.9 m in LTHE apparatus, while it is equal to 0.7 m in DICEA device), even in the wear specimens the data regarding the friction angles can be considered reproducible (Table 5.1.7), being a maximum range of variation of 0.2° for ϕ_0 , 1.3° for ϕ_{lim} and 1° for ϕ_{dyn}^{IP} .

Finally, a comparison between the results obtained by both devices allowed analysing the effect of the specimen size. Changing the specimen dimensions, in addition to other devices differences, no appreciable difference in shear strength is observed. Therefore, the results do not exhibit significant scale effect due to the specimen dimensions involved in these experiments as it could be expected testing fabric-continua interfaces as in the case of geotextile and geomembrane products.

Table 5.1.7. Friction angles of GTX – GMB_s interface obtained at the LTHE and ICEA laboratories applying the UIPP ($T = 20^\circ\text{C}$ and $\sigma_{v0} = 5 \text{ kPa}$).

	LTHE			ICEA		
	$\phi_0 (^\circ)$	$\phi_{lim} (^\circ)$	$\phi_{dyn}^{IP} (^\circ)$	$\phi_0 (^\circ)$	$\phi_{lim} (^\circ)$	$\phi_{dyn}^{IP} (^\circ)$
Virgin Specimens	14.0 \pm 1.0	11.7 \pm 0.2	17.3 \pm 0.8	13.9 \pm 1.3	12.2 \pm 0.3	16.5 \pm 0.3
Wear Specimens	12.3 \div 13.5	10.1 \div 11.0	16.7 \div 17.8	12.7 \div 13.3	9.4 \div 10.7	15.4 \div 16.3

* ϕ_{dyn}^{IP} values are determined applying the variant to Step 2 of the UIPP

5.1.4 Influence of the mean relative velocity

The Inclined Plane test results showed that the interface friction strictly depends on the kinematic conditions (Table 5.1.2 and Table 5.1.3). The Inclined Plane is a suitable device to simulate several kinematic configurations. In this context, in order to assess this specific aspect, the influence of the relative velocity, v , here defined as the upper box average velocity during the slide, was taken into account for interfaces a , b and c (Table 2.3.2).

Depending on the type of motion, the velocity is assessed as follows:

- for uniform motion:

$$v = \frac{du}{dt} \quad 5.1-1$$

- for uniformly accelerated motion:

$$dv = a_{\text{const}} \cdot dt \quad 5.1-2$$

with a_{const} constant upper box acceleration, u , upper box displacement and t , the time.

A special set of tests was especially dedicated to give an insight on the evolution of the dynamic (or kinetic) interface behaviour with velocity and the following approach was used. The Variant to Step 2, with the plane maintained at fixed inclinations, was carried out on both LTHE and ICEA laboratory at a room temperature ($T = 20^\circ\text{C}$) and under a vertical stress, $\sigma_{v0} = 5 \text{ kPa}$. Unlike to test series presented in Figure 5.1.3 - § 5.1.1.1.1, the plane inclinations was varied in a larger range ($12.6^\circ < \beta < 25^\circ$ with $\beta > \beta_0$) in order to study the interface response under a wide set of velocity. These interfaces were selected because, showing a gradual sliding behaviour (§ 5.1.1.1), the velocity can easier be studied from “low – medium” ($v = 1\text{-}10 \text{ cm/s}$) to “high” ($v = 20\text{--}120 \text{ cm/s}$) range of velocity.

Figure 5.1.15 displays the variation of the dynamic friction behaviour with the mean relative velocity. Each dot on the diagrams represents the result of a single test at a fixed plane inclination, v increasing with the inclination β .

Test results can be grouped into two main parts according to the range of velocity. At low – medium velocity, a uniform motion of the upper box is generally observed; in these cases the velocity, almost constant (zero acceleration – uniform motion), is calculated according to Equation 5.1-1 during the steady-state motion of the box and the friction angle, $\phi_{\text{dyn}}^{\text{IP}} (v_{\text{box}} = \text{const})$, is evaluated by using Equation 4.1-8 (noting that β does not vary being fixed)

At high velocities, the upper box slides with a uniformly accelerated motion and the relative velocity varies linearly in the time (Equation 5.1-2). Thus, the dynamic friction angle, $\phi_{dyn}^{IP}(a_{box} = \text{const})$, computed by Equation 4.1-7, is referred to the average value of the box velocity, v , calculated in the range of time where the acceleration reaches a constant value.

The results plotted in Figure 5.1.15 are also summarized in Table 5.1.8.

Table 5.1.8. Influence of the mean relative velocity, v , on the dynamic interface friction angles.

Interface tested	Upper box velocity (cm/s)	$\phi_{dyn}^{IP}(v_{box} = \text{const})$ (°)	Upper box velocity (cm/s)	$\phi_{dyn}^{IP}(a_{box} = \text{const})$ (°)
GTX - GMB_s	1-10	15.0±0.9	20-120	17.3±0.8
GNT - GMB_s	1-10	16.3±0.5	20-120	16.9±0.4
GCD_N - GMB_s	1-10	14.0±0.5	20-120	15.9±0.6

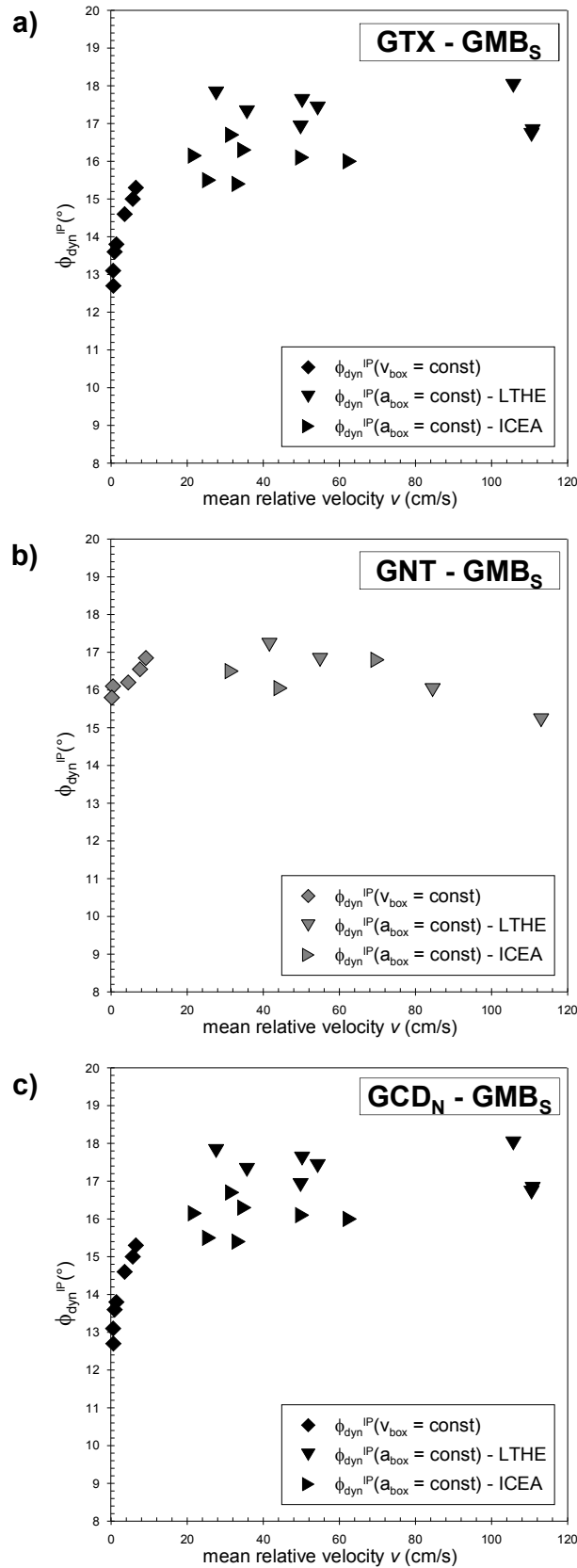


Figure 5.1.15. Influence of the mean relative velocity, v , on the dynamic interface friction angles obtained for uniform ($v_{box} = \text{const}$) and uniformly accelerated motions ($a_{box} = \text{const}$) using ICEA and LTHE inclined plane devices.

The general trend highlighted in all the tests is characterized by an increase in the dynamic friction angle with the increase in the mean relative velocity. In particular, at low velocities, when the motion can be approximated as uniform, the dynamic friction angle increases following a non-linear relationship. Once the uniformly accelerated motion is established, an upper bound of the dynamic friction angle can be defined: here $\phi_{\text{dyn}}^{\text{IP}} (a_{\text{box}} = \text{const})$ does not increase anymore and almost constant values can be calculated even increasing the mean relative velocity.

It is believed that the uniform motion established at the interface may represent the transition between the static and the dynamic phase. This transitory - phase appears clearly in interfaces showing gradual sliding behaviour (during the entire Step 2), while is very short for interfaces displaying a sudden sliding behaviour.

In order to clearly demonstrate this behaviour, Figure 5.1.16 reports inclined plane test results of GTX – GMB_S interface obtained at ICEA laboratory (also included in Figure 5.1.16) in the case of vertical stress, σ_{v0} , equal to 5 kPa.

In the first part, the results of the inclined plane tests when the angle β is close to β_0 is reported while in the second inclined plane tests in which the plane inclination is remarkably higher than β_0 are plotted.

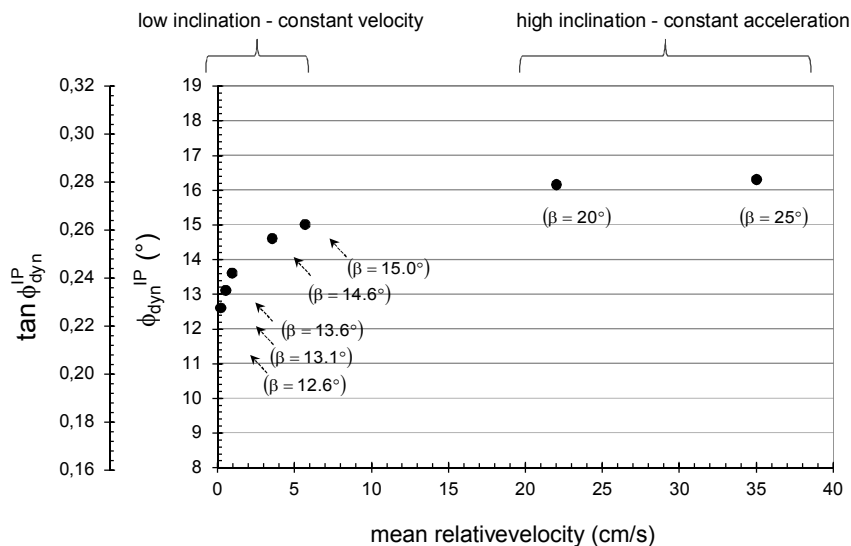


Figure 5.1.16. Dynamic friction angle versus sliding velocity provided by the ICEA inclined plane ($\sigma_{v0} = 5\text{kPa}$) of GTX - GMB_S interface.

When the plane inclination remains beneath the upper bound value corresponding in this case to an angle of about 16.2° , the sliding reaches the condition of uniform motion,

because the driving force can be approximately balanced by the friction force. When the plane inclination exceeds the value of 16.2° , the motion is accelerated, because the friction force is no longer able to fully equilibrate the driving force.

Concluding, as shown by Figure 5.1.16, an increase of the dynamic friction with the velocity can be observed. However, this increase of the dynamic shear strength with the velocity is not unlimited and reaches an upper bound value at high velocities. At this stage the dynamic friction angle is stabilized with respect to the relative velocity so that a constant value can be found for any high velocity. Then, to confirm what stated above, some dynamic interface friction angles of GTX – GMB_s interface obtained applying the variant to Step 2 with plane inclinations $\beta \gg \beta_0$ (high relative velocity) are displayed in Table 5.1.9.

Table 5.1.9. Dynamic interface friction angles of GTX – GMB_s interface obtained applying the variant to Step 2 of the UIPP with plane inclinations $\beta \gg \beta_0$ ($\sigma_{v0} = 5 \text{ kPa}$; $T = 20^\circ\text{C}$; ICEA laboratory).

Interface tested		$\phi_{\text{dyn}}^{\text{IP}}$ (°)	β (°)	v_{box} (cm/s)	a_{box} (m/s ²)
a.	GTX - GMB _s	16.7	18.5	31.8	0.31
		16.3	20.0	22.0	0.72
		16.1	25.0	35.0	1.63

5.1.5 Influence of the normal stress

Interface behaviour can be influenced also by normal stress; the GTX – GMB_s interface was tested under different vertical stress (0.08 kPa; 0.8 kPa; 5 kPa and 12 kPa) to capture variations on friction as function of this parameter.

Figure 5.1.17a reports sliding test results at various normal stresses in terms of a mobilized friction coefficient towards sliding velocity, limited to the range of the medium-low velocities. The interface friction decreases with the increase of the vertical stress. Under the same normal stress, by increasing the velocity the friction angle increases of about $3^\circ - 4^\circ$ (corresponding to a difference of 0.05 – 0.06 in terms of $\tan \phi_{\text{dyn}}^{\text{IP}}$). Figure 5.1.17b is a

zoomed view of Figure 5.1.17a in the field of velocities lower than 1 cm/s where the intercept values of dynamic friction coefficient at zero velocity ($\tan \phi_{v=0}^{IP}$) is compared to the static ones ($\tan \phi_0$ and $\tan \phi_{lim}$). It was found that the intercept values $\tan \phi_{v=0}^{IP}$ matches $\tan \phi_{lim}$ values. Consequently, $\tan \phi_{lim}$ matches the limit value of $\tan \phi_{dyn}^{IP}$ at $v = 0$, reminding that, for definition, ϕ_{lim} corresponds to the static friction angle after shearing. On the other hand, $\tan \phi_0$ is systematically higher.

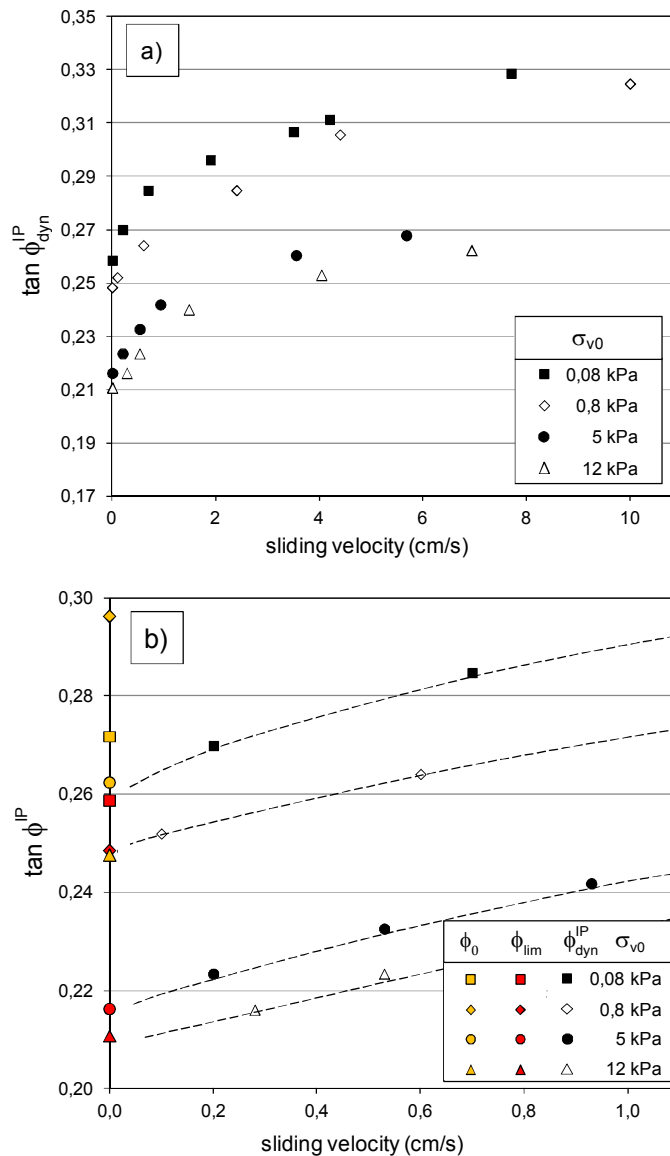


Figure 5.1.17. a) Dynamic friction coefficient versus the sliding velocity for the tests showing uniform motion (ICEA laboratory) of GTX - GMB_s interface; b) Zoomed view of the low relative velocity range of values.

Moreover, it should be noticed that the dynamic friction trends are similar in shape for all the normal stress levels. By normalizing respect to $\tan \phi_{lim}$ (with $\tan \phi_{V=0}^{IP} = \tan \phi_{lim}$ as demonstrated in Figure 5.1.17) and fitting all the data (Figure 5.1.18), a relation independent of the normal stress can be obtained:

$$\frac{\tan \phi_{dyn}^{IP}}{\tan \phi_{lim}} = \left[1 + \alpha \left(1 - e^{-\delta v^\gamma} \right) \right] \quad 5.1-3$$

in which the velocity v is expressed in cm/s and the constants were fixed by regression, thus obtaining $\alpha = 0.36$, $\delta = 0.31$ and $\gamma = 0.75$ for the GTX – GMB_s interface.

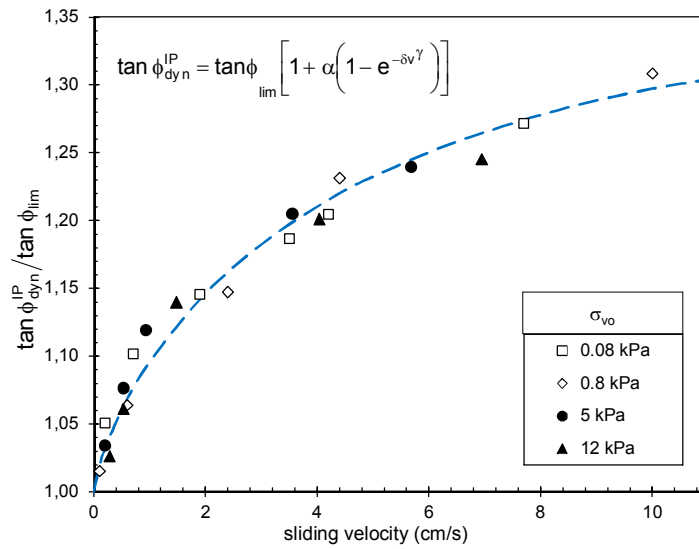


Figure 5.1.18. Normalized dynamic friction coefficient versus sliding velocity (GTX - GMB_s interface - ICEA laboratory).

As previously stated, also $\tan \phi_{lim}$ varies in an inverse proportion with the normal stress (Figure 5.1.19) so that the following relationship can be deduced:

$$\tan \phi_{lim} = \tan \phi_{lim, \sigma_{v0}=0} - \eta \left(1 - e^{-\zeta \sigma_{v0}} \right) \quad 5.1-4$$

In which $\tan \phi_{lim, \sigma_{v0}=0}$ is the value at zero normal stress and σ_{v0} is the vertical stress expressed in kPa. The constants $\tan \phi_{lim, \sigma_{v0}=0}$, η and ζ were evaluated by regression, thus obtaining $\tan \phi_{V=0, \sigma_{v0}=0}^{IP} = 0.2595$, $\eta = 0.05$ and $\zeta = 0.4$ for the GTX – GMB_s interface. As

shown by Equation 5.1-4, a marked non-linearity arises at low stress and the limit friction angle may vary of about 3° (or 20% in terms of $\tan \phi_{lim}$). By exceeding a vertical stress of about 8 kPa, $\tan \phi_{lim}$ approaches an almost constant value (Figure 5.1.19). For comparison, in Figure 5.1.19 also the trend of $\tan \phi_0$ is displayed.

It's worth noting that this trend could be specific to this pair of geosynthetics. For the present interface GTX – GMB_S no interpenetration of the structures of the two geosynthetics increasing with the normal stress is expected, unlike other structures.

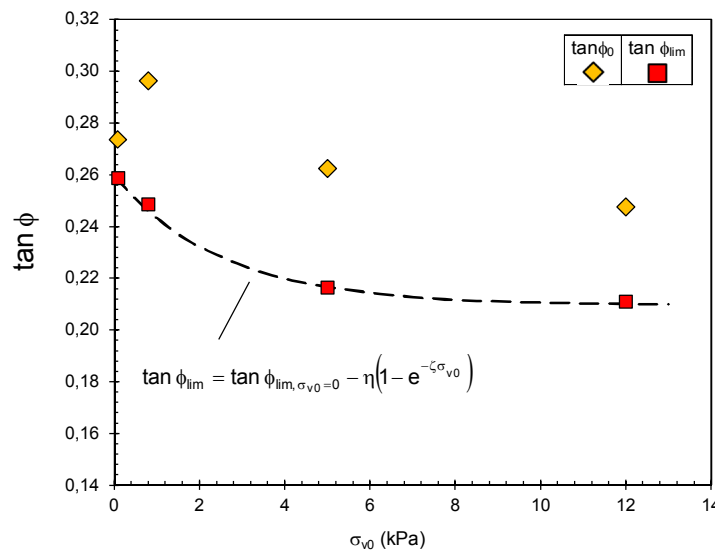


Figure 5.1.19. Variation of the limit interface coefficient of friction with vertical load (GTX - GMB_S interface - ICEA laboratory).

Wasti and Özdüzgün, (2001) comparing inclined plane test with direct shear test results, found a similar trend (Figure 5.1.20), taking into the account that the friction angle obtained from inclined plane tests is the angle of inclination at which sliding occurs applying a static equilibrium analysis.

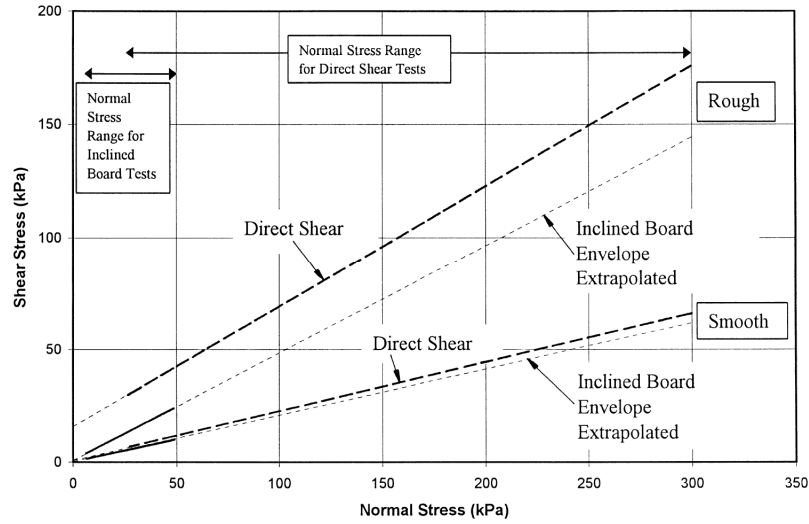


Figure 5.1.20. Effect of normal stress level on the test results: non-woven geotextile – smooth geomembrane (after Wasti and Özdüzgün, 2001).

The interface shear strength can be expressed as a function of the effective normal stress by a Mohr – Coulomb criterion:

$$\tau = \sigma'_{v0} \cdot \tan \phi' \quad 5.1-5$$

It is assumed that when sliding occurs at an interface, the shear stress has overcome a frictional resistance $\sigma'_{v0} \cdot \tan \phi'$ which is dependent on the normal stress acting on the interface. Furthermore, as already demonstrated (Lalarakotoson et al., 1999); Wasti and Özdüzgün, 2001) the inclined plane results of geosynthetic interfaces have a small adhesion that can be neglected, assuming the behaviour as purely frictional.

As studied in literature, for soils, the failure envelope may be curved especially for dense granular soil under low effective normal stresses. Even in the case of geosynthetic interfaces, a slight curvature of the failure envelope can be observed. However, a straight line approximation can still be taken over the effective vertical stress range of interest and the interface shear strength parameters determined for that range (Jones and Dixon, (1998); Wasti and Özdüzgün, (2001)).

In order to investigate the behaviour at low normal stress, failure envelopes of the “static” and “limit” friction coefficient are displayed in Figure 5.1.21. The resulting failures envelopes (Equation 5.1-5) were obtained as the best fitting to the data points of σ_{v0} and τ where the vertical stresses σ_{v0} (varying from 0.08 to 12 kPa) and ϕ is ϕ_0 for the “static” and ϕ_{lim} for the “limit” failure envelope.

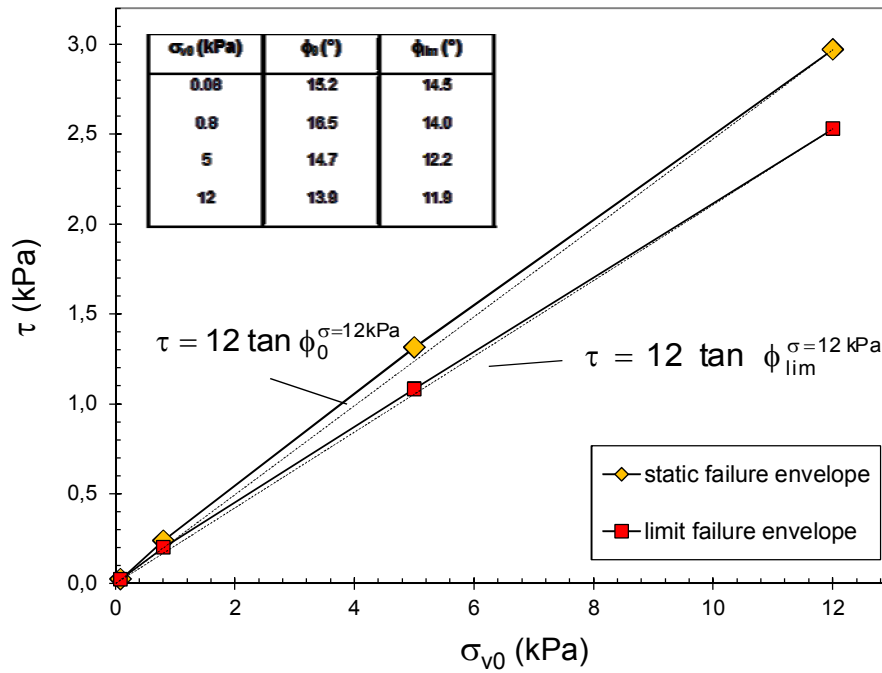


Figure 5.1.21. Comparison between static failure envelopes on GTX-GMB_s interface.

As it could be notice in Figure 5.1.21, a moderate curvature (non-linear envelope) may be observed on both static and limit failure envelopes especially for the range of normal stresses (0.08-5kPa) with a diminishing rise in the amount of increase in the limit shear strength as the normal stress increases. The non-linearity of failure envelopes reduces at higher normal stresses (5-12 kPa). Furthermore, the loss of interface shear strength with displacement can be quantified by considering the ratio of limit to static friction angle, D , where:

$$D = \frac{\tan \phi_{lim}}{\tan \phi_0} \quad 5.1-6$$

The resulting D varies from 0.95 for σ equal to 0.08 kPa to 0.82 for σ_{v0} equal to 5 kPa.

A similar trend was found by Wasti and Özdüzgün, (2001) testing nonwoven needle-punched geotextiles in contact with HDPE and PVC smooth and rough geomembranes on the inclined plane with σ ranging from 5 to 50kPa (Figure 5.1.22 i) taking into account that the interface friction angle was calculated during the upper box sliding applying the static equilibrium. Also, Jones and Dixon (1998) testing a smooth geomembrane in direct contact with a non-woven needle punched geotextile with a large direct shear tests (Figure 5.1.22 ii) under higher normal stress level 25, 50 and 100 kPa. In this case, a reduction passing from the peak to the residual shear strength is observed.

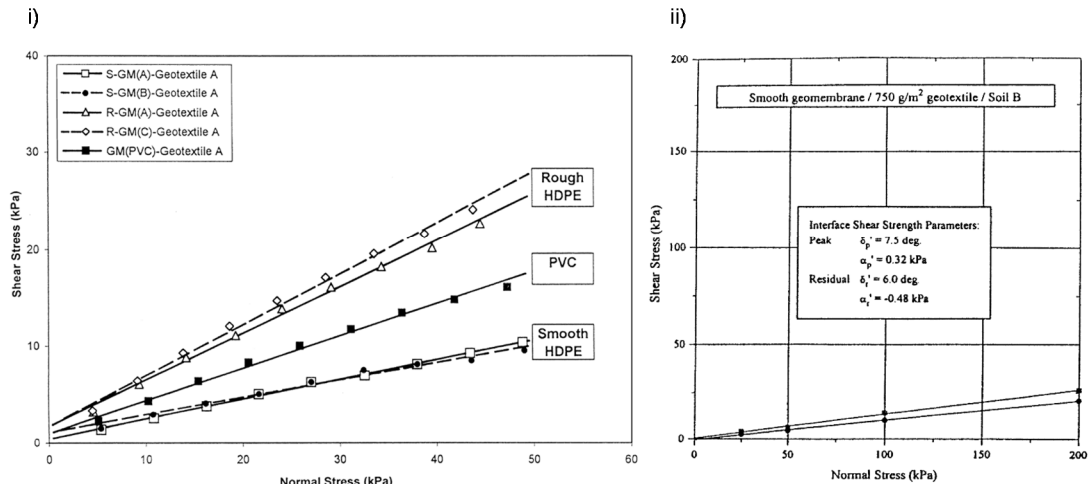


Figure 5.1.22. Shear stress vs normal stress non-woven geotextile - geomembrane: i) inclined plane tests (after Wasti and Özdüzgün, 2001); ii) direct shear tests (after Jones and Dixon, 1998).

5.1.6 Influence of mechanical damage (wear effect)

It is well known that geosynthetics may degrade and damage. The first is mainly related to ageing of the polymer while the second is a consequence of managing (Giroud, 2012).

The processes of damage of geosynthetic surfaces during the installation of the product under construction and during the other stages of the constructive process can enhance the degree of surface wear of interfaces constituted by such polymeric materials (Pitanga et al., 2013).

Wear is related to interactions between surfaces and more specifically the removal and deformation of material on a surface as a result of mechanical action of the opposite surface. The need for relative motion between two surfaces and initial mechanical contact between asperities is an important distinction between mechanical wear compared to other processes with similar outcomes. In geosynthetics, the wear effect is better known as *abrasion* that is defined as the wearing away of a part of the material due to rubbing against another surface (Shukla and Yin, 2006).

Geosynthetic interfaces are sensitive to the surface wear process (Pitanga et al., 2013; Hebel et al., 2005). This sensitivity has consequences in friction properties, and it may increase or decrease their stability under the conditions of service. The damaging effect due to the relative tangential displacement can increase or decrease the interface friction, depending of the pair of associated geosynthetics. Additional factors such as the relative

position among the elements of the interface and the structure of these elements also interfere with the mechanism of wear resistance. In the field, conditions of deployment of the geosynthetic lining systems on slopes, initial wrinkles, and individual conditions of tensile mobilization of the geosynthetics might induce large relative displacements at the interfaces. For these large displacements the alteration of the geosynthetic surface by abrasion can also significantly modify the limit friction angle. The previous knowledge of this sensitivity is, therefore, an important issue of design, which must be considered by the manufacturers of geosynthetics, by the project designers and by the executors of civil works that involve the application of these polymeric materials. Such knowledge can provide a quantitative basis useful for the development of products, for the choice of most appropriate geosynthetic interfaces to the surface wear predicted in work (Pitanga et al., 2013) and also for the care to handle during the laying of geosynthetics in the field.

In addition to the material hardness conveyed by the polymeric constitution, other factors governing the mechanism of interface wear are: the surface roughness (smooth or rough surface), the nature of contact material (natural or synthetic), the level of the effective normal stress acting on the interface (Dove, 1996; Dove et al., 1997; Lee et al., 1998; Frost and Lee, 2001) and the possible influence of aggressive chemical agents (i.e. leakage).

In this context, the goal of this experimental study was to characterize the wear resistance of the geosynthetic interfaces listed in Table 2.3.2.

In order to simulate the effect of wear under conditions similar to operational conditions, repeated inclined plane tests were conducted at the same experimental conditions, under normal stress equal to 5 kPa in dry conditions. The tests were repeated N times on the same specimens, causing a progressive rubbing of the surfaces at contact as schematized in Figure 5.1.23, for a total cumulative displacement of the upper box u_U , at least of 3.6 m (2.7m for interfaces d , e , f and g).

It's worth noting that the kinematic process is not symmetrical for the two geosynthetics, relative shear displacement is far higher for the upper geosynthetic (Figure 5.1.23). The lower specimen is only subjected to a relative displacement u_L corresponding to N times the length of the upper box ($L_U = 180$ mm). Thus, the result of the test is more characteristic of the upper geosynthetic than the lower one.

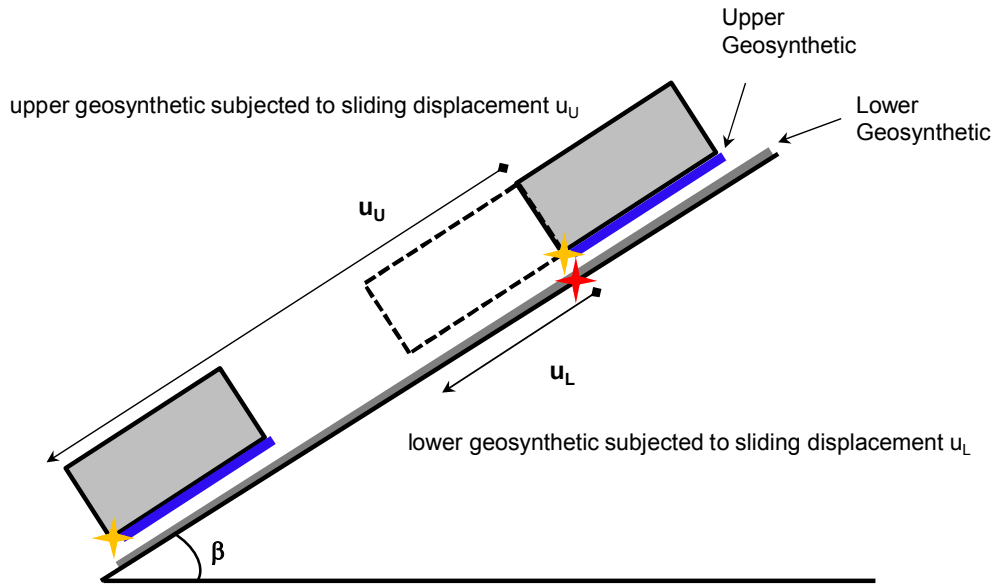


Figure 5.1.23. Schematization of the kinematic processes of the upper and the lower geosynthetics.

5.1.6.1 Wear tests on interfaces involving smooth geomembrane

Figure 5.1.24 displays the sliding behaviour of the GTX - GMB_S, GNT – GMB_S and GCD_N – GMB_S interfaces tested the first time (virgin specimen) and after large displacements (multiple slides). In particular, the wear effect is studied after four and six successive passages of the upper box along the plane. It should be pointed out that in every test, the upper box maximum displacement is equal to $u_{lim} = 0.6$ m for a total cumulative displacement of 3.6 m (for the 6th retest).

Table 5.1.10 summarizes, in terms of ϕ_0 and ϕ_{lim} , test results plotted in Figure 5.1.24. for comparison also the variation of the dynamic friction angles is displayed. From Table 5.1.10, it is possible to observe that, generally, ϕ_{dyn}^{IP} is less sensitive to this parameter (i.e. the range of variation due to the wear effect is similar to the range of repeatability of the tests). For this reason the analysis presented herein is addressed only to ϕ_0 and ϕ_{lim} behaviour.

By analysing test results it could be noticed that, as soon as the number of sliding increases, a progressive modification of both ϕ_0 and ϕ_{lim} , is observed in all the interfaces tested. In particular, for GTX - GMB_S interface both ϕ_0 and ϕ_{lim} tend to reduce. Conversely, the GNT – GMB_S behaviour shows an increase of interface strength with shearing. Finally, the GCD_N – GMB_S interface response displays an increase in ϕ_0 and a decrease in ϕ_{lim} values at large displacements. The loss in shear strength noticed in GTX – GMB_S interface seems to be related to the smoothing of the surfaces in contact as the number of sliding increases and has a more marked effect on ϕ_{lim} which can decrease up to 3° (0.05 in terms

of tangent value). Conversely, visual inspection of specimens after testing highlights that rubbing between GNT – GMB_S at large displacements roughens surfaces increasing the interface friction of about 3° (0.05 in terms of tangent value) for both ϕ_0 and ϕ_{lim} . Finally, the behaviour of GCD_N – GMB_S shows an increase of ϕ_0 and a decrease in ϕ_{lim} values displaying a more marked effect of the support (GNT) in the static friction rather than in the limit one which trend follows the GTX – GMB_S behaviour.

Considering test results of Table 5.1.10, a damage index (DI) is calculated for both coefficient of friction $\tan \phi_0$ and $\tan \phi_{lim}$ as follows:

$$DI = \frac{(\tan \phi_{\text{virgin}} - \tan \phi_{\text{re-tested}})}{\tan \phi_{\text{virgin}}} \cdot 100 \quad 5.1-7$$

In terms of DI the maximum variation of the friction coefficient calculated as difference between results obtained for virgin materials and for the interface tested at 3.6m (6th retest) is about 22.1% regarding $\tan \phi_0$ for GNT – GMB_S interface and 25.9% involving $\tan \phi_{lim}$ for GCD_N - GMB_S interface.

Let notice that DI for ϕ_0 and ϕ_{lim} are not systematically of the same sign.

Table 5.1.10. Effect of wear on interface friction angles of GTX - GMB_s; GNT - GMB_s and GCD_N - GMB_s evaluated for virgin and retested specimens (four and six upper box sliding) ($T = 20^{\circ}\text{C}$; $\sigma_{v0} = 5 \text{ kPa}$, LTHE laboratory).

Interface tested	Number of test	Upper box displacement (m)	ϕ_0 (°)	$DI_{\tan \phi_0}$ (%)	Upper box displacement (m)	ϕ_{lim} (°)	$DI_{\tan \phi_{lim}}$ (%)	$\phi_{dyn}^{IP} (v_{box} = const)$ (°)	$DI_{\tan \phi_{dyn}^{IP} (v = const)}$ (%)	$\phi_{dyn}^{IP} (a_{box} = const)$ (°)	$DI_{\tan \phi_{dyn}^{IP} (a = const)}$ (%)
GTX - GMB_s	virgin	0.001	14.4		0.6	11.6		15.9		17.6	
	4 th retest	1.8	13.4	±15.1	2.4	11.0	±12.3	15.1	±13.2	17.4	±4.5
	6 th retest	3.0	12.3		3.6	10.2		13.8		16.8	
GNT - GMB_s	virgin	0.001	13.3		0.6	13.1		15.9		17.2	
	4 th retest	1.8	14.2	±22.1	2.4	15.7	±29.0	17.0	±4.4	16.8	±6.9
	6 th retest	3.0	16.1		3.6	16.8		16.6		16.0	
GCD_N - GMB_s	virgin	0.001	13.6		0.6	12.6		14.2		16.30	
	4 th retest	1.8	15.4	±19.3	2.4	11.9	±25.9	15.6	±2.1	16.20	±2.4
	6 th retest	3.0	16.1		3.6	9.4		15.3		15.90	

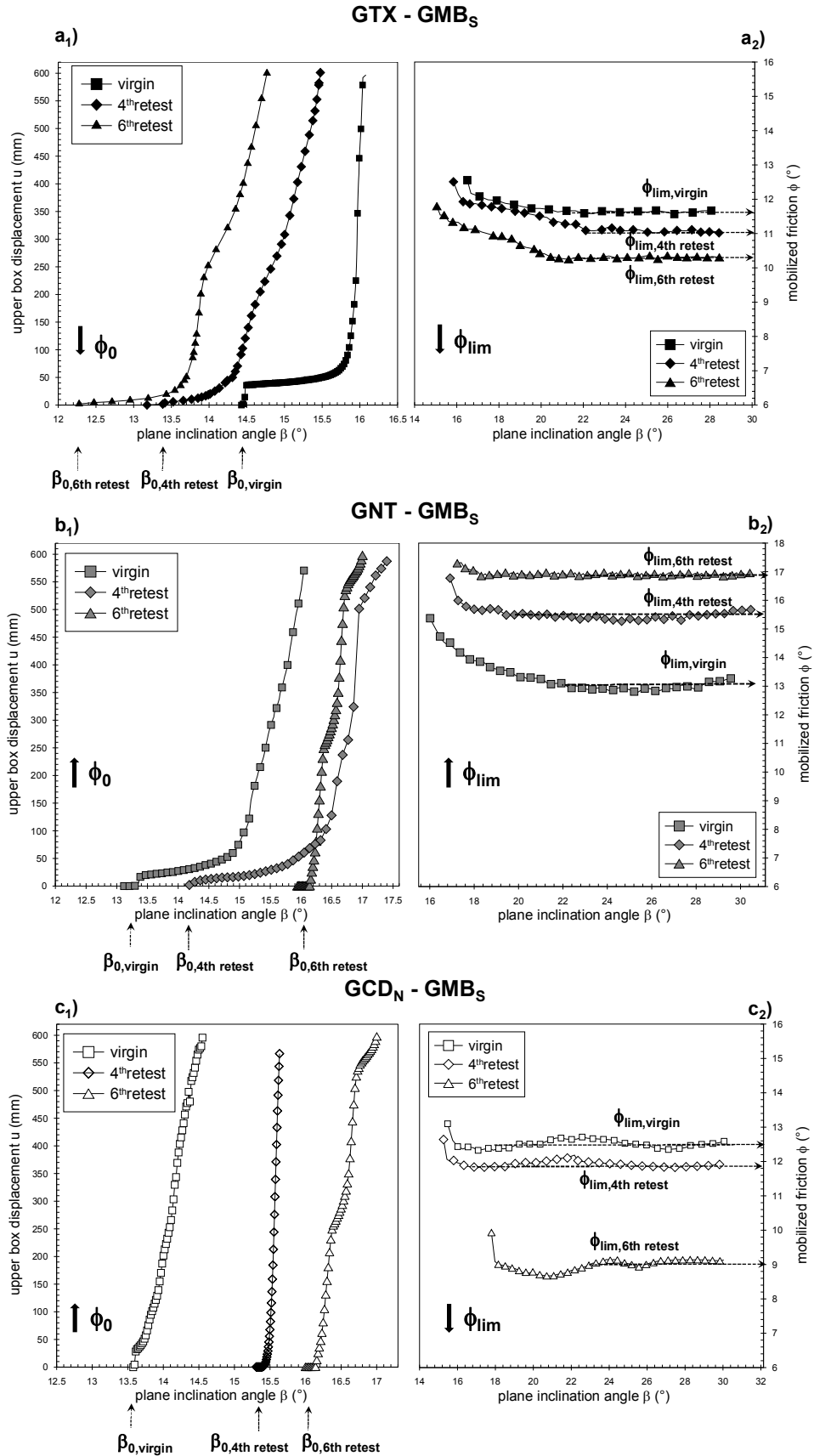


Figure 5.1.24. Wear effect on GTX – GMB_s, GNT – GMB_s, GCD_N – GMB_s interfaces simulated by retesting materials (multiple sliding of the upper box) at the inclined plane ($T = 20^\circ$, $\sigma_{v0} = 5\text{ kPa}$ – LTHE laboratory): a₁), b₁) and c₁) Step 1 and Step 2 of the UIPP; a₂), b₂) and c₂) Step 3 of the UIPP.

5.1.6.2 Wear tests on interfaces involving textured geomembranes

Figure 5.1.24 displays the sliding behaviour of the $GCD_N - GMB_{TMH}$, $GCD_W - GMB_{TMH}$, $GCD_N - GMB_{RMH}$ and $GCD_W - GMB_{RMH}$ interfaces tested the first time (virgin specimen) and after large displacements (multiple slides). In this case, since for these interfaces the surface damage is relevant, it was possible to repeat the test only three times on the same interface. Therefore, wear effect was studied for specimen retested two (2nd retest) and three times (3rd retest) for a maximum cumulative displacement of 2.7 m (0.9 m for a single test).

Test results plotted in Figure 5.1.25 are schematized in Table 5.1.11 in terms of ϕ_0 and ϕ_{dyn}^{IP} . It is worth noting that, due to the difficulties encountered in performing Step 3, the influence of the mechanical damage on ϕ_{lim} values was not investigated.

Table 5.1.11. Effect of wear on interface friction angles of $GCD_N - GMB_{TMH}$, $GCD_W - GMB_{TMH}$, $GCD_N - GMB_{RMH}$ and $GCD_W - GMB_{RMH}$ evaluated for virgin and retested specimens (four and six upper box sliding) ($T = 20^\circ C$; $\sigma_{v0} = 5 \text{ kPa}$, LTHE laboratory).

Interface tested	Number of test	ϕ_0 (°)	$DI_{\tan\phi_0}$ (%)	ϕ_{dyn}^{IP} (°)	$DI_{\tan\phi_{dyn}^{IP}}$ (%)
$GCD_N - GMB_{TMH}$	virgin	25.9		27.9	
	2 nd retest	25.8	±11.3	/	±19.4
	3 th retest	23.6		23.1	
$GCD_W - GMB_{TMH}$	virgin	28.5		25.8	
	2 nd retest	25.4	±14.9	33.2	±43.8
	3 th retest	24.8		34.8	
$GCD_N - GMB_{RMH}$	virgin	38.2		35.9	
	2 nd retest	32.8	±24.8	38.6	±13.0
	3 th retest	30.6		32.2	
$GCD_W - GMB_{RMH}$	virgin	33.4		39.0	
	2 nd retest	31.7	±8.1	39.0	±0.7
	3 th retest	31.2		39.2	

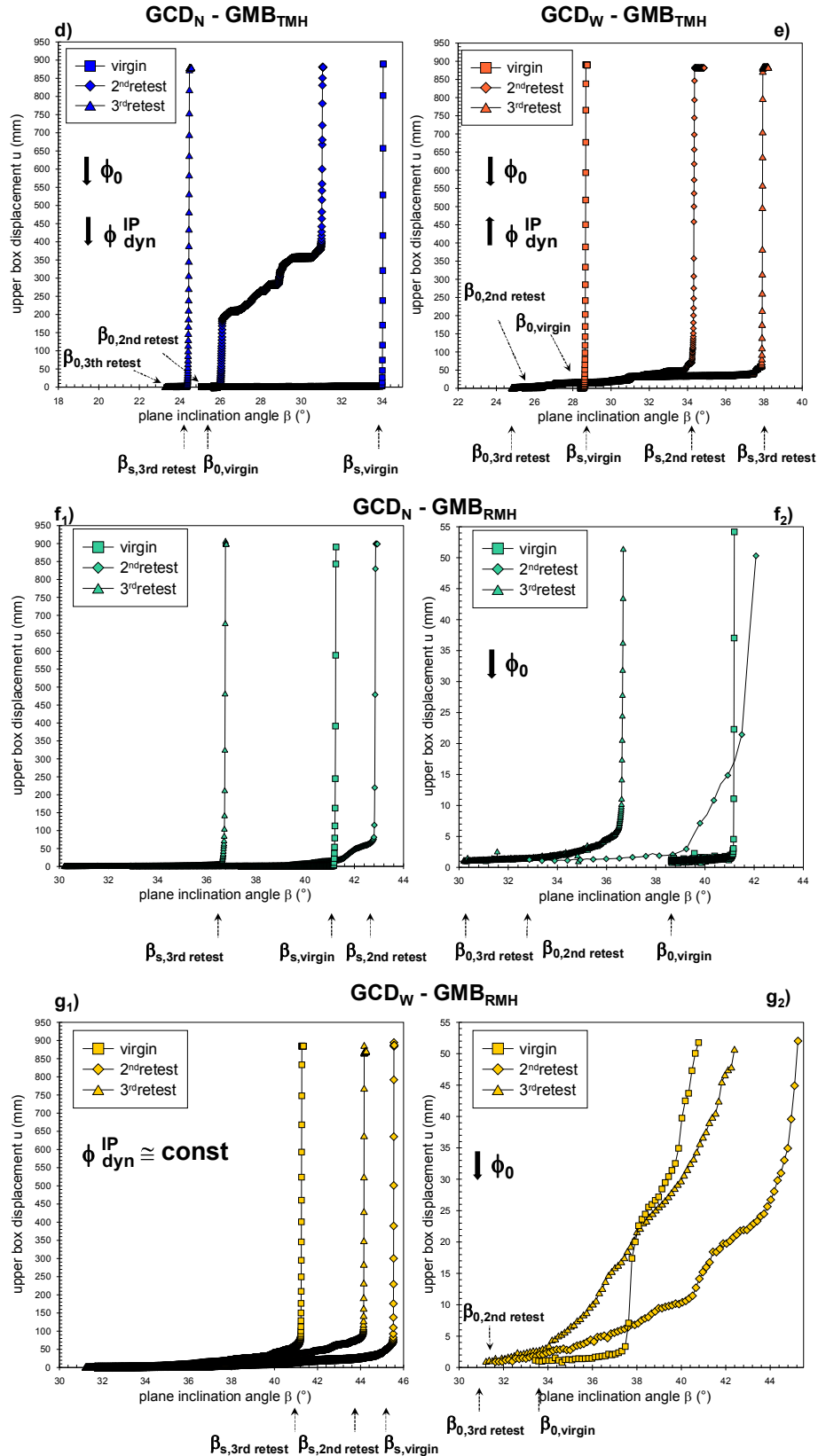


Figure 5.1.25. Wear effect simulated by retesting materials (multiple sliding of the upper box) at the inclined plane ($T = 20^\circ$, $\sigma_{v0} = 5 \text{ kPa}$ – LTHE laboratory): d) Step 1 and 2 of UIPP of GCD_N – GMB_{TMH} interface; e) Step 1 and 2 of UIPP of GCD_W – GMB_{TMH} interface; f₁) Step 1 and 2 of UIPP of GCD_N – GMB_{RMH} interface; f₂) zoomed view of Step1 for GCD_N – GMB_{RMH} interface; g₁) Step 1 and 2 of UIPP of GCD_W – GMB_{RMH} interface; g₂) enlargement view of Step1 for GCD_W – GMB_{RMH} interface.

As it could be noticed by Figure 5.1.26, the texture of the geomembrane can cause a significant alteration of the surface of the upper layer after the multiple passages along the plane. As a consequence, also the interface friction angles change. In particular a reduction in ϕ_0 is observed for all the interfaces tested while ϕ_{dyn}^{IP} trend varies depending on the interface considered.

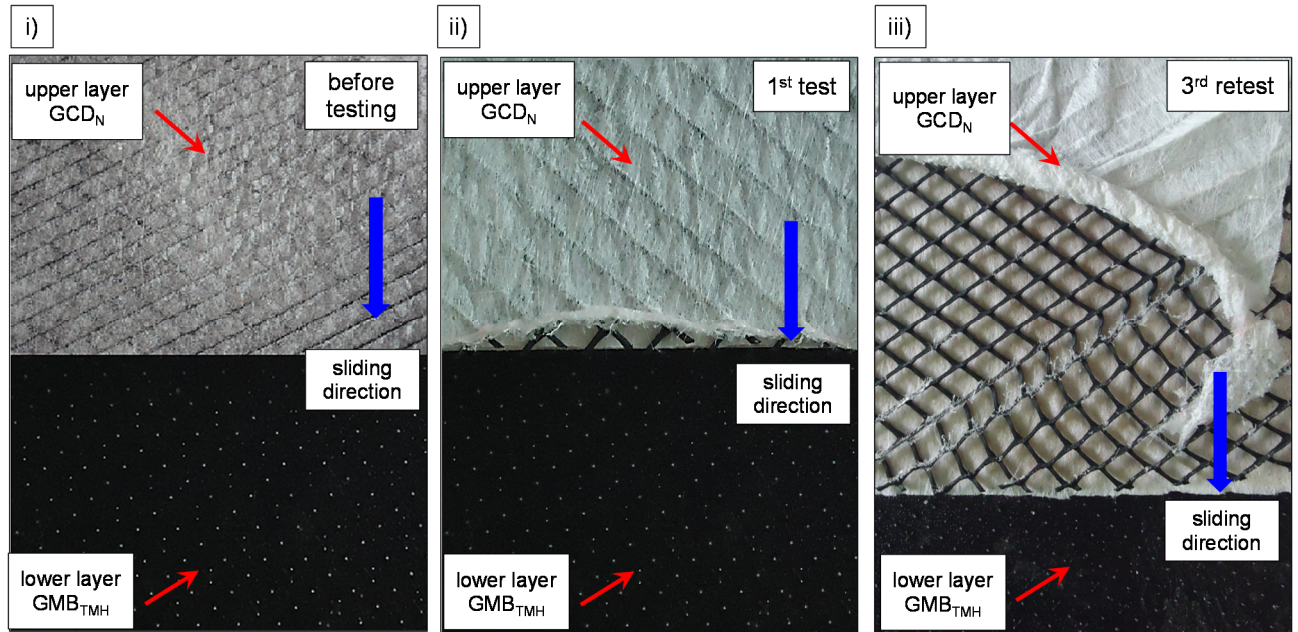


Figure 5.1.26. Damage of the surface in contact: GCD_N after testing in contact with GMB_{TMH} . i) before sliding; ii) after the first passage of the upper box; iii) after three sliding of the upper box ($T = 20^\circ$, $\sigma_{v0} = 5 \text{ kPa}$ – LTHE laboratory).

The damage index (DI) is calculated according to (Equation 5.1-7) for both coefficient of friction $\tan \phi_0$ and $\tan \phi_{dyn}^{IP}$ giving, as maximum variation, 24.8% for ϕ_0 and 43.8% regarding

ϕ_{dyn}^{IP} .

5.1.6.3 Conclusion

Geosynthetic interfaces are sensitive to the surface wear process. This sensitivity has consequences in friction properties, and it may increase or decrease their stability under the conditions of service typical to which when subjected in works. The damaging effect due to the relative tangential displacement can increase or decrease the interface friction, depending on the pair of associated geosynthetics. In addition, the particular type of

geomembrane component of a geosynthetic interface plays an important role in the response of this interface to the surface wear process.

Both systems (interfaces involving smooth and textured geomembranes) show modifications of interface shear strength upon retesting, indicating that wear can occur in the operational stress range.

In particular, the modification of both ϕ_0 and ϕ_{lim} (Figure 5.1.24) in the interfaces *a*, *b* and *c* seems to be related, through visual inspection of the specimens, to the smoothing and polishing of the surfaces in contact as the number of sliding increases and it has a more marked effect on ϕ_{lim} which can change up to 3.7° (DI = 29%).

Test results of interfaces involving textured geomembranes (*d*, *e*, *f* and *g*) show that the wear effect can be relevant and seems to be related to the alteration caused by the macrotextural features of the geomembrane on the upper layer.

In the field, large displacements at interface can occur as a consequence of particular conditions of deployment on slopes, initial wrinkles and/or individual conditions of tensile mobilization of the geosynthetics. For these large displacements, which are not considered in the standard interpretation, the alteration of the geosynthetic surface by abrasion can also significantly modify the limit friction angle.

In the case of geosynthetic systems design on slope, the alteration may cause (i) a possible failure of the system if friction of geosynthetic interfaces decreases or (ii) a tensile failure of the geomembrane in case of an increase of shearing stresses mobilized on geomembrane if friction properties of geosynthetic interfaces increase.

The previous knowledge of this sensitivity is, therefore, an important issue of design, which must be considered by the manufacturers of geosynthetics, by the project designers and by the executors of civil works that involve the application of these polymeric materials. Such knowledge can provide a quantitative basis useful for the development of products and for the choice of most appropriate geosynthetic interfaces according to the surface wear predicted in work.

5.1.7 Influence of temperature

The physical and mechanical properties of geosynthetic materials are strongly temperature dependent (Akpınar and Benson, 2005; Karademir and Frost, 2013).

The performance of geosynthetic layered systems with temperature during their service life in terms of interface shear behaviour and strength properties is of major importance for certain geotechnical applications where geosynthetics are subjected to temperature variations.

In landfill liner systems, for example, the change in temperature conditions can be mainly attributed to the seasonal temperature variations (involving overall the covers) during the temporary conditions of the construction phase as well as the heat transfer due to the exothermic reactions occurring in the waste body during its degradation. Consequently, the range of monitored temperatures at the bottom of the landfill is usually higher than that found in the final covers. Table 5.1.12 summarizes some available data about temperature in landfill liners (Karademir, 2011).

Table 5.1.12. Summary of temperature measurements in landfills (adopted from Karademir, 2011).

Authors	Temperature monitored (°C)	Measurement Location	Landfill Site	Notes
Oweis et al. (1990)	As high as 55 °C	At the bottom of refuse in the base	Northern New Jersey, USA	Municipal Solid Waste Landfill
Collins (1993)	Between 30 °C to 40 °C	In refuse from top to the base	Germany	
Bleiker et al. (1995)	Highest at 59 °C	Above the base of refuse	Toronto, Canada	Measurements at the bottom of boreholes drilled to the base
Yoshida et al. (1997)	As high as 50 °C	In landfill base	Tokyo, Japan	
Barone et al. (2000)	Between 10 °C to 37 °C	At the base	Toronto, Canada	Municipal Solid Waste Landfill
Koerner and Koerner (2006)	From 18 °C to 40 °C	In bottom liner	Eastern Pennsylvania, USA	
Montgomery and Parsons (1990)	Between 7 °C and 27 °C	In final cover	Southern Wisconsin, USA	
Corser and Cranston (1991)	As high as 43 °C	In final cover	Southern California, USA	Measurements in a test section simulating a final cover
Khire et al. (1997)	From 1 °C to 30 °C	In final cover	Central Washington State, USA	
Koerner and Koerner (2006)	Between 0 °C and 30 °C	In final cover	Philadelphia, Pennsylvania, USA	

Although composite geosynthetic interfaces are routinely exposed to different temperature conditions, tests to determine interface strengths are normally conducted in the laboratory at about 20°C. Very little information is published in the literature to date on the influence of temperatures on interface shear behaviour and strength characteristics.

The available data indicate that increasing the temperature generally results in an increase in the coefficient of friction (Akpinar and Benson, 2005; Karademir and Frost, 2013). Pasqualini et al. (1993) found an increase in the interface shear strength between a smooth LDPE geomembrane and nonwoven needle-punched geotextiles passing from 26°C to 30°C. Akpinar and Benson (2005) performed shear tests on two geomembrane-geotextile interfaces (smooth geomembrane-nonwoven geotextile and textured geomembrane-nonwoven geotextile) increasing the temperature from 0°C to 33°C at normal stresses between 7.5 and 49.5 kPa. They found that the interface friction angle increased with increasing temperature (Figure 5.1.27), even if the change in the interface friction angle was small (approximately about 2-3°C) in the range of temperatures used.

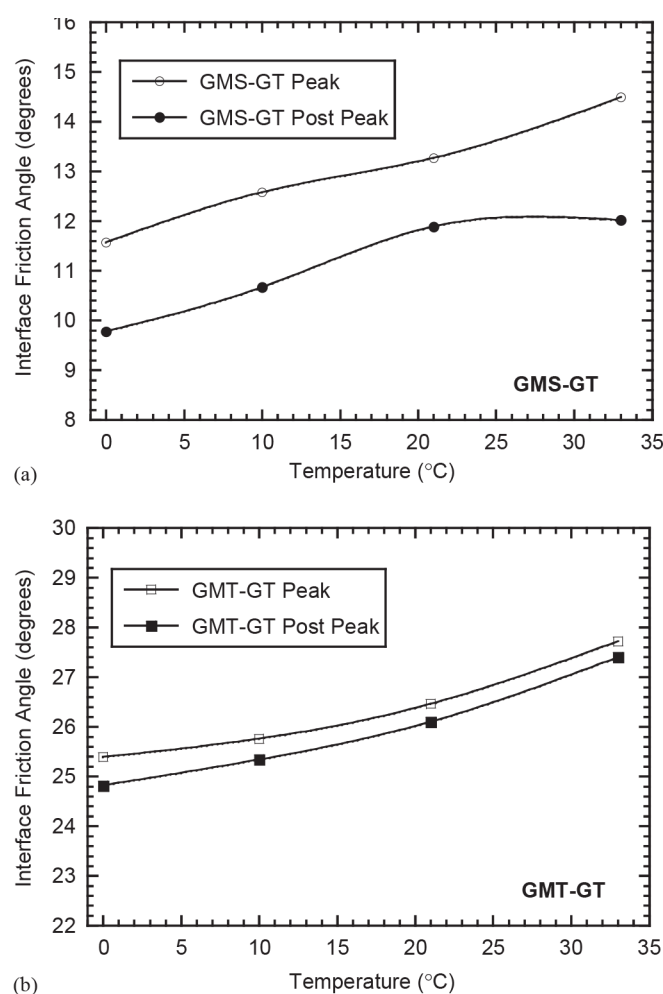


Figure 5.1.27. Friction angles corresponding to peak and post peak conditions as a function of temperature for GMT-GTX and GMS-GTX interfaces (after Akpinar and Benson, 2005).

Karademir and Frost (2013) investigated the interface behaviour of smooth geomembranes (HDPE and PVC) in contact with a nonwoven needle-punched geotextile (PP) under three different temperatures (21, 35 and 50°C) at a normal stress level of 100 kPa. The study confirmed that, increasing the temperature, the interface shear strength increases (Figure 5.1.28). Furthermore, they performed complementary tests to assess the temperature effect on the single components in terms of tensile strength for the geotextile and hardness for the geomembranes. Test results showed that the tensile stiffness of the geotextile filaments and the geomembrane surface hardness are both reduced increasing the temperature, leading to the conclusion that the frictional shear capacity of interfaces between polymeric materials is not just influenced by the effect of temperature on the individual materials but overall by the effect of temperature on the combination of materials. In addition, in the case with contact of geomembranes, it seems that the geomembrane flexibility is the most important factor influencing the interface response (Karademir and Frost, 2013).

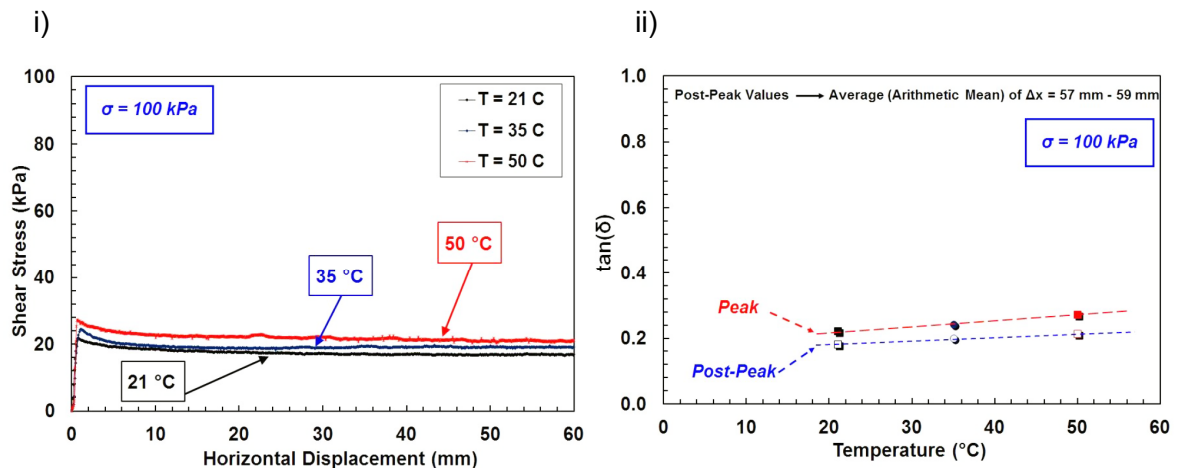


Figure 5.1.28. Smooth HDPE geomembrane- nonwoven needle-punched geotextile interface: i) shear stress – horizontal displacement; ii) coefficient of friction-temperature (Karademir and Frost, 2013).

Few studies investigating the temperature effect on the interface friction by using the Inclined Plane test are presented in literature. Nevertheless, the Inclined Plane test allows studying the variation of interface friction changing temperature conditions for all the applications involving low normal stresses such as landfill covers.

5.1.7.1 Temperature effects on polymeric materials

Before assessing the influence of temperature on the geosynthetic interface shear strength, some fundamental notions about the temperature effect on polymers are briefly presented.

Polymer fibers may consist of both semi-crystalline (aligned molecular chains) and amorphous (disordered atomic-scale structure) regions. Failure can be due to the fracture of the chemical bonds or, more often, to a slippage and separation between the polymer chains when exceeding the intermolecular forces. Therefore, the chemical bonds, the intermolecular force, the sensitiveness to creep under tensile loads and the temperature conditions have a significant effect on the strength response of polymer fibers (Moraci, 2011).

The parameter of particular interest in synthetic polymer manufacturing are the glass transition temperature (T_g), and melting temperatures (T_m) at which amorphous polymers undergo a transition from a glassy state to rubbery state and from rubbery state to melting state, respectively. Below their glass transition temperature, amorphous polymers are usually hard and brittle because of the low mobility of their molecules. Increasing the temperature induces molecular motion resulting in the typical rubber-elastic properties. The melting state has a temperature range above the temperature range of the glassy state and is characterized by greater mobility (visco-plastic behaviour) (Moraci, 2011).

Some polymers such as high-density polyethylene (HDPE), polyvinylchloride (PVC), or polypropylene (PP), commonly used as a base material to manufacture geosynthetics, have different glass transition temperatures (T_g) and melting temperatures (T_m) that are summarized in Table 5.1.13.

Table 5.1.13. Physical properties of some polymeric materials commonly used in manufacturing geosynthetics (after Moraci, 2011).

Polymer	Density (kg/m³)	T_g, Glass Transition Temperature (°C)	T_m, Melting Temperature (°C)	T_d, Decomposition Temperature (°C)
Polyethylene (PE)	915-960	-80	110-135	105-120
Polyvinylchloride (PVC)	1380-1550	80	185	150-160
Polypropylene (PP)	900-910	-10	160-165	380-400
Polyamide (PA)	1140	50-60	250	220-235
Polyester (PET)	1380	80	265	230-240

5.1.7.2 Materials and methodology

Among all the parameters that can influence the interface strength behaviour, also the temperature, as an introductory study, was investigated in this work.

A preliminary laboratory testing program at the Inclined Plane was undertaken over a range of temperature (10°C – 32°C), in dry conditions, under a normal stress equal to 5kPa, to capture variations in shear strength response as a function of ambient temperature. The interfaces tested are a nonwoven geotextile (GTX), a HDPE rhomboidal geonet (GNT) and a geocomposite drain (GCD_N) in direct contact with a smooth HDPE geomembrane (GMB_S) (interfaces a, b and c). In all cases, the geosynthetic materials and the testing equipment were allowed to equilibrate at the testing temperature for at least 24 h before the beginning of the test. At least three replicate tests with virgin materials in the machine direction were conducted for each test condition.

It is worth noting that, this experimental program is only intended to highlight the influence of the testing temperature in the shear strength measurements in the short term. In fact, other temperature-dependent parameters affecting the geosynthetics long term behaviour, such as creep, are not considered in this study.

It's reasonable to point out that the conditions of tests are not totally rigorous, since the temperature is the global laboratory temperature.

5.1.7.3 Results and discussion

The Unified Inclined Plane Procedure (UIPP) was applied to interfaces *a*, *b* and *c* (Table 2.3.2) under a normal stress equal to 5kPa at 10°C, 20°C and 32°C. The static and the limit interface friction angles were determined during Step 1 and Step 3 while the dynamic friction values were found applying the Variant to Step 2 as suggested for the gradual sliding behaviours.

It is worth noting that the change of the interface friction angle over the entire range of test temperatures from 10°C up to 32°C only applies to the particular geosynthetic combinations utilized in this study.

In Table 5.1.14 are displayed the mean values of the interface friction angles and the range of variation in measurement data for each temperature condition. The mean interface friction angles are also schematized in the typical plot of the Inclined Plane test in Figure 5.1.29. Furthermore, in order to better appreciate the friction trend with changing

temperature, the static, the limit and the dynamic interface shear strength in terms of the mean friction angles are presented in Figure 5.1.30.

Table 5.1.14. Interface friction angles at different temperatures applying the UIPP at the Inclined plane test ($\sigma_{v0} = 5kPa$).

T (°C)	GTX - GMBs			GNT - GMBs			GCD _N - GMBs		
	ϕ_0 (°)	ϕ_{lim} (°)	ϕ_{dyn}^{IP} (°)	ϕ_0 (°)	ϕ_{lim} (°)	ϕ_{dyn}^{IP} (°)	ϕ_0 (°)	ϕ_{lim} (°)	ϕ_{dyn}^{IP} (°)
10	16.7±0.6	17.1±0.1	17.5±0.1	15.0±1.4	16.5±0.6	17.3±0.4	16.3±0.1	13.6±0.5	15.0±0.5
20	14.0±1.0	11.7±0.2	17.3±0.8	13.5±1.0	13.1±0.4	16.9±0.4	14.0±1.1	12.6±0.5	16.5±0.6
32	15.5±1.5	13.7±0.1	18.0±0.6	15.5±1.0	16.2±0.6	17.7±0.6	15.7±1.7	14.7±0.6	17.7±0.5

The behaviour, common to all the interfaces, indicates that a modification of the interface shear strength with the temperature occurs. It is noted that the static and the limit coefficient of friction (Figure 5.1.30a and b) are more sensitive to this parameter than the dynamic one (Figure 5.1.30c) which value does not vary significantly. In Figure 5.1.30a and b, for all the interfaces investigated two parts can be recognized. In the first part of the graph, passing from 10°C to 20°C, the coefficient of friction decreases while, ranging from 20°C to 32°C, as the temperature increases an increase in the coefficient of friction is observed. Test results regarding ϕ_0 and ϕ_{lim} at elevated temperatures (20°C ÷ 30°C) are consistent with the observations found in literature. In particular, Karademir and Frost, (2013) performing direct shear tests at 100 kPa in the same temperature range, attributed this behaviour to an increase of the contact area between the counterfaces. In fact, at elevated temperatures a quick dispersion of the concentrated stresses over the interface contact area after the application of load occurs, leading to a more uniform stress distribution over the entire contact surface at the interface during shear displacement. It is also possible that the stiffness decreasing, wrinkles are occurring during the shearing process.

An increase in ambient temperature results in softening of the polymer and a reduction in stiffness allowing a greater flow of the polymeric material under a load application and a greater interaction between the materials (Karademir and Frost, 2013). Conversely, the trend observed between 10°C and 20°C is not in line with the other studies carried out in the same range of temperatures. For example, Akpinar and Benson, (2005) in the aforementioned study, found lower friction values at 0°C and 10°C with respect to the ones obtained at 21°C and 31°C (Figure 5.1.27).

Further, since a common behaviour for the three interfaces can be recognized (Figure 5.1.30), it seems that the major impact in the interface response of the three couple of geosynthetics investigated, may be attributed to the geomembrane properties (i.e. flexibility) as already found by Karademir and Frost, (2013) studying the behaviour between a nonwoven geotextile in direct contact with the HDPE and PVC geomembranes. However, these results should be confirmed by additional tests.

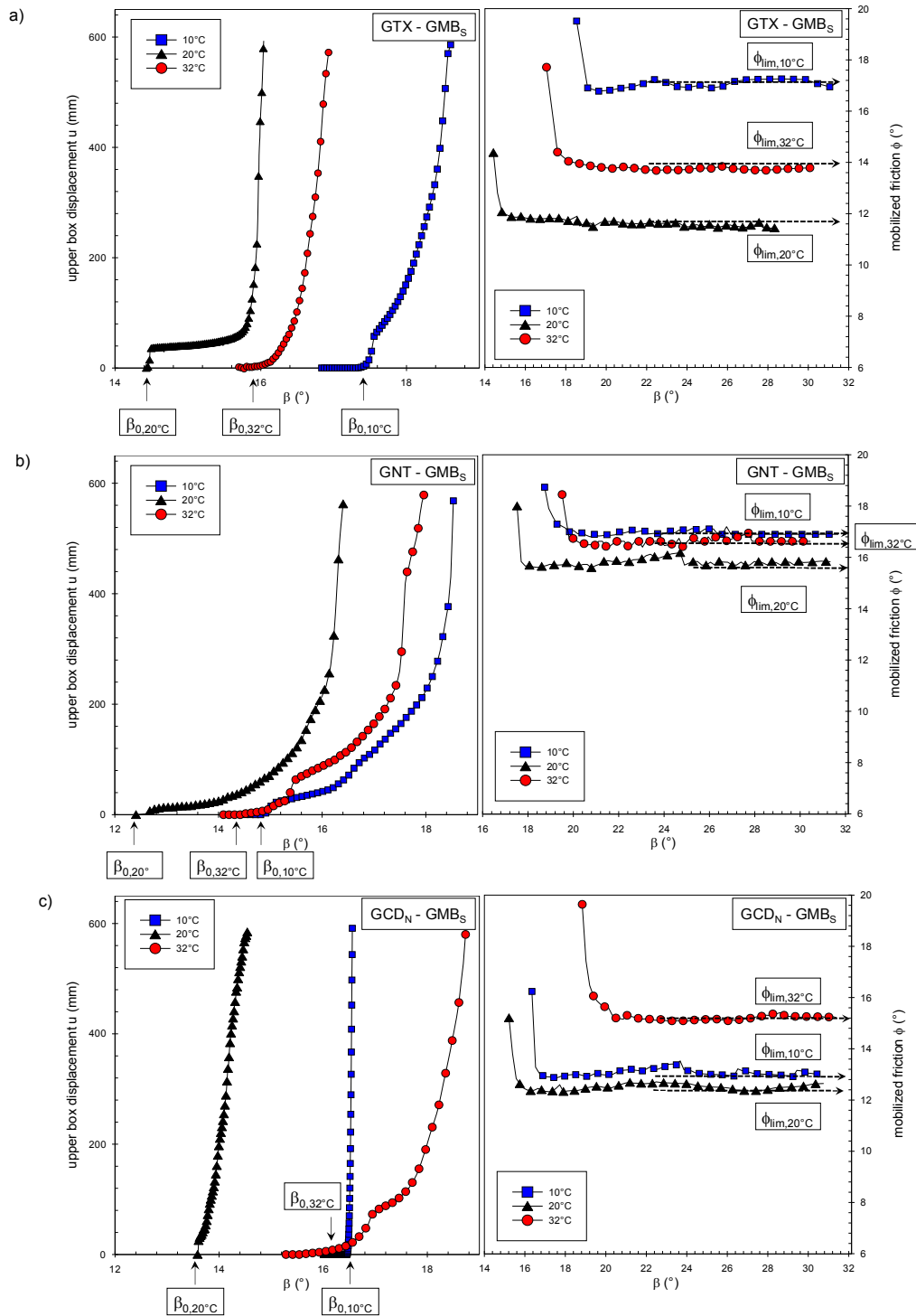


Figure 5.1.29. Inclined Plane test results applying the UIPP at $\sigma_{v0} = 5 \text{ kPa}$: (a) GTX-GMB_S interface; (b) GNT-GMB_S interface; (c) GCDN-GMB_S interface (LTHE laboratory).

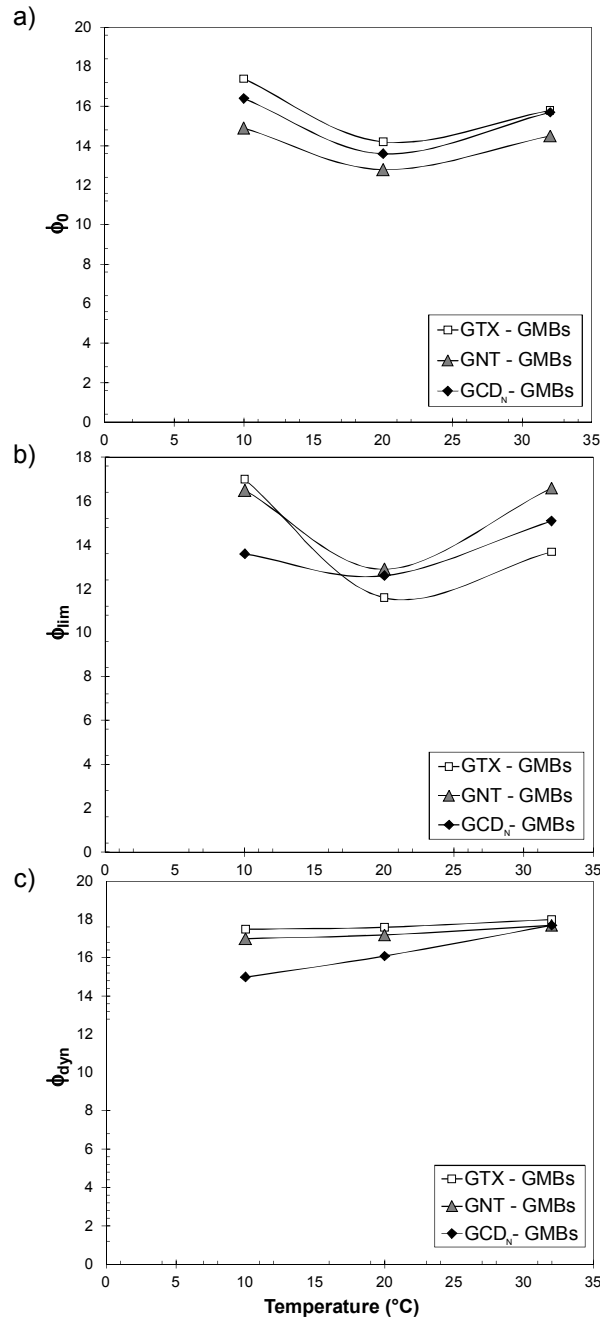


Figure 5.1.30. Static, limit and dynamic interface strength response in terms of coefficient of friction in function of the laboratory temperature for GTX-GMB_s (a), GNT-GMB_s (b) and GCD_N-GMB_s (c) interfaces at $\sigma_{v0} = 5\text{kPa}$ (Inclined Plane test – LTHE laboratory).

5.1.7.4 Summary and conclusions

The mechanical properties of geosynthetic layer systems do not remain constant within the range of temperatures found in typical civil engineering applications. The results presented here were intended to provide insight into the interface shear strength response that may change (i.e. increase or decrease) at different ambient temperature conditions

compared to those determined in conventional laboratory tests conducted at standard room temperatures of 20°C.

The preliminary experimental program confirmed that the temperature can affect the interface shear response. These results must be complemented by other further tests; the observed trends of the friction angles, are specific to the particular geosynthetics used in this study and the results cannot be generalized to other ones.

Therefore, in light of this experimental program, it is suggested to always specify the temperature at which the friction values are obtained.

5.2 SHAKING TABLE TESTS RESULTS

In the present study in order to assess the seismic risk with respect to the sliding failure along the liners, the dynamic behaviour of geosynthetic interfaces was investigated using a shaking table device. A series of fundamental experiments, involving the same interfaces tested at the Inclined Plane, was conducted at the ICEA Shaking Table by applying the sinusoidal horizontal motions as input excitation, as described §4.2.3.

The testing program was carried out with the following aims:

- Development and validation of a procedure able to interpret all the phases of the test.
- Assessment and interpretation of the interface shear strength with the current kinematic conditions.
- Analysis of the parameters influencing test results (as described § 1.4.2).

Dynamic tests were performed on the three different interfaces involving the smooth geomembrane (*a*, *b* and *c* listed in Table 2.3.2) since they are characterized by lower friction angles with respect to the interfaces involving textured geomembranes.

It should be pointed out that these interfaces have shown a “*gradual sliding*” behaviour in the inclined plane tests (§5.1.1.1). In order to investigate the possible behavioural differences for interfaces displaying a “*sudden sliding*” mode of failure, a forth interface (*d* of Table 2.3.2) involving textured geomembrane in contact with the geocomposite drain was also tested.

Table 5.2.1 summarizes the parameters analysed in every test series specifying for each case the experimental conditions.

Table 5.2.1. Schematization of the parameter analysed in the experimental program at the Shaking Table device.

Parameter analysed	Interface tested GSY _{UP} /GSY _{DOWN}	a _{max} (g)	f (Hz)	Sinusoidal excitation	Vertical stress σ _{v0} (kPa)
TAR	a. GTX - GMB _S	0.40	1.5	Standard Lower Faster	5
Frequency (f)	a. GTX - GMB _S	0.40	1.5; 3; 6	Standard	5; 12
	b. GNT - GMB _S	0.40	1.5; 3; 6	Standard	5; 12
	c. GCD _N - GMB _S	0.40	1.5; 3; 6	Standard	5; 12
Normal stress (σ)	a. GTX - GMB _S	0.40	1.5; 3; 6	Standard	5; 12
	b. GNT - GMB _S	0.40	1.5; 3; 6	Standard	5; 12
	c. GCD _N - GMB _S	0.40	1.5; 3; 6	Standard	5; 12
Amplitude (a _{max})	a. GTX - GMB _S	0.34 0.40 0.60	3 3 3	Standard Standard Standard	5 5 5
Mean relative velocity, v	a. GTX - GMB _S	0.34 0.40 0.60	3 1.5; 3; 6 3	Standard Standard Standard	5; 12 5; 12 5; 12
	b. GNT - GMB _S	0.40	1.5; 3; 6	Standard	5
	c. GCD _N - GMB _S	0.40	1.5; 3; 6	Standard	5
Mechanical damage (number of cycles N _d)	a. GTX - GMB _S	0.40	1.5; 3; 6	Standard	5; 12
	b. GNT - GMB _S	0.40	1.5; 3; 6	Standard	5; 12
	c. GCD _N - GMB _S	0.40	1.5; 3; 6	Standard	5; 12

5.2.1 Description and interpretation of a typical test

5.2.1.1 Typical diagrams

In Figure 5.2.1 is shown a typical diagram plotting the table and the box accelerations versus the time for GTX – GMB_S, GNT – GMB_S and GCD_N – GMB_S interfaces during a shaking table test under a sinusoidal base acceleration at a frequency $f = 1.5\text{Hz}$. In this case the “standard signal”, as described in §4.2.3, was used and the maximum amplitude of the base (a_{\max}) was determined on the basis of results from monotonic (inclined plane) and preliminary shaking table tests in order to mobilize the peak shear resistance for the three interfaces tested.

The applied loading allows the observation of the relative box sliding before reaching the maximum amplitude of the table acceleration (a_{\max}) so that the three main phases can be identified (Figure 5.2.1). At the beginning of the test (initial Phase 1), the box and the table have an identical motion [$a_{\text{box}}(t) = a_{\text{table}}(t) < a_{\max}$] and no relative displacement occurs [$a_{\text{table}}(t) < a_{\text{crit}}$]. Once the upper box begins to slide (when $a_{\text{table}}(t) > a_{\text{crit}}$) Phase 2 starts with a table acceleration amplitude not yet stabilized. Finally, when the amplitude of table acceleration reaches the maximum acceleration a_{\max} , Phase 3 takes place. It should be noted that, during Phase 2, the critical acceleration and consequently the dynamic coefficient of friction (Equation 4.2-8), in general, are not stabilized.

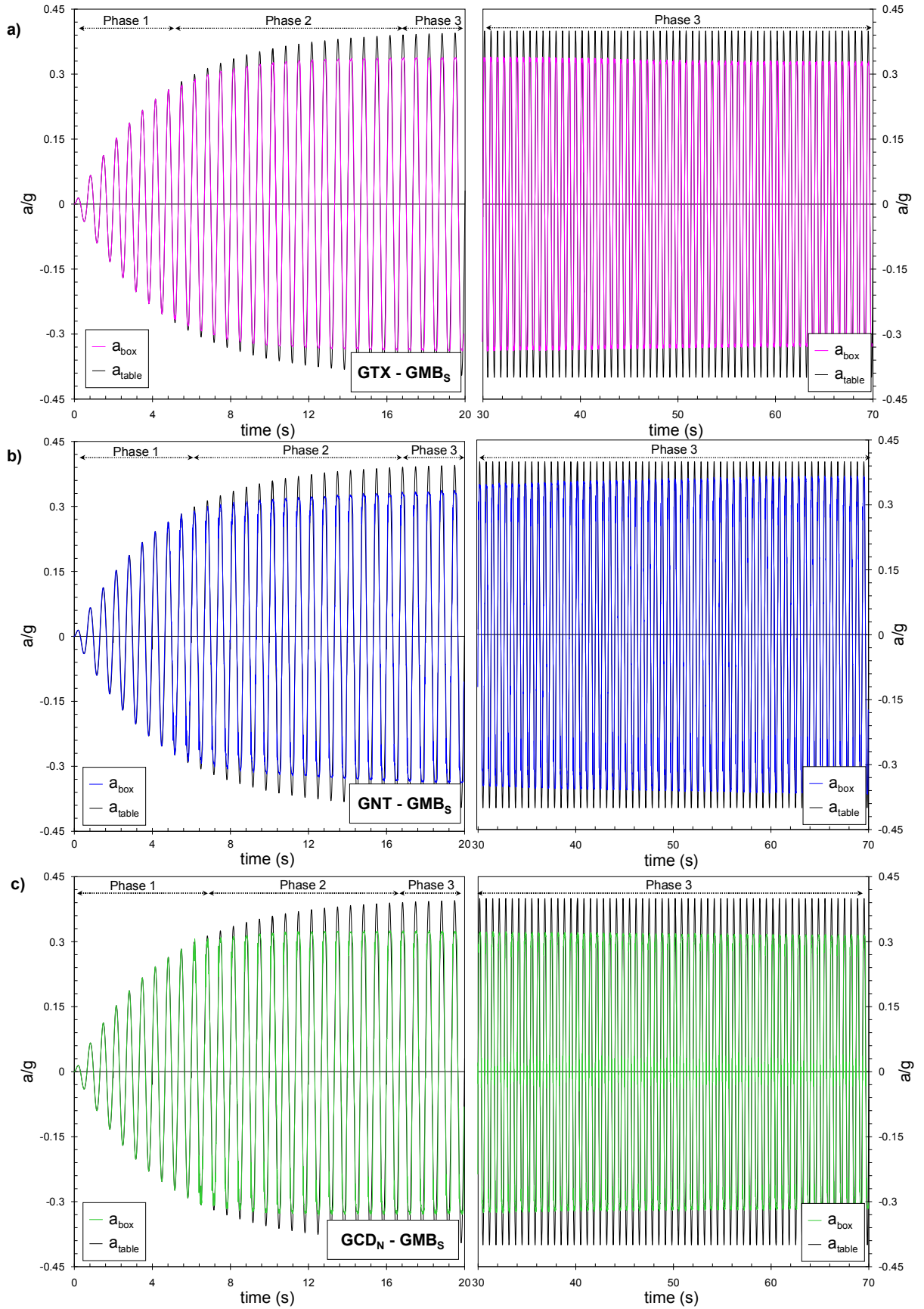


Figure 5.2.1. Evolution of the table and the box accelerations during a shaking table test ("standard" table solicitation, $f = 1.5$ Hz and $\sigma_{v0} = 5$ kPa): a) GTX – GMB_s interface; b) GNT – GMB_s interface; c) GCD_N – GMB_s interface.

The typical diagram of shaking table tests plots the results in terms of the box and table peak accelerations (Figure 5.2.2). The vertical axis shows the recorded box peak acceleration that is transmitted through the interfaces.

For the three interfaces, the results demonstrate that, for a table peak acceleration less than a certain level, the box and the table have the same acceleration (a_{box} follows the bisector) (Figure 5.2.2 a_1 , b_1 and c_1), and no sliding along the interface is observed. Beyond this value, the box acceleration [$a_{\text{box}}(t) = a_{\text{crit}}(t)$] is less than that of the table and a slip occurs. The magnitude of acceleration at which the acceleration of the box fails to increase at the same rate as the acceleration of the table is characterized by a break in the plot (Figure 5.2.2 a_2 , b_2 and c_2) and provides the dynamic friction angle (Equation 4.2-8).

The plots in Figure 5.2.2 show that, prior to slippage, there does not appear to be any dependence on frequency in the frictional behaviour. On the other hand, after the sliding start, a slight variation of the a_{crit} with the frequency can be observed. Similar result was also found by Yegian et al. (1995) testing nonwoven needle-punched geotextile in contact with smooth geomembrane (Figure 5.2.3 *i*), by Park et al., (2004) testing interfaces formed by the combination of three different kinds of geosynthetics, i.e. geotextile, smooth geomembrane and geosynthetic clay liner (Figure 5.2.3 *ii*) and also by De and Zimmie, (1998) testing nonwoven needle-punched geotextile and geonet (put in different orientations of the strands with respect to the direction of the shear displacement) in contact with smooth geomembrane (Figure 5.2.3 *iii and iv*).

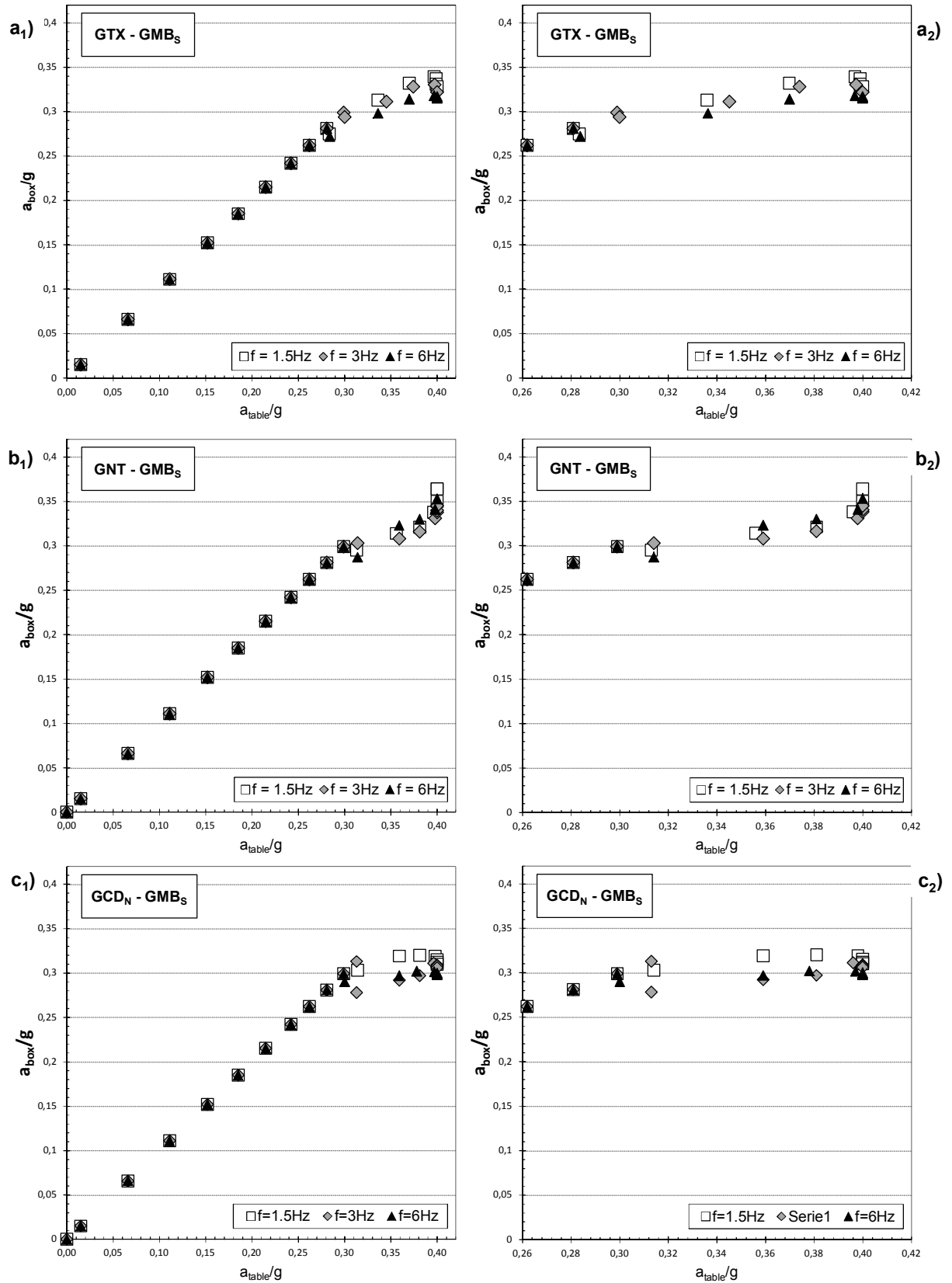


Figure 5.2.2. Box peak acceleration versus table peak acceleration (“standard” table solicitation, $f = 1.5, 3$ and 6Hz and $\sigma_{v0} = 5\text{ kPa}$): GTX – GMB_s interface during the entire test a₁); zoom on Phases 2 and 3 a₂); GNT – GMB_s interface during the entire test b₁), zoom on Phases 2 and 3 b₂); GCD_N – GMB_s interface during the entire test c₁), zoom on Phases 2 and 3 c₂).

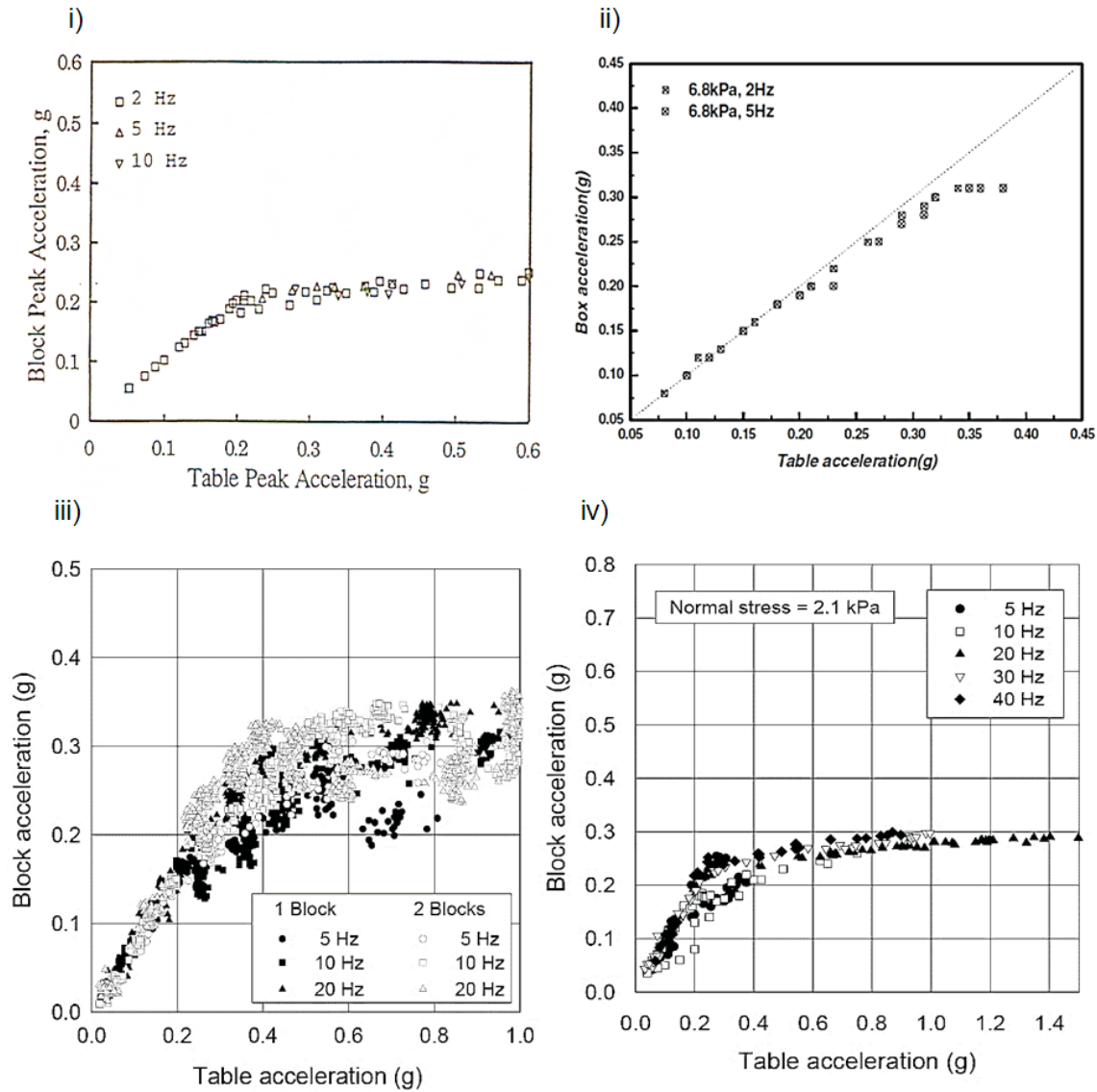


Figure 5.2.3. Box peak acceleration versus table peak acceleration: i) HDPE geomembrane – nonwoven needle-punched geotextile interface (after Yegian et al. 1995); ii) geocomposite clay liner – s,pptH HDPE geomembrane (after Park et al., 2004); iii) and iv) HDPE geomembrane – nonwoven needle-punched geotextile interface (after De and Zimmie, 1998).

5.2.1.1 Basic interpretation

During the same test, the critical acceleration a_{crit} is not constant. In this study, let N_d be the number of cycles from the beginning of relative sliding of the box, in these tests during Phase 2, the evolution of the dynamic friction angle with the number of cycles is considered (Figure 5.2.4).

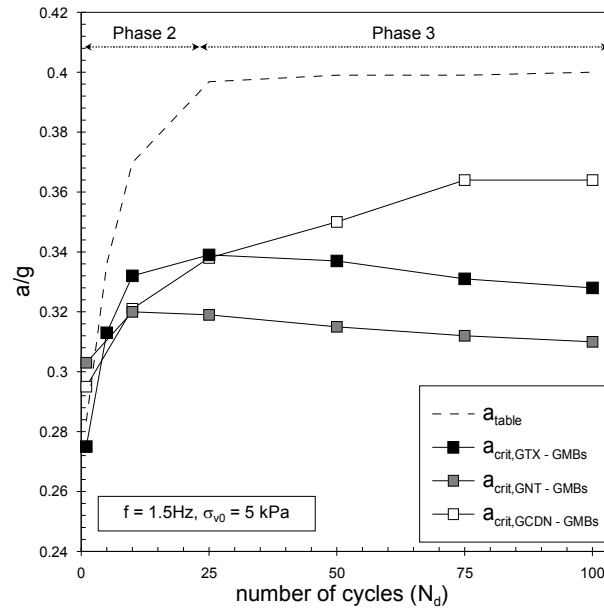


Figure 5.2.4. Typical trend of table and box critical acceleration with the number of cycles of GTX – GMBs, GNT – GMBs and GCDN – GMBs interfaces during Phases 2 and 3 of shaking table tests (“standard” table solicitation, $f = 1.5, 3$ and 6Hz and $\sigma_{v0} = 5\text{ kPa}$).

The typical behaviour observed is characterized by the transitory Phase 2 (for N_d generally ranging from 1 to 20) with a subsequent Phase 3 where the critical acceleration as well as the dynamic friction coefficient (Equation 4.2-8) attain, usually, a relatively steady-state value.

Table 5.2.2 summarizes shaking table test results determined during Phases 2 and 3 of the test applying the “standard” signal at different frequencies. Test results indicate that, for all the interfaces tested:

- $a_{crit, Nd=1}$ values corresponding to the beginning of the sliding does not differ significantly when testing the same interface at various frequencies (the maximum scatter between the different values is of about 1.4° and is of the same order of the repeatability of the results);
- the interface friction increases from its value corresponding to the beginning of the incipient sliding ($a_{crit, Nd=1} < a_{crit, Nd=100}$).

Table 5.2.2. Interface friction angles of GTX - GMB_s; GNT - GMB_s and GCD_N - GMB_s interfaces calculated during the different phases of the shaking table test ($f = 1.5, 3$ and 6 Hz; $T = 20^\circ\text{C}$; $\sigma_{v0} = 5$ kPa).

$\sigma_{v0}= 5 \text{ kPa}$		Number of cylces (Nd)	f = 1.5Hz		f = 3Hz		f = 6Hz	
Interface tested			$\tan \phi_{\text{dyn}}^{\text{ST}}$	$\phi_{\text{dyn}}^{\text{ST}}$	$\tan \phi_{\text{dyn}}^{\text{ST}}$	$\phi_{\text{dyn}}^{\text{ST}}$	$\tan \phi_{\text{dyn}}^{\text{ST}}$	$\phi_{\text{dyn}}^{\text{ST}}$
				(°)		(°)		(°)
a	GTX - GMB_s	1	0.275	15.4	0.294	16.4	0.272	15.2
		10	0.330	18.3	0.311	17.3	0.314	17.4
		25	0.340	18.8	0.328	18.2	0.318	17.6
		50	0.337	18.6	0.330	18.3	0.317	17.6
		75	0.331	18.3	0.328	18.1	0.316	17.5
		100	0.328	18.2	0.325	18.0	0.315	17.5
b	GNT - GMB_s	1	0.295	16.4	0.303	16.9	0.294	16.0
		10	0.321	17.8	0.308	17.5	0.335	18.3
		25	0.338	18.7	0.331	18.3	0.346	18.8
		50	0.350	19.3	0.338	18.7	0.348	18.9
		75	0.364	20.0	0.340	18.8	0.353	19.2
		100	0.364	20.0	0.345	19.0	0.358	19.5
c	GCD_N - GMB_s	1	0.303	16.9	0.278	15.5	0.290	16.2
		10	0.320	17.8	0.297	16.5	0.298	16.8
		25	0.319	17.7	0.311	17.3	0.302	16.8
		50	0.315	17.5	0.309	17.2	0.302	16.7
		75	0.312	17.3	0.308	17.1	0.298	16.6
		100	0.310	17.2	0.306	17.0	0.299	16.7

5.2.1.2 Influence of the table acceleration rate (TAR)

The sinusoidal signal sent to the table (Equation 4.2-9) adopted in this study as described in § 4.2.3, lets a transitory phase (Phase 2) occur. In general, when performing shaking

table tests, the amplitude of vibration is usually increased using a dynamic signal analyzer until a fixed value is reached (Yegian et al. 1995, De and Zimmie, 1998, Lo Grasso et al., 2005, Kotake et al., 2011, Zimmie et al. 1994). Therefore, although the transitory phase is observed, its effect has rarely been addressed in the technical literature.

In this study, in order to further investigate the possible influence of this Phase 2 on the results, a series of tests where the table was forced by sinusoidal signals with “faster” and “slower” table acceleration rate TAR with respect to the “standard” one, was carried out on GTX – GMB_s interface (Figure 5.2.5).

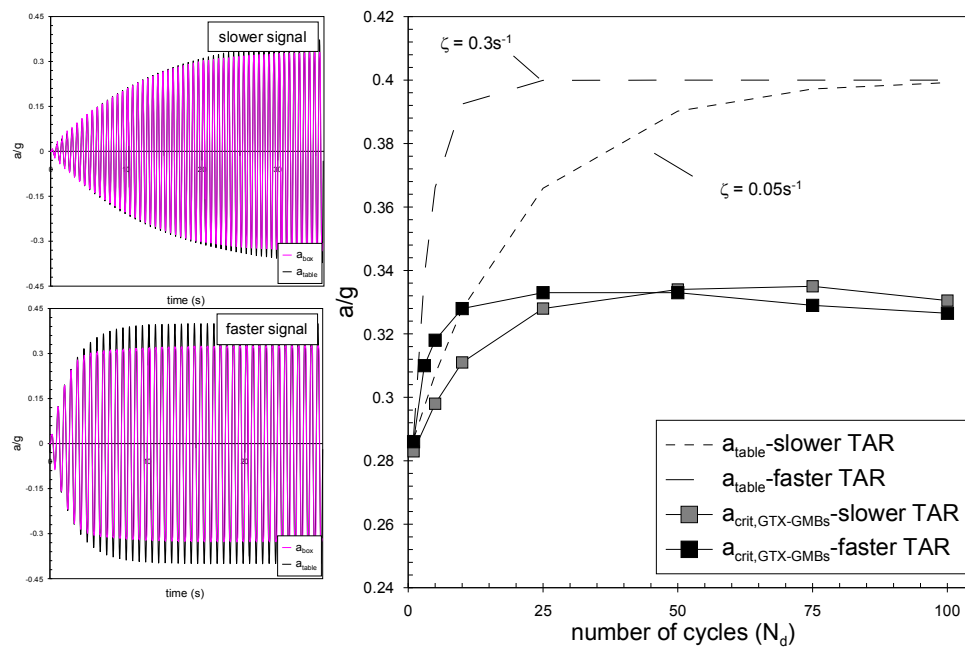


Figure 5.2.5. Influence of the Transitory phase on the dynamic shear strength of GTX – GMB_s interface (“faster” and “slower” TARs, $f = 1.5$ Hz and $\sigma_{v0} = 5$ kPa).

In Figure 5.2.5, it can be noticed that:

- the beginning of the relative motion starts for $a_{crit, Nd=1}$ values very close to each other (being equal to 0.283g and 0.286g for the slower and the faster case respectively). This fact seems to suggest that the interface response is not influenced by the acceleration history sent to the table during Phase 1;
- during Phase 2, the interface response changes depending on the signal shape [i.e. $a_{crit, GTX-GMBs}(slower\ TAR) < a_{crit, GTX-GMBs}(faster\ TAR)$];

- as the TAR increases (faster increase), the steady-state condition is attained more quickly and consequently, also the interface response, in terms of a_{crit} , follows the analogous trend;
- exceeding $N_d = 25$, even if Phase 3 is not reached in the case of the slower TAR, the interface response is no more affected by the shape of the TAR providing similar results.

5.2.2 Influence of frequency

In the determination of the dynamic friction the frequency can play an appreciable role. Several tests are carried out with the same “standard” signal (§4.2.3), the same constant vertical stresses $\sigma_{v0} = 5$ kPa and 12 kPa and different frequencies f for the table solicitations on the interfaces a , b and c (Table 2.3.2).

The experimental results reported in Table 5.2.2 and in Table 5.2.3, are summarized for the three interfaces in terms of the maximum table acceleration and the critical box acceleration (Figure 5.2.6 a_1 , a_3 ; Figure 5.2.7 b_1 , b_3 ; Figure 5.2.8 c_1 , c_3) and in terms of dynamic friction angles ϕ_{dyn}^{ST} (Figure 5.2.6 a_2 , a_4 ; Figure 5.2.7 b_2 , b_4 ; Figure 5.2.8 c_2 , c_4) versus the number of cycles at different frequencies (1.5, 3 and 6 Hz).

Focusing on the effect of the frequency of vibration, for the three interfaces it could be noticed that:

- $a_{crit, Nd=1}$ values corresponding to the beginning of the sliding does not differ significantly when testing the same interface at various frequencies;
- considering the interface response during Phase 3, slight differences in test results can be noticed that, anyway, remain in the order of the results repeatability.

In general, the results obtained for either interfaces do not appear to indicate a marked dependence of the dynamic friction angle on the frequency of vibration. A similar results were found in literature (Yegian et al. 1995, Park et al., 2004, De and Zimmie, 1998) carrying out researches with analogous experimental conditions (geosynthetics interfaces, values of frequency, maximum acceleration and normal stress) as it could be noticed in Figure 5.2.3.

In Figure 5.2.6, Figure 5.2.7 and Figure 5.2.8, it could be also appreciated the behavioural differences of the three interfaces tested. In particular, the dynamic friction angle of GTX – GMB_S and GCD_N – GMB_S interfaces (Figure 5.2.6 and Figure 5.2.8), stabilizes starting from $N_d = 25$ (Phase 3) and also a tendency to decrease with the increase of the number of

cycles (N_d) can be observed. Completely different is the trend followed by GNT – GMB_s interface. In this case, it is quite difficult to identify a stabilization of the dynamic friction angle that continues to increase with the number of cycles. It is believed that, this result is probably related to the different nature of the surfaces in contact. In fact, further tests, reported in the following section § 5.2.6, show that the stabilization of the dynamic friction angle for GNT – GMB_s interface is achieved for $N_d > 100$.

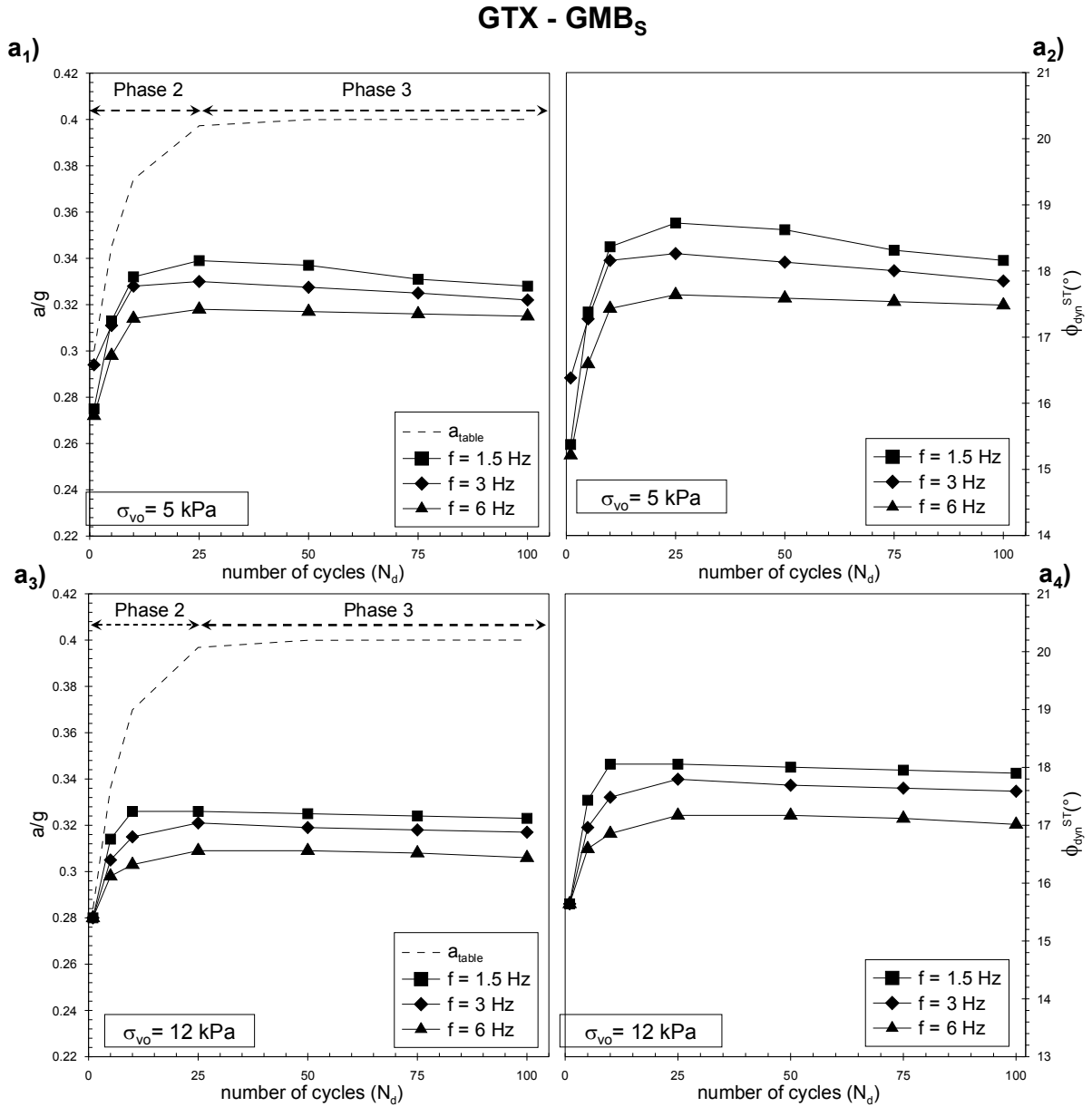


Figure 5.2.6. Influence of frequency and of the number of cycles on the dynamic shear strength of GTX – GMB_s interface (“standard” TAR, $a_{max}=0.4g$, Phases 2 and 3): a₁) and a₂) a/g and ϕ_{dyn}^{ST} values at $\sigma_{v0} = 5 \text{ kPa}$; a₃) and a₄) a/g and ϕ_{dyn}^{ST} values at $\sigma_{v0} = 12 \text{ kPa}$.

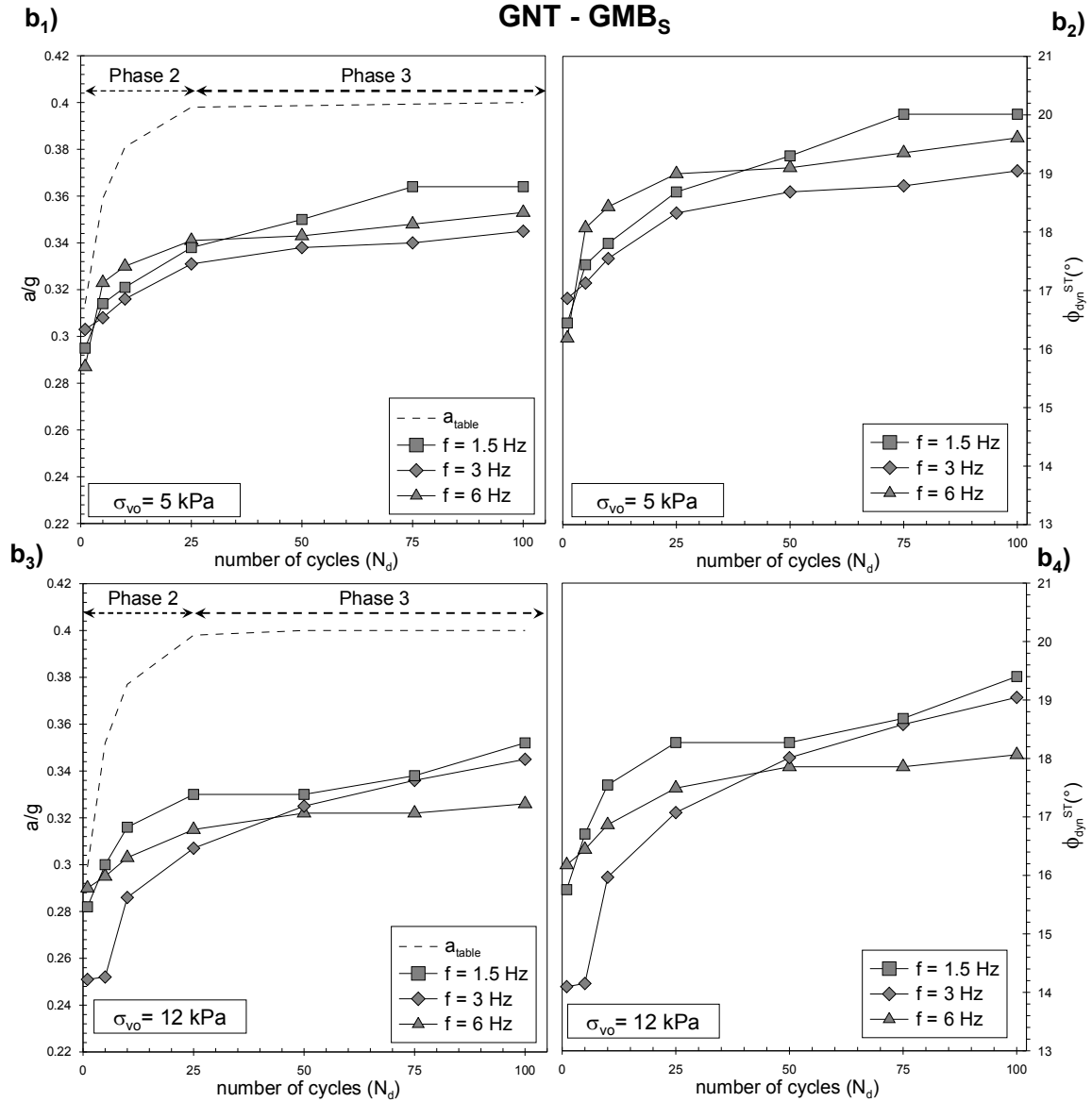


Figure 5.2.7. Influence of frequency and of the number of cycles on the dynamic shear strength of GNT – GMB_s interface (“standard” TAR, $a_{max}=0.4g$, Phases 2 and 3): b₁) and b₂) a/g and ϕ_{dyn}^{ST} values at $\sigma_{v0} = 5 \text{ kPa}$; b₃) and b₄) a/g and ϕ_{dyn}^{ST} values at $\sigma_{v0} = 12 \text{ kPa}$.

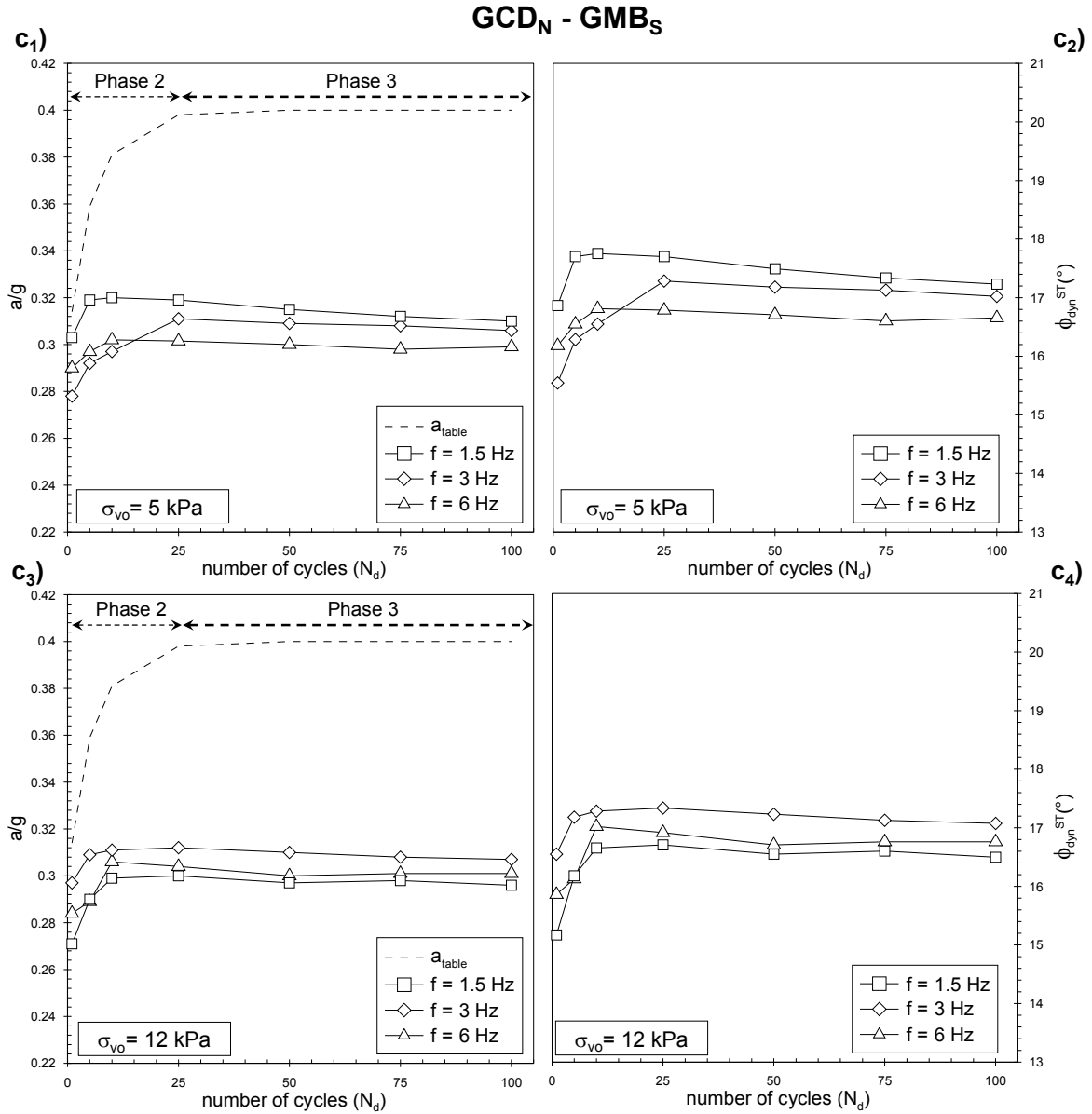


Figure 5.2.8. Influence of frequency and of the number of cycles on the dynamic shear strength of GCD_N - GMB_S interface ("standard" TAR, $a_{max}=0.4g$, Phases 2 and 3): c₁) and c₂) a/g and ϕ_{dyn}^{ST} values

at $\sigma_{v0} = 5$ kPa; c₃) and c₄) a/g and ϕ_{dyn}^{ST} values at $\sigma_{v0} = 12$ kPa.

5.2.3 Influence of the normal stress

The role of the vertical stress is investigated by comparing test results carried out with increasing weighting plate from 5 to 12 kPa. For this purpose the results shown in Figure 5.2.6, and Figure 5.2.8 are compared in Table 5.2.3 for the two compression values. As in the case of the inclined plane tests, it is noted that the dynamic shear strength under

sinusoidal loading is decreasing when the normal stress is increasing to the acting normal stress even if, in the range considered, only a slight difference between the values can be noted (as for example in the case of $GCD_N - GMB_S$ interface, Figure 5.2.9 c₂, c₃).

It is worth noting that, the trend observed refers to the particular geosynthetic interfaces tested under a small normal stress range.

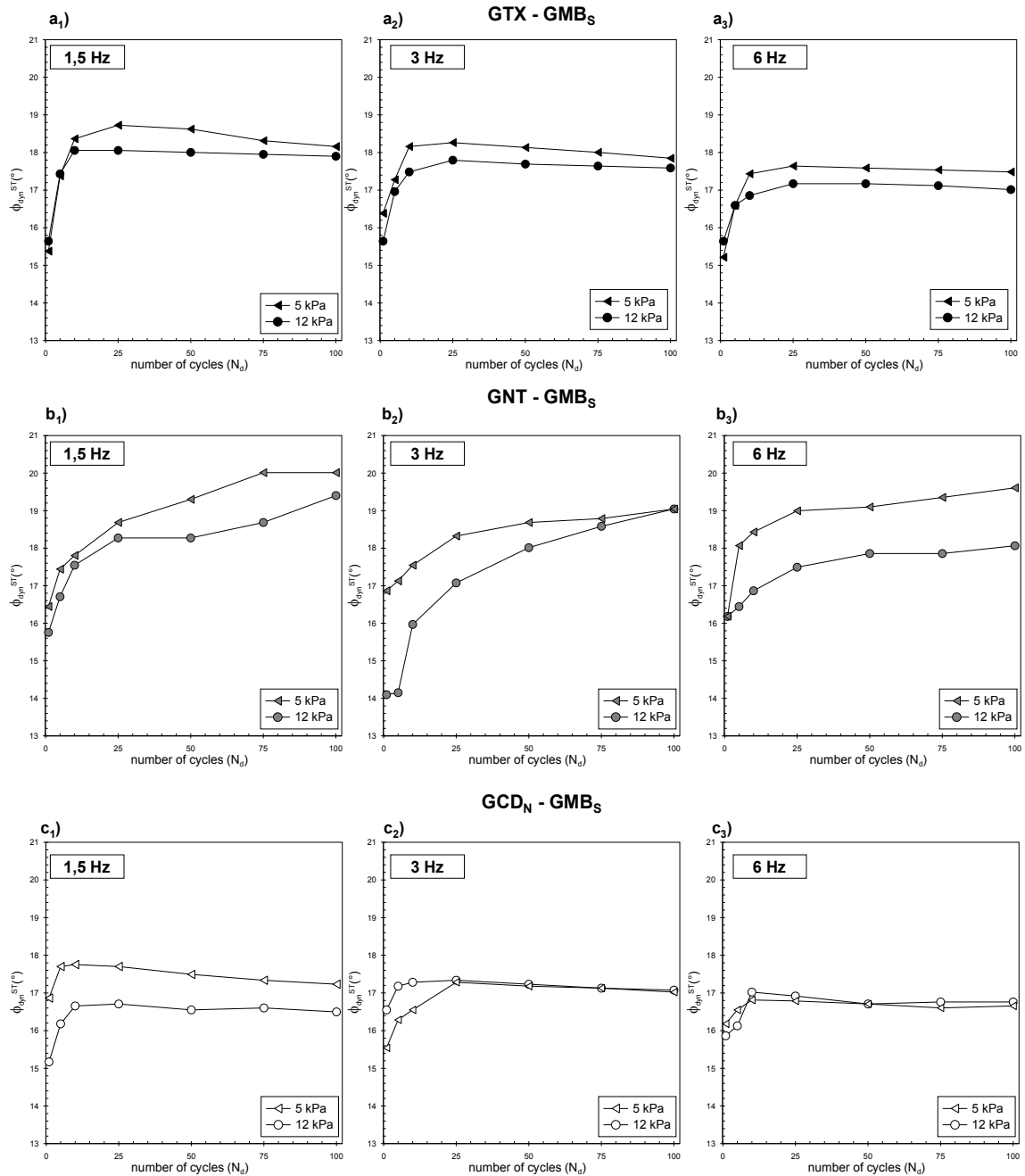


Figure 5.2.9. Influence of normal stress on dynamic friction angle ("standard" TAR and $a_{max}=0.4$ g): (a) GTX - GMB_S , (b) GNT - GMB_S , (c) GCD_N - GMB_S interfaces.

Table 5.2.3. Comparison of the dynamic interface friction angles of GTX - GMB_s; GNT - GMB_s and GCD_N - GMB_s interfaces at $\sigma_{v0} = 5$ and 12 kPa ($f = 1.5, 3$ and 6 Hz; $T = 20^\circ\text{C}$).

Interface tested		Number of cycles (N_d)	Dynamic friction angle					
			$\phi_{\text{dyn}}^{\text{ST}} (^\circ)$					
			$f = 1.5\text{Hz}$		$f = 3\text{Hz}$		$f = 6\text{Hz}$	
			5 kPa	12 kPa	5 kPa	12 kPa	5 kPa	12 kPa
a	GTX - GMB_s	1	15.4	15.6	16.4	15.6	15.2	15.6
		100	18.2	17.9	18.0	17.6	17.5	17.0
b	GNT - GMB_s	1	16.4	15.8	16.9	14.1	16.0	16.2
		100	20.0	19.4	19.0	19.0	19.5	18.1
c	GCD_N - GMB_s	1	16.9	15.2	15.5	16.5	16.2	15.9
		100	17.2	16.5	17.0	17.1	16.7	16.8

In literature, Park et al., (2004) studied the effect of the normal stress carrying out shaking table tests at 1.6, 3.6 and 6.8 kPa on interfaces formed by the combination of three different kinds of geosynthetics (i.e. geotextile, smooth geomembrane and geosynthetic clay liner), found that, for a given frequency of excitation (2 Hz and 5 Hz) the dynamic friction angle was constant varying normal stress (Figure 5.2.10)

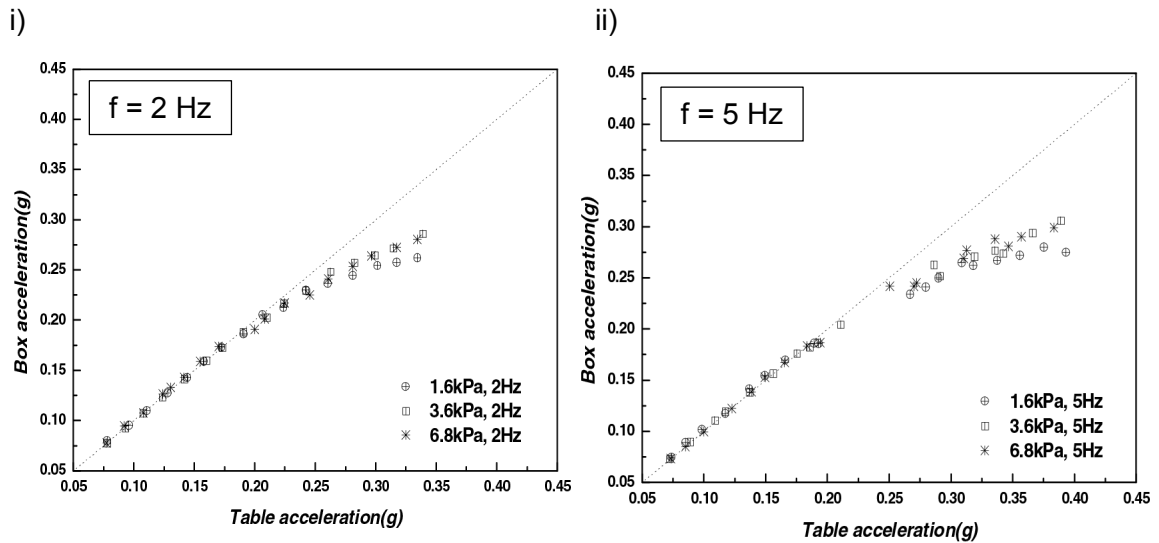


Figure 5.2.10. Effect of normal stress on the dynamic friction angle for geotextile – smooth geomembrane interface (after Park et al. 2004).

5.2.4 Influence of the amplitude

Finally, the effect of the maximum amplitude acceleration of the table motion (a_{\max}) is investigated. For this purpose, the GTX – GMB_s interface was tested under different values of the maximum accelerations ($a_{\max} = 0.34g, 0.40g$ and $0.60g$) at a given frequency equal to 3Hz. Figure 5.2.11 shows the interface response in terms of dynamic friction coefficient versus the number of cycles changing the maximum acceleration values (value reached during Phase 3). These tests indicate that as a_{\max} (i.e. passing from 0.34 to 0.60g) increases, $a_{\text{crit}, N_d=1}$ does not vary significantly while, increasing the number of cycles N_d , during Phase 3, a reduction in a_{crit} values can be observed.

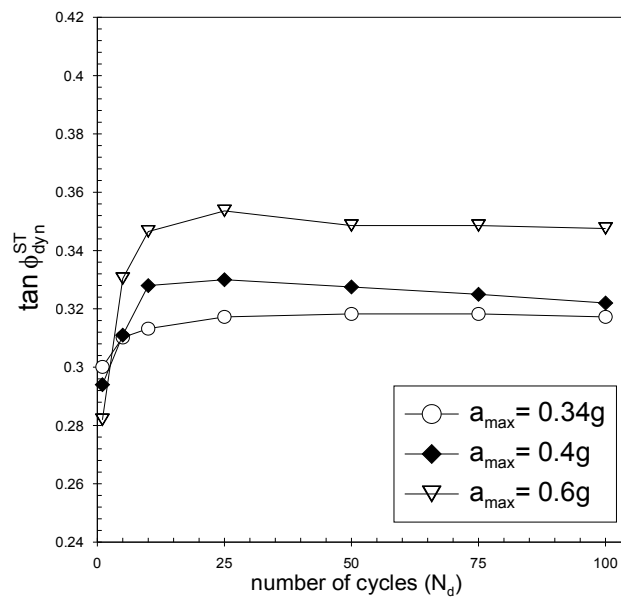


Figure 5.2.11. Influence of the maximum table acceleration on dynamic friction coefficient (“standard” TAR, $f = 3$ Hz and $\sigma_{v0} = 5$ kPa, GTX – GMB_s interface).

5.2.5 Influence of the mean relative velocity

For dynamic loads, the shear strength response is affected by inertial and viscous effects (Carrubba and Massimino, 1998). In this context, as done for inclined plane test results, the influence of the relative velocity was investigated. Regarding the shaking table results it is important to differentiate the load velocity that is the velocity of solicitation (i.e. velocity of the table) and the relative velocity intended here as the upper box velocity during the relative motion. Test results presented in this section only refer to the second definition.

The relative velocity in the time is obtained by integrating the difference between the table and the box accelerations. Furthermore, considering the number of cycles, N_d , from the beginning of relative sliding of the box, the relative velocity can be plotted versus N_d as shown in Figure 5.2.12.

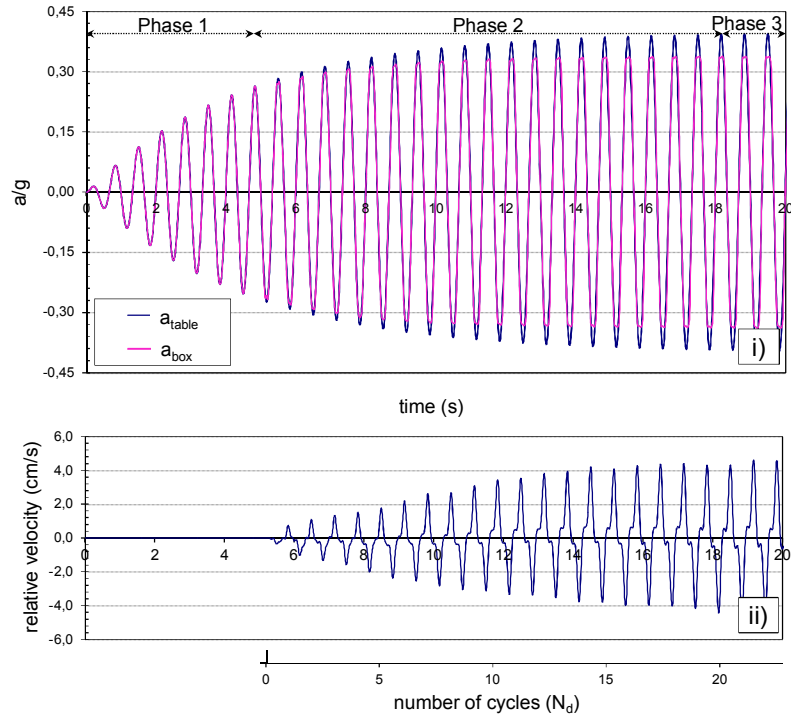


Figure 5.2.12. Relative velocity in shaking table tests. Results of GTX – GMB_s interface subjected to “standard signal” solicitation at frequency, $f = 1.5$ Hz and $\sigma_{v0} = 5$ kPa: i) evolution of the table and the box accelerations; ii) evolution of the relative velocity with the time.

It should be pointed out that the results plotted in Figure 5.2.12, refer to GTX – GMB_s interface at a frequency of solicitation equal to 1.5 Hz. The results displayed in Figure 5.2.12, represent a typical plot of the relative velocity with respect to the time; in addition this series of test provides the higher values of the relative velocity when the sinusoidal standard signal (Figure 4.2.3 § 4.2.3) is applied. In general it could be noticed that a rapid increase of the relative velocity is registered at the beginning of the motion (corresponding in these tests to Phase 2); afterwards, the relative velocity increases linearly and at slowly rate until the end of the test (Phase 3). As shown in Figure 5.2.1 - Table 5.2.2, the critical acceleration behaves in a similar manner increasing during the transitory Phase 2 until the steady condition (Phase 3) is reached.

Considering the mean value of the relative velocity, v , defined as the half of the maximum value of the relative velocity reached in a single cycle (Figure 5.2.12 *ii*) the results during a single test, can be plotted as in Figure 5.2.13. The data plotted in Figure 5.2.13 are reported in Table 5.2.2 ($f = 1.5$ Hz).

In fact, the dependence of the dynamic friction on the mean relative velocity can be detected on both Phases 2 and 3. It is believed that the critical acceleration (also the corresponding dynamic friction) gradually increases in the transitional Phase 2 because also the velocity of the relative displacement gradually increases at every cycle according to the corresponding TAR.

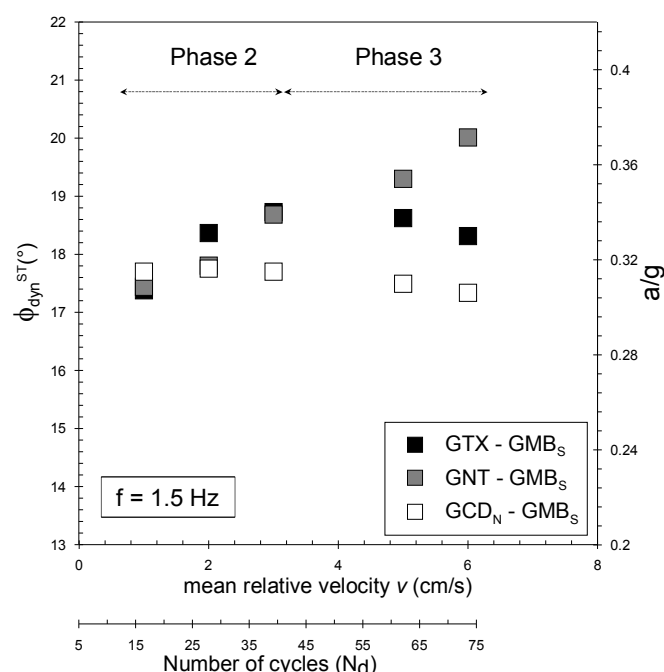


Figure 5.2.13. Evolution of the dynamic friction angle with respect to the mean relative velocity during a single test for GTX – GMB_s; GNT – GMB_s and GCD_N – GMB_s interfaces (“standard signal” solicitation, frequency, $f = 1.5$ Hz and $\sigma_{v0} = 5$ kPa)

Furthermore, being the relative velocity dependent on the table acceleration, the evolution of the dynamic friction angle with different sinusoidal table inputs can be evaluated.

In Figure 5.2.14, for GTX – GMB_s interface, the dynamic friction coefficients obtained at the steady-state Phase 3 of different test series (described in §5.2.2 and §5.2.4) are plotted upon the corresponding mean relative velocity that increases at very slow constant rate (i.e. it can be considered almost constant during this phase). It could be inferred that, especially for this interface, as in the case of the Inclined Plane, the dynamic friction coefficient increases with the mean relative velocity.

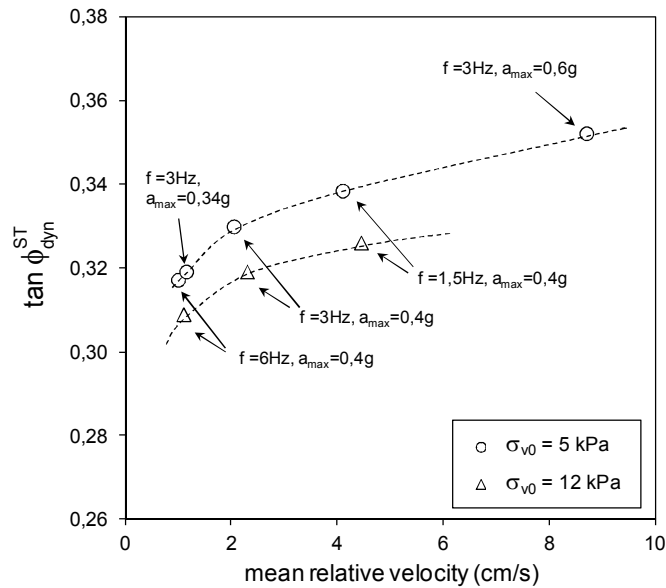


Figure 5.2.14. Evolution of the dynamic friction angle with respect to the mean relative velocity during a single test for GTX – GMB_s interface (“standard signal” solicitation, frequency, $f = 1.5$ Hz and $\sigma_{v0} = 5$ kPa)

Even if, as already stated in §5.2.2, the influence of frequency is negligible, for this interface a specific trend common to all the test performed, can be observed. In fact, as it could be noticed in Figure 5.2.14, at a given maximum acceleration, the dynamic coefficient of friction increases as frequency decreases, being the relative velocity inversely proportional to the frequency. Thus, as shown in Figure 5.2.6, for $a_{max} = 0.4g$, $\tan \phi_{dyn}^{ST}$ at $f = 6$ Hz is lower than $\tan \phi_{dyn}^{ST}$ at $f = 3$ Hz for a_{max} equal to $0.4g$, which is lower than that at $f = 1.5$ Hz.

Conversely, for a given frequency, the increase of the maximum table acceleration induces an increase in the relative velocity and the dynamic coefficient of friction. For example, for a frequency of 3 Hz, the dynamic coefficient of friction at $a_{max} = 0.34g$ is lower than that at $a_{max} = 0.4g$, with the latter being lower than the dynamic coefficient of friction at $a_{max} = 0.6g$ (Figure 5.2.11).

5.2.6 Influence of the mechanical damage (wear effect due to the number of cycles)

In the classical paper by Newmark (1965), it was recognized that the assumption of constant shear strength on the block/plane interface, and therefore the implicit assumption of constant yield acceleration, might not always be appropriate (Matasovic. et al., 1998).

During the steady-state phase (Phase 3) the upper box continues to slide back and forth along the table and a modification of the dynamic friction coefficient can occur. In order to investigate this aspect repeated test series (three tests on the same interface) and tests where the number of cycles N_d was increased from 100 to 300 were performed on the interfaces *a*, *b* and *c* (Table 2.3.2). These two approaches allowed investigating the modification of the dynamic friction angle corresponding to the beginning of the relative sliding, $\phi_{dyn}^{ST}(N_d = 1)$, and after stabilization, $\phi_{dyn}^{ST}(N_d \geq 50)$ respectively. Test results are summarized in Table 5.2.4.

Furthermore, Figure 5.2.15 shows the trend of the dynamic friction angle with the increase of the number of cycles when the table is solicited by the “standard” excitation at the frequency equal to 1.5 Hz.

Test results indicate that, as soon as the number of cycles increases, the dynamic friction changes. This behaviour can be attributed to the repeated relative sliding of the box that could modify the surfaces in contact. As a consequence, a possible alteration of the dynamic friction due to wear of the surfaces occurring under the stress reversal condition of the loading can be observed and differs depending on the surfaces in contact.

Table 5.2.4. Shaking table test results after three successive tests and increasing the number of cycles to 300.

Interface tested	Number of test	$\phi_{dyn}^{ST}(N_d = 1)$			Number of cycles (N_d)	$\phi_{dyn}^{ST}(N_d = 50 - 300)$		
		(°)				(°)		
		1.5Hz	3 Hz	6Hz		1.5Hz	3 Hz	6Hz
GTX - GMB _s	virgin	16.8	16.4	15.4	50	18.6	18.1	17.6
	2 nd retest	16.2	16.2	15.4	100	18.2	17.8	17.5
	3 rd retest	16.1	16.1	15.3	300	17.6	17.0	16.5
GNT - GMB _s	virgin	16.4	16.9	16.0	50	19.3	18.7	19.1
	2 nd retest	19.6	18.3	15.9	100	20.0	19.0	19.6
	3 rd retest	19.8	21.1	18.5	300	20.3	21.6	19.1
GCD _N - GMB _s	virgin	16.9	15.5	16.1	50	17.5	17.2	16.7
	2 nd retest	14.6	15.7	15.1	100	17.2	17.0	16.7
	3 rd retest	14.9	14.9	15.1	300	16.5	16.7	16.9

In particular, for GTX - GMB_s interface (Figure 5.2.15a), an increase in friction angle occurred in approximately the first 25 cycles, after which a tendency to decrease with the

number of cycles (N_d) can be observed. The decrease in shear stress is relatively rapid between 25 - 75 cycles, after which the shear stress reduction continues at a reduced rate.

Conversely, the behaviour of the GNT – GMB_s interface varies substantially with the number of cycles. In the first 50 cycles, ϕ_{dyn}^{ST} increases dramatically with N_d can be observed beyond which the dynamic friction angle remains almost constant. Finally, the GCD_N- GMB_s interface seems to be less affected by the increase of N_d displaying values very close from the beginning to the end of the test.

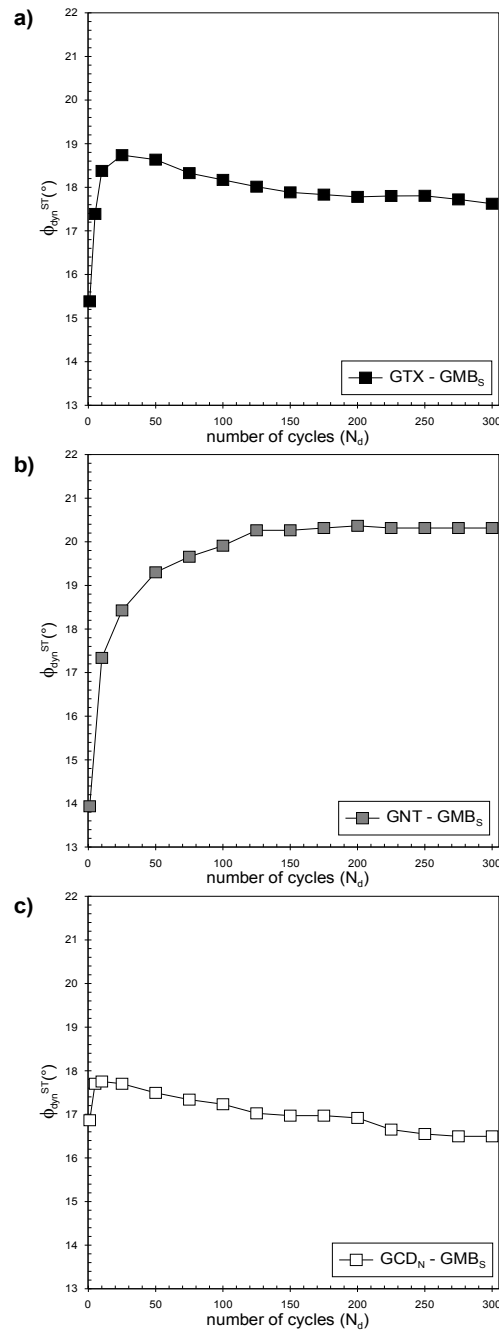


Figure 5.2.15. Influence of the number of cycles, N_d , on the dynamic interface friction angle ("standard" TAR, $f = 1.5$ Hz, $a_{max} = 0.4$ g and $\sigma_{v0} = 5$ kPa) for GTX – GMB_s (a); GNT – GMB_s (b) and GCD_N – GMB_s interfaces (c).

Similar trends of test results were observed in literature by De and Zimmie (1998) carrying out cyclic direct shear tests. They found a decrease in friction angle with the number of direct shear loading cycles for nonwoven geotextile – smooth geomembrane interface and an increase in the friction angle with the number of direct shear loading cycles for geonet – smooth geomembrane interface (Figure 5.2.16). Pasqualini et al. (1995) made the same observations for geotextile/smooth geomembrane interfaces and for a low density polyethylene geomembrane/geonet interface using cyclic direct shear tests.

They attributed a decrease in friction angle observed for geotextile-geomembrane interface to the polishing action of the geotextile on the smooth geomembrane surface while, the increase in friction angle observed for geonet-geomembrane interface can be due to a possible increase in roughness of the geomembrane surface due to shearing with the geonet.

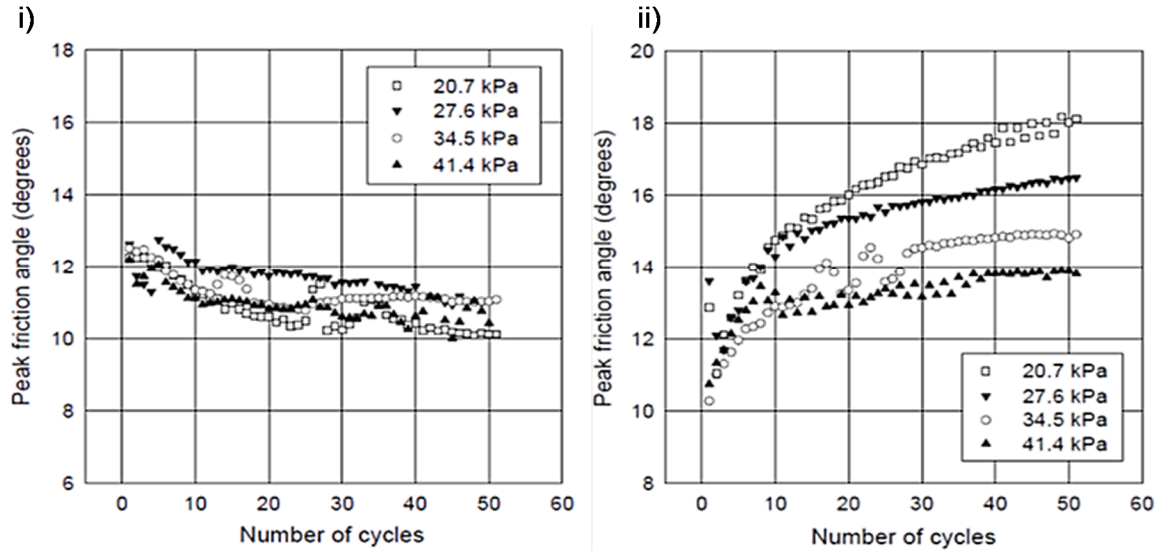


Figure 5.2.16. Variation of the peak friction angle with the number of cycles from cyclic direct shear tests run at a frequency equal to 0.25 Hz for a number of loading cycles equal to 50: i) a geotextile over a smooth geomembrane; ii) a smooth geomembrane over a geonet (after De and Zimmie, 1998).

5.2.7 Interface response comparison

Finally, the response of the interfaces *a*, *b* and *c* (Table 2.3.2) under harmonic excitations is compared in Figure 5.2.17 for the three frequencies investigated. As reported in Table 5.2.2 and Table 5.2.3, the dynamic friction angles determined for the three interfaces, present very close values.

The comparison between test results indicates that:

- the dynamic interface friction angles ϕ_{dyn}^{ST} of the GTX – GMB_s interface with respect to those of the geotextile with its support geonet (GCD_N - GMB_s interface) are influenced by the support which decreases ϕ_{dyn}^{ST} ;
- the contact between GNT – GMB_s is in general quite different than GTX – GMB_s interface with a variation that depends on the nature of the surfaces and on the resulting possible damage effect occurring as soon as the number of cycles N_d increases. In fact, it is believed that, since the contact between the smooth

geomembrane and geonet is maintained primarily at nodal points in the mesh (the nodal points are relatively widely spaced), considerable stress concentrations occur at the contact points, scarring the geomembrane surface during the test. Scar surface leads possibly to an increase in resistance in terms of initial sliding with $\phi_{\text{dyn}, N_d=1, (\text{GNT} - \text{GMBs})}^{\text{ST}} > \phi_{\text{dyn}, N_d=1, (\text{GTX} - \text{GMBs})}^{\text{ST}}$ and also increasing the number of cycles, N_d . In fact, during Phase 3, it is noted that dynamic interface friction values higher than those obtained for GTX – GMB_s interface ($\phi_{\text{dyn}, N_d > 25, (\text{GNT} - \text{GMBs})}^{\text{ST}} > \phi_{\text{dyn}, N_d > 25, (\text{GTX} - \text{GMBs})}^{\text{ST}}$) for all the frequencies investigated.

The trend of the dynamic response of the interfaces tested in this study is consistent with what previously found for similar interfaces in literature. In particular, Maugeri and Seco E Pinto, (2005) in a review of some typical geosynthetic/geosynthetic interface results presented in literature, observed that for geotextile/smooth geomembrane interfaces, the peak dynamic friction angle decreases with increase of the number of excitation cycles, especially for low values of the number of cycles (De and Zimmie, 1998). This reduction is attributed to a polishing action. The polishing effect increases with the addition of moisture, which is common in landfill liners and covers because of the presence of leachate or other fluids (Von Pein and Lewis, 1991). On the contrary, for smooth geomembrane/geonet interfaces a significant increase of the peak dynamic friction angle with cycle numbers is possible. In the first case, the increase in peak dynamic friction can be due to a possible increased roughness of geomembrane caused by the geonet.

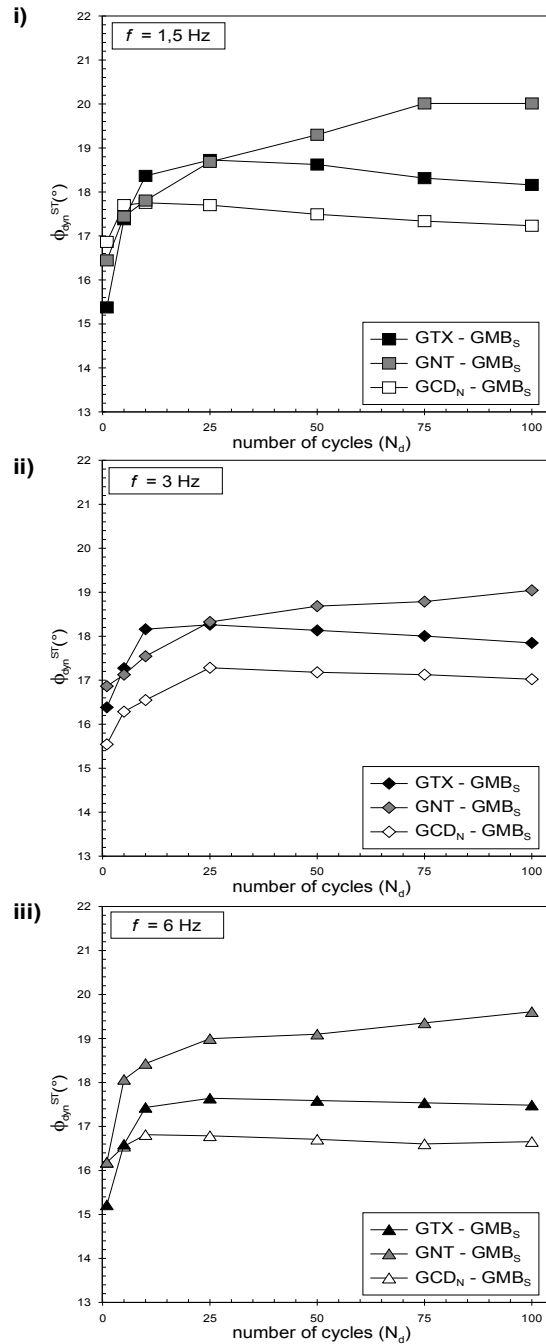


Figure 5.2.17. Comparative behaviour of GTX – GMB_S , GNT – GMB_S and GCD_N – GMB_S interfaces during Phases 2 and 3 of shaking table tests under harmonic excitations (“standard” signal”, $f = 1.5 \text{ Hz}$ (i), 3 Hz (ii) and 6 Hz (iii) at $\sigma_{v0} = 5 \text{ kPa}$).

5.2.8 Influence of the nature of the surfaces

As already found and discussed in inclined plane test results (§ 5.1.1.3), the nature of the surfaces in contact and, in particular, the geomembrane roughness, is of paramount importance in the determination of the interface mechanical behaviour. Tests presented in the previous sections, deal with interface involving smooth geomembrane (GMB_S). These

interfaces have shown a “*gradual sliding*” behaviour and, consequently, the interface mechanical parameters, are different with respect to those observed in interfaces displaying a “*sudden sliding*” mode of failure (see §4.1.1).

In order to investigate the dynamic behaviour of interfaces showing a “sudden sliding” failure, a special series of tests was conducted for geocomposite drain (GCD_N) in contact with structured geomembrane (GMB_{TMH}) (interface *d* of Table 2.3.2). It is worth noting that, thanks to this test series, also the influence of the geomembrane surface can be analysed because the same geocomposite drain (GCD_N) was tested with both smooth (GMB_S) and structured geomembrane (GMB_{TMH}).

In the experimental program the “standard signal”, as described in §4.2.3, at two frequencies equal to 3 Hz and 6 Hz was applied at σ_{v0} equal to 5 kPa. The maximum amplitude of the table (a_{max}) was determined considering the results from inclined plane and preliminary shaking table tests to allow the fully mobilization of the interface shear resistance. Therefore, due to the higher values of the interface friction angles, a_{max} is equal to 0.8g in this case.

The dynamic interface response is schematized in Figure 5.2.18 also plots the results of the geocomposite drain (GCD_N) in contact with the smooth geomembrane (GMB_S) in order to compare the response of interfaces. The resulting dynamic interface friction values (Equation 4.2-8) are summarized in Table 5.2.5 for both interfaces at 3 Hz and 6 Hz.

A completely different interface response can be noticed (Figure 5.2.18.). The interface, *d*, involving the textured geomembrane, displays a higher initial value of $a_{crit, Nd=1}$ [and also of $\phi_{dyn}^{ST} (N_d = 1)$] corresponding to the beginning of the sliding. Subsequently, during the relative movement, the box acceleration dramatically decreases since the first cycles. Similarly to what found in the inclined plane tests for these interfaces, the higher value obtained (Table 5.2.5) corresponds to the beginning of the motion while, during the slide, a drop in the interface friction is registered.

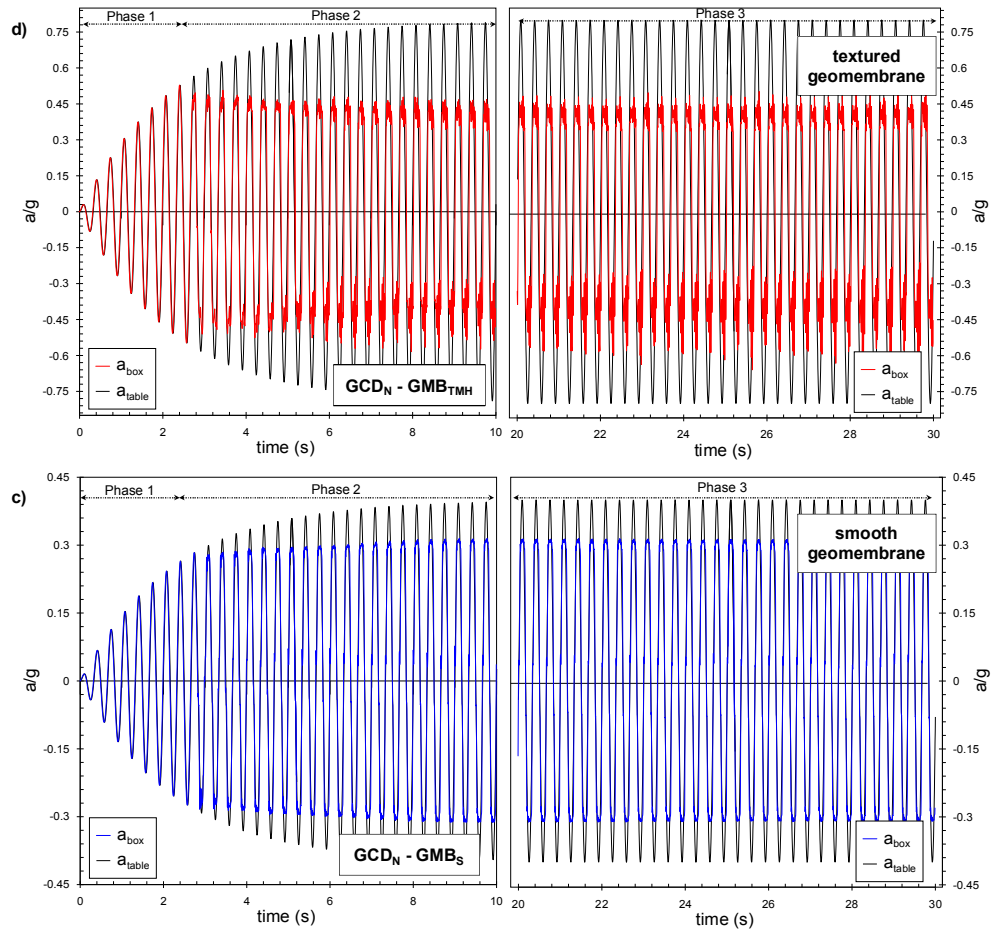


Figure 5.2.18. Dynamic interface response comparison (“standard” TAR, $f = 3$ Hz and $\sigma_{v0} = 5$ kPa): d) table and the box accelerations during Phases 1, 2, and 3 of GCD_N – GMB_{TMH} interface; c) table and the box accelerations during Phases 1, 2, and 3 of GCD_N – GMB_S interface

Table 5.2.5. Comparison between dynamic interface friction angles of geocomposite drain (GCD_N) in contact with the smooth and the structured geomembrane (GMB_{TMH}).

$\sigma_{v0}= 5 \text{ kPa}$		Number of cycles (N_d)	$f = 3\text{Hz}$		$f = 6\text{Hz}$	
Interface tested			$\tan \phi_{dyn}^{ST}$	ϕ_{dyn}^{ST} (°)	$\tan \phi_{dyn}^{ST}$	ϕ_{dyn}^{ST} (°)
c	GCD _N - GMB _S	1	0.278	15.5	0.290	16.2
		10	0.297	16.5	0.298	16.8
		25	0.311	17.3	0.302	16.8
		50	0.309	17.2	0.302	16.7
		75	0.308	17.1	0.298	16.6
		100	0.306	17.0	0.299	16.7
d	GCD _N - GMB _{TMH}	1	0.488	26.0	0.499	26.6
		10	0.433	23.4	0.447	24.1
		25	0.451	24.3	0.452	24.3
		50	0.448	24.1	0.456	24.5
		75	0.439	23.7	0.456	24.5
		100	0.441	23.8	0.450	24.2

The same results can also be plotted versus the number of cycles (N_d) as in Figure 5.2.19. In addition, for comparison, tests results of the $GCD_N - GMB_S$ interface are plotted in the same Figure 5.2.19. In this plot, the difference on the dynamic friction trend can be better appreciated. When the textured geomembrane is tested, in the first 20 cycles a dramatic drop of the dynamic friction angle can be noticed for both the frequencies tested. Subsequently, increasing N_d , as in the case of $GCD_N - GMB_S$ interface, a stabilization of the dynamic friction angle is reached with almost constant values.

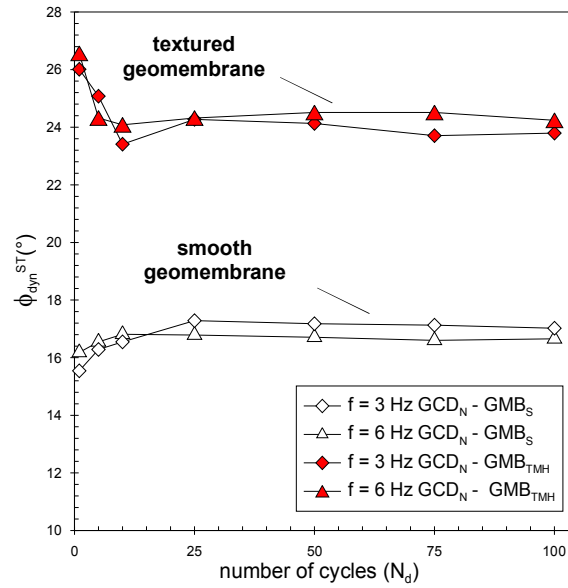


Figure 5.2.19. Comparative behaviour of the dynamic shear strength trend versus the number of cycles (N_d) in the case of “gradual” ($GCD_N - GMB_S$) and “sudden” sliding behaviour ($GCD_N - GMB_{TMH}$).

To summarize, in this section the interface between the geocomposite drain (GCD_N) in contact with the structured geomembrane (GMB_{TMH}) is analysed. This interface displayed “sudden sliding” behaviour in the inclined plane test. Therefore, this specific test series was performed to provide a first insight on the dynamic behaviour also for these kinds of interfaces. The dynamic interface friction trend diverges from the typical trends observed in the previous interfaces (Figure 5.2.6, Figure 5.2.7, Figure 5.2.8) being characterized by a rapid decrease of the dynamic shear strength in the first cycles ($N_d < 25$) after which, a steady – state is reached.

Some common features with respect to test results found in the inclined plane tests can be outlined:

- $\phi_{dyn}^{ST} (N_d = 1) > \phi_{dyn}^{ST} (N_d \geq 5)$ the value required to start the movement is higher than that developed during the sliding (noticed that in the inclined plane test $\phi_0 > \phi_{dyn}^P$)
- during the movement $a_{crit, Nd>1}$ is almost constant ($\phi_{dyn}^P \approx const$),
- the roughness of the geomembrane leads to an increase of the dynamic shear strength angle at the interface $\phi_{dyn}^{ST}(GCD_N - GMB_{TMH}) > \phi_{dyn}^{ST}(GCD_N - GMB_S)$.

5.2.9 Conclusions

The dynamic frictional behaviour of three geosynthetic interfaces (*a*, *b* and *c* listed in Table 2.3.2) were presented in this section. The dynamic shear strength of the interfaces was estimated on the basis of horizontal shaking table tests under harmonic excitations.

Firstly, a procedure able to fully characterize the dynamic shear strength response of the interface under sinusoidal excitations was proposed and carried out.

Tests results revealed various important characteristics regarding the dynamic frictional properties of the geosynthetic interfaces. The possible influence of some experimental parameters was also addressed.

The principal findings of this experimental program are:

- ✓ the critical acceleration, a_{crit} , also called “yield acceleration” is not constant and varies not only from one pulse to another but also during the same test,
- ✓ some interfaces can be sensitive to the influence of the normal stress level, of the frequency, of the maximum table acceleration amplitude and of the mean velocity generated at the interface.

The analyses presented herein further demonstrate that selection of an acceleration time history of appropriate magnitude and/or duration is a key factor in the correct evaluation of the seismic interface response.

In deciding on whether to base a geosynthetic cover design on an analysis using constant yield acceleration or on an analysis using degrading yield acceleration, a variety of other factors should be considered. Factors such as creep and the cyclic nature of earthquake loading may accelerate the degradation of the interface shear strength to the value corresponding to the residual shear strength parameters.

5.3 SHEAR STRENGTH EVOLUTION OF GEOSYNTHETIC INTERFACES FROM STATIC TO DYNAMIC LOADING CONDITIONS

5.3.1 Introduction

The interface shear strength passing from monotonic to dynamic loading condition can be different. Variations of the interface shear strength under dynamic excitations with respect to the static values, can be attributed to the inertial and viscous effects which are linked to the loading velocity and to its variations in the time (Carrubba and Massimino, 1998).

Among the common factors influencing both the static and the dynamic shear strength mobilization at the interface there are:

- ✓ *mean relative velocity*: the interface shear strength is affected by the relative velocity, increasing with the increase of the mean velocity until an upper bound value after which a stabilization of the dynamic interface friction angle is observed;
- ✓ *mechanical damage*: the interface shear strength evolves with respect to the displacement history. Once the peak is reached, the shear strength decays until the residual value. The shear resistance and the displacement levels required to reach these values depend on the nature of the materials at contact;
- ✓ *normal stress*: the coefficient of friction is usually constant based on the fundamental rules of basic theory of friction (Coulomb relationship); however geosynthetic interfaces can show different behaviour: the shear strength may decrease when the normal stress increases.

In light of these statements, a preliminary correlation between the inclined plane and the shaking table test is presented herein. In spite of the different kinematics of both tests, some common trends can be highlighted. Test results of interfaces *a*, *b* and *c* (Table 2.3.2) are compared following the effect of the mean relative velocity, the mechanical damage and the normal stress.

5.3.2 Influence of the mean relative velocity

The whole set of data obtained by means of the inclined plane and the shaking table can be evaluated according to the mean relative velocity. It should be pointed out that, in the inclined plane tests, the sliding velocity of the box is an absolute and a relative velocity at the same time, because the lower geosynthetic is attached to the frame which is motionless. Conversely, in the shaking table, the motion experienced by the interface is the relative

displacement between the box and the table. A mean value of the relative velocity, v , is defined as the half of the maximum value of the relative velocity reached in a single cycle. The definition of relative velocity, v , is different for the two tests. To compare the results, the relative velocity at the interface is always considered in the following.

Figure 5.3.1 summarizes the interface friction mobilised for the three interfaces with respect to the mean relative velocity at σ_{v0} equal to 5kPa. It's worth noting that the values of v in the inclined plane test, are significantly higher than in the shaking table test. As it could be noted from the Figure 5.3.1, the general trend indicates that, as soon as the mean relative velocity increases, also the interface friction angle increases regardless the loading type (monotonic or dynamic). This represents a further confirmation that, for interfaces showing a gradual sliding behaviour, dynamic friction angles higher than the static ones would be expected.

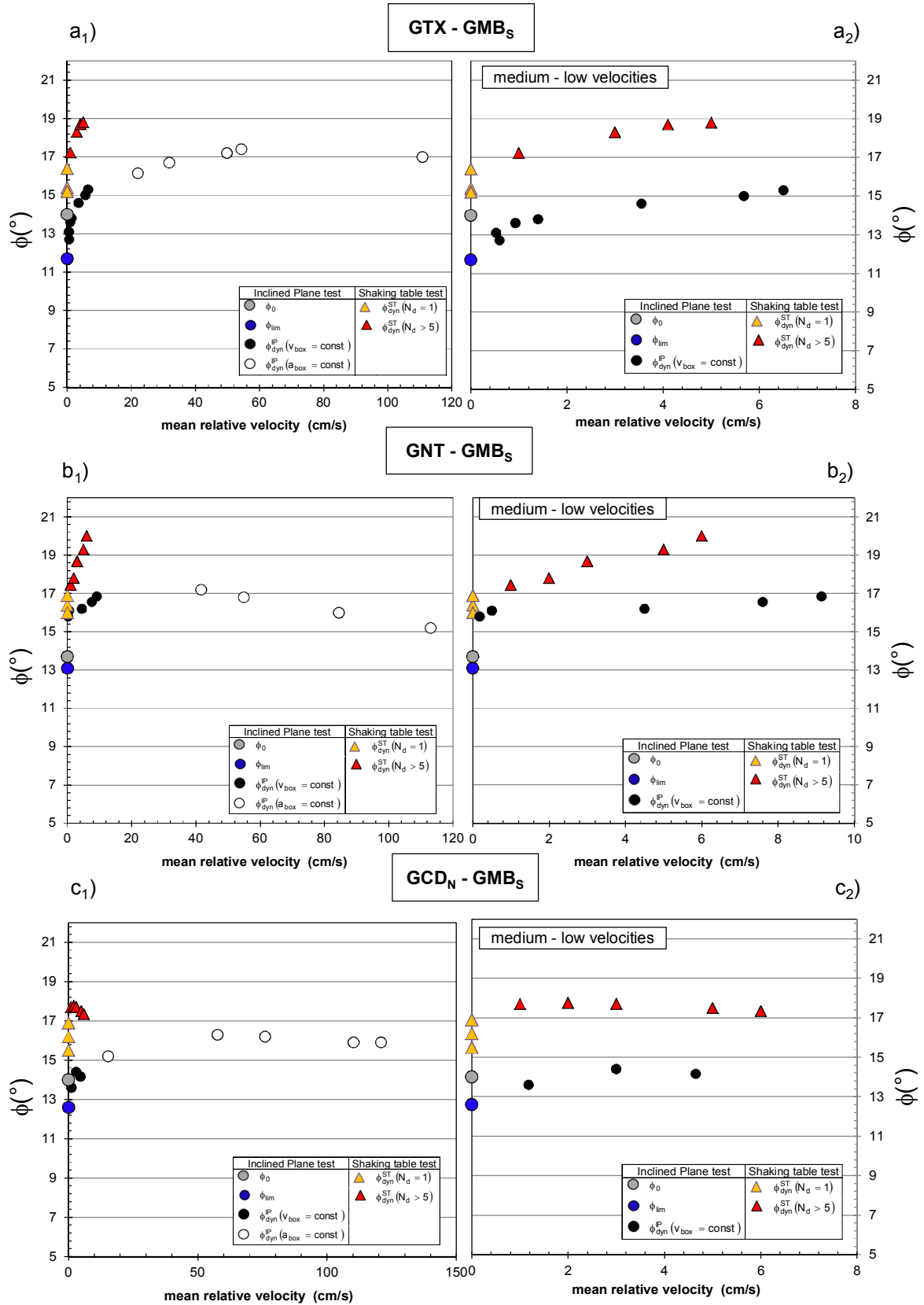


Figure 5.3.1. Mobilised interface friction angle with respect to the mean relative velocity determined through the inclined plane and the shaking table test. GTX -GMB_s interface: a₁) whole set of interface friction angle measured in both tests and a₂) enlarged view on the range of low-medium velocities; GNT -GMB_s interface: b₁) whole set of interface friction angle measured in both tests and b₂) enlarged view on the range of low-medium velocities; GCD_N -GMB_s interface: c₁) whole set of interface friction angle measured in both tests and c₂) enlarged view on the range of low-medium velocities.

Starting the discussion from the static values, for the inclined plane test, shear strength may be identified as ϕ_0 or ϕ_{lim} , for the cases in which displacement has previously occurred or not. In light of the mean relative velocity they correspond to the interface shear strength at relative velocity, v , equal to zero. Similarly, in the shaking table test, even if the table is moving with a certain acceleration, the interface shear strength corresponding to the beginning of the relative motion, $\phi_{dyn}^{ST} (N_d = 1)$ has a relative velocity equal to zero. Table 5.3.1 summarizes the mobilized interface friction angle at zero relative velocity for the three interfaces. The same results are also illustrated in Figure 5.3.2.

Beyond the different operating loading conditions (gravity in the inclined plane and dynamic excitation in the shaking table), if the variability of every friction angle is taken into account, it could be noticed that ϕ_0 values are close to $\phi_{dyn}^{ST} (N_d = 1)$ (Figure 5.3.2). In fact, unlike to ϕ_{lim} , both ϕ_0 and $\phi_{dyn}^{ST} (N_d = 1)$ angles corresponding to the first displacement of the upper box.

Table 5.3.1. Mobilized interface friction angle at zero relative velocity obtained under static and dynamic loading conditions.

Interface tested	Upper box velocity (v) (cm/s)	ϕ_{lim} (°)	ϕ_0 (°)	$\phi_{dyn}^{ST} (N_d = 1)$ (°)		
				1.5Hz	3 Hz	6Hz
GTX - GMB _s	0	11.7±0.2	14.0±1.0	16.1±0.7	16.2±0.1	15.4±0.2
GNT - GMB _s	0	13.1±0.4	13.5±1.0	15.3±1.0	16.5±0.5	16.1±0.2
GCD _N - GMB _s	0	12.6±0.5	14.0±1.1	16.2±0.7	15.4±0.1	16.1±0.2

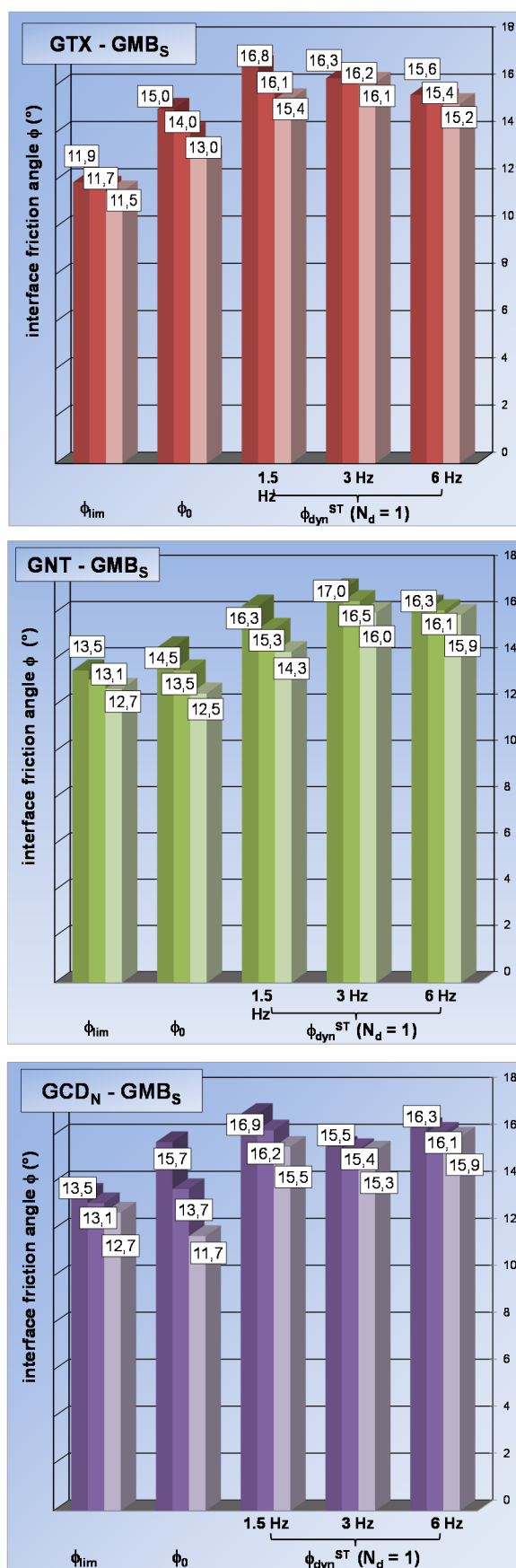


Figure 5.3.2. Comparative analysis between interface friction angles ($\nu = 0$) obtained through inclined plane (ϕ_0 and ϕ_{lim}) and shaking table $\phi_{dyn}^{ST} (N_d = 1)$ tests.

In literature, some studies outlined a correspondence between interface friction angle obtained in static and cyclic/dynamic loading conditions. Matasovic. et al., (1998) studying the degradation of yield acceleration as a function of displacement, found that for a geosynthetic interface, the initial threshold displacement value corresponds to the peak of the interface shear force-displacement curve after which, the yield acceleration degrades with increasing interface displacement until the ultimate “residual” yield acceleration. This second threshold displacement value corresponds to the displacement at which the large deformation, or residual, shear strength of the interface is reached. In agreement with these statements, Kotake et al., (2011), performing inclined plane, direct shear test and shaking table tests, concluded that, for some interfaces, the value corresponding to the beginning of the sliding in the shaking table test can be related to the peak interface friction angle measure through the direct shear test while, the dynamic interface friction angle mobilized during the sliding in the shaking table test, can be associated to the mobilized residual value obtained by the direct shear test. They also attributed the discrepancy between the static peak and residual frictions and the respective observed accelerations to the shear deformation and the dynamic response of the flexible materials. Finally, De and Zimmie, (1998) comparing inclined plane and direct shear tests with cyclic direct shear, shaking table and shaking table with geotechnical centrifuge test results, observed that the initial values of static and dynamic friction angles for the geosynthetic interfaces tested are similar even if the dynamic behaviour of most interfaces is complicated by a dependence on some factors such as the frequency of vibration or the number of cycles.

The dynamic friction angle, was characterized through the inclined plane (ϕ_{dyn}^{IP}) and the shaking table (ϕ_{dyn}^{ST}) devices. The ϕ_{dyn}^{IP} values plotted in Figure 5.3.1, are obtained in the range of high velocities (v ranging from 20 to 120 cm/s) according to Equation 4.1-7 for uniformly accelerated motion (Figure 5.3.1 a₁, b₁, c₁), and in the range of medium-low velocities ($v = 1 - 10$ cm/s) according to Equation 4.1-8 (uniformly motion – Figure 5.3.1 a₂, b₂, c₂). Regarding shaking table tests, the results plotted in Figure 5.3.1 refers to $\phi_{dyn}^{ST} (N_d \geq 5)$ obtained for a standard signal solicitation at 1.5Hz. It is worth noting that, for the shaking table tests, the results at 1.5Hz were chosen because, in these sets of tests, the highest relative velocity values were calculated.

All the dynamic friction angle results were displayed in Table 5.3.2.

Focusing attention on, ϕ_{dyn}^{IP} , for GXT – GMB_S and GCD_N – GMB_S values, inclined plane test results showed that as soon as the mean relative velocity increases, also dynamic

friction angle increases, up to an upper bound value at high velocities (as discussed in § 5.1.4, Figure 5.1.15). As it could be noticed a non-linear relationship between ϕ_{dyn}^{IP} and the relative velocity, at low – medium velocities range, is highlighted. The same trend is also noticed in the shaking table results.

Table 5.3.2. Dynamic interface friction angles, obtained in monotonic and dynamic tests, with respect of the mean relative velocity

Interface tested	Upper box velocity (cm/s)	$\phi_{dyn}^{IP} (v_{box} = const)$ (°)	Upper box velocity (cm/s)	$\phi_{dyn}^{IP} (a_{box} = const)$ (°)	$\phi_{dyn}^{ST} (N_d \geq 5)$ (°)		
					1.5Hz	3 Hz	6Hz
GTX - GMB_s	1-10	15.0±0.9	20-120	17.3±0.8	18.1±0.6	18.1±0.2	17.5±0.1
GNT - GMB_s	1-10	16.3±0.5	20-120	16.9±0.4	19.2±1.0	18.5±0.8	18.9±0.9
GCD_N - GMB_s	1-10	14.0±0.5	20-120	15.9±0.6	17.5±0.4	17.5±0.5	16.7±0.1

The GNT – GMB_s interface, displays a slight different behaviour. In this case, the upper bound corresponding to a stabilization of the dynamic interface friction is not yet reached for $\phi_{dyn}^{ST} (N_d \geq 5)$ in the range investigated and the dynamic friction angles continue to increase.

The systematic dependence of dynamic shear strength on the mean relative velocity seems to be related to the rheology of the geosynthetics. Dependence of mechanical behaviour of polymers influenced by viscosity could affect the interface behaviour (Carrubba and Massimino, 1998). The viscosity is related to the state of the surfaces at contact and depends on normal stress, temperature and progressive smoothing. The major effect related to viscosity is the increase of restraining interface forces with the relative velocity.

Finally, a comparison between ϕ_{dyn}^{IP} and ϕ_{dyn}^{ST} curves (Figure 5.3.1 a₂, b₂ and c₂ reported also in Table 5.3.2) shows that a similar trend is observed for monotonic and dynamic motions even if a difference in the amount of shear strength occurs. The discrepancy can be attributed to the different type of solicitation (monotonic and dynamic) and to the dependence of the mobilized shear strength on specific experimental conditions.

5.3.3 Influence of mechanical damage

The influence of the mechanical damage was simulated by successive monotonic shear experiments of the upper box in the inclined plane test (§ 5.1.6), and by dynamic shearing due to the stress reversal loading in the shaking table test (§ 5.2.6).

Although a sort of mechanical damage is caused in both tests by different mechanisms and the displacement level involved differs by several orders of magnitude, some common trend in the mobilized shear strength can be observed. The aim of this section, in fact is to give a preliminary correlation of results of static and dynamic tests highlighting some common characteristics.

The evolution of the static interface friction angles (ϕ_0 and ϕ_{lim}) obtained after successive sliding at the inclined plane and the angle corresponding to the inception of the motion, $\phi_{dyn}^{ST}(N_d = 1)$, after repeated shaking table tests, is illustrated in Figure 5.3.3. Table 5.3.3 summarizes the corresponding values.

Table 5.3.3. Mechanical damage effect of ϕ_0 and ϕ_{lim} (incline plane test) and of $\phi_{dyn}^{ST}(N_d = 1)$ (shaking table tests).

Interface tested	Number of test	ϕ_0	ϕ_{lim}	Number of test	$\phi_{dyn}^{ST}(N_d = 1)$		
		(°)	(°)		(°)		
					1.5Hz	3 Hz	6Hz
GTX - GMBs	virgin	14.4	11.6	virgin	16.8	16.4	15.4
	4 th retest	13.4	11.0	2 nd retest	16.2	16.2	15.4
	6 th retest	12.3	10.2	3 rd retest	16.1	16.1	15.3
GNT - GMBs	virgin	13.3	13.1	virgin	16.4	16.9	16.0
	4 th retest	14.2	15.7	2 nd retest	19.6	18.3	15.9
	6 th retest	16.1	16.8	3 rd retest	19.8	21.1	18.5
GCD _N - GMBs	virgin	13.6	12.6	virgin	16.9	15.5	16.1
	4 th retest	15.4	11.9	2 nd retest	14.6	15.7	15.1
	6 th retest	16.1	9.4	3 rd retest	14.9	14.9	15.1

***Note:** ϕ_0 and ϕ_{lim} are determined after successive passages of the upper box (see § 5.1.6); ϕ_{dyn}^{ST} values are calculated for “standard” TAR, $f = 1.5$ Hz, $a_{max} = 0.4$ g and $\sigma_{v0} = 5$ kPa (see § 5.2.6).

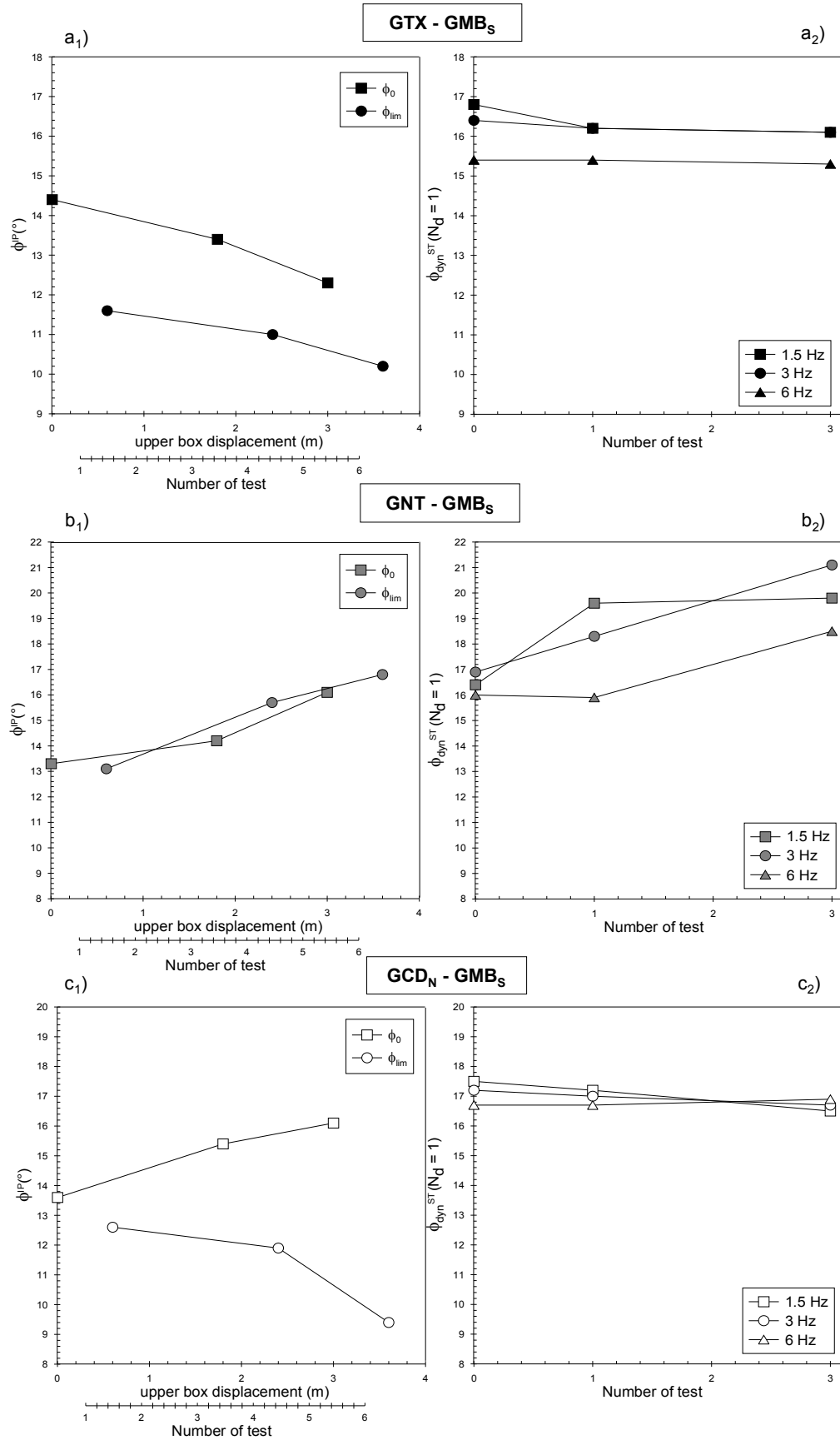


Figure 5.3.3. Comparison of the mechanical damage effect on ϕ_0 and ϕ_{lim} (incline plane test) and on $\phi_{dyn}^{ST} (N_d = 1)$ (shaking table tests: a₁) and a₂) GTX-GMB_s interface; b₁) and b₂) GNT-GMB_s interface; c₁) and c₂) GCD_N-GMB_s interface.

The effect of the mechanical damage for the dynamic friction angles ϕ_{dyn}^{IP} (calculated according to Equations 4.1-7 and 4.1-8 after multiple sliding - § 5.1.6) and ϕ_{dyn}^{ST} (calculated for N_d equal to 50, 100 and 300 cycles as described in § 5.2.6) are reported in Table 5.3.4 and displayed in Figure 5.3.4.

Table 5.3.4. Mechanical damage effect of the dynamic friction angles ϕ_{dyn}^{IP} (incline plane test) and of ϕ_{dyn}^{ST} (shaking table tests).

Interface tested	Number of test	$\phi_{dyn}^{IP} (v_{box} = const)$	$\phi_{dyn}^{IP} (a_{box} = const)$	Number of cycles (N_d)	$\phi_{dyn}^{ST} (N_d = 50 - 300)$		
		(°)	(°)		(°)		
					1.5Hz	3 Hz	6Hz
GTX - GMBs	virgin	15.7-15.9	17.6	50	18.6	18.1	17.6
	4 th retest	14.8-15.1	17.4	100	18.2	17.8	17.5
	6 th retest	13.5-13.8	16.8	300	17.6	17.0	16.5
GNT - GMBs	virgin	15.8-15.9	17.2	50	19.3	18.7	19.1
	4 th retest	16.7-17.0	16.8	100	20.0	19.0	19.6
	6 th retest	16.5-16.6	16.0	300	20.3	21.6	19.1
GCD _N - GMBs	virgin	14.1-14.2	16.30	50	17.5	17.2	16.7
	4 th retest	15.4-15.6	16.20	100	17.2	17.0	16.7
	6 th retest	15.1-15.3	15.90	300	16.5	16.7	16.9

***Note ϕ_{dyn}^{IP} are determined after successive passages of the upper box (see §). ϕ_{dyn}^{ST} values are calculated for “standard” TAR. $f = 1.5$ Hz. $a_{max} = 0.4$ g and $\sigma_{v0} = 5$ kPa.**

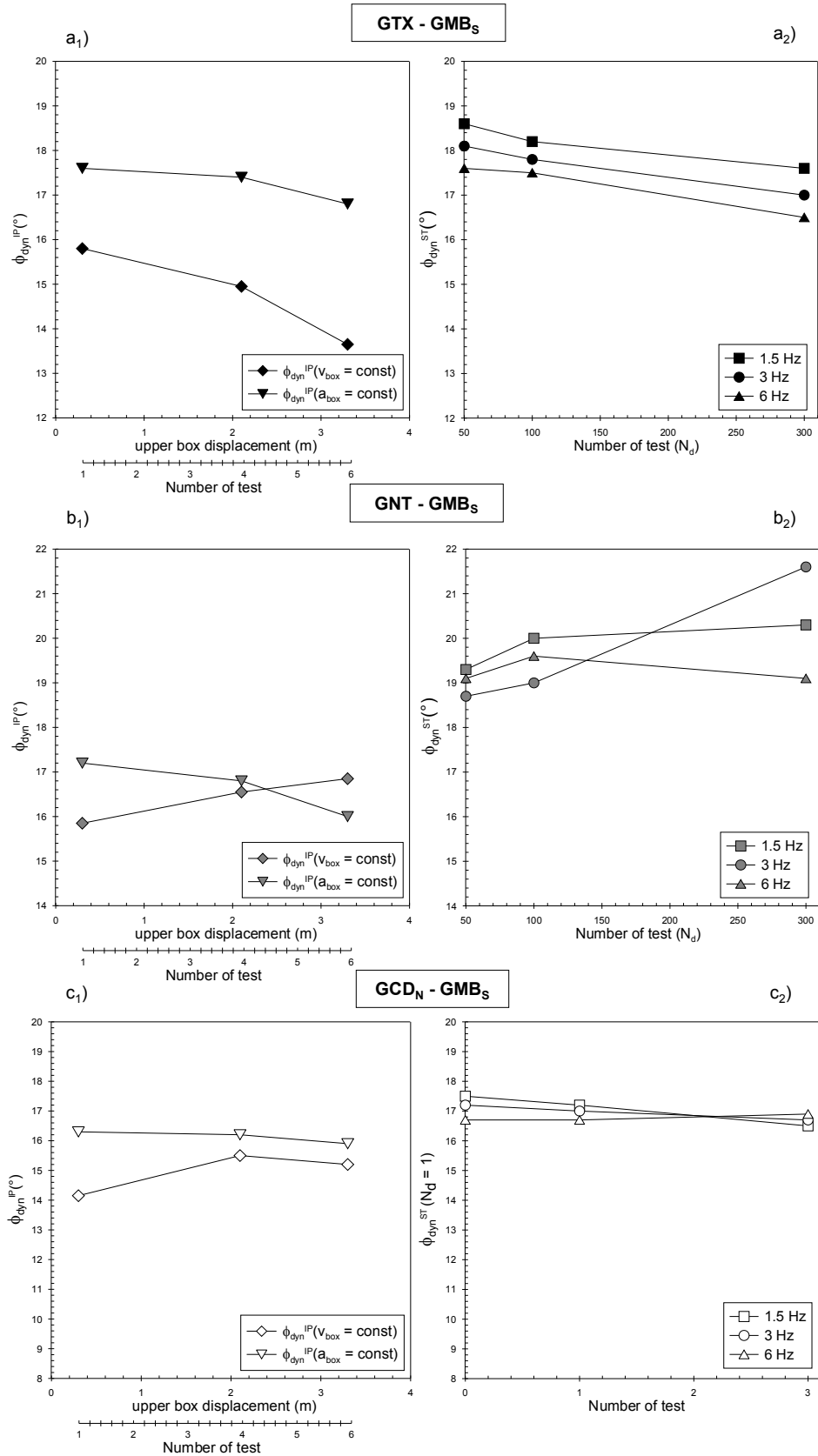


Figure 5.3.4. Mechanical damage effect on dynamic friction angles simulated by successive monotonic shear experiments (a₁, b₁ and c₁) and dynamic shearing due to the stress reversal loading (a₂, b₂ and c₂): a₁) and a₂) GTX-GMB_s interface; b₁) and b₂) GNT-GMB_s interface; c₁) and c₂) GCD_N-GMB_s interface.

It could be noticed that a progressive modification of the surfaces increases increasing the number of tests. In general, a more marked effect is noticed in ϕ_0 and ϕ_{lim} (Table 5.3.3) in monotonic tests while a slight effect is noticed in the case of ϕ_{dyn}^{IP} and ϕ_{dyn}^{ST} obtained from both monotonic (inclined plane) and dynamic (shaking table) tests (Table 5.3.4).

In the case of GTX – GMB_s interface, shear strength tends to reduce increasing the displacement level in both tests. This reduction may be attributed to the polishing action of the geotextile on the smooth geomembrane surface. In particular, De and Zimmie. (1998) studied this phenomenon through microscopic images of geomembrane cross sections before and after cyclic shearing showing an increase in smoothness of the geomembrane surface after being subjected to a successive shearing against a nonwoven geotextile.

On the other hand, the common behaviour of the GNT – GMB_s interface is characterized by an increase in the friction angle increasing the displacement level.

Designers should consider the reduction in the dynamic friction angle due to successive monotonic shear experiments and dynamic shearing due to the stress reversal loading. For interfaces that indicate an increasing dynamic friction angle with an increasing number of shear cycles is important to identify the range of cycles for which the design is intended.

The study presented above attempts to give an insight on the influence of the mechanical damage intended as wear effect of the surfaces using the inclined plane and the shaking table tests.

5.3.4 Influence of normal stress

Interface shear strength evaluation is affected by the normal stress level. A moderate non-linearity is highlighted at very low stresses (0.08 kPa; 0.8 kPa; 5 kPa and 12 kPa) where the coefficient of friction decreases as normal stress increases (Figure 5.1.17, Figure 5.1.19 and Figure 5.1.21). Similar results for the interface friction coefficient variation with the applied vertical stress were obtained by using the shaking table (Figure 5.2.9). It is worth noting that, the trend observed refers to the particular geosynthetic interfaces tested and it should be borne in mind that a small normal stress range was investigated.

Consequently, the characterization of the interface shear strength should be carried out at vertical stresses compatible with those expected on site.

6 CONCLUSIONS AND FUTURE PERSPECTIVES

6.1 INTRODUCTION

Modern engineered landfills are designed and constructed to minimize or eliminate the release of pollutants into the environment. Thus, landfills consist of multi-barrier systems including the bottom and side lining barriers and covers generally composed of a combination of geosynthetics and soils.

The overall integrity of a landfill is closely linked to the slope stability of the lateral and cover barriers under static and seismic loading conditions. When the barrier is installed in the inclined surface for bottom and cover barriers, due to self-weight of the soil for protection layer and the above column of waste in case of bottom barrier, the sliding force will arise along the barrier system that results in shearing force applying to the system. The present report is restricted to the case of cover lining systems. The specificity of this case is the low level of the normal stress along the different geosynthetic and soil interfaces likely to slip.

The interfaces between the different materials composing a multi-layered liner system often represent potential slip surfaces that need to be considered in slope stability analyses. The failure at the interfaces occurs when the driving forces exceed the shear resistance force mobilized at the interface.

The comprised liner and cover systems must withstand the possible applied stresses without being affected in their function. A careful estimation of these stresses as well as strengths of liner and cover systems serves as a basis for safe landfill construction, operation, and post-closure. Furthermore, the performance of solid waste containment

facilities subjected to seismic loading has been the subject of recent concern due to the increased emphasis on the design of landfills against possible seismic disturbance. Although the available examples of modern solid waste landfills subjected to strong earthquakes demonstrated a good ability to withstand to dynamic loadings, the evaluation of the dynamic response of the composite liner systems and in particular of the shear strength at the interface is of paramount importance.

The liner system is designed taking into account the different functions and the efficiency of the materials used. It's important to keep in mind that the design of a composite liner system is based on the separation of functions: one soil or geosynthetic layer-one function.

In particular, the present study focuses on the interface between geocomposite drain in contact with geomembrane because the range of use of this interface is very widespread in geotechnical and environmental engineering and more specifically in landfill covers on slopes. Furthermore, just for the specific interface between the geocomposite drain (GCD_N) and the smooth geomembrane (GMB_S), the influence of the different materials which constitute the geocomposite layer (geonet and geotextile) is assessed by testing them separately in direct contact with the geomembrane.

A wide experimental program was conducted through the inclined plane and the shaking table devices in order to evaluate the interface shear strength under static, dynamic and fully dynamic loading conditions.

In this section, the main conclusions of this research will be drawn as follows:

- limit and capabilities of the new testing procedures proposed and conducted in the experimental program;
- interface shear strength characterization by means of different interface friction angles (ϕ_0 , ϕ_{lim} , ϕ_{dy}^P and ϕ_{dyn}^{ST}): definitions and principal considerations;
- inclined plane and shaking table tests: main conclusions of the first correlation attempt;
- behaviour of the interfaces tested: principal conclusions on the frictional response in both loading conditions.

6.2 INCLINED PLANE AND SHAKING TABLE TESTING METHODS: PRINCIPAL LIMIT AND CAPABILITIES OF TEST PROCEDURES

6.2.1 Unified Inclined Plane Procedure (UIPP)

The present work demonstrates that the information collected from an Inclined Plane Test is far richer than the simple result of friction given from a standard test. In the present research, a comprehensive methodology feasible, easy to perform and able to fully characterize the evolution of the friction angle during the entire test, is proposed and discussed. Hence, the so called “Unified Inclined Plane Procedure (UIPP)” is validated and applied to different geosynthetic interfaces. The new testing method developed, consists of three following steps (Steps 1, 2 and 3 fully described in § 4.1.3) corresponding to different kinematic conditions: static, dynamic and pseudo-static at large displacements.

The UIPP was validated by checking the results repeatability and reproducibility. For this purpose, two inclined plane devices, available at LTHE and ICEA laboratories (see § 3.3 for apparatus details), were used.

Regarding the repeatability, a separate analysis of test results was conducted distinguishing the interfaces involving the smooth geomembrane and the interfaces involving textured geomembranes being the variability of results dependent on the surface properties of the materials in contact. Test results showed a good repeatability for the three interfaces involving smooth geomembrane (GTX - GMB_S, GNT - GMB_S and GCD_N - GMB_S) being the variability, for the interface friction angles determined (ϕ_0 , ϕ_{dyn}^{IP} and ϕ_{lim}), in the range of 0.7 - 9% at $\sigma_{v0} = 5\text{kPa}$. Much more complex is the repeatability analysis of interfaces involving textured geomembranes due to the macrotextural patterns of the geomembrane surface as discussed in § 5.1.1.2. In this case, the coefficients of variability are in the range of approximately 3 - 11% ($\sigma_{v0} = 5\text{kPa}$). Furthermore, matching test results obtained at both inclined plane apparatus (available at LTHE and ICEA laboratories), a good agreement in test results (Table 5.1.4 and Table 5.1.5) can be noticed. Although some operative conditions of the different devices (i.e. the techniques for fixing the interface layers or the stiffness and planarity of the supports made of different materials), being the maximum scatter related to the three interface friction angles (ϕ_0 , ϕ_{dyn}^{IP} and ϕ_{lim}) equal to $\pm 0.8^\circ$, $\pm 0.5^\circ$ and $\pm 1.1^\circ$ respectively, the reproducibility can be considered satisfied. Finally, a comparison between the results obtained by both devices allowed analysing the effect of the specimen size. Changing the specimen dimensions, no appreciable difference in shear strength is observed. Therefore, the results do not exhibit significant scale effect for the specimen dimensions involved in these experiments.

Applying the UIPP, the principal findings can be summarized as follows:

- The interface shear strength cannot be characterised by a single parameter, as proposed by the European Standard EN ISO 12957-2 (2005) depending on the existing kinematic conditions of the interface during the test. Furthermore, since the standard friction angle refers to a conventional displacement of 50 mm, it may correspond to various kinematic conditions, depending on the behaviour of the tested interface, not known a priori.
- The approach proposed and applied in this study tries to overcome the limitations of the “Standard Procedure”. In fact, thanks to the Unified Inclined Plane Procedure (UIPP) it is possible to evaluate, during a single test, different friction angles varying according to the current kinematic conditions (ϕ_0 , ϕ_{dyn}^P and ϕ_{lim}). In particular, the evolution of the interface shear strength in static - dynamic – pseudo-static at large deformations conditions can be investigated during the same test.
- The UIPP seems to be a suitable method even if, in some cases, its application can be difficult and some modifications must be performed. For the interfaces *a*, *b* and *c* displaying a *gradual sliding* behaviour, the dynamic friction angle is difficult to determine during Step 2 (a Variant to Step 2 is proposed) while, in the case of interfaces *d*, *e*, *f* and *g* involving the textured geomembranes, some difficulties were encountered in carrying out Step 3 linked to the device capability.

6.2.2 Shaking Table Test Procedure

In the present study in order to assess the seismic risk with respect to the sliding failure along the liners, the dynamic behaviour of geosynthetic interfaces was investigated using a shaking table device of the ICEA laboratory in the vibrating configuration at zero inclination β of the table.

The test procedure presented and applied in the experimental program, based on the conventional Newmark seismic deformation approach, is able to define the evolution of the dynamic shear strength at the interface during the entire test (§ 4.2.3) when harmonic excitations are applied to the table.

A series of fundamental experiments, on the three different interfaces involving the smooth geomembrane (*a*, *b* and *c* listed) and one interface (interface *d*) involving the structured geomembrane (already tested at the Inclined Plane), was conducted at the ICEA

Shaking Table. The dynamic shear strength of the interfaces was estimated on the basis of horizontal shaking table tests under harmonic sinusoidal excitations.

Firstly, a procedure able to fully characterize the dynamic shear strength response of the interface under sinusoidal excitations was proposed and carried out. In the general case, the adopted testing method consists in three main Phases: an initial (no relative motion - Phase 1), a transitory (beginning of the upper box motion with $a_{crit}(t)$ and $a_{table}(t)$ increasing with the time - Phase 2) and a steady – state (the table acceleration reaches the maximum value a_{max} while $a_{crit}(t)$ can change mainly depending on the particular interface interactions - Phase 3).

It should be pointed out that, during Phase 2, the critical acceleration and consequently the dynamic coefficient of friction, in general, are not stabilized. This kind of behaviour, typically encountered in shaking table test results, has rarely been addressed in the technical literature. Therefore, in order to assess the influence of Phase 2 in the results, a set of tests, sending signals with different table acceleration rates (TARs), was performed. The results indicate that, even changing the TAR, the critical acceleration corresponding to the beginning of motion (Phase1) does not vary significantly. During Phase 2, the interface response varies depending on the considered TAR but, finally, during the steady-state phase, the interface behaviour is no more affected by the signal shape during Phase 2, providing similar results in terms of a_{crit} .

The testing method adopted in this study, allows estimating the dynamic interface friction angle during the entire test by introducing a specific parameter, denoted as number of cycles, N_d where the first cycle, $N_d = 1$, corresponds to the beginning of the relative motion between the box and the table. The variation of the critical acceleration with the number of cycles $a_{crit}(N_d)$, was considered in all the interpretation of test results. The parameter N_d , allowed the assessment of the dynamic interface shear strength in the different phases of the test.

Applying the shaking test method adopted in this study, it could be noticed that:

- the typical behaviour observed is characterized by the transitory Phase 2 (with a subsequent Phase 3 where the critical acceleration as well as the dynamic friction coefficient attain, usually, a relatively steady-state value. The shape of the transitory Phase 2 is more relevant for interfaces involving smooth geomembrane (a , b and c) (observed for N_d generally ranging from 1 to 20) while it is smaller for the interface d , displaying a sudden sliding. Here the steady state value (Phase 3) is already reached for $N_d > 5$.

- $a_{crit, Nd=1}$ values corresponding to the beginning of the sliding do not differ significantly when testing the same interface at various frequencies (1.5 Hz, 3 Hz and 6 Hz). Furthermore, only a slight difference in test results during the steady-state Phase 3 can be noticed and it is, generally, of the same order of the results repeatability.
- The critical acceleration is not constant and can vary not only from one pulse to another but also during the same test. The first condition was investigated testing the interface under different values of the maximum accelerations ($a_{max} = 0.34g, 0.40g$ and $0.60g$) at a given frequency equal to 3Hz. These test results indicate that as a_{max} increases (i.e. passing from 0.34 to 0.60g), $a_{crit, Nd=1}$ does not vary significantly while, increasing the number of cycles N_d , during Phase 3, a reduction in a_{crit} values can be observed. In order to take into account the variation of a_{crit} during the same test, the parameter, N_d , indicating the number of cycles of the upper box during the relative motion, was introduced. It was shown that, contrary to one of the Newmark's hypothesis, the critical acceleration and consequently the dynamic interface friction do not remain constant and generally vary from the value corresponding to the beginning of the initial sliding ($a_{crit, Nd=1} \neq a_{crit, Nd=100}$).

6.3 INTERFACE SHEAR STRENGTH CHARACTERIZATION THROUGH THE INCLINED PLANE AND THE SHAKING TABLE TESTS

The inclined plane and the shaking table tests allowed the evaluation of the interface shear strength at different kinematic conditions. Static conditions are characterized by ϕ_0 corresponding to the initial sliding (determined at the conventional upper box displacement, u , equal to 1 mm) and ϕ_{lim} the interface friction angle after shearing, at large displacements. Dynamic and fully dynamic conditions are evaluated through ϕ_{dyn}^P and ϕ_{dyn}^{ST} obtained, respectively, through the inclined plane and the shaking table tests.

In the inclined plane tests and further confirmed by shaking table test results, the sliding mode is the first parameter that must be taken into account in the analysis of the interface response: following the mode of failure, different considerations about the mechanical interface properties, are expected. In particular, for *gradual sliding* behaviour, observed for the interfaces *a*, *b*, and *c*, the upper box slides progressively, with a nearly uniform motion. In this case, the general trend of test results shows:

- $\phi_0 > \phi_{lim}$,
- $\phi_0 < \phi_{dyn}^P$.

This trend is confirmed also by shaking table test results with $\phi_0 < \phi_{dyn}^{ST}$ and, similarly, it could be noticed that the dynamic friction angle increases from the value corresponding to the beginning of the sliding to the value reached during the steady-state phase $\phi_{dyn}^{ST}(N_d = 1) < \phi_{dyn}^{ST}(N_d = 100)$.

The main features of test results for interfaces showing a *sudden sliding* behaviour, where a uniformly accelerated motion can be recognized (interfaces *d*, *e*, *f*, and *g* listed in Table 2.3.2), can be summarized as follows:

- $\phi_0 > \phi_{lim}$,
- $\phi_0 > \phi_{dyn}^P$.

The inclined plane test results are generally consistent with the mentioned statements. However, some divergences can be noted (Table 5.1.5). In fact, since in this research the interfaces showing a sudden sliding were those involving the textured geomembranes, the discrepancies are mainly related to the “hoop and look” contribution usually encountered in these kind of surfaces, rather than to the mode of sliding. In these cases, the interaction between the geotextile filaments engaged by the geomembrane texture surfaces is the most relevant mechanism influencing the interface response. Test results indicate that, for these interfaces showing a kind of stick-slip behaviour before reaching the brutal rupture, the conventional definition of ϕ_0 could be not relevant. In addition, since $\beta_s > \beta_0$ (in the interfaces *d*, *f* and *g*) also $\phi_{dyn}^{IP} > \phi_0$. Therefore, the aforementioned relationships are satisfied if a new value of the plane inclination, corresponding to the beginning of the sudden sliding (see Figure 5.1.6 and Figure 5.1.7), is considered.

The dynamic response of an interface presenting a *sudden sliding* behaviour was studied at the shaking table device. As discussed in § 5.1.1.2.2, ϕ_0 values, with the conventional definition, cannot be considered in the analysis of the interface response being the interaction between the geotextile filaments and the geomembrane surface the predominant effect on the interface mechanism. However, similarly to what found for interfaces showing a sudden sliding, it could be noticed that:

- $\phi_{dyn}^{ST}(N_d = 1) > \phi_{dyn}^{ST}(N_d > 5)$ (i.e. the value required to start the movement is higher than that developed during the sliding);
- during the movement $a_{crit, Nd>1}$ can be approximated as constant ($\phi_{dyn}^{ST}(N_d > 5) \approx \text{const}$) as in the case of the inclined plane test during Step

2 where, for these interfaces, the uniformly accelerated movement is established ($a_{\text{box}} \approx \text{const}$ and, consequently, $\phi_{\text{dyn}}^{\text{IP}} \approx \text{const}$).

6.4 INCLINED PLANE AND SHAKING TABLE TESTS: MAIN CONCLUSIONS OF THE FIRST CORRELATION ATTEMPT

The assessment of the interface shear strength is quite complex because different experimental parameters can influence the interface response. Among these factors, the influence of the mean relative velocity, the normal stress and the mechanical damage were assessed by both the inclined plane and the shaking table device. Others, such as the temperature or the frequency and the amplitude of the sinusoidal input, were evaluated only by sets of tests carried out at the inclined plane or at the shaking table device.

6.4.1 Mean relative velocity

The whole set of data can be evaluated in the light of the mean relative velocity. Being the kinematics of both tests very different, to compare the results, the mean relative velocity at the interface (i.e. the mean value of the upper box relative velocity) is always considered in the following.

Figure 5.3.1 summarizes test results of the interfaces (*a*, *b* and *c* listed in Table 2.3.2). Both the static and the dynamic interface friction angles are plotted in the same diagram. ϕ_0 , ϕ_{lim} and $\phi_{\text{dyn}}^{\text{ST}} (N_d = 1)$ are considered as interface friction angles corresponding to the mean relative velocity equal to zero; $\phi_{\text{dyn}}^{\text{IP}}$ and $\phi_{\text{dyn}}^{\text{ST}} (N_d \geq 5)$ represent the dynamic and the full dynamic friction angles.

The principal conclusions are summarized below.

Taking into account the different operating loading conditions (gravity in the inclined plane and dynamic excitation in the shaking table), it seems reasonable to relate ϕ_0 to $\phi_{\text{dyn}}^{\text{ST}} (N_d = 1)$ being, unlike to ϕ_{lim} , the angles corresponding to the first displacement of the upper box. In fact, taking into account the different type of solicitations and the variability of the results, similar values can be observed.

The dynamic friction angles, $\phi_{\text{dyn}}^{\text{IP}}$, are determined at the inclined plane for two main velocity ranges: the low-medium (corresponding in these cases to the uniform motion during Step

2) and high (uniformly accelerated motion obtained applying the Variant to Step 2) velocities. Regarding shaking table tests, the results refers to $\phi_{dyn}^{ST} (N_d \geq 5)$ obtained for a standard signal solicitation at 1.5Hz because, the highest relative velocity values were calculated in these sets of tests.

In both inclined plane and shaking table test results, the general trend is characterized by an increase in the dynamic friction angle with the increase in the mean relative velocity. In particular, at low velocities, when the motion can be approximated as uniform, the dynamic friction angle increases following a non-linear relationship. Once the uniformly accelerated motion is established, an upper bound of the dynamic friction angle can be defined: here $\phi_{dyn}^{IP} (a_{box} = \text{const})$ does not increase anymore and almost constant values can be calculated even increasing the mean relative velocity.

It is believed that the uniform motion established at the interface may represent the transition between the static and the dynamic phase. This transitory phase (Step 2) appears clearly in interfaces showing *gradual sliding* behaviour (during the entire Step 2) while, it is very short for interfaces displaying a *sudden sliding* behaviour. Similarly, in the shaking table tests, the transitory Phase 2 can be seen as the transition between the initial phase and the steady-state phase and its shape is more relevant for interfaces involving smooth geomembrane (*a*, *b* and *c*) where N_d generally ranges from 1 to 20 while it is smaller for the interface *d*, where the steady state value (Phase 3) is reached for $N_d > 5$.

Furthermore, the systematic dependence of dynamic shear strength on the mean relative velocity seems to be related to the rheology of the geosynthetics. A possible assumption is that mechanical behaviour of polymers influenced by viscosity could affect the interface behaviour. The viscosity is related to the state of the surfaces at contact and depends on normal stress, temperature and progressive smoothing. The major effect related to viscosity is the increase of restraining interface forces with the relative velocity.

Finally, a comparison between ϕ_{dyn}^{IP} and $\phi_{dyn}^{ST} (N_d \geq 5)$ shows that a similar trend is observed for monotonic and dynamic motions even if a difference in the amount of shear strength occurs. The discrepancy is mainly attributed to the different type of solicitation (monotonic and dynamic), to the discrepancy in the range of displacements and to the dependence of the mobilized shear strength on specific experimental conditions.

6.4.2 Mechanical damage

Geosynthetic interfaces are sensitive to the surface wear process. This sensitivity has consequences in friction properties that may increase or decrease depending on the pair of associated geosynthetics. In addition, the particular type of geomembrane component of a geosynthetic interface plays an important role in the response of this interface to the surface wear process.

In this research, a first insight on the influence of the mechanical damage considered as wear effect of the surfaces, using the inclined plane and the shaking table tests, is provided. The effect of wear, was investigated applying different approaches using the inclined plane and the shaking table tests for interfaces involving smooth geomembranes (*a*, *b* and *c*) while, interfaces involving the textured geomembranes (*d*, *e*, *f* and *g*), were subjected only to mechanical damage simulation (§ 5.1.6) in static loading conditions.

Test results revealed that an alteration of the surfaces of the materials in contact, occurs increasing the number of tests or the number of cycles for all the interfaces investigated in both loading conditions. For the interfaces involving the smooth geomembranes, the general trend indicates that the variation can be mainly attributed to the smoothing and polishing of the surfaces in contact and it has a more marked effect on ϕ_0 and on ϕ_{lim} with respect to ϕ_{dyn}^{IP} and ϕ_{dyn}^{ST} values obtained from both the inclined plane and shaking table tests where only a slight effect is noticed.

Test results of interfaces involving textured geomembranes (*d*, *e*, *f* and *g*) show that the wear effect can be relevant and seems to be related to the alteration caused by the macrotextural features of the geomembrane on the upper layer.

The previous knowledge of this sensitivity is, therefore, an important issue of design, which must be considered by the manufacturers of geosynthetics, by the project designers and by the executors of civil works that involve the application of these polymeric materials. Such knowledge can provide a quantitative basis useful for the development of products and for the choice of the most appropriate geosynthetic interfaces according to the surface wear predicted in work.

6.4.3 Normal stress

Interface shear strength evaluation can be affected by the normal stress level in particular when testing at low normal stress levels. A specific series of tests at the inclined plane, was

dedicated to assess the GTX – GMB_s interface behaviour at very low vertical stresses (0.08 kPa; 0.8 kPa; 5 kPa and 12 kPa). It is found that the coefficient of friction decreases as normal stress increases. Similar results were found testing the materials at two compression values: σ_{v0} equal to 5 kPa and 12 kPa through the shaking table device. However, it could be noticed that, these results refer only to the materials tested in the range of normal stress investigated and cannot be generalized to other interfaces. In general, it is always recommended to perform laboratory tests under the normal stress range consistent with the level expected in the field.

6.4.4 Nature of the surfaces in contact

It is well known that the first parameter influencing the interface shear strength is the nature of the surfaces in contact. Beyond this aspect, test results highlighted that the nature of the geomembrane plays a fundamental role in the development of the shear strength at the interfaces. In fact, for the interfaces involving the smooth geomembrane (*a*, *b* and *c*) a common failure mechanism (*gradual sliding*) is observed in spite of the great difference in the upper layer surface structural pattern (geotextiles, geonet and geocomposite drain). Similarly, the interfaces involving textured geomembranes (*d*, *e*, *f* and *g*) display the feature of the *sudden sliding* mode of failure.

The same trend is confirmed by the shaking table test results.

The use of textured geomembrane in contact with geotextiles, implies that the superficial hook and loop interactions are dominant with respect to the purely frictional interface response occurring in the interfaces with smooth geomembranes.

Furthermore, the interfaces involving textured geomembranes are characterized by friction angles significantly higher than those obtained in the interface involving the smooth geomembrane. One of the main causes of the increase in shear strength, may be attributed to the engagement of the “loop” structure by the “hook” material occurring in systems where textured geomembranes are in contact with the geotextiles. In these interfaces, a dramatic loss in shear strength passing from the initial value required to start the movement [i.e. from ϕ_0 to ϕ_{lim} , in the inclined plane tests and from $\phi_{dyn}^{ST} (N_d = 1)$ to $\phi_{dyn}^{ST} (N_d = 100)$] is noticed in both cases having a more relevant importance in the interfaces involving textured geomembranes.

Concluding, the selection of textured geomembrane results in an increase of the interface friction angles but other complex mechanisms can occur at the interface and, in general, once the failure limit is reached, a brutal rupture takes place.

6.5 RECOMMENDATIONS AND FURTHER PERSPECTIVES

Test results indicate that the assessment of the interface shear strength is a very complex issue. It's worth noting that, on the basis of a design method where every layer of the geosynthetic liner system is limited to one function, the target for the different interface frictions is either a minimal or a maximal value of the friction angle.

It was demonstrated that the interface shear strength cannot be characterized by a single parameter being it very sensitive to the different kinematic conditions. Therefore, it is recommended to evaluate the interface shear strength at the conditions close to those expected in the field identifying the possible critical situation that can occur during the landfill cover lifespan. In this context, it is outlined the importance of performing laboratory tests at the proper normal stress, temperature and, in the analysis of the seismic response, the selection of the acceleration time history.

In particular, regarding temperature, the preliminary inclined plane test results confirmed that geosynthetic are sensitive to this parameter modifying the interface shear response. These results must be complemented by other further tests; the observed trends of the friction angles, are specific to the particular geosynthetics used in this study and the results cannot be generalized to other ones.

The analyses presented in this study, further demonstrate that the selection of an acceleration time history of appropriate magnitude and/or duration is a key factor in the correct evaluation of the seismic interface response. Further tests will be devoted to investigate the performance of the tested interfaces on inclined position of the lower table and to assess the interface shear strength behaviour under earthquake type motion on both horizontal and inclined shaking table configurations.

Finally, it was shown that the nature of the geomembrane is a key factor on determining the interface behaviour. Further tests are planned in order to investigate this phenomenon also at microscopical scale.

The different interface friction angles estimated at both inclined plane and shaking table tests, have direct implications on the design of structure involving composite systems; the evolution of the interface shear strength under different conditions, can help designers in the stability analysis of cover liners on slopes. In addition, in deciding on whether to base a

geosynthetic cover design, a variety of different parameters should be considered. Factors such as creep and the nature of earthquake loading, not treated in this study, may alter the interface shear strength.

7 REFERENCES

- Akpınar, M. V., Benson, C.H., 2005. Effect of temperature on shear strength of two geomembrane–geotextile interfaces. *Geotextiles and Geomembranes* 23, 443–453.
- Akpınar, M., 1997. Interface shear strength of geomembranes and geotextiles at different temperatures. MS Thesis, University of Wisconsin, Madison, WI, USA.
- Amonton, G. 1699. Histoire de l' Académie Royale des Sciences avec les Mémoires de Mathématique et de Physique, 206.
- Augello, A.J., Matasovic, N., Bray, J.D., Kavazanjian, E., Seed, R.B., 1995. Evaluation of solid waste landfill performance during the Northridge earthquake. In: Yegian, M.K., Finn, W.D.L. (Eds.), *Earthquake Design and Performance of Solid Waste Landfills*. Geotechnical Special Publication, ASCE, New York, 54, 17–50.
- Barone, F. S., Costa, J. M. A., and Ciardullo, L. 2000. Temperatures at the base of a municipal solid waste landfill. Proc., 6th Environmental Engineering Specialty Conf. of the CSCE, London, Ontario, Canada, 41–48.
- Bergado, D., Ramana, G., Sia, H., 2006. Evaluation of interface shear strength of composite liner system and stability analysis for a landfill lining system in Thailand. *Geotextiles and Geomembranes* 24, 371–393.
- Bleiker, D.E., Farquhar, G., and McBean, E. 1995. Landfill Settlement and the Impact on Site Capacity and Refuse Hydraulic Conductivity. *Waste Management and Research*, 13 (6), 533-554.
- Blight, G.E., 2007. Failures during construction of a landfill lining: a case analysis. *Waste Management & Research* 25, 327–333.
- Blond, E., Elie, G., 2006. Interface shear-strength properties of textured polyethylene geomembranes, in: *Sea to Sky Geotechnique 2006*, 898–904.
- Bouazza, A., Zornberg, J.G., Adam, D., 2002. Geosynthetics in waste containment facilities : recent advances, in: *Geosynthetics - 7th ICG -Delmas, Gourc & Girard*. 445–507.
- Bowden, F.P. and Tabor, D. 1954. *Friction and Lubrication*, London: Methuen and Company LTD.
- Briançon L, Villard P. 2006. Dimensionnement des renforcements géosynthétiques de plates-formes sur cavités. *Revue Française de Géotechnique* 2006;117, 51–62.
- Briançon, L., Girard, H., Gourc, J.P., 2011. A new procedure for measuring geosynthetic friction with an inclined plane. *Geotextiles and Geomembranes* 29, 472–482.

- Briançon, L., Girard, H., Poulain, D., 2002. Slope stability of lining systems - experimental modeling of friction at geosynthetic interfaces. *Geotextiles and Geomembranes* 20, 147–172.
- Byrne, R. J., 1994. Design issues with strain-softening interfaces in landfill liners. *Proc. Waste Tech.*, Charleston, South Carolina.
- Byrne, R. J., Kendall, J. and Brown, S., 1992. Cause and mechanism of failure, Kettleman Hills Landfill B-19, Phase IA. Stability and performance of slopes and embankments-II. *Geotechnical Special Publication* in: R. B. Seed, R. W. Boulanger (Eds.), 31, 1188-1215.
- Carbone, L., Briançon, L., Gourc, J.P., Moraci, N., Carrubba, P., 2012. Geosynthetic interface friction using Force Procedure at the Tilting Plane, in: *Eurogeo 5*, Valencia, Spain. 93–98.
- Carbone, L., Gourc, J. P., Briançon, L., Moraci, N., Carrubba, P., 2013a. What value of interface friction to select for geosynthetic liner on landfill slopes?, in: *Geosynthetics 2013*, Long Beach, California, 636 – 644.
- Carbone, L., Gourc, J. P., Carrubba, P., Moraci, N., Briançon, L., Pavanello, P., 2013b. New perspectives in the interface shear strength characterization through the inclined plane test., in: *Proceedings Sardinia 2013, Fourteenth International Waste Management and Landfill Symposium*, S. Margherita Di Pula, Cagliari, Italy.
- Carrubba, P. and Massimino, M.R., 1998. Geosynthetic interface strength in dynamic conditions. *L'Ingegnere e l'architetto, ANIAI J.*, 1-12/1998, 33-36.
- Carrubba, P., Massimino, M.R., Maugeri, M., 2001. Dynamic friction of geosynthetic interfaces by shaking table tests, in: *Proc. 8th Int. Waste Management and Landfill Symposium, SARDINIA 2001*. 567 – 576.
- Chareyre, B., Briançon, L., and Villard, P., 2002. Theoretical Versus Experimental Modeling of the Anchorage Capacity of Geotextiles in Trenches, *Geosynthetics International*, 9, (2), 97-123.
- Collins. H., 1993. Impact of the Temperature Inside the Landfill on the Behaviour of Barrier Systems. In: *Proceedings of Sardinia '93, 4th International Landfill Symposium*. S. Margherita di Pula, Cagliari, Italy. CISA, Environmental Sanitary Engineering Center, Cagliari, 417 432.
- Corser, P., and Cranston, M., 1991. Observations on Long-Term Performance of Composite Clay Liners and Covers. *Proceedings of the Conference on Geosynthetic Design and Performance*, Vancouver Geotechnical Society, Vancouver, British Colombia, 1–15.
- De, A., Zimmie, T.F., 1998. Estimation of dynamic interfacial properties of geosynthetics. *Geosynthetics International* 5, 17–39.
- Dellinger, G., Lacey, R., Allen, J., Gilbert, R., 2013. Importance of Variability in the Interface Shear Strength between Textured Geomembrane and Geocomposite Drainage Layer in Landfill Covers. *Geosynthetic 2013 Long Beach*, 688–697.

- Dove, J. E., and Frost, J.D. 1996. A Method for Measuring Geomembrane Roughness, *Geosynthetics International*, 3 (3), 369-392.
- Dove, J. E., Frost, J. D., Han, J., and Bachus, R. C. 1997. The influence of geomembrane surface roughness on interface strength. *Proc., Geosynthetics '97*, 2, Industrial Fabrics Association International, Roseville, Minn., 863-876.
- Eid, H.T., 2011. Shear strength of geosynthetic composite systems for design of landfill liner and cover slopes. *Geotextiles and Geomembranes* 29, 335-344.
- EN ISO 10318, 2005. Geosynthetics - terms and definitions. European Committee for Standardization.
- EN ISO 12957-1, 2005. Geosynthetic - Determination of Friction Characteristics, Part 1: Direct Shear Test. European Committee for Standardization, Brussels.
- EN ISO 12957-2, 2005. Geosynthetic - Determination of Friction Characteristics, Part 2: Inclined Plane Test. European Committee for Standardization, Brussels.
- European Union, 1999. EU Directive 99/31/EC on the landfill of waste. *Off. J. Eur. Communities* L182:1/
- Feki, N. 1996. Modeles physique et numerique de la stabilité des couvertures geosynthetiques en pente. Application aux centres de stockage des dechets, Thesis, Lirigm, Université Joseph Fourier, Grenoble, pp. 156 (in French).
- Frost, J.D., Lee, S.W., 2001. Microscale study of geomembrane - geotextile interactions. *Geosynthetics International* 8, 577-597.
- Girard, H., Fischer, S., Alonso, E., 1990. Problems of friction posed by the use of geomembranes on dam slopes - examples and measurements. *Geotextiles and Geomembranes* 9, 129-143.
- Giroud, J.P., 2012. Geosynthetics: a remarkable discipline with great achievements in the past and exciting challenges for a bright future, in: *Proceedings Keynote Lectures & Educational Session, 5th European Geosynthetics Congress. Valencia 2012 Geosynthetics*, 25 - 28.
- Giroud, J.P., Bachus, R.C. & Bonaparte R. 1995b. Influence of water flow on the stability of geosynthetic-soil layered systems on slopes. *Geosynthetics International* 2(6), 1149- 1180.
- Giroud, J.-P., Beech, J. F., 1989. Stability of soil layers on geosynthetic lining systems. *Proc. Geosynthetics '89, San Diego, USA*, 35-46.
- Giroud, J.P., Williams, N.D., Pelte, T. & Beech, J.F. 1995a. Stability of geosynthetic-soil layered systems on slopes. *Geosynthetics International* 2(6), 1115-1148
- Gourc, J.-P., Lalarakotoson, S., Muller-Rochholz, H., Bronstein, Z., 1996. Friction measurement by direct shearing or tilting process - Development of a European standard, in: *Geosynthetics: Applications, Design and Construction*, De Groot, Den Hoedt & Termaat, Balkema, Rotterdam, 1039-1045.

- Gourc, J.P., Reyes Ramirez, R., 2004. Dynamics-based interpretation of the interface friction test at the inclined plane. *Geosynthetics International* 1, 439 – 454.
- Gourc, J.P., Reyes Ramirez, R., 2004. Dynamics-based interpretation of the interface friction test at the inclined plane. *Geosynthetics International* 11, 439 - 454.
- Gourc, J.P., Reyes-Ramirez, R., Villard, P., 2004. Assessment of Geosynthetics Interface Friction for Slope Barriers of Landfill, in: Keynote Lecture, 3rd Asian Regional Conference on Geosynthetics, GeoAsia 2004, 116–149.
- Guide technique, 2000, Etanchéité par géomembranes des ouvrages pour les eaux de ruissellement routier, co-édité par le SETRA et le LCPC, guide complémentaire, 71p , (in French).
- Hebeler, G., Frost, J., Myers, a, 2005. Quantifying hook and loop interaction in textured geomembrane-geotextile systems. *Geotextiles and Geomembranes* 23, 77–105.
- Hullings D. E., Sansone L. J. 1997 Design concerns and performance of geomembrane anchor trenches. *Geotextiles and Geomembranes*, 15 (4-6), 403-413.
- Hushmand,B. andMartin, G.R., 1990, “Final Report SBIRPhase I Study, Layered Soil-Synthetic Liner Base Isolation System”, Report submitted to the National Science Foundation Small Business Innovative Research Program, The Earth Technology Corporation, Long Beach, California, USA, pp. 86.
- Izgin, M., Wasti, Y., 1998. Geomembrane - sand interface frictional properties as determined by inclined board and shear box tests. *Geotextiles and Geomembranes* 16.
- Jones, D.R. V., Dixon, N., 1998. Shear strength properties of geomembrane/geotextile interfaces. *Geotextiles and Geomembranes* 16, 45–71.
- Karademir, T., 2011. Elevated temperature effects on interface shear behavior. Thesis, Georgia Institute of Technology.pp 628.
- Karademir, T., 2011. Elevated temperature effects on interface shear behavior. Georgia Institute of Technology.
- Karademir, T., Frost, D., 2013. Elevated Temperature Effects on Smooth Geomembrane – Geotextile Interfaces. *Geosynthetic* 2013 1-4 April, 610–619.
- Kavazanjian, E., 1999. Seismic Design of Solid Waste Containment Facilities. *Proceedings of the Eight Canadian on Earthquake Engineering* 51 – 89.
- Kavazanjian, E., Hushmand, B. andMartin, G.R., 1991. Frictional Base Isolation Using a Layered Soil-Synthetic Liner System, *Proceedings of the Third U.S. Conference on Lifeline Earthquake Engineering*, Cassaro, M.A., Editor, ASCE Technical Council on Lifeline Earthquake Engineering Monograph No. 4, Los Angeles, California, USA, August 1991, pp. 1140-1151.
- Khire, M., Benson, C., and Bosscher, P. 1997. Water Balance Modeling of Earthen Landfill Covers. *Journal of Geotechnical and Geoenvironmental Engineering*, ASCE 123 (8), 744–754.

- Kim, J.M., 2001. Probabilistic approach to evaluation of earthquake-induced permanent deformation of slopes, Ph.D. Thesis, University of California, Berkeley, USA, pp.361.
- Koerner, G.R., and Koerner, R.M. 2006. Long-Term Temperature Monitoring of Geomembranes at Dry and Wet Landfills. *Geotextiles and Geomembranes*, 24 (1), 72-77.
- Koerner, R. M., Hwu, B. L., 1991. Stability and tension considerations regarding cover soils on geomem- brane lined slopes. *Geotextiles and Geomembranes* 10, 335 - 355.
- Koerner, R.M., 1998. *Designing with Geosynthetics*, Fourth ed. Prentice- Hall, Upper Saddle River, NJ., 761 pp.
- Koerner, R.M., 2005. *Designing with Geosynthetics*. Fifth ed. Pearson-Prentice Hall Publ. Co., Upper Saddle River, NJ, 796 pp.
- Koerner, R.M., Soong, T.Y., 2000. Stability assessment of ten large lanffill failures. In: *Proceedings of GeoDenver 2000 Congress: Advances in Transportation and Geoenvironmental Systems Using Geosynthetics*, vol. 103, pp. 1-38. ASCE Geotechnical Special Publication.
- Kotake, N., Matsubara, S., Kamon, M., 2011. Dynamic Interface Behaviors of Geosynthetic Barriers by Shaking Table Tests. *Geo - Environmental Engineering* 2011.
- Lalarakotoson, S., Villard, P., Gourc, J.P., 1999. Shear strength characterization of geosynthetic interfaces on inclined planes. *Geotechnical Testing Journal* 22, 284 - 291.
- Lee, S.W. 1998. Influence of Surface Topography on Interface Strength and Counterface Soil Structure, Ph.D. Dissertation, School of Civil and Environmental Engineering, Georgia Institute of Technology, 336 pp.
- Ling, H.I., Burke, C., Mohri, Y., Matsushima, K., 2002. Shear strength parameters of soil-geosynthetic interfaces under low confining pressure using a tilting table. *Geosynthetics International* 9, 373–380.
- Ling, H.I., Leshchincky, D., 1997. Seismic stability and permanent displacement of landfill cover systems. *Journal of geotechnical and geoenvironmental engineering* 113 – 122.
- Long, J. H., Gilbert, R. B., Daly, J. J., 1994. Geosynthetic loads in landfill slopes: Displacement compatibil- ity. *Journal of Geotechnical Engineering* 120 (11), 2009-2025.
- Lopes, P.C., Lopes, M.L., Lopes, M.P., 2001. Shear behaviour of geosynthetics in the inclined plane test – Influence of soil particle size and geosynthetic structure. *Geosynthetics International* 8, 327–342.
- Manassero, M., Benson, C.H., Bouazza, A., 2000. Solid waste containment systems, in: *International Conference on Geotechnical & Geological Engineering*, Melbourne. 520–642.

- Manfredi S. and Christensen T.H., 2009. Environmental assessment of solid waste landfilling technologies by means of LCA-modeling (EASEWASTE). Waste Management, 29, 32–43.
- Matasovic., N., Kavazanjian, E.J., Giroud, J. P., 1998. Newmark seismic deformation analysis for geosynthetic covers. Geosynthetics International 5, 237–264.
- Maugeri, M., Seco E Pinto, P.S., 2005. Seismic design of solid waste landfills and lining systems. TC5 Report Chapter 5, 1 – 27.
- Mitchell, J. K., Seed, R. B., Seed, H. B., 1990. Stability considerations in the design and construction of lined waste repositories. Geotechnics of waste fills theory and practice ASTM STP 1070, Landva&Knowles, Eds., ASTM, Philadelphia.
- Monteiro, C.B., Araújo, G.L.S., Palmeira, E.M., Cordão Neto, M.P., 2013. Soil-geosynthetic interface strength on smooth and texturized geomembranes under different test conditions In: 18th International Conference on Soil Mechanics and Geotechnical Engineering, Paris, France, 02-06 September 2013, 3053-3056.
- Montgomery, R., and Parsons, L. 1990. The Omega hills cover test plot study: fourth year data summary. Proceedings of the 22nd Mid-Atlantic Industrial Waste Conference, Technomic Publishing Company, Inc., Lancaster, PA, USA, pp. 1–12.
- Moraci, N., 2011. Il rinforzo del terreno con geosintetici - recenti sviluppi tecnologici, progettuali e normativi, in: Relazione Generale. XXIV Convegno Nazionale Geotecnica. Innovazione Tecnologica nell'Ingegneria Geotecnica. Ed.AGI. Napoli, 22-24 Giugno, 1. 149–198.
- Moraci, N., Cardile, G., 2009. Influence of cyclic tensile loading on pullout resistance of geogrids embedded in a compacted granular soil. Geotextiles and Geomembranes 27, 475 - 487.
- Newmark, N. M. 1965. Effects of earthquakes on dams and embankments. Geotechnique, 15, (2), pp. 139–160.
- NTC, 2008 - DM 14/1/2008. Norme Tecniche per le Costruzioni. S.O. n. 30 - Gazzetta Ufficiale della Repubblica Italiana, n. 20-4/2/2008.
- Oweis, J.S., Smith, D.A., Ellwood, R.B., and Green, D.S. 1990. Hydraulic Characteristics of Municipal Refuse. Journal of Geotechnical Engineering, 116 (4): 539-553.
- Palmeira, E.M., 2009. Soil–geosynthetic interaction: Modelling and analysis. Geotextiles and Geomembranes 27, 368–390.
- Palmeira, E.M., Lima, N.R.J., Mello, L.G.R., 2002. Interaction between soils and geosynthetic layers in large-scale ramp tests. Geosynthetics International 9, 149–187.
- Palmeira, E.M., Viana, H.N., 2003. Effectiveness of geogrids as inclusions in cover soils of slopes of waste disposal areas. Geotextiles and Geomembranes 21, 317–337.

- Park, I.J., Seo, M.W., Park, J.B., Kwon, S.Y., Lee, J.S., 2004. Estimation of the dynamic properties for geosynthetic interfaces, in: 13 Th World Conference on Earthquake Engineering, Vancouver, Canada, August 1-6. 3210 pp.
- Pasqualini, E., Roccato, M., and Sani D., 1993. Shear Resistance at the Interfaces of Composite Liners, Proceedings Sardina 93, Cagliari, Italy, 1457-1471.
- Pavanello P., Carrubba P., 2012. Taratura e primi riscontri sperimentali su tavola vibrante. IARG 2012, Incontro Annuale dei Ricercatori di Geotecnica, Padova, 2-4 Luglio 2012, pp.6.
- Pitanga, H.N., Gourc, J.-P., Vilar, O.M., 2009. Interface shear strength of geosynthetics: Evaluation and analysis of inclined plane tests. *Geotextiles and Geomembranes* 27, 435–446.
- Pitanga, H.N., Gourc, J.-P., Vilar, O.M., 2011. Enhanced Measurement of Geosynthetic Interface Shear Strength Using a Modified Inclined Plane Device. *Geotechnical Testing Journal* 34, 10.
- Pitanga, H.N., Vilar, O.M., Gourc, J.-P., 2013. Wear resistance of geosynthetic interfaces constituted by geomembrane and geospacers. *REM: R. Escola Minas, Ouro Preto* 66, 227–232.
- prEN 1998-5, 2003. Eurocode 8: Design of structure for earthquake resistance,. Part 5: Foundations, retaining structures and geotechnical aspects. CEN European Committee for Standardisation, Bruxelles, Belgium.
- Reyes Ramirez, R., Gourc, J.P., 2003. Use of the inclined plane test in measuring geosynthetic interface friction relationship. *Geosynthetics International* 10, 165–175.
- Rowe, R.K., 2005. Long-term performance of contaminant barrier systems. *Geotechnique* 55 (9), 631–678.
- Seed, R.B., Mitchell, J.K., and Seed, H.B., 1990. Kettleman Hills Waste Landfill Slope Failure II: Stability Analysis, *ASCE Journal of Geotechnical Engineering*, 116, (4), 669-689.
- Shukla, S.K. and Yin, J.-H. 2006. *Fundamentals of Geosynthetic Engineering*. Taylor and Francis, London, UK, 410 p.
- Sia, a. H.I., Dixon, N., 2007. Distribution and variability of interface shear strength and derived parameters. *Geotextiles and Geomembranes* 25, 139–154.
- Stark, T., Williamson, T., Eid, H., 1996. HDPE geomembrane/geotextile interface shear strength. *Journal of Geotechnical Engineering, ASCE* 122 (3), 197–203.
- Stark, T.D., Arellano, D., Evans, W.D., Wilson, V.L., Gonda, J.M., 1998. Unreinforced geosynthetic clay liner case history. *Geosynthetics International* 5 (5), 521-544.
- Tropeano, G., 2010. Previsione di spostamenti di pendii in condizioni sismiche. Thesis, Mediterranean University of Reggio Calabria. pp. 230. (in Italian).

- Vashi Jigisha M., Desai M. D., Desai A.K., Solanki C.H., 2010. Geosynthetic Materials and Its Properties for Reinforced Earth Structures, Swarnim Jayanti, All India Seminar on Geosynthetics for Civil Engg.; Organizer Institute of Eng. (India) Ahmedabad Centre, Ahmedabad November, 2010.
- Villard, P., Chareyre, B., 2004. Design methods for geosynthetic anchor trenches on the basis of true scale experiments and discrete element modeling. Canadian Geotechnical Journal, 41 (6), 1193-1205.
- Von Pein R.T., Lewis S.P., 1991. Composite Lining System Design Issues. Geotextiles and Geomembranes, 10, (5-6), 125-131.
- Wasti, Y., Özdüzgün, Z.B., 2001. Geomembrane - geotextile interface shear properties as determined by inclined board and direct shear box tests G zdu. Geotextiles and Geomembranes 19, 45–57.
- Wu, W., Wang, X.T., Aschauer, F., 2008. Investigation on failure of a geosynthetic lined reservoir. Geotextiles and Geomembranes 26, 363–370.
- Yegian, M.K., Harb, J.N., 1995. Slip displacements of geosynthetic systems under dynamic excitation, in: Earthquake Design and Performance of Solid Waste Landfills, Geotechnical Special Publication N° 54. pp. 212–236.
- Yegian, M.K., Kadakal, U., 1998. Geosynthetic interface behavior under dynamic loading. Geosynthetics International 5, 1–16.
- Yegian, M.K., Lahlaf, A.M., 1992. Dynamic interface shear strength properties of geomembranes and geotextiles. ASCE Journal of Geotechnical Engineering 118 (5), 760–778.
- Yegian, M.K., Yee, Z.Y., Harb, J.N., 1995a. Seismic response of geosynthetic-soil systems, in: Geoenvironment 2000, 2, 1113 – 1125.
- Yegian, M.K., Yee, Z.Y., Harb, J.N., 1995b. Response of Geosynthetics Under Earthquake Excitations, in: Geosynthetics 1995, 677 –689.
- Yoshida, H., Tanaka, N., and Hozumi, H., 1997. Theoretical Study on Heat Transport Phenomena in a Sanitary Landfill. Proceedings of Sardinia: Sixth International Landfill Symposium, Cagliari, Italy.